Calculation and Analysis of the Rejected Takeoff Speed of a Commercial Airliner Under Various Environmental Conditions

a project presented to
The Faculty of the Department of Aerospace Engineering
San José State University

in partial fulfilment of the requirements for the degree
Master of Science in Aerospace Engineering

by

James D. Gonzalez

August 2023

approved by

Thomas Lombaerts, Ph.D.
Faculty Advisor

San José State
UNIVERSITY

Abstract

Considered the world's largest commercial aircraft in civilian aviation history, the Airbus A380-800 provides safe and reliable transportation to people and customers all over the world. To uphold the A380's impeccable safety record, critical parameters such as, but not limited to, the rejected takeoff (RTO) speed is calculated with sophisticated software algorithms and real time data. The RTO speed of an A380 is a critical calculation that is determined before each departure to reduce the likelihood of catastrophic lateral and longitudinal runway excursions in the event of an aborted takeoff. Given the size, capacity, and power requirements of commercial airliners, a runway excursion can be disastrous and fatal if the takeoff procedure during the ground roll phase is aborted after the predetermined RTO speed is exceeded. As a result, large commercial airliners include a dependable and robust flight management system (FMS) which calculates the RTO speed as accurately as possible so that flight crews make the appropriate go/no-go decisions. In addition to aircraft geometry and performance specifications, thermodynamic properties, and airport information, environmental factors such as headwinds, tailwinds, crosswinds, and runway surface conditions have a significant impact on the calculation of both the RTO speed and the location of the RTO speed. The primary objective of this master's project is to analyze the effects and overall impacts of realistic wind conditions and unfavorable runway surface conditions on the RTO speed of an A380. First, a 1-D RTO speed model is constructed given fundamental equations of motion, published data, and proven numerical methods to calculate critical parameters at every timestep. Moreover, the 1-D RTO speed model serves as a benchmark for more complicated models, which exercises multiple environmental factors simultaneously. Once the benchmark RTO speed model is validated with published data, environmental factors are analyzed from a 1-D (e.g., pure headwinds, pure tailwinds, and average dry and wet runway surface conditions) and 3-D (e.g., crosswinds and varying runway surface conditions dependent on ground speed and sideslip angle) perspective. Furthermore, realistic environmental conditions such as wind speed, wind direction, temperature, and altimeter readings are obtained from 2022 Meteorological Aerodrome Reports (METAR), and runway surface schemes are obtained from publications and other baseline models. To further assess the impacts of the aforementioned environmental conditions on the RTO speed, sensitivity analyses are conducted to quantify the results. The secondary objectives of this master's project are to investigate and analyze the effects of mechanical failures, as well as hot and high conditions, on the A380's performance during the ground roll procedure. Moreover, the engine failures are analyzed before, at, and after the RTO speed to assess the A380's capabilities and limitations in the event of a bird strike or major engine malfunctions. Regarding hot and high conditions, and the overall impacts on the A380 performance capabilities, temperature and altimeter values obtained from 2022 METAR observations are used to calculate realistic air density values which have a direct impact on thrust and aerodynamic properties.

Acknowledgments

First and foremost, I would like to express my deepest gratitude to my faculty advisor Dr. Thomas Lombaerts for his continuous support and guidance throughout this master's project. Thank you Dr. Lombaerts for all of your feedback, direction, and invaluable insight. My success throughout the MSAE program at SJSU would be impossible without your support.

Thank you Mom and Dad for your encouragement while I completed my master's degree in aerospace engineer. I really enjoyed our late night phone calls while working on this project.

Finally, I express my profound gratitude and love to Emily Regan, who endlessly supported me, brought me joy when I was stressed, and believed in me from the beginning. I am forever grateful for you, Emily, and will forever cherish your love and support.

Table of Contents

List of Tables

List of Figures

Nomenclature

Symbol	Definition	Units
AR	Aspect ratio	$-$
b	Wingspan	m
C_{D_0}	Parasitic drag coefficient	$-$
C_D	Total drag coefficient	$-$
C_L	Lift coefficient	$-$
C_l	Non-dimensional roll moment coefficient	$^1/_{\text{rad}}$
C_n	Non-dimensional yaw moment coefficient	$^1/_{\text{rad}}$
C_Y	Non-dimensional side force coefficient	$^1/_{\text{rad}}$
D	Total drag	N
dt	Timestep	s
e_1	Span efficiency factor	$-$
F	Force acting on aircraft	N
g	Acceleration constant due to gravity	$^{\text{m}}/_{\text{s}^2}$
h	Wingtip above runway	m
H_{g}	Airport elevation	m
I_{zz}	Moment of inertia about the z-axis	kg m^2
k	Proportional gain constant for crosswind model	$-$
L	Total lifting force	N
m	Mass of aircraft	kg
M	Moment	N m
q	Dynamic pressure	Pa
$q_{\text{air,lift}}$	Dynamic pressure used for lift calculations	Pa
R	Resistance force	N
R_{air}	Gas constant for air	$^{\text{J}}/_{\text{kg K}}$
r	Yaw rate	$^{\text{rad}}/_{\text{s}}$
$\dot{r}$	Yaw rate of change with time	$^{\text{rad}}/_{\text{s}^2}$
r_1	Distance between nose wheel and C.G.	m
r_4	Distance between main wheels and C.G.	m
r_{eng}	Lateral distance between engine and C.G.	m
S_1	Location of rejected takeoff speed	m
S_w	Wing surface area	m^2
S	Runway distance	m
T	Engine thrust	m
T_K	Absolute temperature	K

u	Forward velocity with respect to the body frame	m/s
$\dot{u}$	Forward acceleration with respect to the body frame	m/s^2
v	Lateral velocity with respect to the body frame	m/s
$\dot{v}$	Lateral acceleration with respect to the body frame	m/s^2
V_1	Rejected takeoff speed	m/s
V	Airspeed for 1-D environmental model	m/s
$V_{\text{air,lift}}$	Airspeed used for lift calculations in crosswind model	m/s
W	Aircraft weight	N
W_b	Wheel base	m
$\ddot{x}(t)$	Instantaneous inertial acceleration	m/s^2
$\dot{x}(t)$	Instantaneous ground speed	m/s
$x(t)$	Instantaneous position	m
z_1	Distance between outboard engines and C.G.	m
z_2	Distance between inboard engines and C.G.	m
Greek Symbols		
β	Sideslip angle	rad
δ_n	Nose wheel deflection angle	rad
δ_r	Rudder deflection angle	rad
μ	Runway surface friction coefficient	–
μ_s	Lateral runway surface friction coefficient	–
κ	Track angle relative to runway centerline	rad
ϕ	Ground effect factor	–
ρ	Free-stream density	kg/m^3
ψ	Aircraft heading angle	rad
θ_{air}	Wind direction with respect to RWY centerline	rad
Subscripts		
aero	Aerodynamic	–
avg	Average	–
∞	At elevation conditions	–
0	Sea-level conditions	–
28R	Runway 28R at KSFO	–
dry	Dry runway conditions	–
contam	Contaminated runway conditions	–
eff	Effective	–
eng	Engine	–
f	Fuel	–
g	Ground or runway surface	–
gear	Main and nose wheel gear	–
inboard	Inboard engines	–
L	Landing	–

max	Maximum value	–
MTOW	Maximum takeoff weight	–
mw	Main wheel	–
nw	Nose wheel	–
outboard	Outboard engines	–
pub	Published value	–
rev	Reverse for thrust applications	–
r	Runway condition	–
TO	Takeoff	–
wet	Wet runway conditions	–
wind	Wind conditions	–
x	x-direction in reference frame	–
y	y-direction in reference frame	–
z	z-direction in reference frame	–
ZFW	Zero fuel weight used to determine 1-D landing profile	–
Acronyms		
ATC	Air traffic control	–
AGL	Above ground level	–
ARTCC	Air Route Traffic Control Center	–
C.G.	Center of gravity	–
EFTO	Engine failure on takeoff	–
FAA	Federal Aviation Administration	–
FMS	Flight management system	–
FOD	Foreign object damages	–
FoS	Factor of Safety	–
IEM	Iowa Environmental Mesonet	–
ISA	International Standard Atmosphere	–
JAA	Joint Aviation Authorities	–
KDEN	Denver International Airport	–
KSFO	San Francisco International Airport	–
METAR	Meteorological Aerodrome Reports	–
NAS	National Airspace System	–
OEP	Operational Evolution Partnership	–
RTO	Rejected takeoff	–
RWY	Runway	–
SEQM	Quito/Mariscal Sucre International Airport	–
TRACON	Terminal Radar Approach Control Facility	–

Chapter 1: Introduction

1.1 Motivation

Over the last couple of years, the Federal Aviation Administration (FAA) noted an increase in runway near miss incidents at several U.S. airports across the National Airspace System (NAS) [1]. In addition to the alarming number of runway incursions in previous years, bird strikes across the NAS and at Operational Evolution Partnership (OEP) 35 airports (e.g., San Francisco International Airport) have also increased due to a parallel increase in large bird populations [2, 3]. In addition to operating a large network of facilities (e.g., Air Route Traffic Control Centers, Terminal Radar Approach Control facilities, and airport towers), maintaining communication equipment, integrating new technology such as the NextGen Air Transportation System into the NAS, and providing reliable transportation services, aviation safety remains at the forefront of the administration's activities. Furthermore, developments and improvements in aircraft subsystems, such as the flight management system (FMS), can mitigate the likelihood of both runway incursions and excursions by accurately calculating critical parameters such as the rejected takeoff (RTO) speed with real time data streams [4].

Having a great understanding of the RTO speed of a large commercial airliner can reduce the likelihood of disastrous lateral and longitudinal runway excursions in the event of an aborted takeoff. To uphold the FAA's safety objectives, the accuracy of the RTO speed calculation under various environmental conditions is of great importance to the aerospace community because both runway incursions (e.g., pilot deviations and near misses) and excursions (e.g., longitudinal and lateral runway overshoot) could decrease significantly with the development of robust, dependable algorithms and various data streams (e.g., hour or half-hour METAR observations for realistic wind speeds, wind directions, precipitation conditions, and improved sensors on board the aircraft, etc.). While the overall takeoff procedure includes multiple phases, the work described in this master's project is focused specifically on the ground roll procedure and does not account for the lift-off process. Moreover, the environmental conditions are obtained from readily accessible METAR databases, and the runway conditions account for various surfaces (e.g., dry and wet conditions).

The primary motivation for this master's project is to explore and analyze various environmental factors, such as wind speed, wind direction, unfavorable runway conditions, temperature, and pressure, and to assess the overall impact on the rejected takeoff (RTO) speed of the world's largest civilian passenger aircraft: the Airbus A380-800 [5]. In addition to environmental factors, the impacts of random propulsion equipment malfunctions (e.g., multiple engine failure due to bird strikes) on the RTO speed of the A380 are investigated and analyzed.

1.2 Literature Review

The RTO speed, commonly referred to as V_1 in the aviation industry, is defined as the maximum speed by which a rejected takeoff must be initiated to ensure an aircraft does not overshoot the runway [6]. Moreover, there are several circumstances and instances when flight crew members have to conduct an RTO. For example, if an aircraft commits a runway incursion and crosses an airstrip not authorized by air traffic control (ATC), similar to the Delta and American Airlines incident at New York-JFK in January 2023, the departing aircraft is forced to conduct an RTO to protect lives onboard both aircraft[7]. In addition to runway incursions, engine mechanical failures as well as bird strikes during the ground roll procedure are other instances where flight crews may initiate an RTO. While turbofan technology has advanced significantly since the 1960s, and the current failure rate of commercial turbofan engines are less than 1 per 100,000 flights, bird strikes can arise unexpectedly and may force flight crews to conduct an RTO [8].

Given fundamental expressions related to flight mechanics, aircraft specifications (e.g., weight of the aircraft), thermodynamic properties (e.g., ambient pressure and temperature), and airport information (e.g., runway elevation) significantly impact the calculation of the RTO speed of commercial airliners [9]. In addition, other factors such as wind conditions (e.g., headwinds and tailwinds), unfavorable runway surfaces (e.g., contaminated runway surfaces), and engine failures also have a significant impact on both the RTO speed and the location of the RTO speed along the runway. The literature review described in this master's project explores previous studies and publications, and highlights key findings related to the present work. Furthermore, a pivotal goal is to integrate the models and algorithms described in this master's project with existing research to further explore and investigate the RTO speed of an A380 given a wide range of environmental conditions and random mechanical failures.

1.2.1 Wind Conditions During Ground Roll

During the ground roll procedure, commercial airliners are subjected to three types of wind conditions: pure headwinds, pure tailwinds, and crosswinds [10]. Moreover, the aforementioned wind classifications have unique impacts on commercial airliners departing a runway. For instance, it is ideal for aircraft to depart directly into the wind (e.g., pure headwind conditions) as more lift is generated over the wings, the ground speed is ultimately reduced, and the aircraft is able to lift-off in a shorter distance [9]. On the other hand, a penalty occurs when an aircraft departs with a pure tailwind since the airflow over the wing is slowed down and the aerodynamic forces are ultimately reduced [9]. In extreme conditions, commercial airliners may be subjected to crosswind conditions, which is a portion of the wind that is orthogonal to the runway [11]. In addition, strong and gusting crosswind conditions are more frequent due to global warming and other climate conditions [11, 12].

Regarding published factors and specifications (e.g., minimum control ground speed), manufacturers typically obtain these values based on favorable and nominal conditions (e.g., dry runways, negligible wind conditions, etc.) [13, 14]. However, depending on the severity of the wind conditions (e.g., strong crosswinds), the aircraft may become unstable and the RTO speed, as well as the location of the RTO speed, is reduced significantly [15]. A reduction in the RTO speed gives flight crews less time to safely abort the takeoff in the event of an emergency. In addition to airframe risk and safety analysis, the aforementioned wind classifications must be accounted for in the RTO speed calculation.

1.2.2 Runway Surface Conditions

According to regulations from the FAA and the Joint Aviation Authorities (JAA), there are three runway classifications: dry, wet, and contaminated [16]. For the present work, dry and wet runway conditions are considered for the 1-D RTO models. To alleviate ambiguity, the wet runway conditions described in the present work follow the FAA definition, and the depth of standing water is assumed to be equal to, or is less, than 3-mm [16, 17]. In addition to dry and wet runway surface conditions, the runway friction coefficient varies between takeoff and landing procedures due to brake applications. For instance, the value of the runway friction coefficient during the takeoff procedure is smaller compared to the landing procedure because the application of main wheel brakes result in larger friction coefficients [9]. Moreover, these findings are noticeable for dry and ideal runway surface conditions because the main wheels typically have better traction when several brakes are applied at high speeds [9]. For analyses which rely on 1-D equations of motion in the present work, such as the baseline and environmental models, approximations for dry and wet runway conditions are easily obtainable from previous studies [16, 18].

Regarding non-ideal runway surface conditions, several sources indicate that wet runway friction conditions are significantly reduced compared to dry runway conditions, and traction failure can lead to catastrophic accidents [19, 20, 21]. For realistic runway conditions, several models and algorithms have been developed for all three runway classification types [19, 20]. For instance, existing finite element (FE) models are capable of simulating rolling aircraft wheels with different surface conditions (e.g., dry, wet, etc.) and runway materials (e.g., asphalt) [21]. Moreover, existing literature related to dry and wet runway conditions present linear and non-linear sensitivity analyses to quantify uncertainly levels and identify which independent variables impact the runway coefficient the most [20]. Other established runway surface models include empirical relationships for all three runway surface classifications, where the runway friction coefficient is dependent on both the ground speed as well as the wheel sideslip angle [22].

1.2.3 Engine Failure

If a commercial airliner experiences an engine failure on takeoff (EFOT), flight crew members must make the appropriate go/no-go decision to either proceed with the takeoff or abort the departure entirely to avoid a longitudinal or lateral runway excursion [13]. Moreover, the RTO speed serves as a critical threshold for this go/no-go decision. There are several instances where a commercial airliner can experience an EFOT. In addition to airframe damage, bird strikes account for more than 90% of foreign object damages (FODs), and have been known to interfere with ground roll operations [23]. Moreover, most bird strikes occur during the takeoff, approach, and landing phases of flight at altitudes less than 100 ft above ground level (AGL) [23]. While modern turbofan engines are reliable from a mechanical standpoint, compressor surges and stalls can occur due to a disturbed operating cycle and result in an EFOT. In addition to compressor stalls, general oil and fuel system issues can result in an EFOT, in which case an RTO must be initiated. As a result, EFOTs in addition to various environmental factors must be accounted for to enhance the accuracy of the calculated RTO speed.

1.2.4 Hot and High Conditions

Temperature, pressure, and airport elevation have a significant impact on the performance, as well as the RTO speed, of a commercial airliner. Moreover, the lower air density common at high elevation airports (e.g., Denver International Airport) has a direct impact on the thrust generated by the turbofan engines and overall aircraft performance [24]. To ensure large aircraft can safely operate under hot and high conditions, longer runways are implemented in the airfield design phase [24]. However, if large commercial airliners are operating under MTOW conditions, it is imperative the performance calculations are as accurate as possible to ensure the aircraft can depart safely. Under extreme temperature conditions, which are common in the summertime at Phoenix Sky Harbor, temperatures can get close to or exceed the maximum operating temperature and must be accounted for prior to departure [25]. As a result, significant density and temperature conditions should be accounted for in performance calculations to ensure the aircraft can depart and operate safely.

1.3 Project Proposal

The RTO speed of a commercial airliner is a pivotal parameter that is determined prior to departure to reduce the likelihood of catastrophic runway excursions in the event of an aborted takeoff. Moreover, runway excursions are likely to occur if the ground roll procedure is aborted after the RTO speed is exceeded, which may result in the loss of life, cargo, and building infrastructure. As a result, flight crew members must determine whether to proceed with the takeoff procedure or abort the takeoff entirely in the event of an emergency (e.g., engine failures due to bird strikes, runway incursions by nearby aircraft, etc.) given the airspeed at the time of the incident. Moreover, the FMS uses sophisticated software algorithms, real time data, and a certain level of redundancy to ensure the calculation of the RTO speed is as accurate as possible.

The calculation of the RTO speed of a commercial airliner is primarily dependent on aircraft properties and specifications (e.g., aircraft weight, aerodynamic properties, wingspan and wing surface area, etc.), airport information (e.g., runway elevation, runway length, etc.), thermodynamic properties (e.g., temperature, pressure, etc.), and environmental factors (e.g., pure headwinds, pure tailwinds, crosswinds, varying runway surface conditions, etc.) [9]. Furthermore, the calculation of the RTO speed is based on the fundamental aircraft equations that govern both transnational and rotational motion along the runway, which are derived from Newton's second law of motion [9].

The primary objective of this master's project is to analyze the effects and overall impacts of realistic, readily accessible varying wind conditions (e.g., wind speed and wind direction) and unfavorable runway surface conditions (e.g., wet surfaces) on both the RTO speed as well as the location of the RTO speed through sensitivity analyses. For this master's project, the A380 is analyzed at maximum takeoff weight (MTOW) conditions and departs several airports depending on the RTO speed study. For environmental studies, which primarily focus on wind conditions and unfavorable runway surface conditions, the aircraft departs runway 28R at San Francisco International Airport. First, a 1-D RTO speed model is developed with fundamental equations of motion related to flight mechanics, A380 specifications and properties, and proven numerical schemes (e.g., Explicit Euler method) to calculate critical parameters at every timestep (e.g., force, acceleration, velocity, position, etc.) and ultimately calculate the nominal (e.g., negligible wind conditions, dry runway surface conditions, International Standard Atmosphere, etc.) RTO speed for an A380 at MTOW. The 1-D RTO speed model is validated with published A380 data (e.g., nominal takeoff distance, nominal landing distance, etc.), and will serve as a benchmark for more complicated environmental models, which include varying wind conditions and unfavorable runway surface conditions. The impacts of 1-D environmental factors (e.g., pure headwinds, pure tailwinds, and averaged runway surface conditions) on both the RTO speed as well as the location of the RTO speed are assessed through 2-D sensitivity analyses conducted in MATLAB. Moreover, realistic wind speeds and directions are obtained from readily-accessible METAR observation reports.

The secondary objectives of this master's project are to investigate and analyze the effects of 1-D mechanical failure (e.g., multiple engine failures due to bird strike), 1-D hot and high conditions, and 3-D crosswind impacts on the overall performance of the A380 at MTOW. Regarding the engine failure analysis due to a bird strike, the objective is to analyze the performance of the A380 at MTOW when the engine failure occurs before, at, and after the RTO speed, and plot the corresponding deceleration profile to assess whether or not the aircraft can safely depart. Regarding 1-D hot and high conditions, realistic temperature and altimeter values are obtained from readily-accessible METAR observations which ultimately capture lower and realistic air density values through the ideal gas law. Moreover, the lower air density under hot and high conditions significantly impacts both the performance as well as the calculation of the RTO speed of an A380 at MTOW, and are analyzed in this master's project. Regarding the crosswind analysis, and the overall impact on both the performance and the RTO speed, realistic wind conditions are obtained from the aforementioned METAR observation reports. Moreover, the 3-D crosswind model includes three separate submodels in order to enhance the fidelity of the dynamics. For instance, the aerodynamic submodel captures both aerodynamic forces and moments, whereas the gear submodel captures the resistance forces in both the longitudinal and lateral directions.

1.4 Methodology

The objective of this master's project is to determine the effects of environmental factors, engine failures, and hot and high conditions on the RTO speed, V_1, of an Airbus A380 at maximum takeoff weight (MTOW) departing various airports (e.g., San Francisco International Airport, Denver International Airport, and Quito/Mariscal Sucre International Airport). To accomplish this objective, a 1-D RTO speed model is first constructed and validated with published A380 data. Next, environmental factors, engine failures, and hot and high conditions are integrated into the baseline algorithm to develop both 1-D and 3-D studies. Moreover, the 1-D analyses in this master's project include averaged data (e.g., pure headwinds and pure tailwinds, wind directions obtained from METAR observation reports, average dry and wet runway surface conditions, etc.), whereas the 3-D analysis includes complex scenarios (e.g., crosswind conditions, various lateral and longitudinal runway surface conditions based on ground speed, well-defined aerodynamic and gear submodels, etc.). As a result, the analyses presented in this master's project also capture limitations for the A380 at MTOW for safety measures, which aim to reduce the likelihood of overshooting the runway in the event of an aborted takeoff.

The goal of the 1-D baseline model is to calculate both the RTO speed as well as the location of the RTO speed of an A380 at MTOW under nominal conditions (e.g., negligible wind conditions, dry and ideal runway surface conditions, no mechanical failures, ISA conditions, etc.) and validate the algorithm by comparing the results with readily-accessible published A380 data (e.g., nominal takeoff speed, nominal landing speed with minimal fuel, runway required for takeoff under ISA conditions, etc.). The 1-D governing equations of motion are derived from Newton's second law, and include several equations related to flight mechanics which are included in the baseline model [9]. First, specifications, properties, and published data (e.g., nominal takeoff distance assuming negligible airfield pressure altitude) for the A380 are collected from aircraft characteristics and maintenance data sheets [14, 26]. With the A380 specifications defined, required parameters such as, but not limited, the aspect ratio, ground effect factor, and the weight of the aircraft at zero fuel conditions are calculated and approximated with expressions related to flight mechanics and conservation of mass [9]. Next, the coefficient of lift and coefficient of drag are approximated with nominal, published takeoff and landing velocities [14]. Regarding the total coefficient of drag, the term includes both parasitic and induced drag components caused by the aircraft geometry (e.g., skin friction and pressure drag) and lift, respectively. Following the lift and drag coefficients, the total lifting force as well as the total drag force for both the takeoff and landing procedures are calculated. With 1-D equations of motion, as well as a baseline free body diagram, the effective force is calculated for both takeoff and landing profiles. Given the effective force and the mass of the aircraft, the acceleration, velocity, and position for both profiles are calculated at each timestep, dt, with a series of explicit Euler numerical methods [27]. Regarding initial conditions, a majority of the A380 is position aft of the displaced threshold (refer to Fig. 1.1 on pg. 7) where aircraft are allowed to taxi and takeoff, but not land [28]. Therefore, the departing A380 is assumed to have an initial position of 0 m, and starts at rest (i.e., negligible acceleration and velocity). In addition, the boundary condition for the 1-D baseline RTO model is the length of the runway since the goal is to prevent the A380 from overshooting the runway. The 1-D baseline RTO speed model is then validated with readily-accessible published data, and serves as a benchmark algorithm for environmental, engine failures, and hot and high models and analyses.

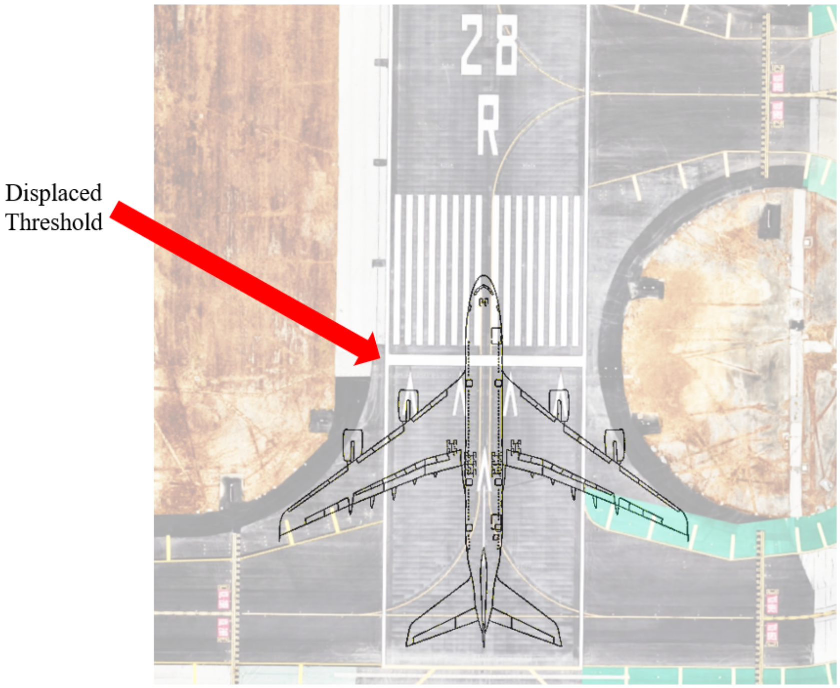

Figure 1.1: A380 aft of the displaced threshold at RWY 28R

Upon completion of the 1-D baseline RTO speed model, the second 1-D study for this master's project integrates varying and averaged environmental factors such as pure headwinds, pure tailwinds, and both dry and wet runway surface conditions which are common at San Francisco International Airport (KSFO). Realistic headwinds, tailwinds, and wind directions are obtained from readily-accessible 2022 METAR observations [29]. Since most METAR observations are issued hourly, the data is averaged and sorted with Python libraries and built-in functions (e.g., Python pivot tables within pandas library) to obtain realistic, averaged conditions at KSFO [29]. The pivot tables are then exported to CSV files for additional processing (e.g., chart creation). Once the data is processed with various computational tools, design variables and arrays for both wind conditions and varying runway surface conditions are included as inputs to the aforementioned 1-D baseline RTO model. To test every possible environmental combination in this 1-D environmental study, the 1-D baseline RTO model is retrofitted with a double loop and a series of surface plots are created. The surface plots will primarily focus on the RTO speed as well as the location of the RTO speed with varying environmental conditions. Given the surface plots, a 2-D sensitivity analysis is conducted to assess the largest impact on both the RTO speed as well as the location of the RTO speed. Similar to the 1-D baseline RTO model, the 1-D environmental study is validated with a pair of environmental conditions (e.g., a specific wind speed with a specific pair of runway surface coefficients) in conjunction with the 1-D RTO baseline model. Lastly, this 1-D environmental model serves as a benchmark to the 3-D environmental study, which includes more complex factors such as crosswinds and varying runway friction conditions dependent on ground speed and wheel sideslip angles.

The third 1-D study presented in this master's project analyzes the impact on the performance of an A380 in the event of multiple engine failures during the ground roll procedure. Moreover, the 1-D engine failure study illustrates the importance of the RTO process in the event of an emergency. A two engine out scenario is implemented to simulate a bird strike impacting the #1 and #2 engines. The 1-D engine failure analysis implements a built-in MATLAB function to initiate engine failures at random locations along the runway (e.g., engine failures before, at, and after the location of the RTO speed) during the takeoff procedure. In addition, deceleration plots are included to illustrate how quickly the A380 at MTOW can slow down, and if the aircraft can slow down prior to overshooting the runway. In addition, the 1-D engine failure study serves as a benchmark for complex 3-D engine failure analysis.

Chapter 2: Baseline RTO Speed

2.1 Free-body Diagrams

Considered the world's largest civilian passenger jet in history, the four-engine Airbus A380-800 at maximum takeoff weight (MTOW) is the commercial airliner selected for this study [26]. Furthermore, the airport and runway selected for this study are San Francisco International Airport (KSFO) and runway 10L/28R, respectively. Of the four runways at KSFO, 10L/28R is the longest and is the most appropriate option for an A380 at MTOW [30]. Moreover, the A380 is setup for a west departure based on average wind conditions obtained from METAR observations [29].

The primary objective of the present work is to analyze the effects of headwinds, tailwinds, and wet runway conditions on the RTO speed of an A380 with 1-D equations of motion. Prior to the implementation of environmental factors, a baseline model is constructed given readily accessible, published A380 data and specifications such as MTOW, wing geometry, and the height of the wingtip above the ground [14, 26]. Moreover, KSFO information such as runway length are included in the baseline model. The baseline case assumes negligible wind speeds and regular, dry runway conditions. In addition, the baseline model is validated with published, nominal A380 takeoff and landing data [14]. Given a proven model, realistic wind conditions obtained from METAR observations as well as approximated expressions for wet runway friction coefficients are implemented to assess environmental impacts on V_1 [16, 29].

The 1-D governing equation of motion used in the present work is Newton's second law as shown in Eq. (2.1) below. Moreover, the positive convention in the present work is in the same direction as the ground speed $\dot{x}$. The calculation of the RTO speed in this study is determined based on the intersection point between the takeoff and landing velocity profiles during the ground roll. Moreover, the velocity profiles are obtained by integrating the instantaneous acceleration $\ddot{x}\,(t)$ in Eq. (2.1), which is dependent on the effective forces.

$$\Sigma\vec{F}_{\text{net}} = m_{MTOW}\ddot{x}\,(t) \tag{2.1}$$

For the baseline study, the effective forces acting on the aircraft are thrust, drag, lift, weight, and friction resistance between the runway and the landing gear wheels as shown in Fig. 2.1 on pg. 10. Furthermore, the configuration and arrangement of the force vectors in the baseline takeoff FBD (refer to the top schematic in Fig. 2.1 on pg. 10]) agree with existing literature [9]. In the baseline landing FBD (refer to the bottom schematic in Fig. 2.1), reverse thrust is engaged to decelerate the A380 in the event of an RTO. Additionally, the lifting force in the baseline landing FBD is omitted because the spoilers along the wing are engaged. Furthermore, the smaller $\dot{x}$ vector in the baseline landing FBD indicates the aircraft is decelerating.

The FBD for the environmental factor study includes the same effective forces as the baseline study with the addition of a wind speed component, as shown in Fig. 2.2 on pg. 11. Moreover, headwinds as depicted in Fig. 2.2 increase the airspeed of an aircraft as well as the magnitude of the aerodynamic forces (e.g., lift and drag). On the other hand, tailwinds slow down the airflow over the wing which ultimately reduces the aerodynamic forces during the takeoff procedure.

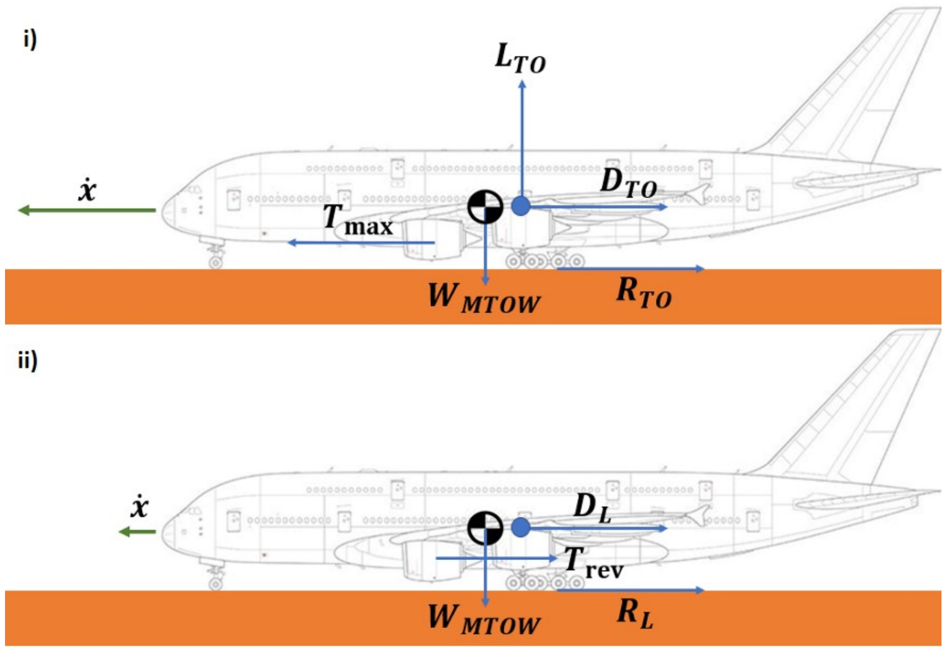

Figure 2.1: Baseline free body diagrams and effective forces acting on the aircraft

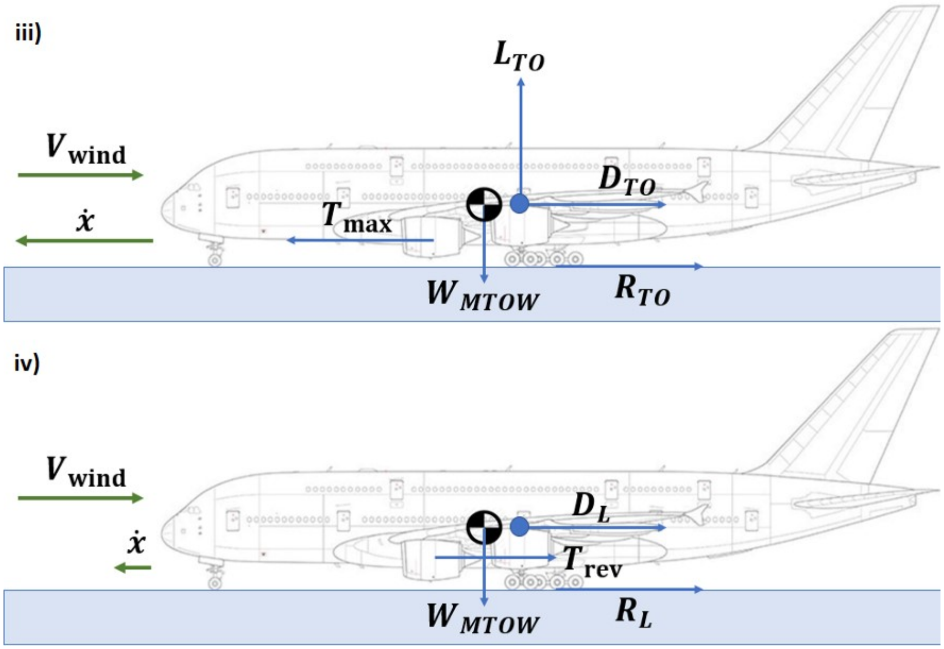

Figure 2.2: Environmental free body diagrams and effective forces acting on the aircraft

2.1.1 Assumptions

For simplification purposes, several assumptions are implemented in the 1-D baseline RTO speed model. Regarding San Francisco International Airport, the runway slope is omitted because the difference in elevation between the runway ends, RWY 28R (elevation circled in blue in Fig. 2.3 on pg. 12) and RWY 10L (elevation circled in red in Fig. 2.3 on pg. 12), is negligible compared to the overall runway length [30]. Furthermore, the runway surface conditions for RWY 28R are assumed to be paved, smooth, and dry for the nominal study. As a result, an averaged runway coefficient for a dry surface is easily obtainable from existing, published literature [9]. Moreover, the elevation of San Francisco International Airport is negligible, and thermodynamic properties (e.g., density and temperature) are evaluated at sea-level conditions [30].

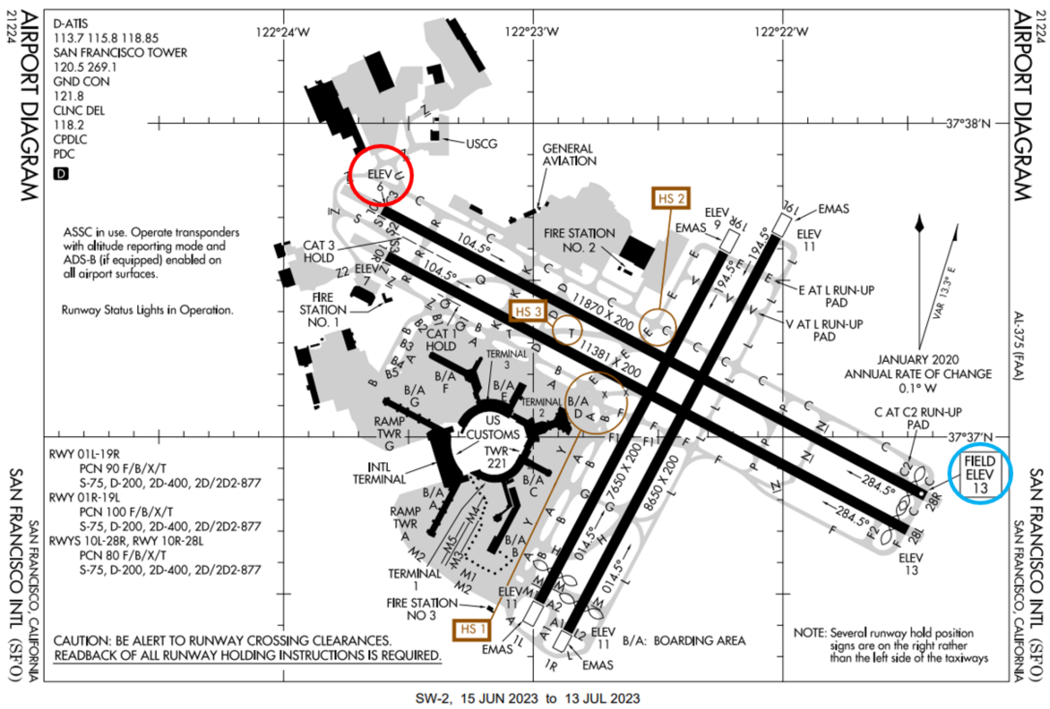

Figure 2.3: San Francisco International Airport diagram [30]

Regarding the aircraft, the weight is assumed to remain constant since the present work is focused specifically on the ground roll. During the takeoff procedure, the thrust force is directly in-line with the engines and the thrust inclination angle is negligible. With the spoilers engaged in the landing configuration, it is assumed all of the lift is disturbed based on the spoiler coverage along the wing [14]. Since the model specifically captures the ground roll, moments about the center of mass and the aerodynamic center are not considered in the analysis. Due to the limited information on the planform geometry, a span efficiency factor, e_1, of 0.90 is assumed. Moreover, the value selected for e_1 lies within an acceptable range for typical subsonic aircraft [9]. Regarding the effective force calculations, the lift generated by the fuselage and horizontal stabilizer is neglected. For the ground effect calculation, the A380 winglet design is neglected for simplification purposes. For the environmental factors described in the present work, the runway friction coefficients are averaged and remain constant throughout the ground roll and pure headwinds and tailwinds are assumed. Regarding applied thrust, it is assumed the brakes are engaged while the four turbofan engines spool up from idle conditions to maximum takeoff thrust conditions. This ensures the maximum acceleration at the beginning of the ground roll procedure, and ultimately shortens the runway length requirements [31]. In the case of crosswind conditions, the present work neglects the crosswind impact on the individual turbofan engines, which impacts the intake performance of the engines.

2.2 1-D Baseline Study and Model Development

Specifications and characteristics of the A380 are obtained from readily available fact sheets and maintenance manuals, and are presented in Table 2.1 below [14, 26]. The published landing velocity of the A380, $V_{L,\text{pub}}$, is the indicated airspeed with certified maximum flap setting and standard atmospheric conditions [14]. The published takeoff distance of the A380 $S_{TO,\text{pub}}$ used for this analysis assumes zero pressure altitude based on the airport elevation, International Standard Atmosphere (ISA) conditions, and negligible wind factors [14]. In addition, the published landing distance $S_{L,\text{pub}}$ is based on dry runway conditions as well as field elevation [14].

Table 2.1: Published data for Airbus A380-800 at sea-level [14, 26]

Parameter	Value	Units
b	79.75	m
S	845	m
AR	7.53	–
h	7.8	m
$V_{TO,\text{pub}}$	87.5	$^{\text{m}}/_{\text{s}^2}$
$V_{L,\text{pub}}$	71.0	$^{\text{m}}/_{\text{s}^2}$
$S_{TO,\text{pub}}$	3,000	m
$S_{L,\text{pub}}$	2,150	m
m_{MTOW}	575,000	kg
W_{MTOW}	5,638,800	N
W_f	2,490,700	N

Information related to KSFO is obtained from readily accessible published data, and is noted in Table 2.2 below[30]. Moreover, the density and the acceleration due to gravity are evaluated at sea-level since the airport elevation H_g is negligible compared to the radius of Earth [9].

Table 2.2: KSFO airport information [30]

Parameter	Value	Units
S_{28R}	3,618	m
H_g	4.10	m
ρ_0	1.225	$^{\text{kg}}/_{\text{m}^3}$
g_0	9.81	$^{\text{m}}/_{\text{s}^2}$

The aerodynamic properties for both the takeoff and landing configurations are calculated with published aircraft and airport data noted in Table 2.1 and Table 2.2. Moreover, the aerodynamic properties assume steady, level flight conditions where the weight of the aircraft is equivalent to the lifting force. The coefficient of lift for the takeoff procedure, $C_{L,TO}$, incorporates MTOW conditions as well as the A380 published takeoff speed as shown in Eq. (2.2) on the following page. Similarly, the coefficient of lift for the landing procedure,

$C_{L,L}$, incorporates the weight of the aircraft without fuel W_{ZFW} (refer to Eq. (2.3) below) and the published landing speed as shown in Eq. (2.4) below. Moreover, the flap settings for the takeoff and landing configurations are captured in $V_{TO,\text{pub}}$ and $V_{L,\text{pub}}$, respectively. Recall, the lifting force in the landing configuration is negligible due to the deployment of spoilers.

$$C_{L,TO} = \frac{W_{MTOW}}{\frac{1}{2}\rho_0 V_{TO,\text{pub}}^2 S_w} \tag{2.2}$$

$$W_{ZFW} = W_{MTOW} - W_f \tag{2.3}$$

$$C_{L,L} = \frac{W_{ZFW}}{\frac{1}{2}\rho_0 V_{L,\text{pub}}^2 S_w} \tag{2.4}$$

Since the present work is focused specifically on the ground roll, the approximated ground effect factor, ϕ, is obtained with Eq. (2.5) [9]. The approximated ground effect factor is included in the analysis to diminish the strength of the wing-tip vortices due to the interaction with the runway surface [9]. Moreover, the disturbance of the wing-tip vortices ultimately reduces the induced drag and the overall drag penalty. The approximated downwash for this study was calculated to be $\phi = 0.71$.

$$\phi = \frac{\left(\frac{16h}{b}\right)^2}{1 + \left(\frac{16h}{b}\right)^2} \tag{2.5}$$

The total drag coefficient for the takeoff configuration, $C_{D,TO}$, includes both the parasitic and induced drag components and is obtained with Eq. (2.6). Moreover, a span efficiency factor of $e_1 = 0.90$ is selected for this study since the value lies halfway between the acceptable range for typical subsonic aircraft [9]. In addition, the induced drag component of Eq. (2.6) is reduced by ϕ since it is less than unity. The total drag coefficient for the landing configuration $C_{D,L}$ only includes the parasitic drag component as shown in Eq. (2.7) since the spoilers are engaged and all of the lift over the wing is disturbed. Moreover, the parasitic drag components for Eq. (2.6) and Eq. (2.7) were approximated with Breguet's equations [9]. All of the required dimensionless aerodynamic properties for the present work are included in Table 2.3 on pg. 15.

$$C_{D,TO} = C_{D_0,TO} + \phi \frac{C_{L,TO}^2}{\pi e_1 AR} \tag{2.6}$$

$$C_{D,L} = C_{D_0,L} \tag{2.7}$$

The forces acting on the aircraft for the takeoff and landing baseline case are obtained from the FBD (refer to Fig. 2.1 on pg. 10). Given $C_{L,TO}$ and $C_{L,L}$, the lifting forces for the takeoff and landing configurations are obtained with Eq. (2.8) and Eq. (2.9), respectively. Similarly, given $C_{D,TO}$ and $C_{D,L}$, the drag forces for the takeoff and landing configurations are obtained with Eq. (2.10) and Eq. (2.11), respectively. For the present work, the maximum takeoff thrust is set to $T_{\max} = 979,968$ N and the reverse thrust T_{rev} is approximated at

Table 2.3: Approximated Airbus A380-800 aerodynamic properties

Parameter	Value
$C_{L,TO}$	1.4245
$C_{L,L}$	1.2069
$C_{D_0,TO}$	0.0130
$C_{D_0,L}$	0.0143

15% of $T_{\max}$. Regarding the baseline runway conditions, the dimensionless runway friction coefficients are defined as $\mu_{\mathrm{r,TO}} = 0.02$ and $\mu_{\mathrm{r,L}} = 0.065$ based on a smooth, paved surface [9]. In addition, $\mu_{\mathrm{r,L}} > \mu_{\mathrm{r,TO}}$ since brakes are engaged during the landing procedure. With all of the baseline forces defined, the instantaneous effective forces for the takeoff and landing configurations are obtained with Eq. (2.12) and Eq. (2.13), respectively.

$$L_{TO} = C_{L,TO}\frac{1}{2}\ \rho_0 V^2 S_w \tag{2.8}$$

$$L_L = C_{L,L}\frac{1}{2}\ \rho_0 V^2 S_w \tag{2.9}$$

$$D_{TO} = C_{D,TO}\frac{1}{2}\rho_0 V^2 S_w \tag{2.10}$$

$$D_L = C_{D,L}\frac{1}{2}\rho_0 V^2 S_w \tag{2.11}$$

$$F_{\mathrm{eff},TO} = T_{\max} - \left[D_{TO} + \mu_{\mathrm{r,TO}}\left(W_{MTOW} - L_{TO}\right)\right] \tag{2.12}$$

$$F_{\mathrm{eff},L} = -T_{\mathrm{rev}} - \left[D_L + \mu_{\mathrm{r,L}} W_{MTOW}\right] \tag{2.13}$$

Since the analysis described in the present work is purely centered around the ground roll procedure, the baseline lift and drag forces are determined for both takeoff and landing configurations to ensure the A380 does not lift-off. As shown in Fig. 2.4 on pg. 16, the lifting force L_{TO} does not exceed W_{MTOW} prior to the nominal takeoff speed $V_{TO,\mathrm{pub}}$ (refer to Table 2.1 on pg. 13) and therefore the aforementioned ground roll condition is satisfied. Recall, the lifting force in the landing configuration L_L is negligible due to the deployment of spoilers, and D_L is noticeably smaller than D_{TO} for airspeeds greater than approximately 40 $\frac{m}{s}$ due to absence of induced drag. For robustness, a maximum function is implemented in the algorithm to ensure the lifting force does not exceed W_{MTOW}.

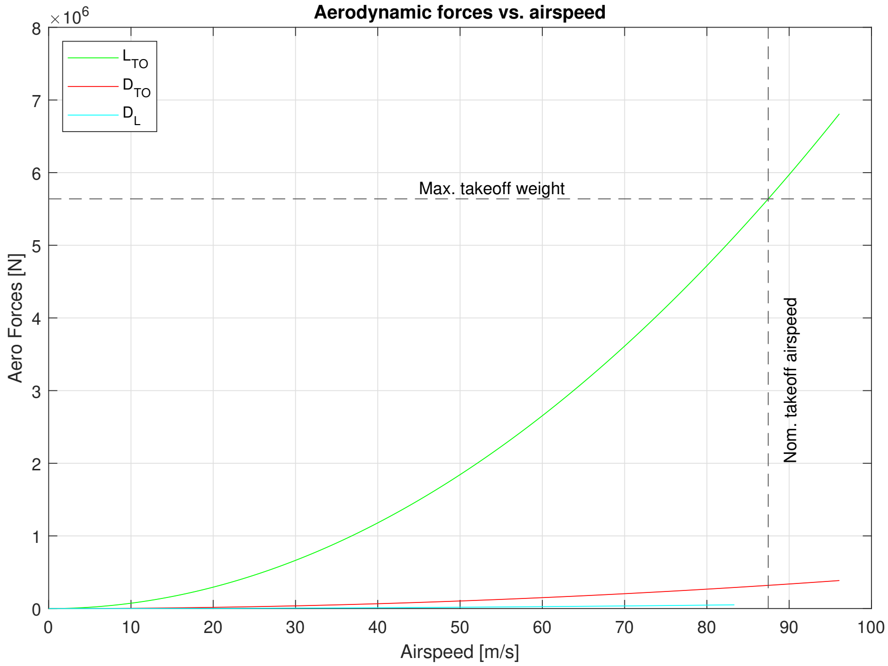

Figure 2.4: Baseline aerodynamic forces on the A380

Since the effective forces change with time, the instantaneous acceleration $\ddot{x}(t)$ is obtained with Eq. (2.14), a manipulated expression of the original 1-D equation of motion described by Eq. (2.1) on pg. 9. Given $\ddot{x}(t)$, the instantaneous ground speed $\dot{x}(t)$ is numerically approximated with the explicit Euler method as shown in Eq. (2.15), with a timestep of $dt = 0.1\ s$ [27]. Since wind conditions are neglected in the baseline study, the instantaneous ground speed is equivalent to the airspeed. Given $\dot{x}(t)$, the instantaneous position $x(t)$ is approximated with the same explicit Euler method as shown in Eq. (2.16). Regarding initial conditions, the aircraft is initially at rest and all of the parameters (e.g., ground speed, lifting force, etc.) are initialized to zero. The boundary condition used in the present work is the length of the runway $S_{28\mathrm{R}}$. For visualization purposes, a mapping between the fundamental equations and the explicit Euler methods is presented in Fig. 2.5 on pg. 17.

$$\ddot{x}(t) = \frac{g_0}{W_{MTOW}} F_{\mathrm{eff}} \tag{2.14}$$

$$\dot{x}(t) = \dot{x}(t - dt) + \ddot{x}(t - dt)\,dt \tag{2.15}$$

$$x(t) = x(t - dt) + \dot{x}(t - dt)\,dt \tag{2.16}$$

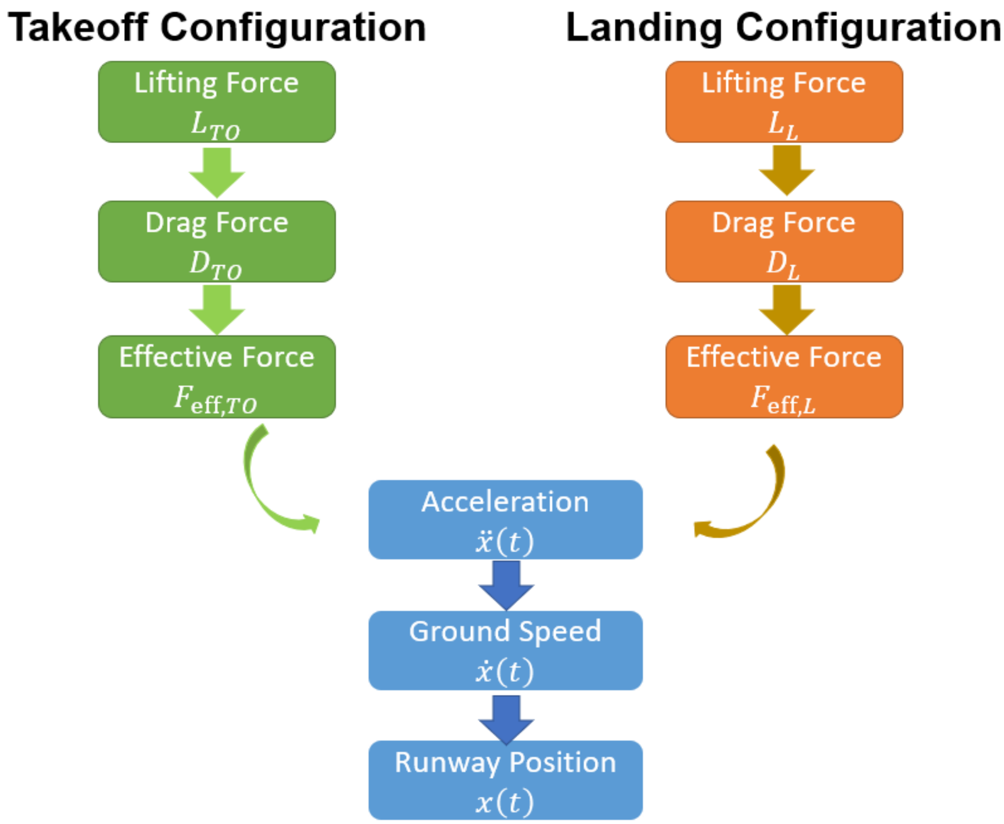

Figure 2.5: Baseline mapping for numerical schemes

Given the readily available published data in Tables 2.1 and 2.2 on pg. 13, approximated aerodynamic properties presented in Table 2.3 on pg. 15, and expressions for the ground roll procedure defined by Eqs.(2.2) through (2.14), the baseline RTO speed model is constructed and presented in Fig. 2.6 on pg. 18. The numerical schemes defined by Eqs. (2.14) through (2.16) are implemented to obtain three velocity profiles: one for the takeoff configuration, one for the landing configuration which considers MTOW conditions, and another landing configuration which considers zero fuel (ZFW) conditions. For verification and validation purposes, the takeoff profile as well as the landing profile with ZFW conditions are computed and compared with published takeoff and landing information. Once validated, the 1-D baseline RTO of the A380 is determined with the takeoff profile as well as the landing profile with MTOW conditions, as shown in Fig. 2.6 on pg. 18.

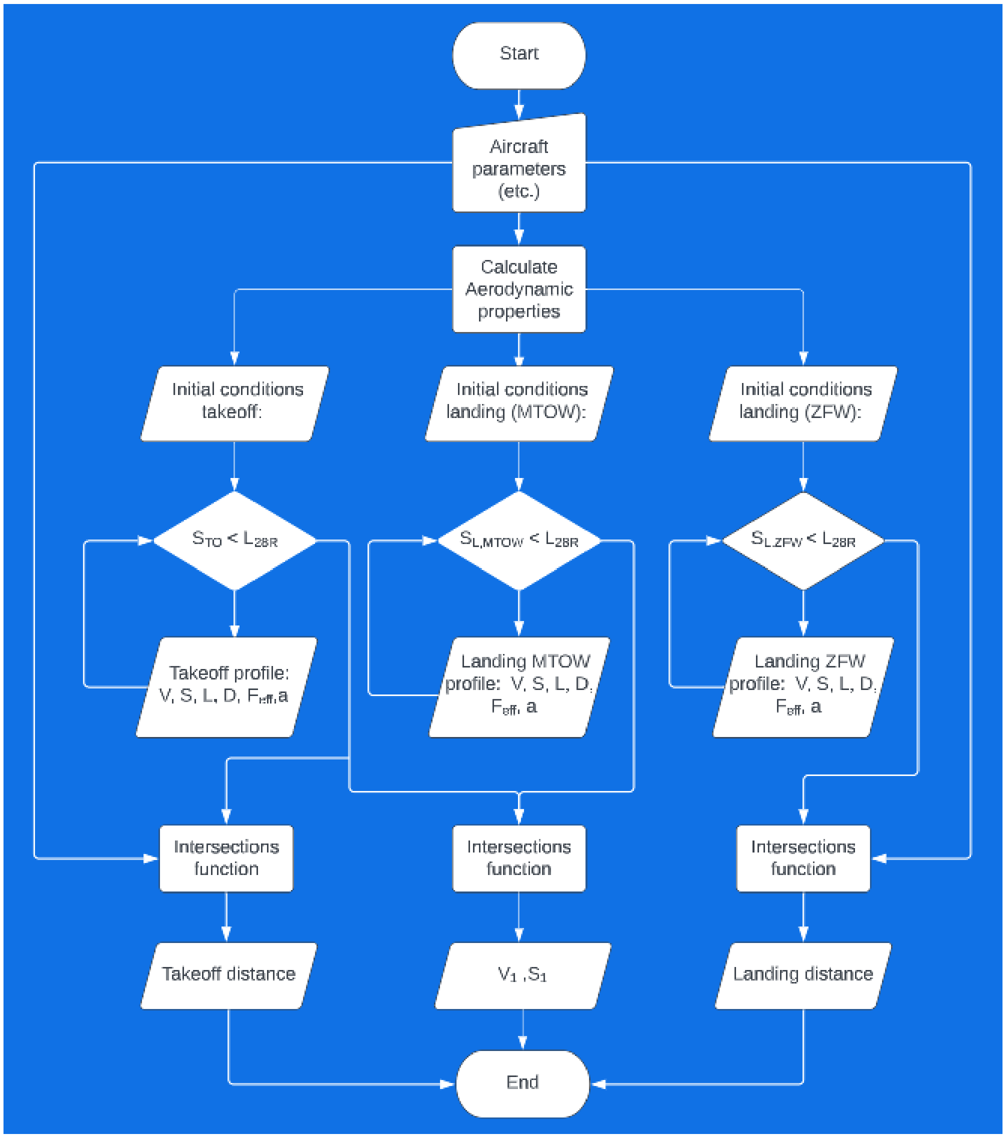

Figure 2.6: Baseline RTO speed flowchart

The intersection point between the takeoff and landing velocity profiles is determined with the intersections function, and the RTO speed is numerically approximated to be $V_1 = 63.9\ ^m/_s$ with the algorithm presented in Fig. 2.6 [32, 33]. To validate the baseline model, the nominal takeoff distance $S_{TO,\text{pub}}$, as well as the nominal landing distance $S_{L,\text{pub}}$ are numerically approximated by the baseline model. Compared to the published A380 data (refer to Table 2.1 on pg. 9), $S_{TO,\text{pub}}$ and $S_{L,\text{pub}}$ obtained from the numerical scheme (refer to Fig. 2.7 on the following page) have percent differences of -3.63% and 0.2%, respectively. Given the results in Fig. 2.7, the numerical scheme described in this section is deemed valid and is used to assess the impact of environmental factors on the RTO speed of an A380 at MTOW.

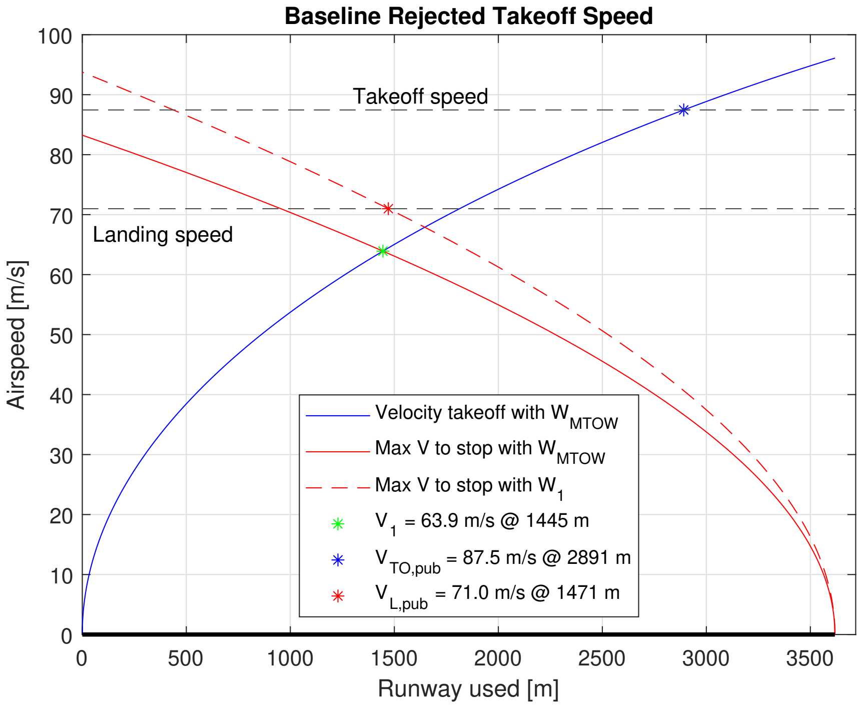

Figure 2.7: Baseline RTO speed of an Airbus A380

Chapter 3: 1-D Environmental RTO Speed

3.1 1-D Environmental Model and Sensitivity Analysis

With the proven 1-D baseline RTO speed model presented in the previous chapter, environmental factors such as varying wind speed and unfavorable runway conditions are included to assess realistic impacts on the RTO speed as well as the location of the RTO speed along the runway. Regarding wind conditions, pure headwinds and tailwinds are included in the 1-D environmental model to capture both favorable and unfavorable wind conditions, respectively. Regarding surface conditions, the two runway classes selected for the 1-D environmental study are dry and wet surfaces. For simplicity purposes, the dry runway conditions used in the environmental study are the same nominal conditions referenced in the baseline study presented in Chapter 2. Moreover, for wet runway conditions it is assumed that the depth of standing water along the runway is less than 3-mm, and the runway friction coefficients for a wet surface are approximated with previous studies available in literature [16].

3.2 Environmental Inputs

Realistic headwind and tailwind conditions were obtained from 2022 KSFO METAR observations, which were made weekly for one year, via the ASOS network available through Iowa Environmental Mesonet (IEM) [29]. The maximum headwind and tailwind conditions were approximately 16.5-kts and 3.3-kts, respectively (refer to Table 3.1 on pg. 21) [29]. Moreover, a factor of safety (FoS) of 1.50 is included to account for stronger, unforeseen wind conditions. Once converted to the appropriate units, the design wind speed array used in the 1-D environmental RTO speed model was $-2.55\ {}^{m}\!/\!{}_{s} \leq V_{\text{wind}} \leq 12.70\ {}^{m}\!/\!{}_{s}$. In the 1-D baseline RTO speed model, the ground speed was equivalent to the airspeed due to negligible wind conditions. In addition, the wind speed ultimately impacts the aerodynamic forces described in Eqs. (2.8) through (2.11), and the new airspeed is obtained with Eq. (3.1) below. Headwinds are added to the ground speed $\dot{x}$ due to the increase in aerodynamic performance during the ground roll, whereas tailwinds are subtracted from $\dot{x}\,(t)$ and ultimately reduce the lift due to a smaller value of V [18].

$$V = \dot{x}\,(t) \pm V_{\text{wind}} \tag{3.1}$$

Regarding the dry runway surface conditions, the dimensionless runway friction coefficient values for the takeoff and landing configuration are $\mu_{\text{r,TO}} = 0.02$ and $\mu_{\text{r,L}} = 0.065$,

Table 3.1: KSFO weekly wind conditions from 2022 METAR Observations [29]

Week no.	Avg. wind speed (kts)	Avg. wind direction
21	16.45	281.16°
18	15.49	266.59°
25	14.82	283.35°
20	14.68	281.09°
27	13.44	278.32°
16	13.23	253.81°
30	12.77	302.39°
01	4.79	168.18°
04	4.63	128.67°
07	3.90	130.94°
48	3.63	134.22°
52	3.46	077.63°
05	3.30	121.89°
03	2.88	084.41°

which are identical to the 1-D baseline RTO speed study. Based on acceptable runway surface expressions for the landing configuration, the friction coefficient for the wet runway is approximated to be $\mu_{\mathrm{r_{wet}},\mathrm{L}} = 0.5\mu_{\mathrm{r,L}}$ [16]. Moreover, the present work assumes the same factor is applied to the takeoff configuration, and $\mu_{\mathrm{r_{wet}},\mathrm{TO}} = 0.5\mu_{\mathrm{r,TO}}$. As a result, the design runway friction coefficient arrays for the takeoff and landing configurations are $0.01 \leq \mu_{\mathrm{r,TO}} \leq 0.02$ and $0.033 \leq \mu_{\mathrm{r,L}} \leq 0.065$, respectively.

3.3 Sensitivity Analysis

The design arrays for the constant wind speed and the varying runway surface conditions described in the previous section are the two independent variables used in the 2-D sensitivity analysis. Moreover, the 2-D sensitivity analysis described in this section satisfies one of the project objectives and determines how varying headwinds, tailwinds, and runway surface conditions impact the RTO speed of the A380 in a 1-D coordinate system. Given a proven model, the 1-D environmental model is integrated with the 1-D baseline RTO speed model presented in the previous chapter. Furthermore, the environmental model calculated the RTO speed for every condition within the design wind speed array, given a pair of runway friction coefficients for the takeoff and landing configurations (e.g., tailwind with a wet runway, headwind with a wet runway, etc.) with a double for loop (refer to the flowchart of the 1-D environmental RTO speed model in Fig. 3.1 on pg. 22).

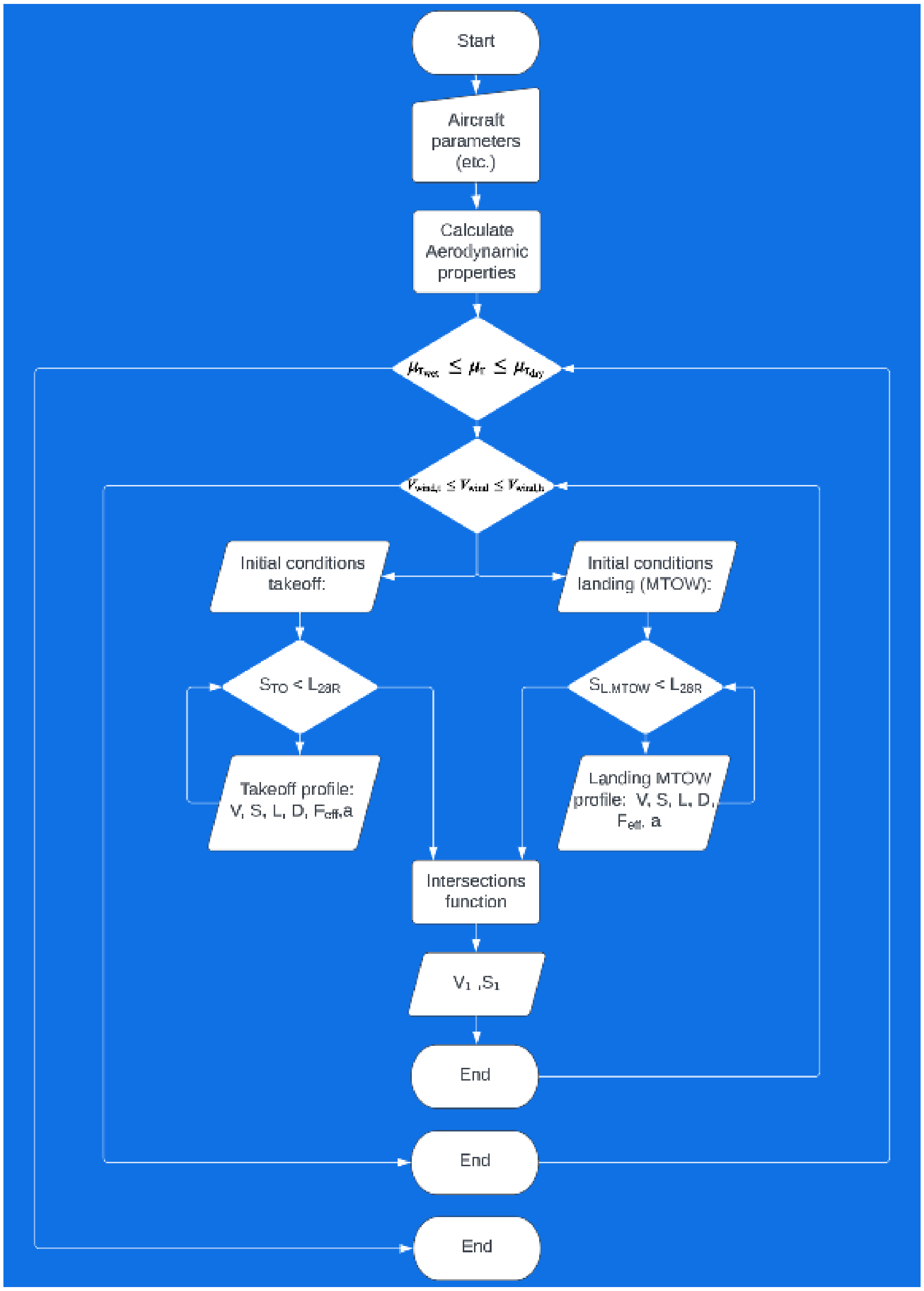

Figure 3.1: Environmental RTO speed flowchart

The RTO speed of an A380 under various environmental conditions is presented in Fig. 3.2 on pg. 23. The independent variables had different impacts on V_1, as well as the location of the RTO speed S_1, for an A380 at MTOW. For example, V_1 increased parabolically as the runway friction coefficient increased. Moreover, the parabolic trend is expected because the runway friction coefficient is impacted by the lifting force, which depends on the square of the airspeed (refer to Eq. (2.12) and Eq. (2.13) on pg. 15). Additionally, if the wind speed was held constant, V_1 evaluated under dry runway surface conditions increased by approximately 12.0% when compared to wet runway conditions. Of the independent variables, the wind speed had the largest impact on V_1 (refer to Fig. 3.2 below). With the strongest tailwind and headwind considered, V_1 increased by approximately 20.4% when the runway surface conditions were held constant. Moreover, the linear trend is expected because V_{wind} is added or subtracted from the ground speed (refer to Eq. (3.1)) on pg. 20) based on the wind conditions.

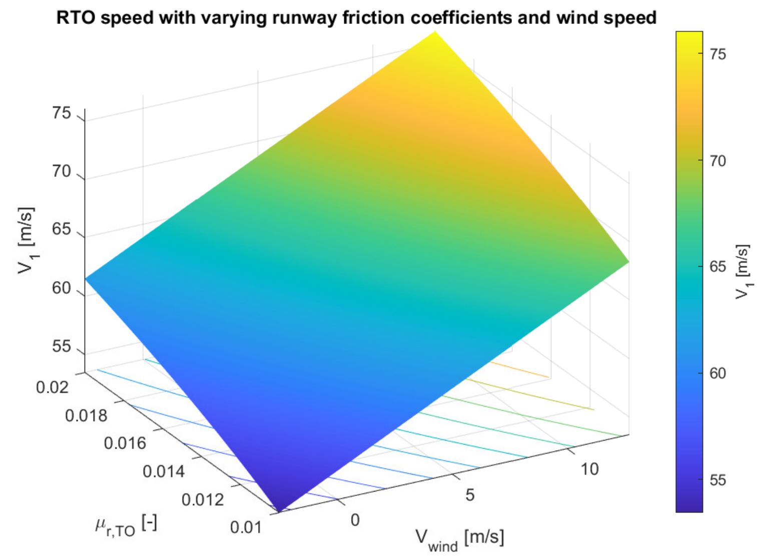

Figure 3.2: Rejected takeoff speed with varying environmental conditions

In addition to the RTO speed, the location of the RTO speed S_1 is numerically approximated and is shown in Fig. 3.3 on pg. 24. Regarding S_1, the runway surface conditions have a significant impact compared to the wind speed. Assuming constant wind conditions, S_1 evaluated under dry runway conditions increased by approximately 40% when compared to wet surface conditions. On the other hand, the varying wind speed had little effect on S_1. For example, S_1 increased approximately 3.1% when the maximum tailwind and headwind conditions were considered.

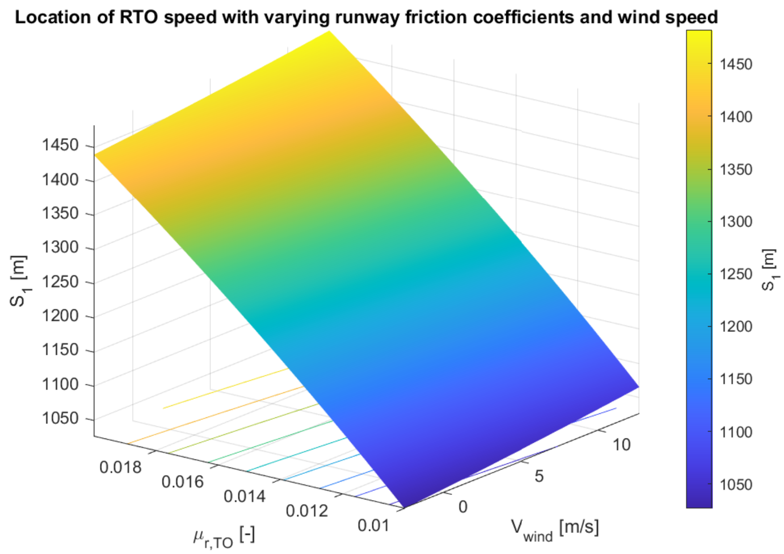

Figure 3.3: Location of rejected takeoff speed with varying environmental conditions

The relationships and observations between V_1 and S_1 and varying environmental conditions are further illustrated when considering the minimum and maximum wind speed and runway surface conditions. As shown in Fig. 3.4 on pg. 24, the location of the RTO speed did not change significantly with varying wind speeds, assuming the runway friction coefficient remained constant. However, the RTO speed was significantly impacted by varying wind speeds assuming the runway friction coefficient remained constant. The results provided in this section further illustrate the importance of considering various environmental conditions to accurately assess the impact on both the RTO speed and the location of the RTO speed of commercial airliners.

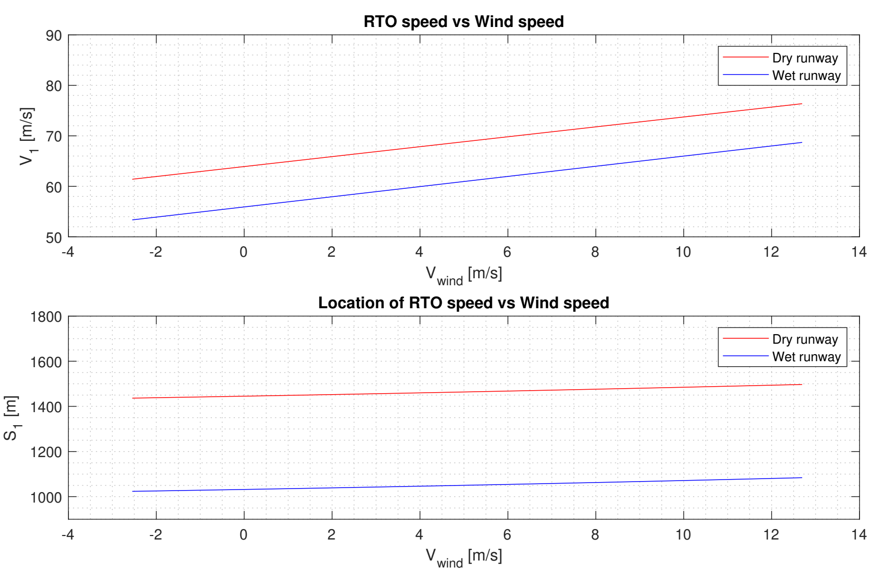

Figure 3.4: Constant runway friction coefficient with varying wind speeds

3.4 Validation of 1-D Environmental Model

For verification purposes, the landing distance with respect to V_1 is numerically approximated and presented in Fig. 3.5 on pg. 25. Because V_1 is the intersection point between the takeoff velocity profile and the landing velocity profile, the sum of the takeoff and landing distances with respect to V_1 is expected to be equal to the length of runway, $S_{28\mathrm{R}}$. The random environmental inputs selected for verification are presented in Table 3.2 below. Regarding the takeoff and landing velocity profiles with respect to V_1, the length of runway used was numerically calculated to be 1,326.21 m and 2,291.79 m, respectively. Moreover, the landing and takeoff distances with respect to V_1 for the validation case are presented in Fig. 3.5 and Fig. 3.6, respectively. Furthermore, the sum of the takeoff and landing distances with respect to V_1 was equal to $S_{28\mathrm{R}}$, which agrees with the RTO concept and definition.

Table 3.2: Environmental model verification inputs

Parameter	Value	Units
$\mu_{\mathrm{r,TO}}$	0.0163	–
$\mu_{\mathrm{r,L}}$	0.0547	–
V_{wind}	5.486	$^{\mathrm{m}}/_{\mathrm{s}}$

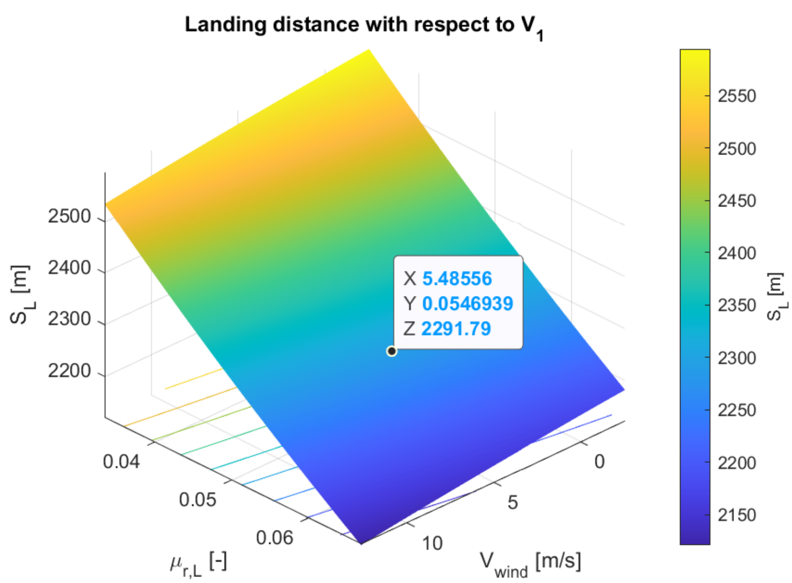

Figure 3.5: Landing distance with respect to the RTO speed

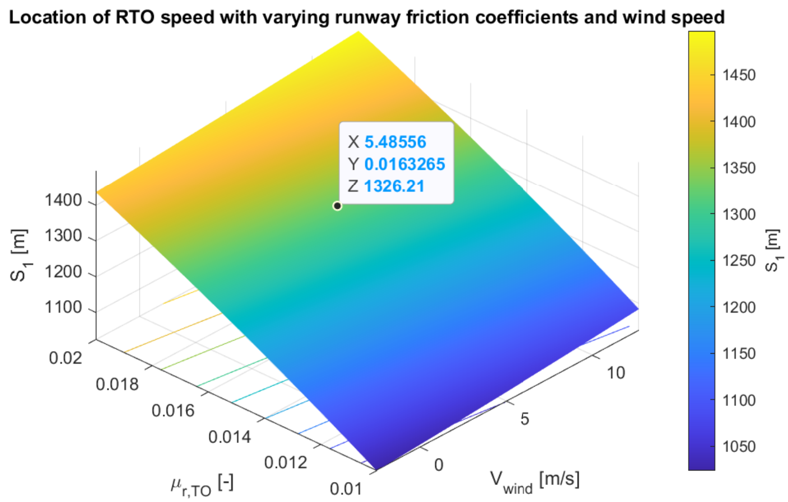

Figure 3.6: Takeoff distance with respect to the RTO speed

Chapter 4: 1-D Off Normal Conditions

This chapter explores off normal conditions with the aforementioned 1-D scheme and looks into engine failure as well as performance limitations in hot environments and higher altitude airfields. The A380 is equipped with four Engine Alliance GP 7200 or Rolls Royce Trent 900 turbofan engines, which are susceptible to failure in the event of a bird strike. Regarding the 1-D engine failure analysis, it is assumed a flock of large birds flying orthogonal to the runway impact the #1 and #2 engines, as shown in Fig. 4.1. Moreover, the impact results in a two engine out scenario. The airports selected for the 1-D hot and high analysis are Denver International Airport and Quito/Mariscal Sucre International Airport based on historical weather data and geographical location.

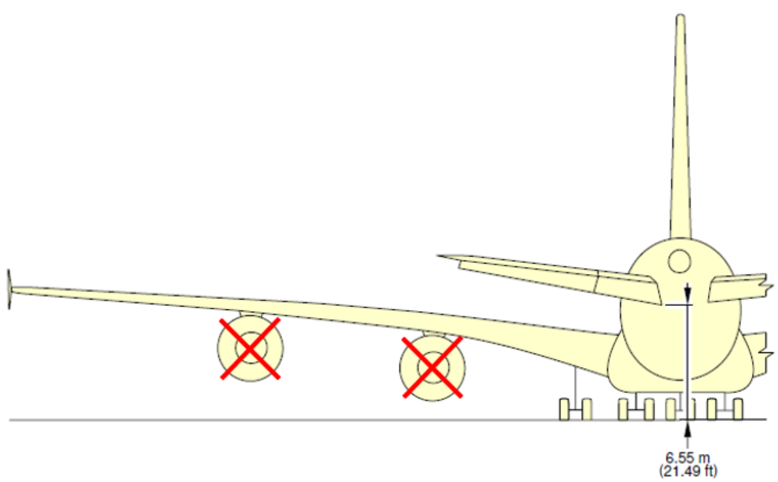

Figure 4.1: 1-D bird strike resulting in two engines out [14]

4.1 Engine failure

With the #1 and #2 engines out due to the bird strike, the takeoff thrust T_{TO} is half of the maximum takeoff thrust $T_{\max}$ noted in Chapter 2, or approximately $490,000$ N Moreover, the 1-D bird strike during the ground roll procedure considers three instances: the strike before, at, and after V_1. If the bird strike occurs at the location of V_1, the A380 will have just enough velocity to lift-off before reaching the end of the runway at KSFO as depicted in Fig. 4.2 on pg. 28.

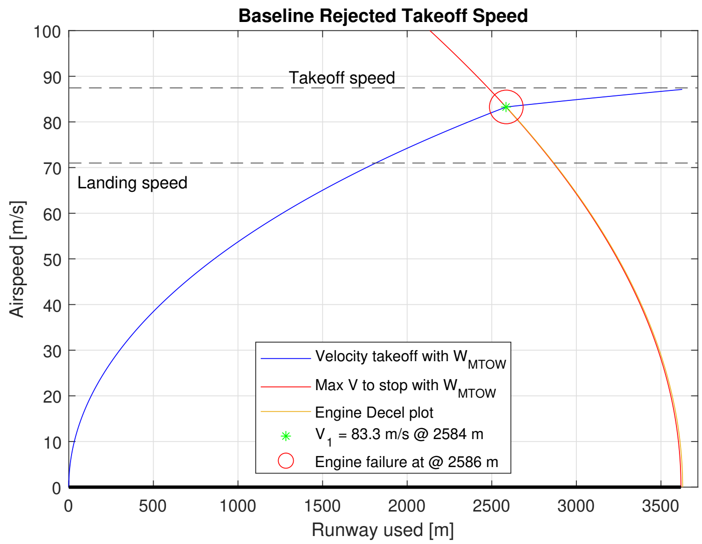

Figure 4.2: Two engines out at the RTO speed

The remaining two scenarios are highlighted in Fig. 4.3 on pg. 28. In the event the bird strike occurs before the location of V_1, the A380 will not have enough speed to lift-off before reaching the end of the runway, as shown in Fig. 4.3(a) on pg. 28. As a result, the flight crew has adequate time to reject the takeoff as the yellow deceleration profile is before the solid red landing profile in Fig. 4.3(a). If the bird strike occurs after the location of V_1, the flight crew must proceed with the takeoff since the aircraft has exceeded the deceleration curve as shown in Fig. 4.3(b) on pg. 28. Moreover, the A380 has adequate velocity to takeoff before reaching the end of the runway, per Fig. 4.3(b). In the event an RTO is attempted in the last scenario, a longitudinal runway excursion is certainly imminent as the A380 has insufficient runway to slow down in time. It is important to note the engine out analysis presented in this master's project does not account for pilot reaction delays, hence the immediate yellow deceleration profiles presented in Fig. 4.2 and Fig. 4.3.

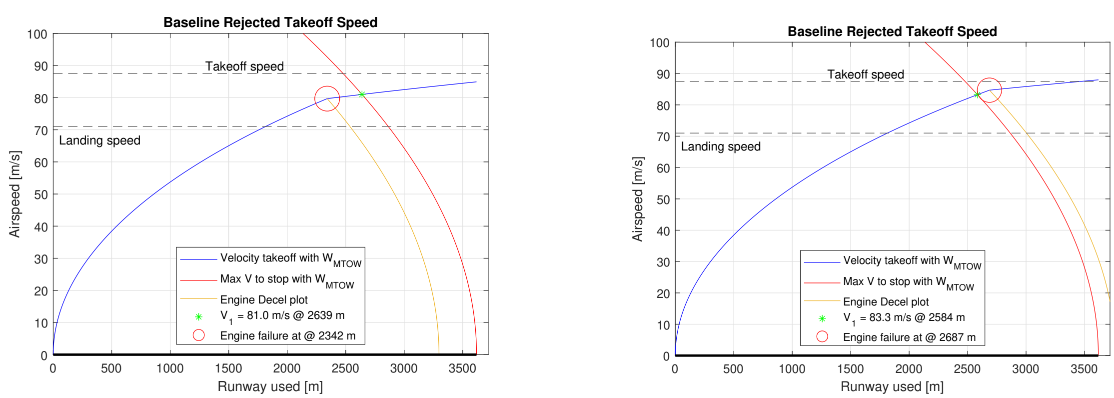

(a) Two engines out prior to the RTO speed

(b) Two engines out after the RTO speed

Figure 4.3: Two engines out before and after RTO speed

4.2 Higher Airfields

In addition to wind and unfavorable runway conditions, other environmental factors such as temperature and airport elevation can significantly impact the performance of various commercial airliners - especially an A380 at MTOW [24]. In addition, the amount of thrust generated by the turbofan engines is hindered by the ambient conditions in hot and high environments, as described by Eq. (4.3) where ρ_∞ is the density at the airport.

To capture realistic conditions, historical altimeter readings and temperature values are obtained from readily-accessible 2022 METAR observations. For Denver, a linear trend line was applied to the daily averaged altimeter readings as shown in Fig. 4.4 on pg. 29. Based on the results for KDEN, an altimeter reading of approximately 29.98 in Hg is collected as an input to the hot and high model. Moreover, the altimeter reading will have a significant impact on the air density, and more importantly the performance of the aircraft.

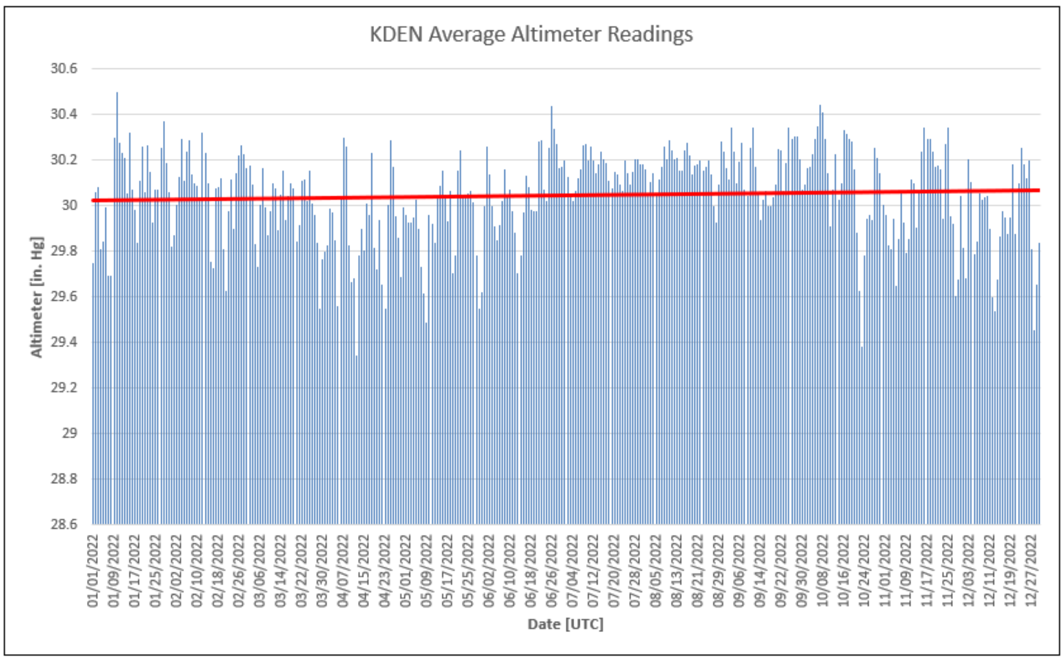

Figure 4.4: Average altimeter readings at KDEN

Similar analysis is conducted with the daily averaged ambient temperature at KDEN. Unlike the altimeter reading, the trend line for the ambient temperature is more parabolic, which is in-line with the seasons (refer to Fig. 4.5 on pg. 30). Since temperature has a significant impact on the ambient air density, a FoS of 1.75 was included. Considering the average ambient temperature at KDEN was approximately 21-degrees Celsius, the ambient temperature selected as input was approximately 37.2-degrees Celsius.

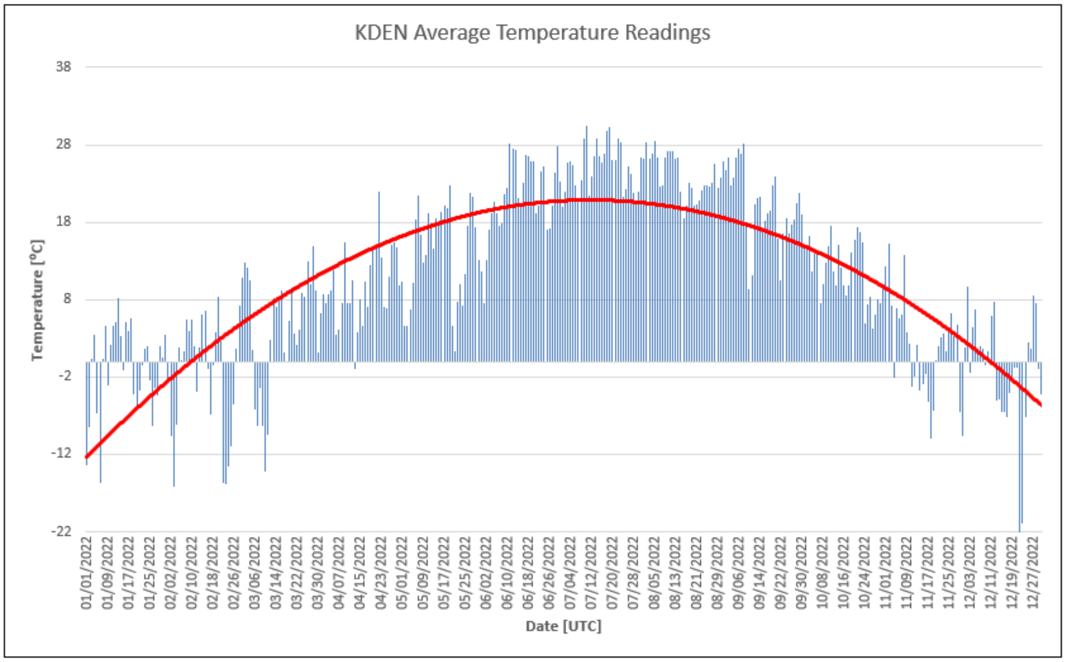

Figure 4.5: Average temperature conditions at KDEN

In this analysis, both Denver International Airport and Quito/Mariscal Sucre International Airport (SEQM) are selected based on historical weather data and geographical location. Moreover, the same analysis presented in Fig. 4.4 and Fig. 4.5 was applied to SEQM. Similar to the 2-D environmental study presented in Chapter 3, airport information is gathered from historical METAR observations as presented in Table 4.1 on pg. 30 [29].

Table 4.1: Hot and high airport conditions [29]

Parameter	KDEN	SEQM
RWY elevation, H_g (m)	1621.84	2370.13
RWY length (m)	4,876.8	4,098.0
Temperature °C	37.2	27.0
Altimeter (in Hg)	29.98	30.15
Density, ρ_∞ ($^{\text{kg}}/_{\text{m}^3}$)	0.9557	0.9071

To calculate the pressure at altitude P_∞, the altimeter readings from Table 4.1 are converted to actual pressure values with Eq. (4.1) given a proven pressure factor [34]. Once P_∞ is converted to Pascals, and the temperature values are converted to absolute conditions, the density at altitude ρ_∞ is calculated with the ideal gas law described by Eq. (4.2). Moreover, the density values for both airports are presented in Table 4.1. As noted in the literature review, a smaller ambient air density has a significant impact on aircraft performance, especially thrust, as shown in Eq. (4.3) [9].

$$P_\infty = \left(\text{altimeter} - \frac{0.91}{1000\text{ft}}\right) * H_g \tag{4.1}$$

$$\rho_\infty = \frac{P_\infty}{R_{\text{air}} T_K} \tag{4.2}$$

$$T_\infty = \frac{\rho_\infty}{\rho_0} T_{\max} \tag{4.3}$$

The performance of the A380 at both airports is depicted in Fig. 4.6 on pg. 31. If the A380 at MTOW departs Denver International Airport under the environmental conditions described in Table 4.1, the aircraft has enough velocity to takeoff. This is mainly possible due to the long runways at Denver International Airport, which provides commercial airliners with more space to roll during the takeoff procedure [24]. At Quito airport, the A380 has insufficient velocity and will not be able to takeoff under the conditions presented in Table 4.1. In order to takeoff, the weight of the A380 must be reduced by removing fuel, passengers, or cargo.

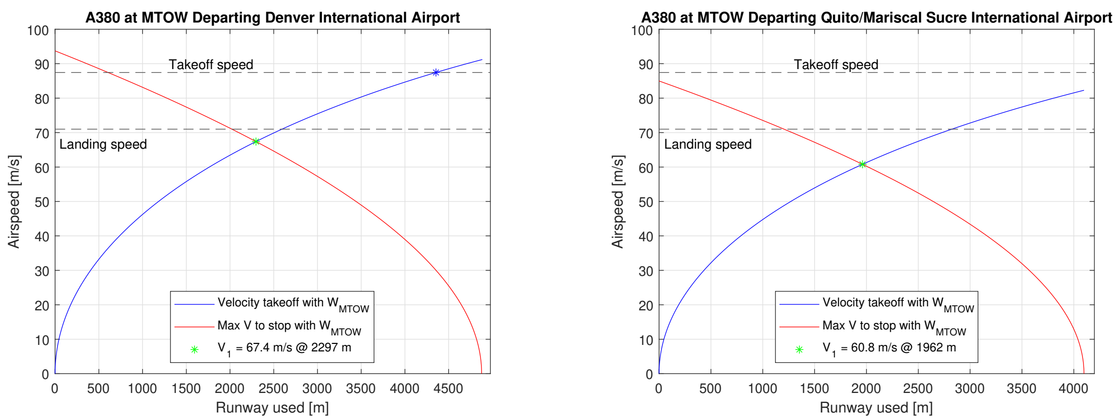

(a) Denver airport velocity profiles

(b) Quito airport velocity profiles

Figure 4.6: A380 departing hot and high conditions

Chapter 5: 3-D Crosswind Conditions

5.1 Realistic Wind Conditions at KSFO

In Chapter 3, pure headwind and tailwind conditions were assumed and integrated into the environmental model. While these conditions were considered for the 1-D environmental model, crosswind conditions are more likely to occur in reality. As a result, realistic wind conditions are obtained from readily-accessible historical METAR observations [29] to assess the overall impact of an A380 departing under crosswind conditions. Since METAR observations are typically released every hour, the average wind speed as well as the average wind direction were determined by taking a daily average. First, the average wind speed was obtained and plotted for the entire 2022 year. The red parabolic trend line indicates an increase in average wind speed in the spring and summer months, and a decrease in average wind speed in the fall and winter months, with the peak average wind speed occurring in April (refer to Fig. 5.1 on pg. 32).

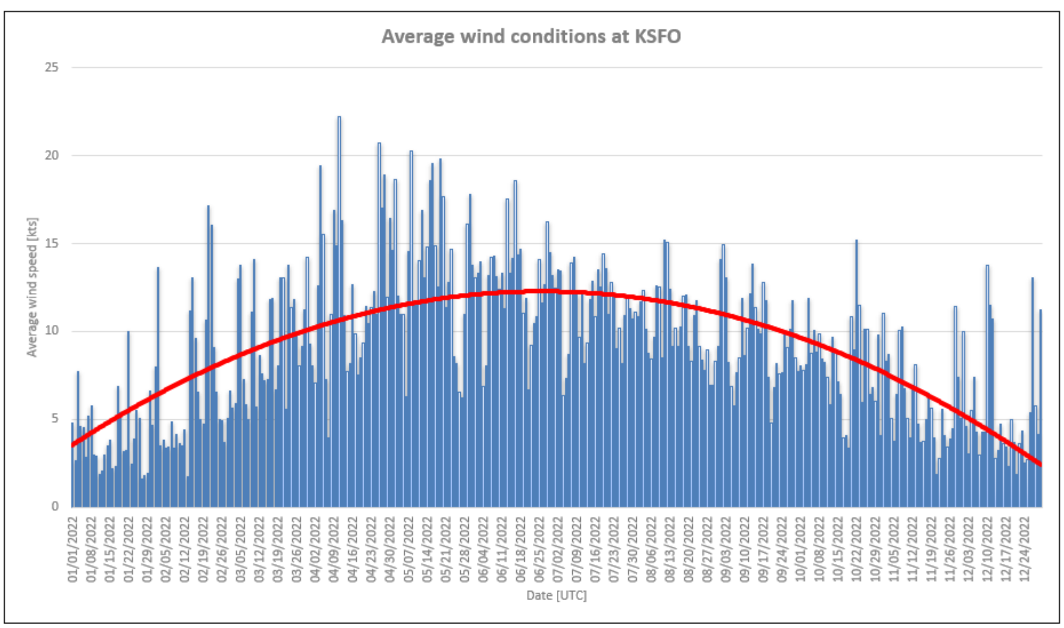

Figure 5.1: Average wind speed conditions at KSFO

In addition to the average wind speed, the average wind direction is analyzed and plotted with readily accessible METAR data [29]. Similar to the average wind speed, a trend line is included to analyze findings. The average wind direction is predominately out of the west and southwest in the spring and summer months, and out of the south and east in the fall and winter months, as illustrated by the red trend line (refer to Fig. 5.2 on pg. 33). The black horizontal line on Fig. 5.2 indicates the magnetic heading of RWY 28R at KSFO [30]. Per Fig. 5.2, the average wind direction rarely coincides with the magnetic heading of the runway, and thus, the A380 departing RWY 28R at KSFO is likely to experience crosswind conditions. As a result, crosswind conditions must be taken into consideration when calculating the RTO speed of the aircraft.

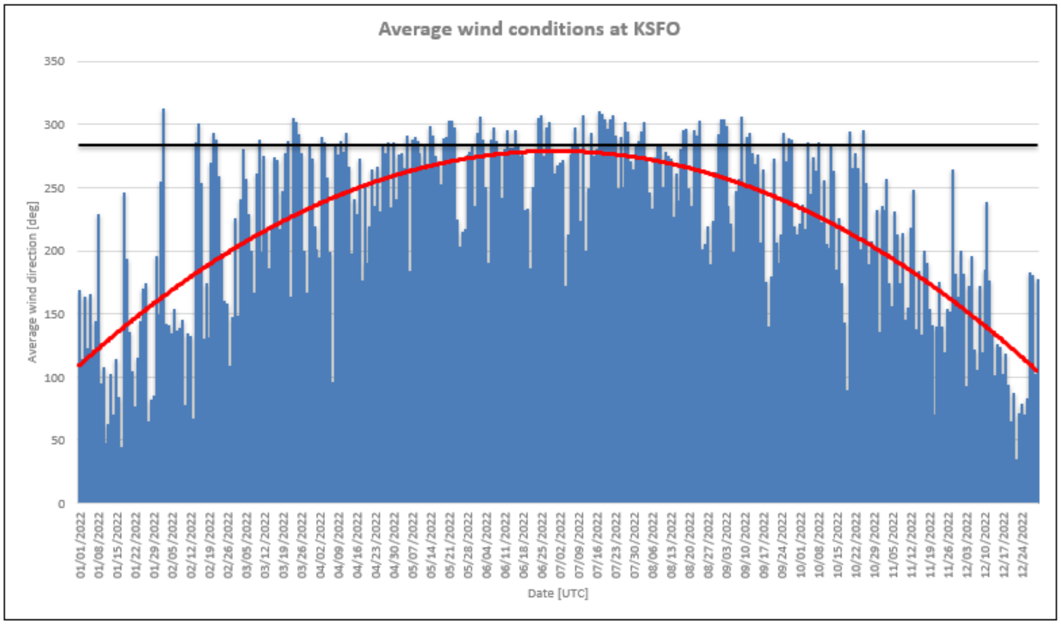

Figure 5.2: Average wind direction at KSFO

5.2 Crosswind Study Parameters

Similar to the previous algorithms and studies discussed thus far, the crosswind model purely focuses on the ground roll procedure. Same as the environmental model discussed in Chapter 3, a FoS of 1.50 is applied to the average wind speed to account for a severe crosswind case. Based on the METAR data presented in Fig. 5.1 (refer to pg. 32), the largest average wind conditions at KSFO in 2022 was approximately 23.3-kts. As a result, the magnitude of the crosswind used as input for the crosswind model was set to 35-kts. Based on the METAR results presented in Fig. 5.2 (refer to pg. 33), the corresponding wind direction for the largest average wind condition was approximately 285-degrees - almost in-line with the magnetic heading of RWY 28R at KSFO. To implement the crosswind, a wind direction of approximately 312-degrees (which is seen around early February 2022 per Fig. 5.2) was selected as an input for the crosswind model.

5.3 Crosswind Model

A general schematic of the crosswind model is presented in Fig. 5.3 on pg. 34. Based on the study parameters, the crosswind comes from the right of the A380-800. Similar to the environmental model discussed in Chapter 3, the headwind component of the crosswind is expected to increase the airspeed of the A380 during the ground roll procedure. From the perspective of air molecules (i.e., the airspeed), the total velocity vector of the aircraft is represented by the solid green vector as shown in Fig. 5.3, which is the sum of the ground speed and wind speed. The crosswind shown in Fig. 5.3 will naturally want to pull the nose of the aircraft to the right, based on the weathervane effect. To counteract the weathervane effect, left rudder input from the pilot is required to maintain runway centerline.

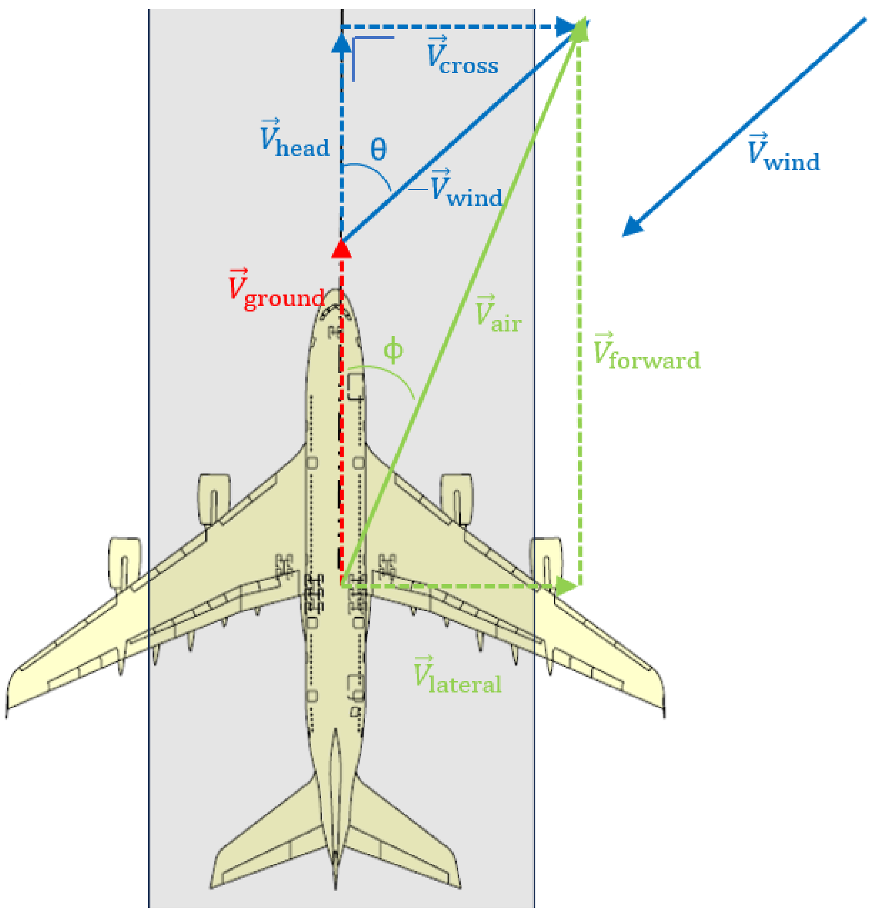

Figure 5.3: Airspeed velocity vector in a crosswind configuration

Similar to the other models discussed in Chapter 2 and 3, a flow chart of the crosswind model is presented in Fig. 5.4 on pg. 36. First, airport, weather, and specific A380-800 information is collected and imported as inputs. Given approximations of various A380-800 dimensions, an input file for the DATCOM Plus Program in constructed [14, 35]. While the outputs (i.e., stability and control derivatives) from the DATCOM Plus Program are highly approximated, the values are compared to, and corrected with, published Boeing

747 stability and control derivatives [35, 36]. There are three submodels within the main crosswind model: aerodynamics model, gear model, and dynamics model. Variables within the aerodynamic model (e.g., aerodynamic forces and moments) are initialized based on a series of initial conditions. The initial aerodynamic parameters, coupled with a runway surface model developed by NASA, are used to initialize the gear model [13, 22]. The initial outputs from both the aerodynamic and gear models are used to approximate the dynamics of the A380-800 [13]. Once the initial conditions are determined for each submodel, an Explicit Euler numerical method, similar to the 1-D baseline and environmental models, is implemented to approximate velocities (e.g., forward, lateral, and yaw rate) and positions (e.g., longitudinal, lateral, and directional) at every timestep until the boundary condition (i.e., the length of the runway) is satisfied (refer to the while loop in Fig. 5.4 on pg. 36).

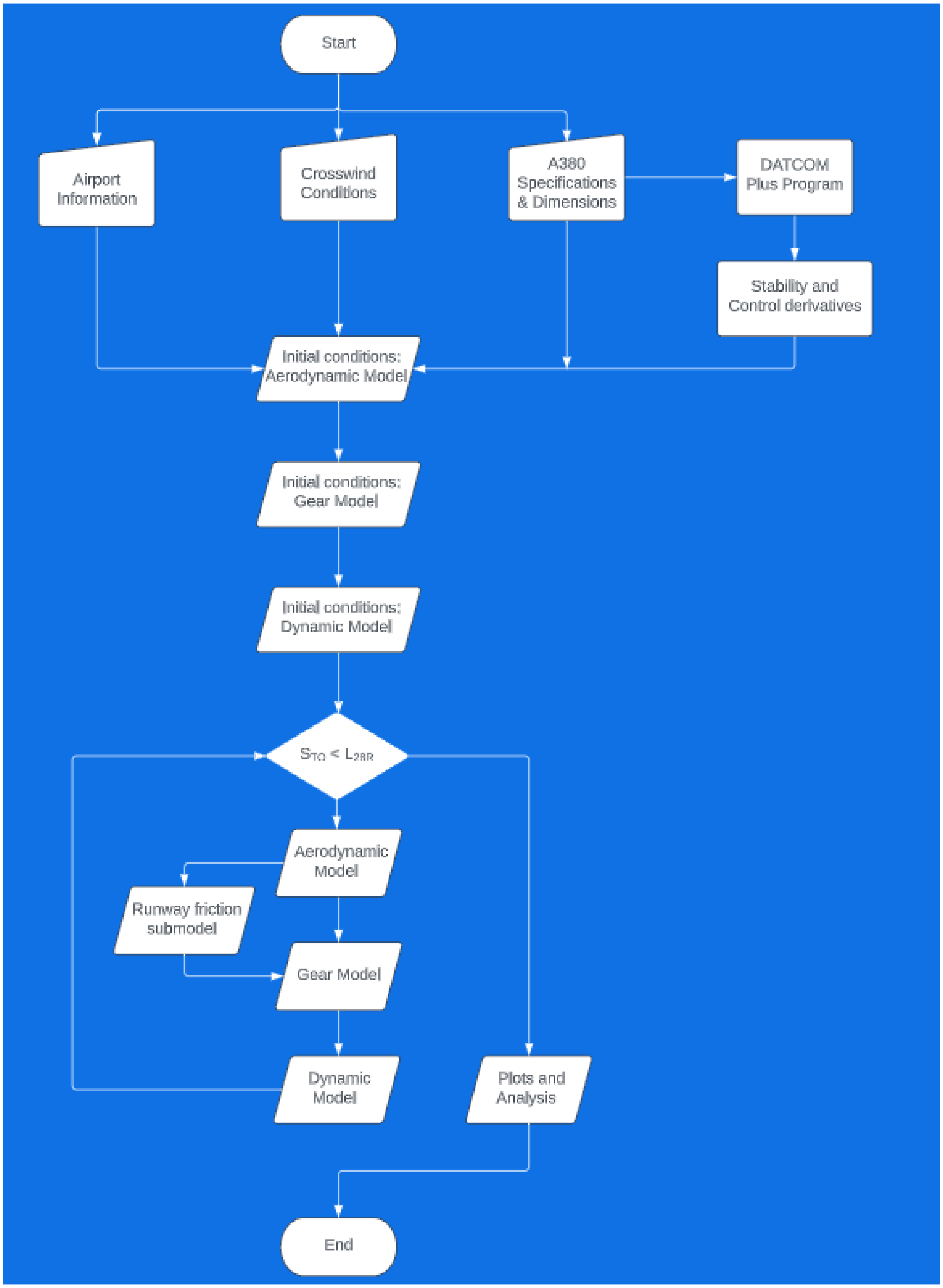

Figure 5.4: Flowchart of crosswind analysis

5.3.1 Assumptions

Similar to the algorithms discussed thus far, the 3-D crosswind model incorporates several assumptions. Regarding the A380, constant thrust is produced by all four engines, and maximum thrust is applied at the first timestep. Throughout the ground roll procedure, the non-dimensional stability and control derivatives remain constant. Moreover, non-dimensional stability or control derivatives for pitch and roll rate are neglected since the analysis purely focuses on the ground roll procedures (i.e., elevator and aileron input from the pilot is small and negligible). Due to limited information related to airfoils, a NACA-W-6-63-210 airfoil was considered for the wings, horizontal tail, and the vertical tail. Throughout the ground roll procedure, it is assumed the fuselage and the horizontal stabilizer do not generate any lift. Regarding the location of the C.G., it is assumed to remain constant due to the minimal fuel burn during the takeoff procedure. Moreover, the location of the C.G. is approximated based on general A380 dimensions provided by Airbus [14]. When countering the weathervane effect, it is assumed the nose wheel is coupled with the rudder and follows the same sign convention as the rudder deflection angle. Regarding actuation, control surface and wheel deflections do not account for pilot reaction times and are assumed to be instantaneous. Regarding environmental conditions, crosswind conditions (wind magnitude and direction) are assumed to remain constant throughout the takeoff procedure. Regarding runway surface conditions, similar to the 1-D baseline model, the longitudinal runway friction coefficient remains constant throughout the takeoff procedure. The gear model discussed in this master's project only considers the nose wheel, the left main wheel, and the right main wheel based on available information.

5.3.2 Coordinate System and Dimensions

The 3-D coordinate system used for the crosswind analysis is in-line with the coordinate system referenced in Aerospace Engineering courses at San Jose State University, and the positive conventions are noted in Fig. 5.5 on pg. 38 [37]. By convention, the positive body x-axis $\hat{b}_x$ goes through the nose of the A380, the positive body y-axis $\hat{b}_y$ goes through the right wing of the A380, and the positive body z-axis $\hat{b}_z$ goes through the C.M. and points downwards, as shown in Fig. 5.5 on pg. 38 [37]. As previously mentioned, the crosswind model includes three separate submodels: aerodynamic, gear, and dynamics. These models presented in this analysis were originally obtained from literature and later altered to accommodate the A380 [13]. In order to fully-develop all three submodels, several A380 dimensions were approximated based on readily-accessible diagrams (the approximated dimensions are presented in Table 5.1 on pg. 38). For this analysis, positive rudder deflection occurs when the trailing edge of the rudder is deflected to the left. As a result, the camber is increased and the vertical tail lifts to the right, which ultimately pivots the aircraft about the C.G. and points the nose to the left [37]. As presented in literature, positive nose wheel deflection follows the same convention as the rudder [13]. Moreover, this analysis includes two primary reference frames: the fixed runway frame and the varying aircraft frame.

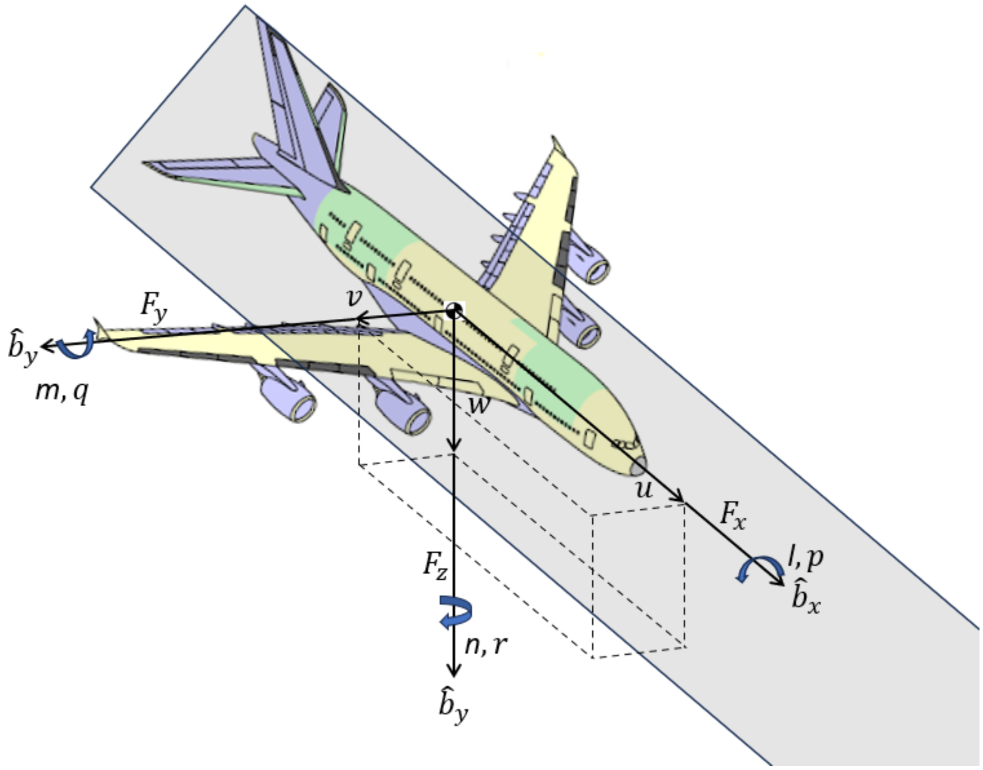

Figure 5.5: Body reference frame

Table 5.1: Approximated dimensions of A380-800 [14]

Parameter	Value	Units	Defined in
$r_{y,\text{eng},1/4}$	25.70	m	Fig. 5.10
$r_{y,\text{eng},2/3}$	14.80	m	Fig. 5.10
r_1	28.61	m	Fig. 5.15
r_4	1.00	m	Fig. 5.17
W_{b_x}	28.61	m	Fig. 5.15
W_{b_y}	12.46	m	Fig. 5.17
W_{b_z}	5.50	m	Fig. 5.12
z_1	1.25	m	Fig. 5.12
z_2	2.25	m	Fig. 5.12
$\delta_{r,\max}$	26.00	deg	Fig. 5.10
$\delta_{nw,\max}$	10.00	deg	Fig. 5.15

Given the forward and lateral velocities with respect to the aircraft, u and v, respectively, the tire sideslip angle β_g is calculated with Eq. (5.1). The tire sideslip angle is a critical parameter when calculating the lateral runway friction coefficient [22, 13].

$$\beta_g = \tan^{-1}\left(\frac{v}{u}\right) \tag{5.1}$$

The ground speed is obtained by applying the Pythagorean theorem to the forward and lateral velocities with respect to the aircraft, as shown in Eq. (5.2) (refer to Fig. 5.6 on pg. 39 for illustration). The track angle κ is the sum of the aircraft heading angle ψ and the ground sideslip angle, and is used to calculate the velocities in the runway frame (refer to Eq. (5.4) and Eq. (5.5)).

$$V_g = \sqrt{u^2 + v^2} \tag{5.2}$$

$$\kappa = \psi + \beta_g \tag{5.3}$$

$$V_{g,x} = V_g \cos(\kappa) \tag{5.4}$$

$$V_{g,y} = V_g \sin(\kappa) \tag{5.5}$$

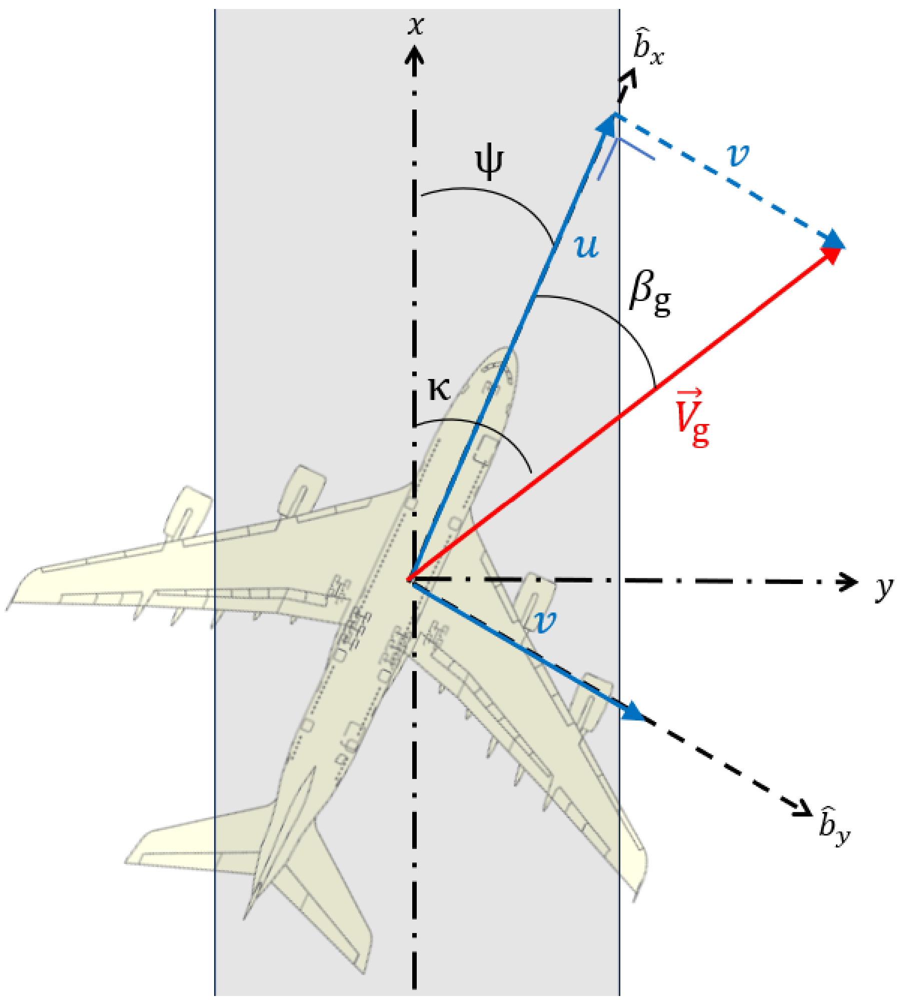

Figure 5.6: Ground speed in a crosswind configuration

Next, the headwind $V_{x,\text{wind}}$ and crosswind $V_{y,\text{wind}}$ components are calculated given the magnitude of the wind speed (i.e., 35-kts), as well as the wind direction relative to the runway centerline θ_{wind} and the aircraft heading angle, with Eq. (5.6) and Eq. (5.7), respectively (refer to Fig. 5.7 and pg. 40). The aerodynamic sideslip angle is then determined with Eq. (5.8), which has an impact on the aerodynamic forces and moments [13]. Moreover, the total airspeed is obtained with Eq. (5.9), which is then used to calculate the total dynamic pressure as shown in Eq. (5.10). Similar to β, the total dynamic pressure is a critical parameter required for aerodynamic forces and moments [13].

$$V_{x,\text{wind}} = V_{\text{wind,avg}} * \cos\left(\theta_{\text{wind}} - \psi\right) \tag{5.6}$$

$$V_{y,\text{wind}} = V_{\text{wind,avg}} * \sin\left(\theta_{\text{wind}} - \psi\right) \tag{5.7}$$

$$\beta = \tan^{-1}\left(\frac{v + V_{y,\text{wind}}}{u + V_{x,\text{wind}}}\right) \tag{5.8}$$

$$V_{\text{air}} = \sqrt{\left(V_{g,x} + V_{\text{wind,x}}\right)^2 + \left(V_{g,y} + V_{\text{wind,y}}\right)^2} \tag{5.9}$$

$$q = \frac{1}{2}\rho_0 V_{\text{air}}^2 \tag{5.10}$$

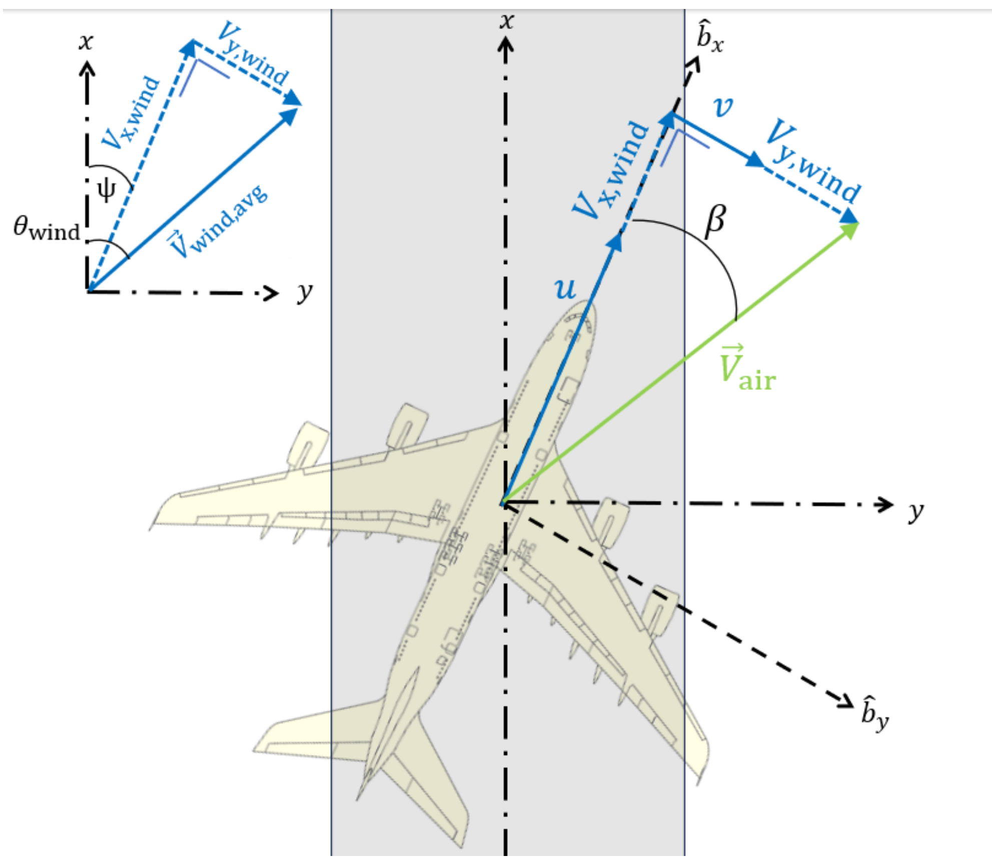

Figure 5.7: Wind velocity vector and aerodynamic sideslip angle

5.3.3 Non-dimensional Stability and Control Derivatives

Due to limited A380 information available to the public, some of the control derivatives were first approximated with the DATCOM Plus Program [35]. This program requires a wide variety of inputs such as, but not limited to, mach number, aircraft weight, location of C.G., fuselage dimensions, and airfoil dimensions for the wings, horizontal tail, and vertical tail. The input file to the DATCOM Plus Program is shown in Fig. 5.8 on pg. 41.

```
CASEID ----- AIRBUS A380 -----
 $FLTCON NMACH=1.0,MACH(1)=0.2,NALPHA=1.0,ALSCHD(1)=0.0,
  NALT=1.0,ALT(1)=0.0,WT=1267659.0,LOOP=1.$
 $SYNTHS XCG=115.00,ZCG=0.0,XW=64.50,ZW=2.0,ALIW=2.0,XH=192.39,
  ZH=2.0,ALIH=0.0,XV=176.97,ZV=9.33$
 $OPTINS SREF=243.0$
 $BODY NX=6.0,
  X(1)=0.0,16.31,51.14,150.58,192.39,238.09,
  S(1)=58.49,228.85,511.11,521.17,231.54,231.54$
NACA-W-6-63-210
 $WGPLNF CHRDTP=13.06,SSPNOP=97.62,SSPNE=119.12,SSPN=130.83,
  CHRDBP=46.00,CHRDR=57.97,SAVSI=33.5,SAVSO=33.5,CHSTAT=0.25,
  TWISTA=0.0,DHDADI=5.6,DHDADO=5.6,TYPE=1.0$
NACA-H-6-63-210
 $HTPLNF CHRDTP=12.2,SSPNE=44.26,SSPN=49.82,CHRDR=37.96,SAVSI=33.5,
  CHSTAT=0.25,TYPE=1.0$
NACA-V-6-23-210
 $VTPLNF CHRDTP=15.42,SSPNE=47.87,SSPN=50.00,CHRDR=39.57,SAVSI=33.5,
  CHSTAT=0.25,TYPE=1.0$
DIM FT
BUILD
PLOT
NEXT CASE
```

Figure 5.8: DATCOM Input file for A380

MATLAB programs have been developed to configure the aircraft given a DATCOM Plus input file (refer to Fig. 5.9 on pg. 42) [38]. Regarding the fuselage, a circular cross-section was assumed for simplicity purposes. Since the A380 dimensions included in the DATCOM Plus Program input file were highly approximated, the control derivatives were compared with published Boeing 747 data [36]. In some cases, a correction factor was applied to the DATCOM Plus Program results, and the control derivatives used in the crosswind analysis are presented in Table 5.2 on pg. 42.

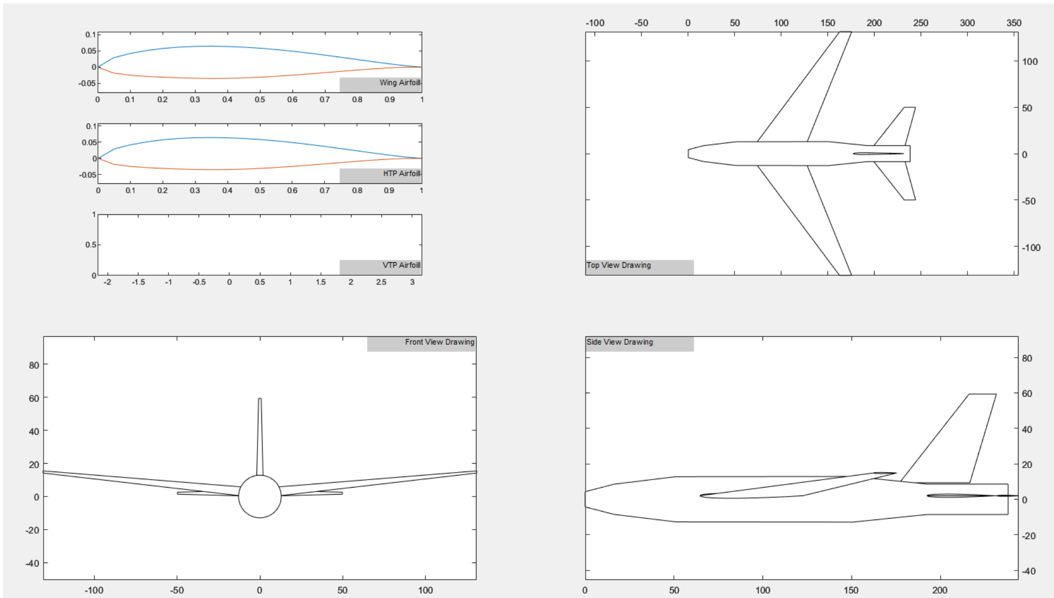

Figure 5.9: DATCOM Input visualization for A380 [38]

Table 5.2: Stability and control derivatives

Parameter	Value	Units
C_{l_β}	-0.221	$^1/_{\text{rad}}$
$C_{l_{\delta_r}}$	0.007	$^1/_{\text{rad}}$
C_{l_r}	0.101	$^1/_{\text{rad}}$
C_{Y_β}	-0.96	$^1/_{\text{rad}}$
$C_{Y_{\delta_r}}$	0.175	$^1/_{\text{rad}}$
C_{n_β}	0.150	$^1/_{\text{rad}}$
$C_{n_{\delta_r}}$	-0.109	$^1/_{\text{rad}}$
C_{n_r}	-0.30	$^1/_{\text{rad}}$

5.3.4 Aerodynamic Forces and Moments

The first component of the crosswind model is the aerodynamic model, which consists of forces acting on the aircraft body in the $\hat{b}_x$, $\hat{b}_y$, and $\hat{b}_z$ directions. First, the aerodynamic forces parallel to the $\hat{b}_x$ direction (refer to Fig. 5.10 on pg. 44) are determined with Eq. (5.11). Similar to the 1-D baseline and environmental cases, constant thrust evaluated at maximum conditions is assumed at the first timestep of the simulation. Moreover, it is assumed the angle of attack throughout the ground roll procedure remains constant, hence the overall drag coefficient C_d remains constant [13]. Moreover, the aerodynamic force in the $\hat{b}_x$ direction will ultimately decrease due to a stronger dynamic pressure increase over time. While the exact lateral dimensions between the C.G. and the centerline of each engine are unknown, the values are approximated based on general A380-800 dimensions [14]. Next, the aerodynamic moment about the $\hat{b}_z$ axis is computed at every timestep with Eq. (5.12). Regarding this simulation, the thrust components in Eq. (5.12) will cancel due to constant thrust and symmetry, however, the terms are included in the event engine failure analysis is pursued. Since this study focuses specifically on the ground roll procedure, and moment in pitch and roll is assumed to be negligible, the roll and pitch derivatives in Eq. (5.12) are neglected. As a result, the derivatives in focus are the sideslip angle, the rudder deflection angle, and the yaw rate, or β, δ_r, and r, respectively. While there are different ways to non-dimensionalize r, the component in Eq. (5.12) is obtained from literature [13].

$$F_{x,\text{aero}} = T_{\text{eng},1} + T_{\text{eng},2} + T_{\text{eng},3} + T_{\text{eng},4} - qS_wC_d \tag{5.11}$$

$$\begin{aligned} M_{z,\text{aero}} =& qS_wb\left(C_{n_\beta}\beta + C_{n_{\delta_r}}\delta_r + C_{n_r}\frac{rb}{2V_{\text{air}}}\right) \\ &+ T_{\text{eng},1}r_{y,\text{eng},1} + T_{\text{eng},2}r_{y,\text{eng},2} - T_{\text{eng},2}r_{y,\text{eng},2} - T_{\text{eng},4}r_{y,\text{eng},4} \end{aligned} \tag{5.12}$$

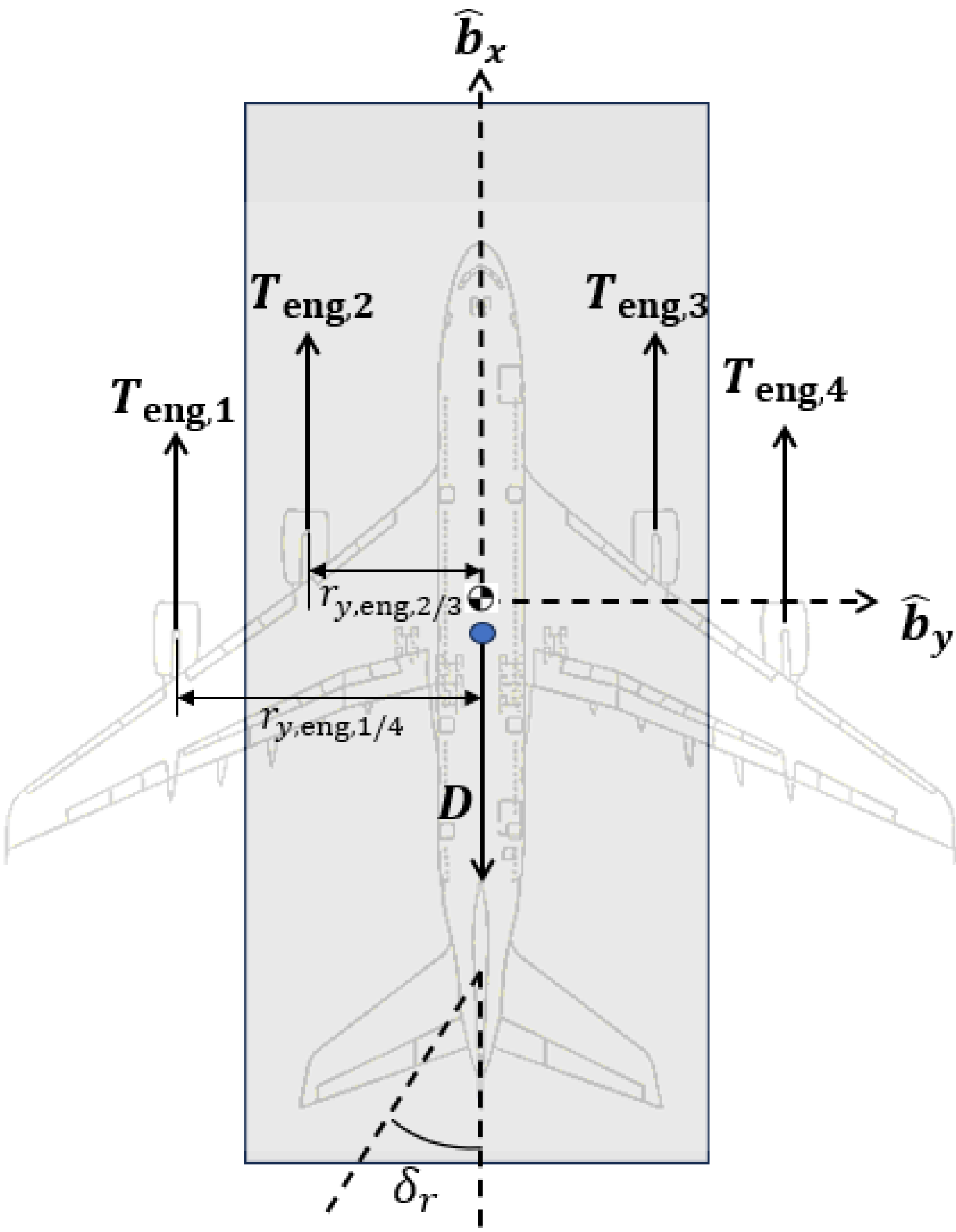

Figure 5.10: FBD of forces parallel with the roll axis

Next, the aerodynamic force along the $\hat{b}_y$ axis, as well as the aerodynamic moment about the $\hat{b}_x$ axis, is determined from the FBD depicted in Fig. 5.11 on pg. 45. In this crosswind analysis, only β and δ_r have a significant impact on the side force, as mentioned in Eq. (5.13), similar to other models found in literature [13]. Since the crosswind in this model comes from the right, this will cause the aircraft to naturally yaw into the wind due to the weathervane effect which results in a positive aerodynamic sideslip angle, β.Therefore, the crosswind results in a positive heading angle (also due to the weathervane effect), which is in the same direction as β in this case. As a result, a negative side force is initially exerted on the vertical tail along the negative $\hat{b}_y$ axis. Regarding the aerodynamic moment about the $\hat{b}_x$ axis, the aircraft has a tendency to roll to the left, especially with no aileron input from the pilot. This results in a negative rolling moment, and is described by Eq. (5.14) [37]. Similar to the yawing moment (refer to Eq. (5.12) on pg. 43), the contributing derivatives are β, δ_r, and r, with r non-dimensionalized with an expression found in literature [13].

$$F_{y,\text{aero}} = qS_w \left(C_{Y_\beta}\beta + C_{Y_{\delta_r}}\delta_r \right) \tag{5.13}$$

$$M_{x,\text{aero}} = qS_w b \left(C_{l_\beta}\beta + C_{l_{\delta_r}}\delta_r + C_{l_r}\frac{rb}{2V_{\text{air}}} \right) \tag{5.14}$$

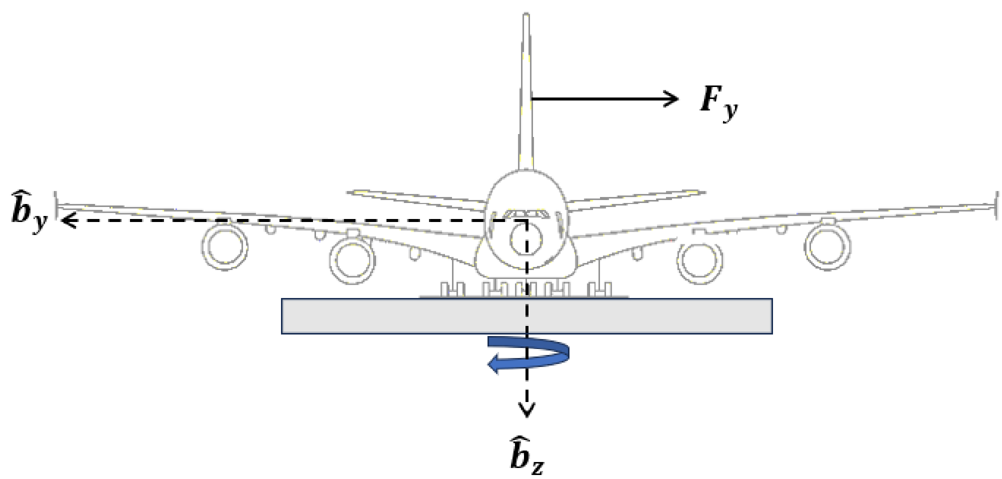

Figure 5.11: FBD of forces parallel with the pitch axis

The last portion of the aerodynamic model includes aerodynamic forces along the $\hat{b}_z$ axis, as well as the aerodynamic moment about the $\hat{b}_y$ axis, or the pitching moment. Moreover, these expressions are derived from a FBD in the profile view (refer to Fig. 5.12 on pg. 46). When calculating the lift at every timestep, the x-component of V_{air} is only considered since that term accounts for the streamlines going over the wings, which are parallel to the $\hat{b}_x$ axis, as shown in Eq. (5.15). Moreover, the dynamic pressure is also impacted by the reduced airspeed (since the orthogonal component is neglected) and is calculated with Eq. (5.16). Finally, the dynamic pressure calculated at every timestep with Eq. (5.16) is used to calculate the lift generated by the wings with Eq. (5.17).

Based on similar readily accessible studies found in literature, this analysis assumes the pitching moment coefficient, as well as the elevator deflection coefficient, cancel each other out [13]. Therefore, the only forces which contribute to the pitching moment are thrust generated by all four engines, and their respective moment arms as shown in Eq. (5.18). Since the thrust remains constant for this crosswind study, the aerodynamic moment about the $\hat{b}_y$ axis will also remain constant. While the exact moment arms could not be determined, the values were approximated based on general A380 dimensions [14].

$$V_{\text{air,lift}} = \sqrt{\left(V_{g,x} + V_{\text{wind,x}}\right)^2} \tag{5.15}$$

$$q_{\text{lift}} = \frac{1}{2}\rho_0 V_{\text{air,lift}}^2 \tag{5.16}$$

$$F_{z,\text{aero}} = W_{MTOW} - q_{\text{lift}} S_w C_L \tag{5.17}$$

$$M_{y,\text{aero}} = z_1 \left(T_{\text{eng},1} + T_{\text{eng},4}\right) + z_2 \left(T_{\text{eng},2} + T_{\text{eng},3}\right) \tag{5.18}$$

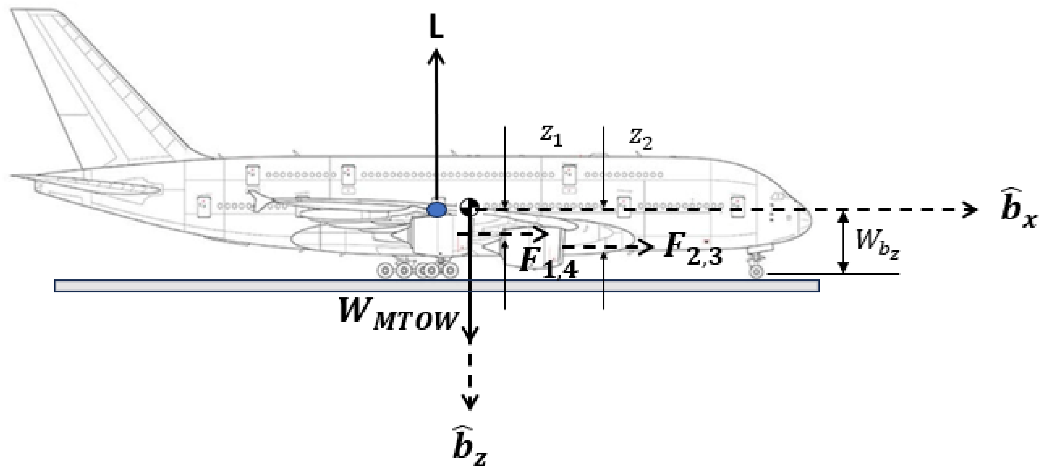

Figure 5.12: FBD of forces parallel with the yaw axis

5.3.5 Gear Model

The next portion of the crosswind analysis is related to the gear model. Based on available A380 information, the gear model includes the nose wheel and both main gears [14]. For this analysis, the runway friction coefficients are accounted for in two directions: the rolling friction coefficient along the forward direction and a lateral runway friction coefficient orthogonal to the runway centerline. The rolling coefficient used in this analysis is identical to the value used in the 1-D RTO speed model as well as the environmental model ($\mu_{\text{r,TO}} = 0.02$ for a dry runway surface). The side runway friction coefficient is approximated with a runway NASA model for dry surfaces, and other publications [13, 22]. Moreover, the lateral runway friction coefficient for a dry runway is approximated with an empirical expression as shown in Eq. (5.19) [13]. To calculate the lateral runway coefficient for each wheel, the proper sideslip angle was substituted into Eq. (5.19). A graphical representation of Eq. (5.19) is presented in Fig. 5.13 on pg. 47. Moreover, Fig. 5.13 assumes a constant ground speed of 100-kts, with varying ground sideslip angles [13, 22]. As shown in Fig. 5.13, the lateral runway friction coefficient yields a symmetrical plot, thus the absolute value of the lateral runway friction coefficient is considered depending on the sign of β_g.

$$\mu_{s,\text{dry}} = 0.39\exp\left(-0.015\sqrt{\text{V}_\text{g}}\right)\tan^{-1}\left(0.33\beta_\text{g}\right) \tag{5.19}$$

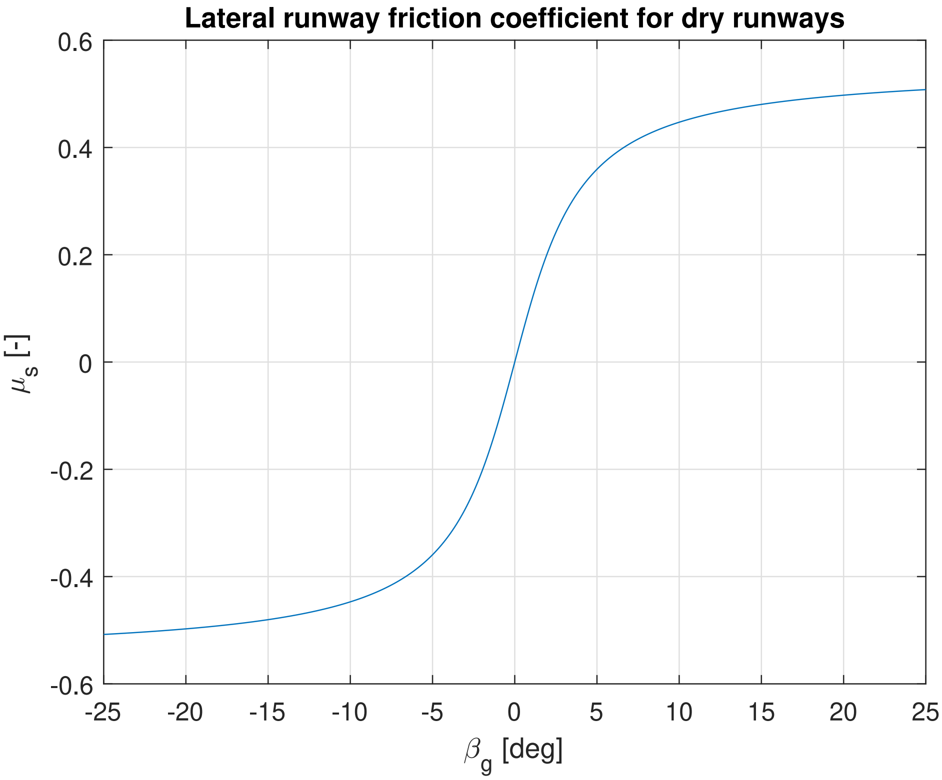

Figure 5.13: Lateral runway friction coefficient for dry runways [22]

Similar to the aerodynamic model, FBDs are constructed for each wheel in order to identify critical force and moment expressions. Regarding the nose wheel, there are three main forces acting on the component: a force parallel to the forward direction along the $\hat{b}_x$ direction, a side force orthogonal to the forward direction, and a vertical normal force in the negative $\hat{b}_z$ direction. The nose gear forces are presented in a FBD, as shown in Fig. 5.14 on pg. 48. Note, the two forces along the $\hat{b}_y$ axis account for both configurations, and the direction depends on the sign of the nose wheel sideslip angle.

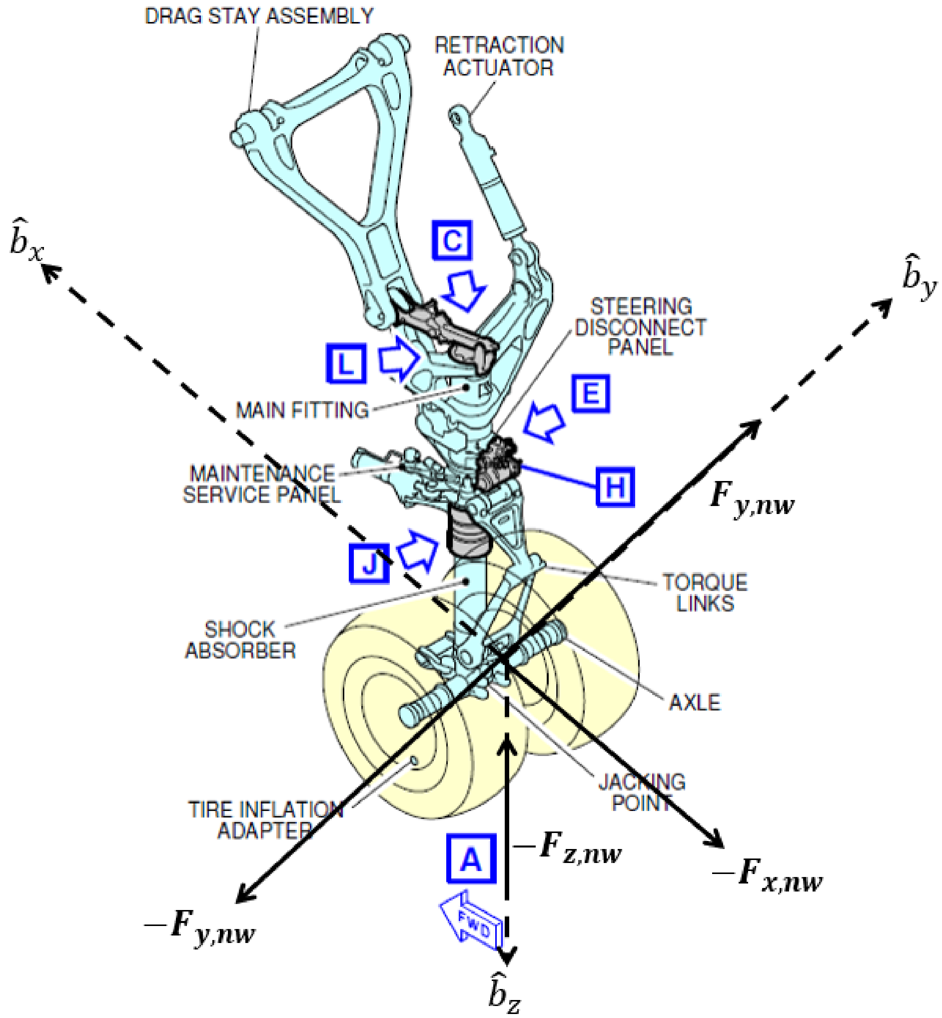

Figure 5.14: FBD of an A380 nose wheel [14]

In addition to the forces exerted on the nose gear, the conventions for various angles are presented in Fig. 5.15 on pg. 49. The sideslip angle of the nose wheel is calculated with Eq. (5.20), which has a direct impact on the direction of the lateral gear force. As stated previously, the nose wheel deflection angle δ_{nw} shares the same convention as the rudder deflection angle δ_{r} [13, 37]. For this analysis, a proportional gain is included to calculate δ_{nw}, and is dependent on the lateral position of the aircraft (refer to Eq. (5.21)). To counteract the weathervane effect, the proportional constant k is multiplied by the lateral position of the aircraft S_{y} as shown in Eq. (5.21). Since the crosswind causes a negative lateral displacement, and k is set to a constant of -0.0050, a positive wheel deflection angle is calculated to counteract the weathervane effect. Furthermore, since the rudder and nose wheel are coupled in this analysis, the rudder deflection angle is calculated by taking the ratio of both deflection angles as shown in Eq. (5.22), a technique available in literature [13].

$$\beta_{g,\mathrm{nw}} = \delta_{\mathrm{nw}} + \tan^{-1}\left(\frac{v + r\ r_1}{u}\right) \tag{5.20}$$

$$\delta_{\mathrm{nw}} = kS_{\mathrm{y}} \tag{5.21}$$

$$\delta_{\mathrm{r}} = \delta_{\mathrm{nw}} \left(\frac{\delta_{\mathrm{r,max}}}{\delta_{\mathrm{nw,max}}} \right) \tag{5.22}$$

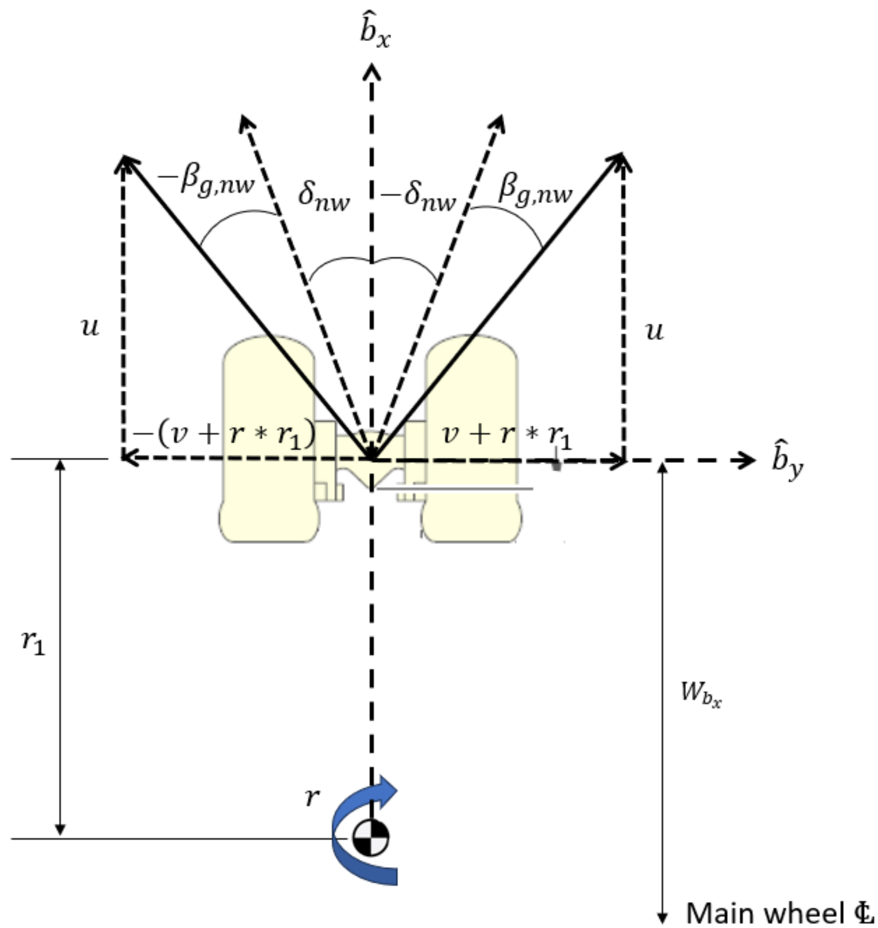

Figure 5.15: Nose wheel Sideslip and nose wheel deflection angles [13, 14]

Similar to the nose wheel analysis, the same methodology is applied to the left and right main wheels. The forces exerted on each main wheel are developed with a FBD (refer to Fig. 5.16 on pg. 50). The left and right main wheels have a negative friction force in the negative $\hat{b}_x$ direction, similar to the nose wheel. If the nose wheel deflection angle is negative, the sideslip angles for each main wheel are positive, which ultimately results in a lateral force parallel to the negative $\hat{b}_y$ direction (refer to Fig. 5.15 on pg. 49 for nose wheel deflection angle convention). Lastly, both normal forces are noted in Fig. 5.16, along the negative $\hat{b}_z$ direction.

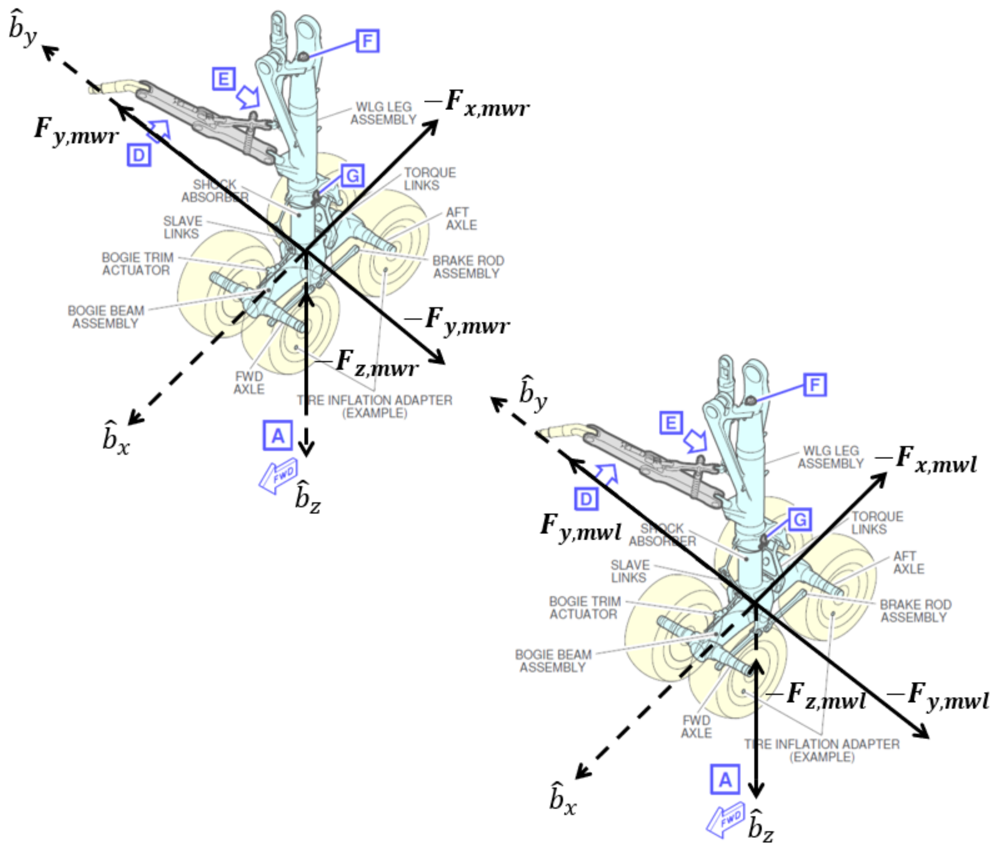

Figure 5.16: FBD of main wheels on an A380 [14]

The sideslip angles for each main wheel differ depending on the nose wheel deflection angle and the yaw rate r [13]. For a negative nose wheel deflection angle (as shown in Fig. 5.17 on pg. 51), the left main wheel will have a smaller sideslip angle $\beta_{g,\text{mw,left}}$ in comparison to the right main wheel. Moreover, the comparison between the left and right main wheel sideslip angles is Eq. (5.23) and Eq. (5.24), respectively [13]. Moreover, the blue and red sectional views in Fig. 5.17 illustrate the detailed velocity vectors caused by the yaw rate [13]. The center-to-center distance between the left and right main wheels W_{b_y}, as well as the distance from the C.G. to the center of the main wheels r_4, are approximated with general A380 dimensions (refer to Table 5.1 on pg. 38) [14].

$$\beta_{g,\text{mw,left}} = \tan^{-1}\left(\frac{v - r\ r_4}{u + r\left(\frac{W_{b,y}}{2}\right)}\right) \tag{5.23}$$

$$\beta_{g,\text{mw,right}} = \tan^{-1}\left(\frac{v - r\ r_4}{u - r\left(\frac{W_{b,y}}{2}\right)}\right) \tag{5.24}$$

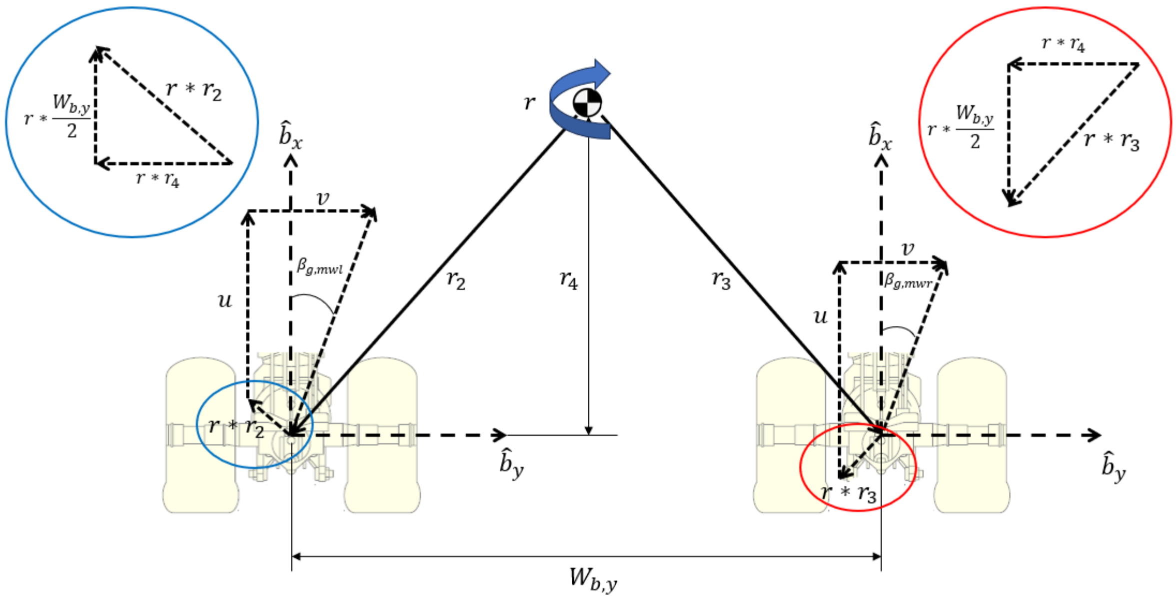

Figure 5.17: Main wheel sideslip angles and velocity triangles [13, 14]

Given the FBDs for the nose gear and both main gears (refer to Fig. 5.14 and Fig. 5.16, respectively), the gear forces are derived for each axis. Regarding the forces parallel to the $\hat{b}_x$ direction, the normal forces for each wheel are multiplied by the rolling friction coefficient, as shown in Eq. 5.25. Regarding the forces parallel to the $\hat{b}_y$ direction, the normal forces for each wheel are multiplied by the lateral runway friction coefficient μ_s, as shown in Eq. (5.26). Recall, the lateral runway friction coefficient is calculated with the empirical formula defined by Eq. (5.19) on pg. 46 [13]. Moreover, the sign functions in Eq. (5.26) determine the direction of the lateral force applied to the wheel.

$$F_{x,\text{gear}} = F_{z,\text{nw}}\mu_{r,\text{TO}} + F_{z,\text{mw,left}}\mu_{r,\text{TO}} + F_{z,\text{mw,right}}\mu_{r,\text{TO}} \tag{5.25}$$

$$\begin{aligned} F_{y,\text{gear}} =& F_{z,\text{nw}}\mu_{s,\text{nw}}\text{sgn}\left(\beta_{\text{g,nw}}\right) + \text{F}_{\text{z,mw,left}}\mu_{\text{s,mw,left}}\text{sgn}\left(\beta_{\text{g,mw,left}}\right) \\ &+ F_{z,\text{mw,right}}\mu_{s,\text{mw,right}}\text{sgn}\left(\beta_{\text{g,mw,right}}\right) \end{aligned} \tag{5.26}$$

Moreover, expressions for the gear moments about the $\hat{b}_x$ direction and $\hat{b}_y$ axes are defined by Eq. (5.27) and Eq. (5.28), respectively, where W_{b_z} is the vertical distance between the center of the wheels to the C.G. (refer to Table 5.1 on pg. 38 for value) [13].

$$\begin{aligned} M_{x,\text{gear}} =& -W_{b_z}[F_{z,\text{mw,left}}\mu_{s,\text{mw,left}}\text{sgn}\left(\beta_{\text{g,mw,left}}\right) + \text{F}_{\text{z,mw,right}}\mu_{\text{s,mw,right}}\text{sgn}\left(\beta_{\text{g,mw,right}}\right) \\ &+ F_{z,\text{nw}}\mu_{s,\text{nw}}\text{sgn}\left(\beta_{\text{g,nw}}\right)] \end{aligned} \tag{5.27}$$

$$M_{y,\text{gear}} = -W_{b_z}\left(F_{z,\text{mw,left}}\mu_{r,\text{TO}} + F_{z,\text{mw,right}}\mu_{r,\text{TO}} + F_{z,\text{nw}}\mu_{r,\text{TO}}\right) \tag{5.28}$$

With the gear forces and moments defined in both the $\hat{b}_x$ and $\hat{b}_y$ directions, a linear gear model is implemented to compute the normal forces for each wheel. Moreover, the general setup of the linear system was obtained from literature [13]. The linear model is separated into two constant matrices: the aerodynamic matrix and the gear matrix. The aerodynamic matrix is represented with matrix B, as shown in Eq. (5.29), and the transpose of the gear matrix A is shown in Eq. (5.30). Since the crosswind analysis purely focuses on the ground roll procedure, and the normal forces on each wheel must balance moments about the $\hat{b}_x$ and $\hat{b}_y$ axes, the linear equation shown in Eq. (5.31) is equal to zero. The normal forces are then solved with Eq. (5.32) for each timestep, in order to calculate the gear forces and moments in the $\hat{b}_x$ and $\hat{b}_y$ directions.

$$B = \begin{bmatrix} M_{x,\text{aero}} \\ M_{y,\text{aero}} \\ F_{z,\text{aero}} \end{bmatrix} \tag{5.29}$$

$$A^T = \begin{bmatrix} -W_{b,z}\mu_{s,\text{nw}}\text{sgn}\left(\beta_{\text{g,nw}}\right) & -W_{b,z}\mu_{\text{roll}} - r_1 & 1 \\ \left(-W_{b,z}\mu_{s,\text{mw,left}}\text{sgn}\left(\beta_{\text{g,mw,left}}\right)\right) - \frac{1}{2}W_b & -W_{b,z}\mu_{\text{roll}} + r_4 & 1 \\ \left(-W_{b,z}\mu_{s,\text{mw,right}}\text{sgn}\left(\beta_{\text{g,mw,right}}\right)\right) + \frac{1}{2}W_b & -W_{b,z}\mu_{\text{roll}} + r_4 & 1 \end{bmatrix} \tag{5.30}$$

$$0 = B + A \begin{Bmatrix} F_{z,\text{nw}} \\ F_{z,\text{mw,left}} \\ F_{z,\text{mw,right}} \end{Bmatrix} \tag{5.31}$$

$$\begin{Bmatrix} F_{z,\text{nw}} \\ F_{z,\text{mw,left}} \\ F_{z,\text{mw,right}} \end{Bmatrix} = A^{-1}\left(-B\right) \tag{5.32}$$

To validate the gear model, the sum of the normal forces parallel to the $\hat{b}_z$ direction is subtracted from the aerodynamic force parallel to the same axis. As shown in Fig. 5.18 on pg. 53, this check was calculated for each timestep in the simulation. Moreover, a constant result of zero over the entire simulation is expected, and the gear model is validated. Furthermore, the derivation for the gear submodel is available in Appendix H.

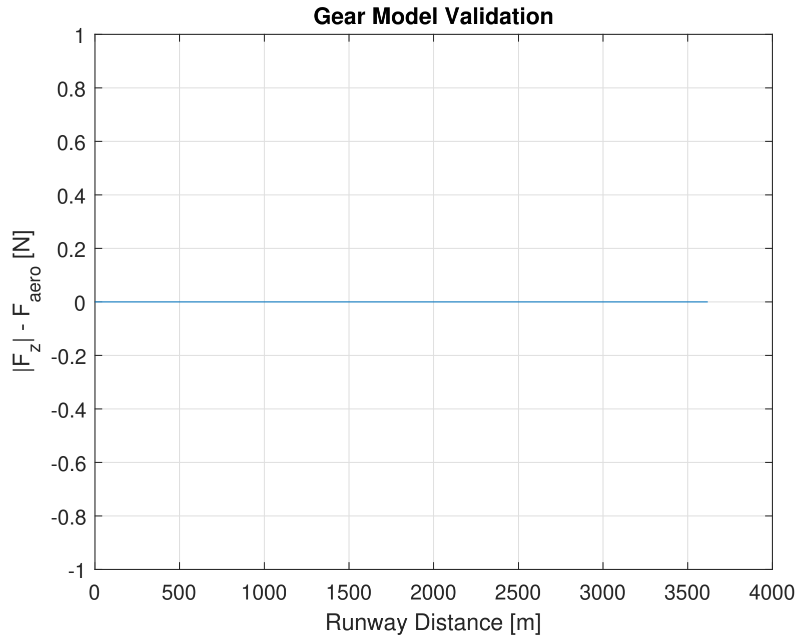

Figure 5.18: Validation of gear model used in crosswind analysis

5.3.6 Dynamics Model

Lastly, the forward acceleration $\dot{u}$ as well as the lateral acceleration $\dot{v}$ are computed with Newton's second law and 3-D equations of motion. Moreover, the crosswind analysis presented in this master's project assumes a stiff landing gear, and the following dynamics are neglected: $\dot{w}$, $\dot{p}$, and $\dot{q}$ [13]. Due to minimal aileron and elevator input from the pilot, the roll and pitch rates are neglected in the analysis.

$$\dot{u} = \frac{(F_{x,\text{aero}} + F_{x,\text{gear}})}{m_{MTOW}} + rv \tag{5.33}$$

$$\dot{v} = \frac{(F_{y,\text{aero}} + F_{y,\text{gear}})}{m_{MTOW}} - ru \tag{5.34}$$

The gear moment about the $\hat{b}_z$ axis is calculated with Eq. (5.35), and is developed from the FBDs in Fig. 5.15 and Fig. 5.17 [13]. The moment of inertia about the z-axis I_{zz} is approximated with an expression readily-accessible in literature (refer to Eq. (5.36)) [13]. Lastly, neglecting the vector products of both the angular velocity and angular momentum, considering we only assume rotation about the $\hat{b}_z$ axis, $\dot{r}$ is approximated with Eq. (5.37).

$$\begin{aligned} M_{z,\text{gear}} = &- \left[F_{z,\text{mw,left}}\mu_{s,\text{mw,left}}\text{sgn}\left(\beta_{\text{g,mw,left}}\right) + \mathrm{F}_{\text{z,mw,right}}\mu_{\text{s,mw,right}}\text{sgn}\left(\beta_{\text{g,mw,right}}\right)\right] r_4 \\ &+ F_{z,\text{nw}}\mu_{s,\text{nw}}\text{sgn}\left(\beta_{\text{g,nw}}\right) + \mathrm{F}_{\text{z,mw,left}}\mu_{\text{r,TO}}\frac{\mathrm{W}_{\mathrm{b_y}}}{2} - \mathrm{F}_{\text{z,mw,right}}\mu_{\text{r,TO}}\frac{\mathrm{W}_{\mathrm{b_y}}}{2} \end{aligned} \tag{5.35}$$

$$I_{zz} = 0.037 m_{MTOW} b^2 \tag{5.36}$$

$$\dot{r} = \frac{(M_{z,\text{aero}} + M_{z,\text{gear}})}{I_{zz}} \tag{5.37}$$

Similar to the models presented in Chapter 2 and Chapter 3, the crosswind model implements a series of Explicit Euler methods to approximate the integration of several parameters [27]. Once the initial conditions are calculated, the forward velocity and position are approximated with Eq. (5.38) and Eq. (5.39), respectively. Next, the lateral velocity, as well as the lateral position, are approximated with Eq. (5.40) and Eq. (5.41), respectively. Recall, the lateral position S_y is a critical parameter which significantly impacts the nose wheel deflection angle (refer to Eq. (5.21) on pg. 49). Regarding directional parameters, the yaw rate and aircraft heading are approximated with Eq. (5.42) and Eq. (5.43), respectively. Moreover, these parameters are calculated at every timestep until the boundary condition (i.e., the length of the runway) is satisfied.

$$u\left(t\right) = u\left(t-1\right) + \dot{u}\left(t-1\right)dt \tag{5.38}$$

$$S_x\left(t\right) = S_x\left(t-1\right) + u\left(t-1\right)dt \tag{5.39}$$

$$v\left(t\right) = v\left(t-1\right) + \dot{v}\left(t-1\right)dt \tag{5.40}$$

$$S_y\left(t\right) = S_y\left(t-1\right) + v\left(t-1\right)dt \tag{5.41}$$

$$r\left(t\right) = r\left(t-1\right) + \dot{r}\left(t-1\right)dt \tag{5.42}$$

$$\psi\left(t\right) = \psi\left(t-1\right) + r\left(t-1\right)dt \tag{5.43}$$

5.3.7 Crosswind Results and Discussion

The first parameter investigated in the crosswind analysis was the aircraft heading angle ψ over the trajectory of the ground roll procedure (refer to Fig. 5.19 on pg. 55). The aircraft heading has a sharp increase within the first 500-m of the takeoff procedure, which is a result of the weathervane effect caused by the crosswind. While the nose of the aircraft rotates into the wind, the lateral velocity causes a lateral displacement in the negative $\hat{b}_y$ direction. Around 500-m into the takeoff procedure, left rudder is applied which results in a positive rudder deflection angle. The rudder application counteracts the weathervane effect such that the A380 can maintain a straight, consistent trajectory.

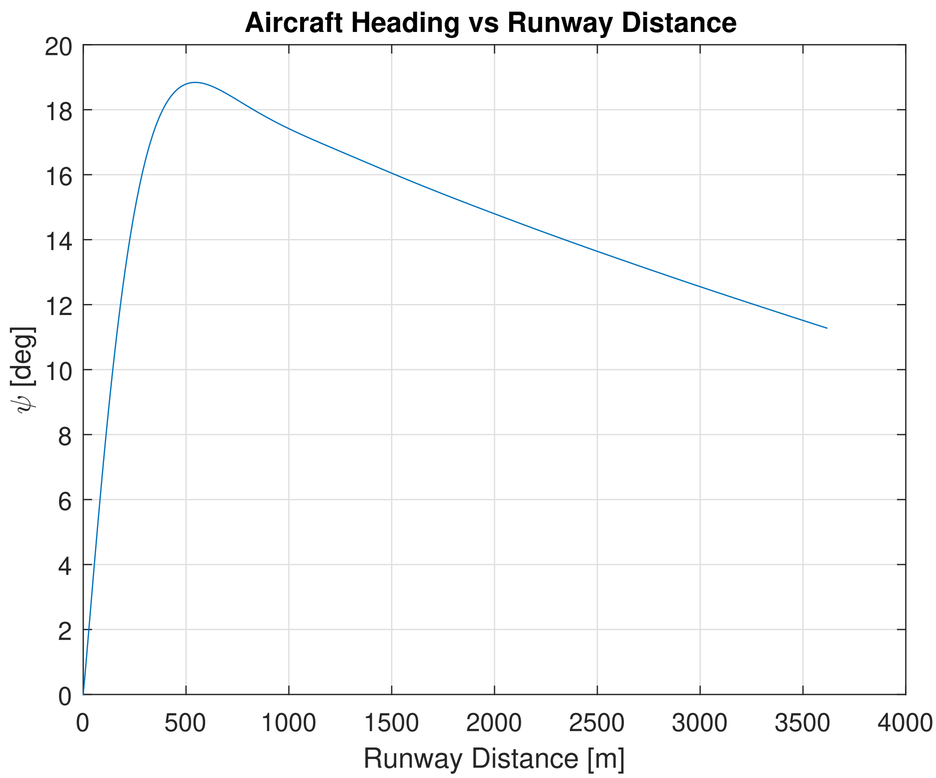

Figure 5.19: A380 heading angle over runway distance

In addition to the aircraft heading angle, the nose wheel and rudder deflection angles are presented in Fig. 5.20 on pg. 56. By convention, the nose wheel and rudder in the analysis are coupled and have positive deflection angles to counteract the weathervane effect. Moreover, the trends for both deflection angles are quite similar due to the calculation of the rudder deflection angle (refer to Eq. (5.22) on pg. 49). Moreover, the fairly consistent rudder actuation between 2000-m and 3500-m prevents the aircraft from over rotating (due to the weathervane effect) and overshooting in the lateral direction.

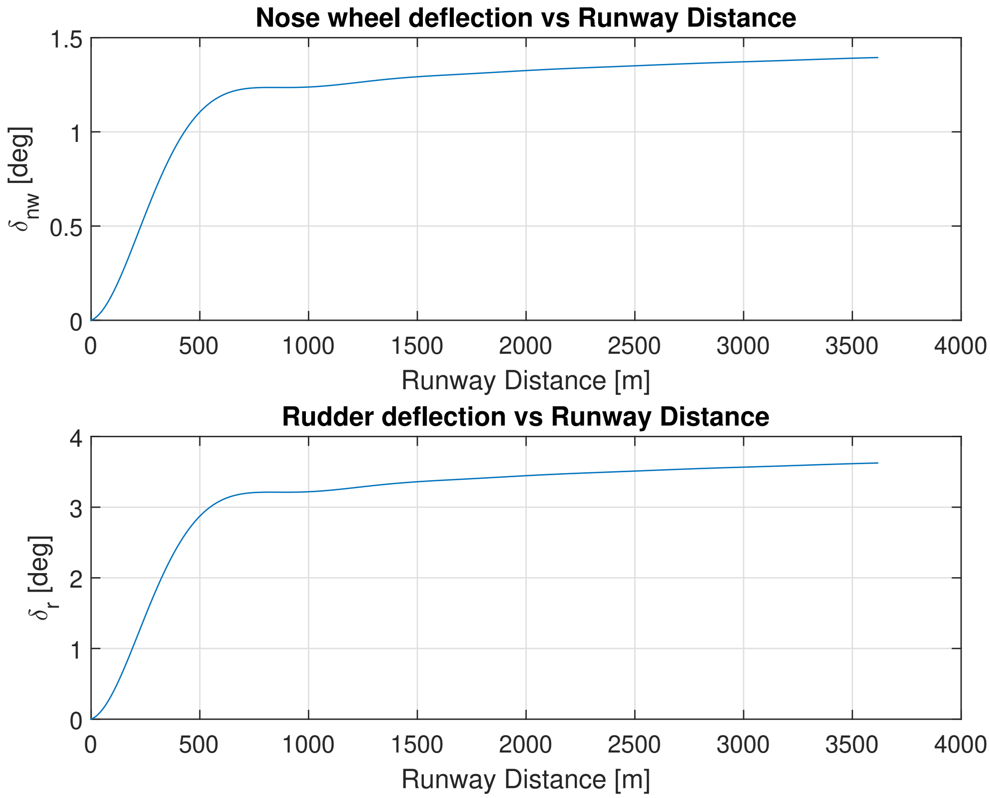

Figure 5.20: Nose wheel and rudder deflection angle in crosswind configuration

For visualization purposes, the orientation of the A380 is depicted in Fig. 5.21 on pg. 57, and is developed with existing MATLAB tools [39]. Similar to the heading angle shown in Fig. 5.19 on pg. 55, the weathervane effect due to the crosswind has a significant impact on the departing A380 especially at the beginning of the ground roll procedure (the weathervane effect is clearly illustrated in Fig. 5.22(a) on pg. 57). With the application of the rudder, as well as an increase in airspeed, the A380 corrects for the crosswind and avoids a lateral runway excursion. Moreover, the nose of the aircraft aligns closer to the runway centerline toward the end of the ground roll procedure (refer to Fig. 5.22(b) on pg. 57). Moreover, the maximum lateral displacement during the ground roll procedure was less than 5-meters, and the A380 successfully remained on the runway due to the rudder input (refer to Fig. 5.23 on pg. 58).

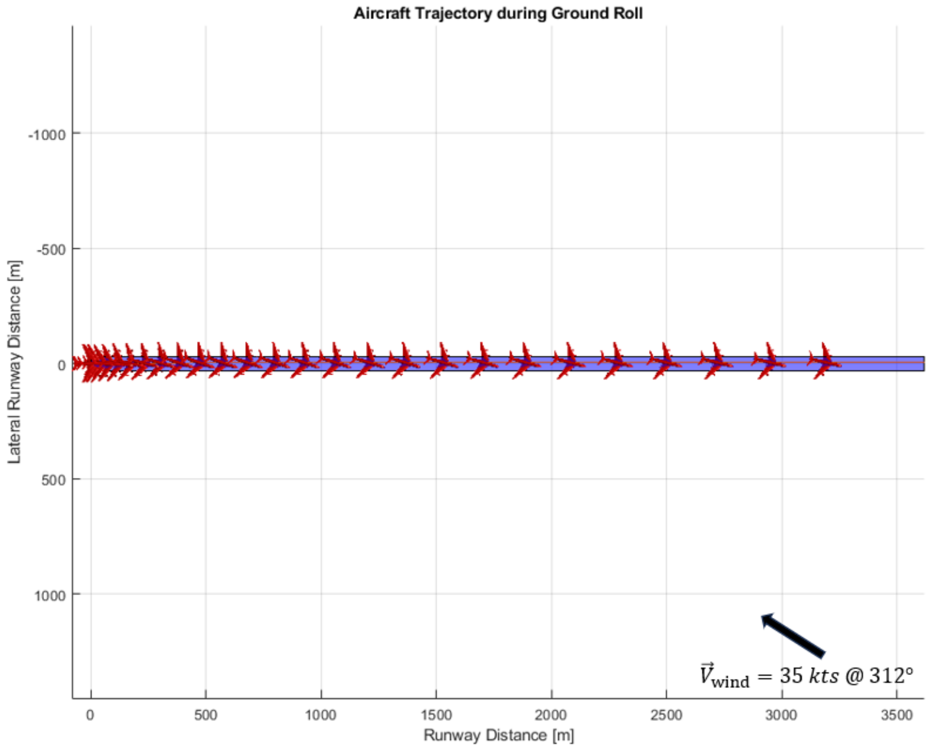

Figure 5.21: Trajectory of A380 in a crosswind configuration [39]

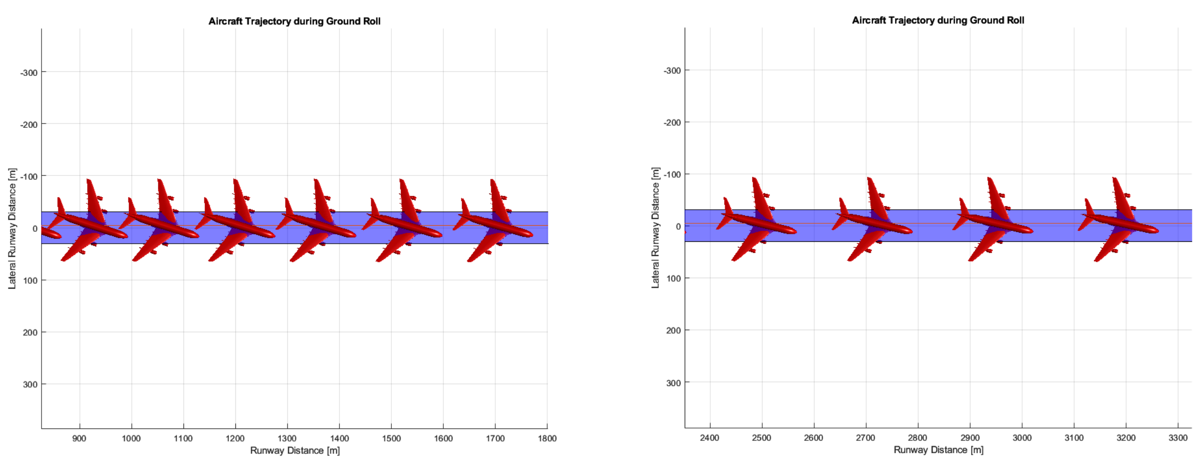

(a) One-third into ground roll procedure

(b) End of ground roll procedure

Figure 5.22: Beginning and end of ground roll procedure [39]

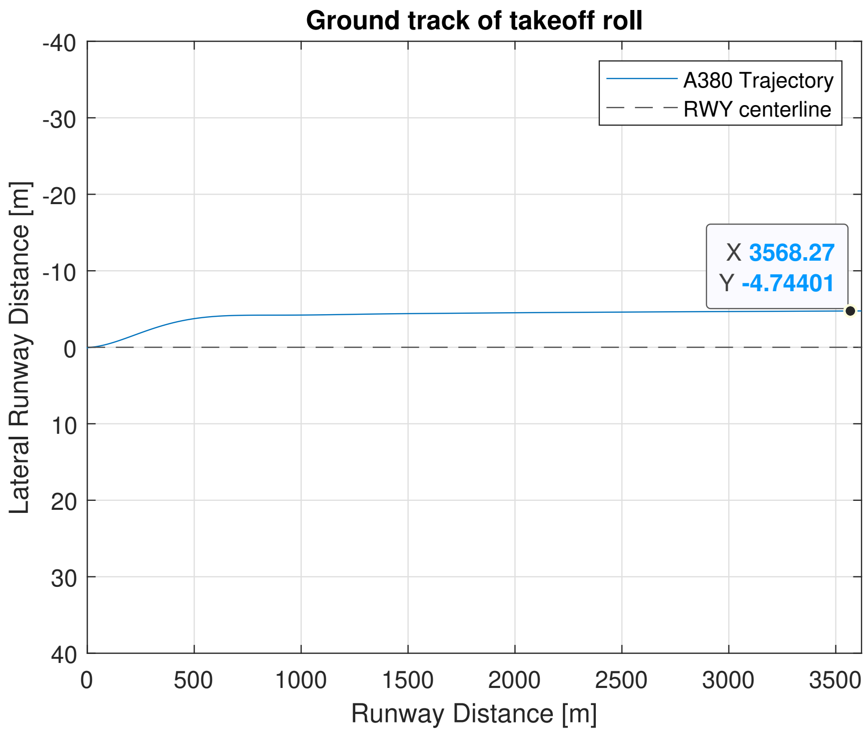

Figure 5.23: Lateral deviation from runway centerline

Lastly, both the forward and lateral velocities were plotted over the entire ground roll procedure. For validation purposes, the average wind speed in the crosswind model was set to zero to simulate nominal conditions. Given the nominal takeoff speed and distance for an A380 is approximately 88 m/s at 2,900 m, respectively, the crosswind model under nominal conditions yielded a takeoff speed of approximately 93.7 m/s at 2,900 m (roughly 6% off from the 1-D baseline RTO speed model). Under the crosswind conditions specified in Section 5.2, the negative lateral velocity between 0 m and 1500 m is a result of the weathervane effect. However, the rudder actuation significantly reduces the lateral velocity, and the A380 does not have to reject the takeoff.

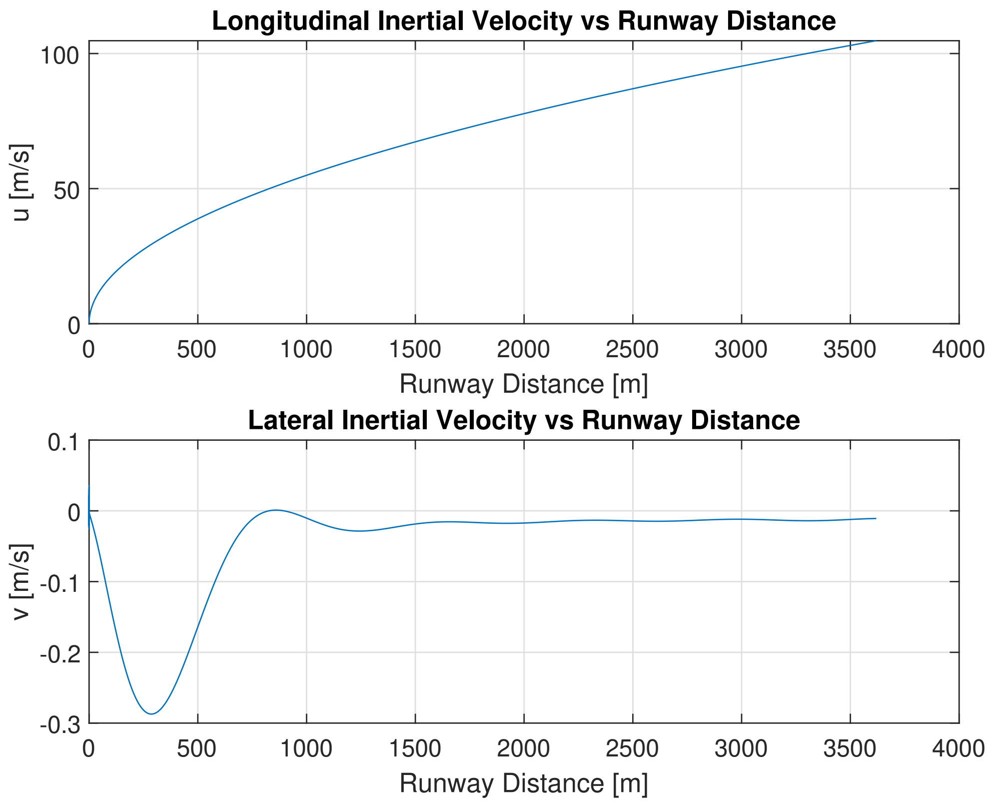

Figure 5.24: Longitudinal and lateral speed in crosswind configuration

Chapter 6: Conclusion and Future Work

The RTO speed of a commercial airliner, especially an A380-800, is a critical calculation that is determined before each departure to ensure the safety of passengers and flight crews and reduce the likelihood of catastrophic lateral and longitudinal runway excursions. In Chapter 2, the 1-D baseline RTO speed model was constructed to assess the validity of the RTO speed calculation. Moreover, the model was verified with readily accessible published data based on the nominal takeoff and landing distances considering airport conditions at KSFO [14, 26, 30]. Once verified, the 1-D environmental model discussed in Chapter 3 was integrated with the 1-D baseline model, and included both headwinds and tailwinds, as well as varying runway surface conditions. Moreover, the 1-D model was validated by comparing the takeoff and landing distances with respect to the location of the RTO speed, the sum of which was equivalent to the length of the runway - and hence the aircraft was able to reject the takeoff without overshooting the runway. In addition to aircraft geometry and performance specifications, thermodynamic properties, and airport information, several environmental factors such as pure headwinds, pure tailwinds, significant crosswinds, and runway surface conditions have a significant impact on the calculation of both the RTO speed V_1 and the location of the RTO speed S_1.

6.1 Future Work

In addition to the crosswind ground roll procedure, a 2-D sensitivity analysis, similar to the 1-D environmental model discussed in Chapter 3, can be applied to the 3-D model discussed in Chapter 5. To do this, a triple loop would be integrated with the existing crosswind model: one loop for the magnitude of the wind speed, another loop for the wind direction to account for the crosswind component, and the last loop to incorporate a key to toggles between dry, wet, and contaminated runway surface conditions. Regarding the NASA runway surface model discussed in Chapter 5, the results may be improved by conducting experiments on actual runway surfaces, with varying conditions, and applying empirical formulas to approximate the runway surface coefficients as a function of ground speed and sideslip angle. Regarding the gear submodel discussed in Section 5.3.5, the bogie wheels can be included for more realistic analysis. Lastly, additional work such as the development of a parametric model which can analyze a wide variety of aircraft, at several airports across the NAS, would be a beneficial tool in the preliminary stages of evaluating aircraft performance during the ground roll procedure. This would include storing various aircraft parameters, aircraft specifications, airport information, and historical METAR observations in a database (e.g., SQL) which the RTO speed model could reference. Future work should also include reaction times from pilots (e.g., human in the loop simulations) to simulate realistic responses.

References

[1] Maile, A. and Kelly, J., "Airport runway incidents have risen but serious close calls have decreased over 20 years: Federal Aviation Administration," *ABC News*, 2023, Retrieved on 2023-03-02, `https://abcnews.go.com/Politics/airport-runway-incidents-risen-close-calls-decreased-20/story?id=97358077#:~:text=The%20number%20of%20runway%20incursions,the%20987%20reported%20in%202002.`

[2] Marek, G., "SFO flight makes emergency landing after potential bird strike during takeoff," *SFGATE*, 2022, Retrieved on 2023-02-05, `https://www.sfgate.com/travel/article/sfo-flight-makes-emergency-landing-17607356.php`.

[3] Packard, J., "Bird strikes happening more while flying, but the Federal Aviation Administration (FAA) may have a solution," *News Channel 5: Nashville*, 2023, Retrieved on 2023-05-12, `https://www.newschannel5.com/bird-strikes-happening-more-while-flying-but-faa-may-have-a-solution#:~:text=An%20FAA%20study%20published%20in,electric%20or%20hydrogen%2Dpowered%20engines.`

[4] Moir, I. and Seabridge, A., *Aircraft Systems: Mechanical, electrical, and avionics subsystems integration*, chap. 1, John Wiley & Sons Ltd, Chichester, England, 3rd ed., 2008, pp. 38–44.

[5] Nelson, C., *Investigating the Airbus A380: Was it a success, failure, or combination?*, Master's thesis, Lundquist College of Business, 2020.

[6] White, W. J., "Takeoff Safety Training Aid," *FAA AC Document No. 120-62*, 1994.

[7] Hernandez, J., "The FAA is investigating a near-miss between two passenger planes at JFK airport," *npr*, 2023, Retrieved on 2023-02-15, `https://www.npr.org/2023/01/15/1149330980/jfk-delta-american-airlines-near-miss-faa-investigation#:~:text=The%20FAA%20is%20investigating%20a,planes%20at%20JFK%20airport%20%3A%20NPR&text=Tiny%20Desk-,The%20FAA%20is%20investigating%20a%20near%2Dmiss%20between%20two%20planes,York%20City%20airport%20Friday%20night.`

[8] Reid, C., "SWISS Airbus A320 Rejects Takeoff In Zurich Amid Engine Failure," *Simple Flying*, 2023, Retrieved on 2023-03-30, `https://simpleflying.com/swiss-airbus-a320-rejects-takeoff-engine-failure/`.

[9] Anderson, J. D., *Introduction to Flight*, chap. 6, McGraw-Hill, New York, 8th ed., 2016, pp. 522–531.

[10] Administration, F. A., "Wind Analysis," *Document No. AC 150/5300-13 CHG 6*, 2000.

[11] Castilho, D. S., Urbina, L. M., and de Andrade, A., "STPA for continuous controls: A flight testing study of aircraft crosswind takeoffs," *Safety Science*, Vol. 108, 2018, pp. 129–139.

[12] Edenhofer, O.and Pichs-Madruga, R. and Sokona, Y., *Climate Change 2014: Mitigation of Climate Change*, chap. 8, Cambridge University Press, United Kingdom, 2014, pp. 622–623.

[13] Koolstra, Herman J.and Huijbrechts, E.-J. A. M. and Mulder, J. A., "Analyzing Aircraft Controllability After Engine Failure During Takeoff in Adverse Weather Conditions," *Journal of Aircraft*, Vol. 56, No. 4, 2019, pp. 1330–1341.

[14] Airbus, "Aircraft Characteristics - Airport and Maintenance Planning," *Revision No. 17*, 2016.

[15] Huijbrechts, E.-J. A. M., Koolstra, H. J., and Mulder, J. A., "Using Vmcg-Limited V1, Controllability Issues on Contaminated Runways and in Crosswind," *Journal of Aircraft*, Vol. 56, No. 4, 2019, pp. 1342–1352.

[16] Jiang, Y., "Review on flight performance certification standard for wet and contaminated runway," *Procedia Engineering*, Vol. 17, Elsevier, 2011, pp. 7–12.

[17] Firdiyan, N. and Muntini, M., "The Effect of Rainfall on the Detection of Standing Water on Runway," *Journal of Physics*, Vol. 1951, No. 1, 2021, pp. 1–13.

[18] Zhu, Y., Wang, J., Chen, Y., and Wu, Y., "Calculation of Takeoff and Landing Performance under different Environments," *International Journal of Modern Physics*, Vol. 42, No. 1660174, 2016, pp. 1–12.

[19] Xiang, X., Zhang, S., and Xie, L., "Research on Calculation for Rejected Takeoff Distance of Civil Aircraft on Wet and Contaminated Runway," *IPEC*, 2022, pp. 60–63.

[20] Curry, D. C., *Estimation of Real-Time Runway Surface Contamination Using Flight Data Recorder Parameters*, Master's thesis, Embry-Riddle Aeronautical University, 2013.

[21] Anupam, K.and Santosh, S., Kasbergen, C., Scarpas, A., and Kane, M., "Finite Element Framework for the Computation of Runway Friction of Aircraft Tires," *Transportation Research Record*, Vol. 2641, No. 1, 2017, pp. 126–138.

[22] Yager, T. and Mccarty, J., "Friction characteristics of three 30 by 11.5-14.5, type 8, aircraft tires with various tread groove patterns and rubber compounds," *NASA*, 1977.

[23] Hedayati, R. and Sadighi, M., *Bird Strike : An Experimental, Theoretical and Numerical Investigation*, chap. 1,3, Woodhead Publishing, Cambridge, 1st ed., 2016, pp. 1–2, 35–45.

[24] Maaz, M. A., "How Hot And High Conditions Affect Aircraft Takeoffs And Landings," *Simple Flying*, 2022, Retrieved on 2023-02-12, `https://simpleflying.com/how-hot-and-high-conditions-affect-aircraft-take-offs-and-landings/#:~:text=When%20it%20comes%20to%20landing,with%20the%20correct%20glide%20path`.

[25] Carpenter, B. T., "An Overview and Analysis of the Impacts of Extreme Heat on the Aviation Industry," *The Journal of Undergraduate Research at The University of Tennessee*, Vol. 9, No. 1, 2019, pp. 3.

[26] Airbus, "Airbus A380 Facts and Figures," *Airbus*, 2021.

[27] Lomax, H., Pulliam, T., and Zingg, D., *Fundamentals of Computational Fluid Dynamics*, chap. 6, Springer-Verlag Berlin Heidelberg, New York, 1st ed., 2001, p. 83.

[28] Speidel, D. J., "Airfield Marking Handbook," *Report IPRF 01-G-002-05-1*, 2008.

[29] Herzmann, D., editor, *Iowa Environmental Mesonet ASOS Network*, Iowa State University, 2023.

[30] Administration, F. A., "Airport Master Record," *FAA Document No. OMB 2120-0015*, 2022.

[31] Clark, A. W., *Predicting the Crosswind Performance of High Bypass Ratio Turbofan Engine Inlets*, Master's thesis, The Ohio State University, 2016.

[32] Schwarz, D., "Fast and Robust Curve Intersections," *MATLAB Central File Exchange*, 2023.

[33] MATLAB, *version 9.13.0.2105380 (R2022b)*, The MathWorks Inc., Natick, Massachusetts, 2022.

[34] Skilling, T., "Shouldn't air pressure in Denver be much lower than it is in Chicago?" *Chicago Tribune*, 2017, Retrieved on 2023-04-25, `https://www.chicagotribune.com/weather/ct-wea-asktom-0522-20170521-column.html`.

[35] Fink, R., "USAF Stability and Control DATCOM," *McDonnell Douglas Corporation, Douglas Aircraft Division,, for the Flight Controls Division, Air Force Flight Dynamics Laboratory, Wright-Patterson AFB*, 1978.

[36] Heffley, R. and Jewell, W. F., "Aircraft Handling Qualities," 1972.

[37] Hunter, J. M., *Aerospace Vehicle Dynamics and Control*, chap. 2, San Jose State University, NCalifornia, 2021, pp. 8–11.

[38] Sahrun, S., "drawDATCOMaircraft," *MATLAB Central File Exchange*, 2023.

[39] Scordamaglia, V., "Trajectory and Attitude Plot Version 3," *MATLAB Central File Exchange*, 2023.

Appendix A: Baseline RTO Speed Code

```
clear
clc
close
% James D. Gonzalez III
% Dr. Lombaerts

% Goal of the Project:
% Calculate the maximum rejected takeoff speed (also known as V1) and the
% corresponding position the furthest along the runway from where an Airbus
% A380 with MTWO can still safely come to a full standstill before it runs
% over the end of runway 28R at KSFO. Consider a baseline model with no
% headwind or tailwind, and assume standing rolling friction coefficients.

% Subscripts:
% TO   == Takeoff
% L    == Landing
% pub  == Published data
% MTOW == Maximum Takeoff Weight

% Published data:
V_TO_pub = 170;                 % High-end of published takeoff speed for A380
 [knots]
V_TO_pub = V_TO_pub*0.51444;    % High-end of published takeoff speed for A380
 [m/s]
V_L_pub  = 138;                 % Published landing speed for A380 [knots]
V_L_pub  = V_L_pub*0.51444;     % Published landing speed for A380 [m/s]
%l_TO     = 2900;                % Takeoff distance for an Airbus A380 [m]
%l_L      = 2150;                % Landing distance for an Airbus A380 [m]

% KSFO Airport Information:
l_28R = 3618;                   % Length of the runway 29R at KSFO [m]
rho_air =1.225;                % Density of air at sea-level conditions [kg/
m^3].
%%%%%%%%%%%%%%%%%%%%%%%%%%%%%%%%%%%%%%%%%%%%%%%%%%%%%%%%%%%%%%%%%%%%%%%%%%%%%%
%%%%%%%%%%%%%%%%%%%%%%%%%%%%%%%%%%%%%%%%%%%%%%%%%%%%%%%%%%%%%%%%%%%%%%%%%%%%%%
%%%%%%%%%%%%%%%%%%%%%%%%%%%%%%%%%%%%%%%%%%%%%%
% Variables:
u_r_TO = 0.02;                  % Normal coefficient of rolling friction for
 (takeoff conditions) [-]
%u_r_TO = 0.0;
u_r_L = 0.067;                  % Coefficient of rolling friction while
 braking (landing conditions) [-]
%u_r_L = 0.067;
V_wind = 0;                     % Wind speed (+ for headwind; - for tailwind)
 [knots]
V_wind = V_wind*0.51444;        % Wind speed [m/s]
%%%%%%%%%%%%%%%%%%%%%%%%%%%%%%%%%%%%%%%%%%%%%%%%%%%%%%%%%%%%%%%%%%%%%%%%%%%%%%
%%%%%%%%%%%%%%%%%%%%%%%%%%%%%%%%%%%%%%%%%%%%%%%%%%%%%%%%%%%%%%%%%%%%%%%%%%%%%%
%%%%%%%%%%%%%%%%%%%%%%%%%%%%%%%%%%%%%%%%%%%%%%%

% Aircraft weight, engine, and geometric information:
```

```
% https://www.airbus.com/sites/g/files/jlcbta136/files/2021-12/EN-Airbus-A380-
Facts-and-Figures-December-2021_0.pdf
g_0 = 9.80665;                  % Acceleration due to gravity at sea-level [m/
s^2]
M_MTOW = 575000;                % Maximum takeoff mass [kg]
W_MTOW = M_MTOW*g_0;            % Maximum takeoff weight (MTOW) [N]
Wfuel = 253.983e3*g_0;          % Fuel capacity [N]
Wzerofuel = W_MTOW - Wfuel;     % Max zero fuel weight [N]
T_max = 0.704*4*348e3;          % Total/max thrust for all four engines [N]
T_rev = T_max*.15;              % Maximum reverse thrust (i.e. 15% of maximum
 thrust) [N]
h_wingtip = 7.8;                % Height of wingtip above the ground [m]
b = 79.75;                      % Wingspan [m]
S = 845;                        % Total wing surface area [m^2]
AR = (b^2)/S;                   % The aspect ratio [-]
e1 = 0.90;                      % Span efficiency coefficient [-]

% Aircraft aerodynamic properties:
CL_TO = W_MTOW/(0.5*rho_air*V_TO_pub^2*S);                   % Maximum lift
 coefficient in takeoff configuration [-]
CL_L = (Wzerofuel)/(0.5*rho_air*V_L_pub^2*S);                % Maximum lift
 coefficient in landing configuration [-]
CD0_TO = 0.013;                                              % Parasitic drag
 coefficient at takeoff [-]
CD0_L = 1.1*CD0_TO;                                          % Parasitic drag
 coefficient with spoilers deployed [-]

% Step 1: Calculate the total drag coefficient for both takeoff and landing
 profiles:
phi = ((16*(h_wingtip)/b)^2)/(1+((16*(h_wingtip)/b)^2));    % Ground effect
 factor [-]
CD_TO = (CD0_TO + phi*CL_TO^2/(pi*e1*AR));                   % Total drag
 coefficient for the takeoff profile [-]
CD_L = CD0_L;                                                % Total drag
 coefficient for the landing profile. Note, the induced drag component is zero
 because the spoilers are deployed, which destroys the lift over the wings [-]

% Step 2: Using double integration over time, determine the takeoff profile

% First, initialize the parameters for the takeoff roll:
i = 1;                                                       % First index,
 terms evaluated at x = 0 m [-]
% Perhaps something to consider in the future, is s_TO evaluated at the
% center of mass? Or, does it not matter?
s_TO(i)  = 0;                                                % Initial distance
 of the A380 [m]
V_TO(i)  = 0;                                                % Initial ground
 speed of the A380 [m/s]
L_TO(i) = CL_TO*0.5*rho_air*(V_TO(i)+V_wind)^2*S;            % Initial lift
 evaluated at x = 0 m [N]
D_TO(i) = CD_TO*0.5*rho_air*(V_TO(i)+V_wind)^2*S;            % Initial drag
 evaluated at x = 0 m [N]
Feff_TO(i) = T_max - (D_TO(i) + u_r_TO*(W_MTOW - L_TO(i))); % Effective force
 evaluated at x = 0 m [N]
```

```
disp(W_MTOW-L_TO(i))
a_TO(i) = g_0/W_MTOW*Feff_TO(i); % Acceleration evaluated at x = 0, using
 Newton's Second Law of motion [m/s^2]

dt = 0.1; % Select a time step for the numerical method [s]

% Set up the integration loop for the takeoff profile. Apply the explicit
 Euler method:
% Explicit Euler Method: u_{n+1} = u_{n} + dt*u'_{n} pg. 83 Lomax, Pulliam,
% Zingg

 while s_TO < l_28R
    i = i+1; % Move to next time step [-]
    V_TO(i) = V_TO(i-1) + dt*a_TO(i-1);                         % Calculate
 the velocity at the next time step [m/s]
    s_TO(i) = s_TO(i-1) + dt*V_TO(i-1);                         % Calculate
 the position along runway at the next time step [m]
    L_TO(i) = CL_TO*0.5*rho_air*(V_TO(i)+V_wind)^2*S;           % Initial lift
 evaluated at the next time step [N]
    D_TO(i) = CD_TO*0.5*rho_air*(V_TO(i)+V_wind)^2*S;           % Initial drag
 evaluated at the next time step [N]
    Feff_TO(i) = T_max - (D_TO(i) + u_r_TO*(max([(W_MTOW - L_TO(i)) 0]))); %
 Effective force evaluated at the next time step [N]
    a_TO(i) = g_0/W_MTOW*Feff_TO(i);                            % Acceleration
 evaluated at the next time step, using Newton's Second Law of motion [m/s^2]
 end

% Step 3: Using double integration over time, determine the landing profile
% First, initialize the parameters for landing (MTOW)
i = 1;                                                                  %
 First index, terms evaluated at x = 0 m [-]
s_L_MTOW(i)  = 0;                                                       %
 Initial distance of the A380 [m]
V_L_MTOW(i)  = 0;                                                       %
 Initial ground speed of the A380 [m/s]
L_L_MTOW(i) = 0;                                                        % Will
 not contribute, as the spoilers are deployed [N]
D_L_MTOW(i) = CD_L*0.5*rho_air*(V_L_MTOW(i)+V_wind)^2*S;                %
 Initial drag evaluated at x = 0 m [N]
Feff_L_MTOW(i) = T_rev + (D_L_MTOW(i) + u_r_L*(W_MTOW - L_L_MTOW(i)));  %
 Effective force evaluated at x = 0 m [N]
a_L_MTOW(i) = g_0/W_MTOW*Feff_L_MTOW(i);                                %
 Acceleration evaluated at x = 0, using Newton's Second Law of motion [m/s^2]

while s_L_MTOW < l_28R
    i = i+1;
    V_L_MTOW(i) = V_L_MTOW(i-1)+a_L_MTOW(i-1)*dt;
    s_L_MTOW(i) = s_L_MTOW(i-1)+V_L_MTOW(i-1)*dt;
    L_L_MTOW(i) = 0;%CL_L*0.5*rho_air*(V_L_MTOW(i)+V_wind)^2*S;
      % spoilers deployed!
    D_L_MTOW(i) = CD_L*0.5*rho_air*(V_L_MTOW(i)+V_wind)^2*S;
    Feff_L_MTOW(i) = T_rev + D_L_MTOW(i) + u_r_L*(W_MTOW);%-0*L_L_MTOW(i));
    a_L_MTOW(i) = g_0/W_MTOW*Feff_L_MTOW(i);
end
```

```
% Step 4: Using double integration over time, determine the landing profile

% First, initialize the parameters for landing (W_zerofuel)

i = 1;
              % First index, terms evaluated at x = 0 m [-]
s_L_Wzerofuel(i)  = 0;
              % Initial distance of the A380 [m]
V_L_Wzerofuel(i)  = 0;
              % Initial ground speed of the A380 [m/s]
L_L_Wzerofuel(i) = 0;
              % Will not contribute, as the spoilers are deployed [N]
D_L_Wzerofuel(i) = CD_L*0.5*rho_air*(V_L_Wzerofuel(i)+V_wind)^2*S;
              % Initial drag evaluated at x = 0 m [N]
Feff_L_Wzerofuel(i) = T_rev + (D_L_Wzerofuel(i) + u_r_L*(Wzerofuel -
 0*L_L_Wzerofuel(i)));  % Effective force evaluated at x = 0 m [N]
a_L_Wzerofuel(i) = g_0/Wzerofuel*Feff_L_Wzerofuel(i);
               % Acceleration evaluated at x = 0, using Newton's Second Law of
 motion [m/s^2]

while s_L_Wzerofuel < l_28R
    i = i+1;
    V_L_Wzerofuel(i) = V_L_Wzerofuel(i-1)+a_L_Wzerofuel(i-1)*dt;
    s_L_Wzerofuel(i) = s_L_Wzerofuel(i-1)+V_L_Wzerofuel(i-1)*dt;

    L_L_Wzerofuel(i) = CL_L*1/2*rho_air*V_L_Wzerofuel(i)^2*S; % spoilers
 deployed!
    D_L_Wzerofuel(i) = CD_L*1/2*rho_air*V_L_Wzerofuel(i)^2*S;
    Feff_L_Wzerofuel(i) = T_rev + D_L_Wzerofuel(i) +
 u_r_L*(Wzerofuel-0*L_L_Wzerofuel(i));
    a_L_Wzerofuel(i) = g_0/Wzerofuel*Feff_L_Wzerofuel(i);
end

% Apply intersection function [1]
[S_1,V_1,c,d] = intersections(s_TO,V_TO+V_wind,(l_28R-s_L_MTOW),V_L_MTOW
+V_wind,true);

% Determine required runway for takeoff given the takeoff velocity profile
% and V_TO_pub
V_TO_pub_array = V_TO_pub*ones(1,length(V_TO));
% Apply intersection function [1]
[S_TO_RWYUsed,V_TO_check,e,f] = intersections(s_TO,V_TO
+V_wind,s_TO,V_TO_pub_array);

V_L_pub_array = V_L_pub*ones(1,length(V_L_MTOW));
% Apply intersection function [1]
if max(V_L_MTOW+V_wind) < V_L_pub
    S_L_RWYUsed = NaN;
    V_L_check = NaN;
else
    [S_L_RWYUsed,V_L_check,g,h] = intersections((l_28R-s_L_MTOW),V_L_MTOW
+V_wind,(l_28R-s_L_MTOW),V_L_pub_array);
```

```
end

V_L_pub_Wzero_array = V_L_pub*ones(1,length(V_L_Wzerofuel));
% Apply intersection function [1]
if max(V_L_Wzerofuel+V_wind) < V_L_pub
    S_L_RWYUsed_Wzerofuel = NaN;
    V_L_check_Wzerofuel = NaN;
else
    [S_L_RWYUsed_Wzerofuel,V_L_check_Wzerofuel,t,y] =
 intersections((l_28R-s_L_Wzerofuel),V_L_Wzerofuel+V_wind,(l_28R-
s_L_Wzerofuel),V_L_pub_Wzero_array);
end


% Step 5: Combine all three velocity profiles together:
figure
% Plot the Ground speed vs. runway used:
plot(s_TO,V_TO+V_wind,'b')
hold on
plot((l_28R-s_L_MTOW),V_L_MTOW+V_wind,'r')
plot(l_28R-s_L_Wzerofuel,V_L_Wzerofuel+V_wind,'r--')
%plot(l_28R-s_L_Wzerofuel,V_L_Wzerofuel+V_wind,'r--')
%xline(S_TO_RWYUsed,'k--')
txt_LO = 'Takeoff speed'; % Add text to curve.
text(1300,90,txt_LO)
txt_LO = 'Landing speed'; % Add text to curve.
text(50,67,txt_LO)
plot(S_1,V_1,'g*') % V1, depicted on the plot.
plot(S_TO_RWYUsed,V_TO_check,'b*') % V_TO, depicted on the plot.
%plot(S_L_RWYUsed,V_L_check,'c*')
plot(S_L_RWYUsed_Wzerofuel,V_L_check_Wzerofuel,'r*')
% Plot the runway
plot([0 l_28R], [0 0],'k',LineWidth=2)
yline(V_TO_pub,'k--')  % Nominal takeoff speed
yline(V_L_check,'k--') % Nominal landing speed
xlim([0,l_28R+100])
ylim([0,100])
xlabel('Runway used [m]')
ylabel('Airspeed [m/s]')
title('Baseline Rejected Takeoff Speed')
V_1_str = sprintf('V_{1} = %3.1f m/s @ %3.0f m',V_1,S_1); % String to note the
 value for V1 in the legend.
V_TO_str = sprintf('V_{TO,pub} = %3.1f m/s @ %3.0f
 m',V_TO_check,S_TO_RWYUsed); % String to note the value for V1 in the legend.
%V_L_str = sprintf('V_{L} = %3.1f m/s @ %3.0f m',V_L_check,S_L_RWYUsed);%
 String to note the value for V1 in the legend.
V_L_str = sprintf('V_{L,pub} = %3.1f m/s @ %3.0f
 m',V_L_check_Wzerofuel,S_L_RWYUsed_Wzerofuel);% String to note the value for
 V1 in the legend.
%legend ({'Velocity takeoff with W_{MTOW}','Max V to stop with W_{MTOW}','Max
 V to stop with W_{1}',V_1_str,V_TO_str,V_L_str},'Location','south')
legend ({'Velocity takeoff with W_{MTOW}','Max V to stop with W_{MTOW}','Max V
 to stop with W_{1}',V_1_str,V_TO_str,V_L_str},'Location','south')
grid on
```

```
% Plot the Lift and Drag Profiles:
figure
plot(V_TO,L_TO)
hold on
plot(V_TO,D_TO)
plot(V_L_MTOW,L_L_MTOW)
plot(V_L_MTOW,D_L_MTOW)
%ylim([0,8E6])
grid on
yline(W_MTOW,'k--','Max. takeoff weight')
%yline(Wzerofuel,'k--','Zero fuel weight')
xlabel('Airspeed [m/s]')
ylabel('Aero Forces [N]')
title('Aerodynamic forces vs. airspeed')
legend('L_{TO}','D_{TO}','L_{L}','D_{L}','Location','northwest','NumColumns',2)

% References:

% [1] Douglas Schwarz (2022). Fast and Robust Curve Intersections (https://
www.mathworks.com/matlabcentral/fileexchange/11837-fast-and-robust-curve-
intersections), MATLAB Central File Exchange. Retrieved November 28, 2022.
% https://www.mathworks.com/matlabcentral/fileexchange/11837-fast-and-robust-
curve-intersection
%-----------------------------------------------------------------------------------------
```

5.6388e+06

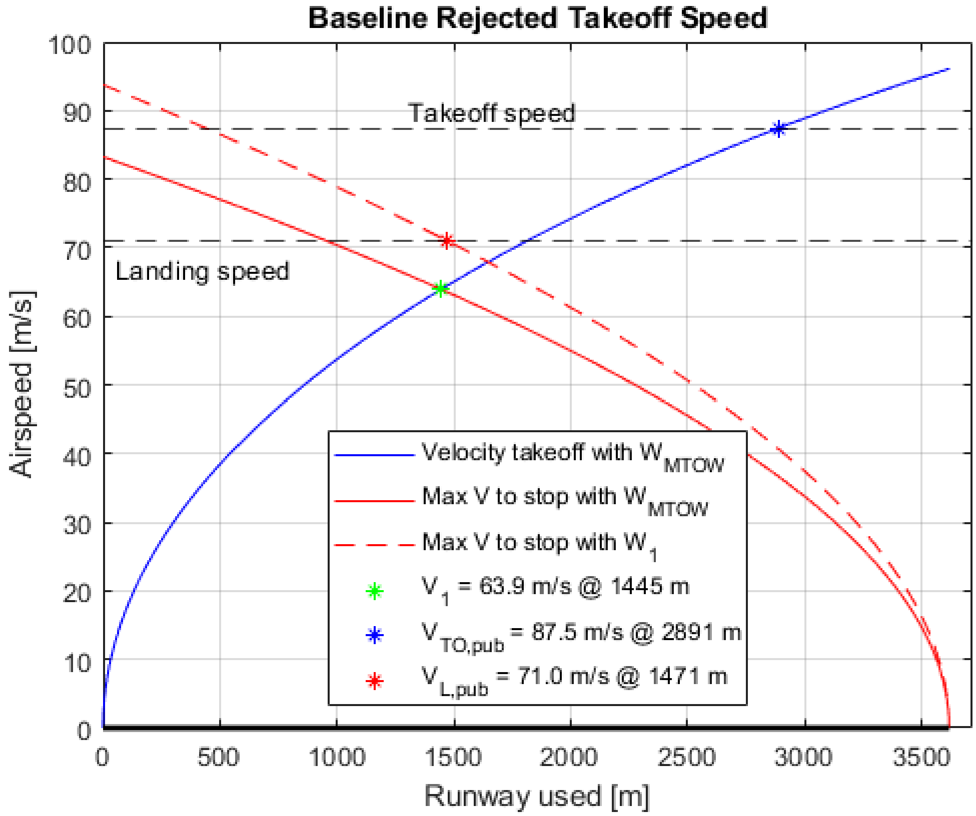

Baseline Rejected Takeoff Speed
Takeoff speed
Landing speed
Velocity takeoff with W_MTOW
Max V to stop with W_MTOW
Max V to stop with W_1
V_1 = 63.9 m/s @ 1445 m
V_TO,pub = 87.5 m/s @ 2891 m
V_L,pub = 71.0 m/s @ 1471 m
Airspeed [m/s]
Runway used [m]

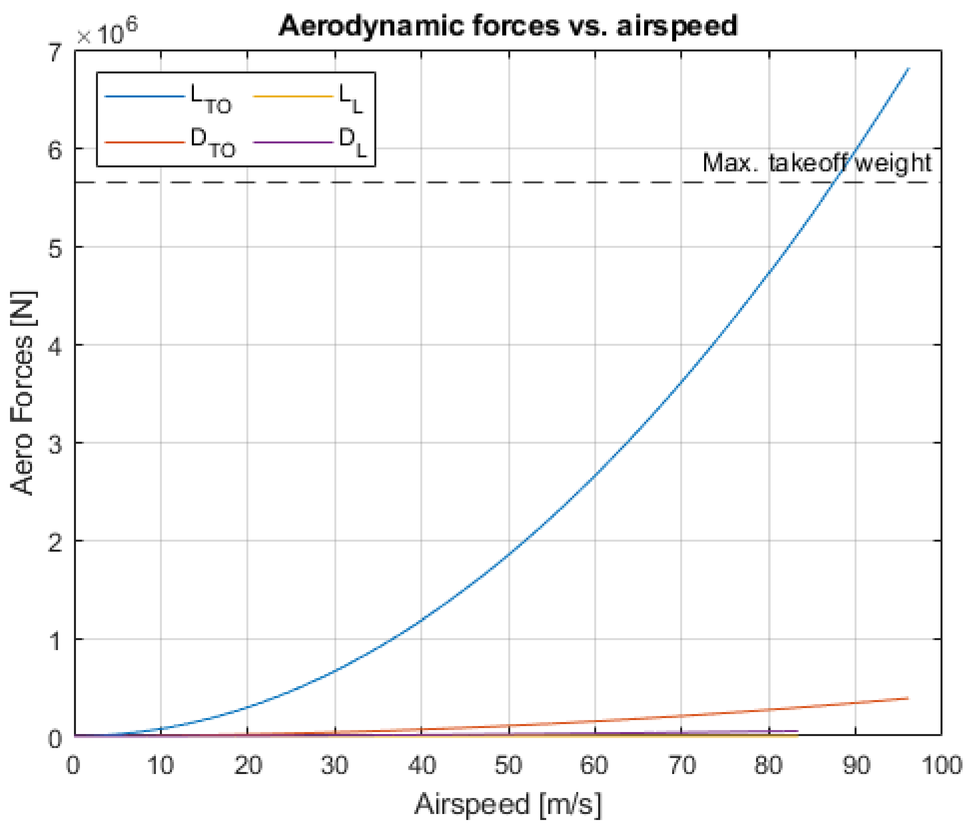

Aerodynamic forces vs. airspeed
×10^6
L_TO
L_L
D_TO
D_L
Max. takeoff weight
Aero Forces [N]
Airspeed [m/s]

Published with MATLAB® R2022b

Appendix B:
1D Environmental RTO Speed Code

```
clear
clc
% James D. Gonzalez III
% Dr. Lombaerts

% Goal of the Project:
% Calculate the maximum rejected takeoff speed (also known as V1) and the
% corresponding position the furthest along the runway from where an Airbus
% A380 with MTWO can still safely come to a full standstill before it runs
% over the end of runway 28R at KSFO. Consider a baseline model with no
% headwind or tailwind, and assume standing rolling friction coefficients.

% Subscripts:
% TO   == Takeoff
% L    == Landing
% pub  == Published data
% MTOW == Maximum Takeoff Weight

% Published data:
V_TO_pub = 170;
      % High-end of published takeoff speed for A380 [knots]
V_TO_pub = V_TO_pub*0.51444;
      % High-end of published takeoff speed for A380 [m/s]
V_L_pub  = 138;
      % Published landing speed for A380 [knots]
V_L_pub  = V_L_pub*0.51444;
      % Published landing speed for A380 [m/s]
l_TO     = 2900;
      % Takeoff distance for an Airbus A380 [m]
l_L      = 2150;
      % Landing distance for an Airbus A380 [m]

% KSFO Airport Information:
l_28R = 3618;
      % Length of the runway 29R at KSFO [m]
rho_air = 1.225;
      % Density of air at sea-level conditions [kg/m^3].
g_0 = 9.80665;
      % Acceleration due to gravity at sea-level [m/s^2]
%%%%%%%%%%%%%%%%%%%%%%%%%%%%%%%%%%%%%%%%%%%%%%%%%%%%%%%%%%%%%%%%%%%%%%%%%%%%%%%%%%
%%%%%%%%%%%%%%%%%%%%%%%%%%%%%%%%%%%%%%%%%%%%%%%%%%%%%%%%%%%%%%%%%%%%%%%%%%%%%%%%%%
%%%%%%%%%%%%%%%%%%%%%%%%%%%%%%%%%%%%%%%%%%%%%%%%%
% User Inputs:
%u_r_TO = 0.02
      % Normal friction coefficient for a smooth paved runway.
u_r_TO = linspace(0.02/2,0.02,50);
      % Normal coefficient of rolling friction for (takeoff conditions) [-]s
u_r_L = linspace(0.067/2,0.067,50);
      % Coefficient of rolling friction while braking (landing conditions) [-]
V_wind = linspace(-3.3*1.50,16.45*1.50,75);
      % Wind speed (+ for headwind; - for tailwind) [knots]
% Convert the wind speed to appropriate units: [m/s]
```

```
V_wind = V_wind*0.51444;
      % Wind speed [m/s]
%%%%%%%%%%%%%%%%%%%%%%%%%%%%%%%%%%%%%%%%%%%%%%%%%%%%%%%%%%%%%%%%%%%%%%%%%%%%%%%%
%%%%%%%%%%%%%%%%%%%%%%%%%%%%%%%%%%%%%%%%%%%%%%%%%%%%%%%%%%%%%%%%%%%%%%%%%%%%%%%%
%%%%%%%%%%%%%%%%%%%%%%%%%%%%%%%%%%%%%%%%%%%%%%%%%%

% Aircraft weight, engine, and geometric information:
M_MTOW = 575000;
      % Maximum takeoff mass [kg]
W_MTOW = M_MTOW*g_0;
      % Maximum takeoff weight (MTOW) [N]
Wfuel = 253.983e3*g_0;
      % Fuel capacity [N]
Wzerofuel = W_MTOW - Wfuel;
      % Max zero fuel weight [N]
T_max = 0.704*4*348e3;
      % Total/max thrust for all four engines [N]
T_rev = T_max*.15;
      % Maximum reverse thrust (i.e. 15% of maximum thrust) [N]
h_wingtip = 7.8;
      % Height of wingtip above the ground [m]
b = 79.75;
      % Wingspan [b]
S = 845;
      % Total wing surface area [m^2]
AR = (b^2)/S;
      % The aspect ratio [-]
e1 = 0.90;
      % Span efficiency coefficient [-]

% Aircraft aerodynamic properties:
CL_TO = W_MTOW/(0.5*rho_air*V_TO_pub^2*S);
      % Maximum lift coefficient in takeoff configuration [-]
% When we calculate V1, would the lift coefficient for the landing profile
% also include W_MTOW???

%CL_L = (Wzerofuel)/(0.5*rho_air*V_L_pub^2*S);
      % Maximum lift coefficient in landing configuration [-]
% Talk with Dr. Lombaerts about WzeroFuel and WMTOW?
CL_L = (Wzerofuel)/(0.5*rho_air*V_L_pub^2*S);
      % Maximum lift coefficient in landing configuration [-]

CD0_TO = 0.013;
      % Parasitic drag coefficient at takeoff [-]
CD0_L = 1.1*CD0_TO;
      % Parasitic drag coefficient with spoilers deployed [-]

% Step 1: Calculate the total drag coefficient for both takeoff and landing
 profiles:
phi = ((16*(h_wingtip)/b)^2)/(1+((16*(h_wingtip)/b)^2));
      % Ground effect factor [-]
CD_TO = (CD0_TO + phi*CL_TO^2/(pi*e1*AR));
      % Total drag coefficient for the takeoff profile [-]
```

```
CD_L = CD0_L;
      % Total drag coefficient for the landing profile. Note, the induced drag
 component is zero because the spoilers are deployed, which destroys the lift
 over the wings [-]

% Initialize variables for storage:
S_1 = zeros(length(u_r_TO),length(V_wind));
V_1 = zeros(length(u_r_TO),length(V_wind));

% Introduce double for loop for runway surface and wind speed:
for j = 1:length(u_r_TO)
    for o = 1:length(V_wind)
        % Step 2: Using double integration over time, determine the takeoff
 profile
        % First, initialize the parameters for the takeoff roll:
        i = 1;
      % First index, terms evaluated at x = 0 m [-]
        s_TO(i)  = 0;
      % Initial distance of the A380 [m]
        V_TO(i)  = 0;
      % Initial ground speed of the A380 [m/s]
        L_TO(i) = CL_TO*0.5*rho_air*(V_TO(i)+V_wind(o))^2*S;
      % Initial lift evaluated at x = 0 m [N]
        D_TO(i) = CD_TO*0.5*rho_air*(V_TO(i)+V_wind(o))^2*S;
      % Initial drag evaluated at x = 0 m [N]
        Feff_TO(i) = T_max - (D_TO(i) + u_r_TO(j)*(max([(W_MTOW - L_TO(i))
 0])));              % Effective force evaluated at x = 0 m [N]
        a_TO(i) = g_0/W_MTOW*Feff_TO(i);
       % Acceleration evaluated at x = 0, using Newton's Second Law of motion
 [m/s^2]
        dt = 0.1; % Select a time step for the numerical method [s]

    % Set up the integration loop for the takeoff profile. Apply the explicit
 Euler method:
    % Explicit Euler Method: u_{n+1} = u_{n} + dt*u'_{n} pg. 83 Lomax,
 Pulliam,
    % Zingg

        while s_TO(i) < l_28R
            i = i+1; % Move to next time step [-]
            % Given acceleration, integrate to find velocity:
            V_TO(i) = V_TO(i-1) + dt*a_TO(i-1);
      % Calculate the ground speed at the next time step [m/s]
            % Given velocity, integrate to find position
            s_TO(i) = s_TO(i-1) + dt*V_TO(i-1);
      % Calculate the position along runway at the next time step [m]
            % Calculate new lifting force given current velocity
            L_TO(i) = CL_TO*0.5*rho_air*(V_TO(i)+V_wind(o))^2*S;
      % Initial lift evaluated at the next time step [N]
            % Calculate new drag force given current velocity
            D_TO(i) = CD_TO*0.5*rho_air*(V_TO(i)+V_wind(o))^2*S;
      % Initial drag evaluated at the next time step [N]
            % Select engine out at 1/4 of RWY distance, for example
            % If statement here for engine failure; T_max*1/2
```

```
            Feff_TO(i) = T_max - (D_TO(i) + u_r_TO(j)*(max([(W_MTOW - L_TO(i))
 0])));          % Effective force evaluated at the next time step [N]
            a_TO(i) = g_0/W_MTOW*Feff_TO(i);
       % Acceleration evaluated at the next time step, using Newton's Second
 Law of motion [m/s^2]
        end

        % Step 3: Using double integration over time, determine the landing
 profile
        % First, initialize the parameters for landing (MTOW)
        i = 1;
      % First index, terms evaluated at x = 0 m [-]
        s_L_MTOW(i)  = 0;
      % Initial distance of the A380 [m]
        V_L_MTOW(i)  = 0;
      % Initial ground speed of the A380 [m/s]
        L_L_MTOW(i) = 0;
      % Will not contribute, as the spoilers are deployed [N]
        D_L_MTOW(i) = CD_L*0.5*rho_air*(V_L_MTOW(i)+V_wind(o))^2*S;
      % Initial drag evaluated at x = 0 m [N]
        Feff_L_MTOW(i) = T_rev + (D_L_MTOW(i) + u_r_L(j)*(max([(W_MTOW -
 L_L_MTOW(i)) 0])));   % Effective force evaluated at x = 0 m [N]
        a_L_MTOW(i) = g_0/W_MTOW*Feff_L_MTOW(i);
       % Acceleration evaluated at x = 0, using Newton's Second Law of motion
 [m/s^2]

        while s_L_MTOW(i) < l_28R
            i = i+1;
            V_L_MTOW(i) = V_L_MTOW(i-1)+a_L_MTOW(i-1)*dt;
            s_L_MTOW(i) = s_L_MTOW(i-1)+V_L_MTOW(i-1)*dt;
            L_L_MTOW(i) = CL_L*0.5*rho_air*(V_L_MTOW(i)+V_wind(o))^2*S;
                  % spoilers deployed!
            D_L_MTOW(i) = CD_L*0.5*rho_air*(V_L_MTOW(i)+V_wind(o))^2*S;
            Feff_L_MTOW(i) = T_rev + D_L_MTOW(i) + u_r_L(j)*(max([(W_MTOW -
 0*L_L_MTOW(i)) 0])); % spoilers deployed; lift is zero.
            a_L_MTOW(i) = g_0/W_MTOW*Feff_L_MTOW(i);
        end

        % Apply intersection function [1]
        [S_1(j,o),V_1(j,o),c,d] = intersections(s_TO,V_TO+V_wind(o),(l_28R-
s_L_MTOW),V_L_MTOW+V_wind(o),true);

        % Determine required runway for takeoff given the takeoff velocity
 profile and V_TO_pub:
        V_TO_pub_array = V_TO_pub*ones(1,length(V_TO));
        [S_TO_RWYUsed(j,o),V_TO_check(j,o),e,f] = intersections(s_TO,V_TO
+V_wind(o),s_TO,V_TO_pub_array,true);

        % Determine required runway for landing given the landing velocity
 profile and V_TO_pub:
        if max(V_L_MTOW+V_wind(o)) < V_L_pub
            S_L_RWYUsed(j,o) = NaN;
        else
            V_L_pub_array = V_L_pub*ones(1,length(V_L_MTOW));
```

```
            [S_L_RWYUsed(j,o),V_L_check(j,o),g,h] = intersections((l_28R-
s_L_MTOW),(V_L_MTOW+V_wind(o)),(l_28R-s_L_MTOW),V_L_pub_array,true);
        end

        % Reset parameters to zero:
        s_TO = 0;
        V_TO = 0;
        s_L_MTOW = 0;
        V_L_MTOW = 0;

    end
    if j ==1
        S_1_wet = S_1;
        V_1_wet = V_1;
        S_TO_RWYUsed_wet = S_TO_RWYUsed;
        S_L_RWYUsedwet = S_TO_RWYUsed;
    end
end

% Display/print the values for V_1
%disp(V_1);

% CreaSte the meshgrid for wind speed and rolling friction coefficient for
% takeoff
[V_wind_TO_mesh,u_r_TO_mesh] = meshgrid(V_wind,u_r_TO);

% Create the meshgrid for wind speed and rolling friction coefficient for
% takeoff
[V_wind_L_mesh,u_r_L_mesh] = meshgrid(V_wind,u_r_L);


% Create surface plot for V_1:
figure(1)
surfc(V_wind_TO_mesh,u_r_TO_mesh,V_1)
xlabel('V_{wind} [m/s]')
ylabel('\mu_{r,TO} [-]')
zlabel('V_1 [m/s]')
title('RTO speed with varying runway friction coefficients and wind speed')
colorbar
c = colorbar;
c.Label.String = 'V_1 [m/s]';
shading interp
% Use view () to capture 2-axes on surface plot

% Create surface plot for V_1 (V_wind + u_r_L):
figure(2)
surfc(V_wind_L_mesh,u_r_L_mesh,V_1)
xlabel('V_{wind} [m/s]')
ylabel('\mu_{r,L} [-]')
zlabel('V_1 [m/s]')
title('RTO speed with varying runway friction coefficients and wind speed')
c = colorbar;
c.Label.String = 'V_1 [m/s]';
shading interp
```

```
% Use view () to capture 2-axes on surface plot

% Create surface plot for S_1 (V_wind + u_r_L):
figure(3)
surfc(V_wind_L_mesh,u_r_L_mesh,S_1)
xlabel('V_{wind} [m/s]')
ylabel('\mu_{r,L} [-]')
zlabel('S_1 [m]')
title('Location of RTO speed with varying runway friction coefficients and
 wind speed')
c = colorbar;
c.Label.String = 'S_1 [m]';
shading interp
% Use view () to capture 2-axes on surface plot

% Create surface plot for S_1 (V_wind + u_r_TO):
figure(4)
surfc(V_wind_TO_mesh,u_r_TO_mesh,S_1)
xlabel('V_{wind} [m/s]')
ylabel('\mu_{r,TO} [-]')
zlabel('S_{1} [m]')
title('Location of RTO speed with varying runway friction coefficients and
 wind speed')
c = colorbar;
c.Label.String = 'S_{1} [m]';
shading interp

% Create surface plot for takeoff distance:
figure(5)
surfc(V_wind_TO_mesh,u_r_TO_mesh,S_TO_RWYUsed)
xlabel('V_{wind} [m/s]')
ylabel('\mu_{r,TO} [-]')
zlabel('S_{TO} [m]')
title('Environmental impacts on the takeoff distance')
c = colorbar;
c.Label.String = 'S_{TO} [m]';
shading interp

% Create surface plot for landing distance:
figure(6)
surfc(V_wind_TO_mesh,u_r_L_mesh,l_28R-S_1)
xlabel('V_{wind} [m/s]')
ylabel('\mu_{r,L} [-]')
zlabel('S_{L} [m]')
title('Landing distance with respect to V_{1}')
c = colorbar;
c.Label.String = 'S_{L} [m]';
shading interp

% Print the results:
% Location of V1 vs wind speed
figure(7)
subplot(2,1,1)
% V1 vs wind speed
```

```
% Dry conditions
plot(V_wind,V_1(end,:),'r')
hold on
% Wet conditions
plot(V_wind,V_1(1,:),'b')
ylim([50,90])
xlim([-4,14])
title('RTO speed vs Wind speed')
ylabel('V_{1} [m/s]')
xlabel('V_{wind} [m/s]')
legend('Dry runway','Wet runway','location','northeast')
grid minor

subplot(2,1,2)
% Dry conditions:
plot(V_wind,S_1(end,:),'r')
hold on
% Wet conditions:
plot(V_wind,S_1(1,:),'b')
ylim([900,1800])
xlim([-4,14])
title('Location of RTO speed vs Wind speed')
ylabel('S_{1} [m]')
xlabel('V_{wind} [m/s]')
legend('Dry runway','Wet runway','location','northeast')
grid minor
```

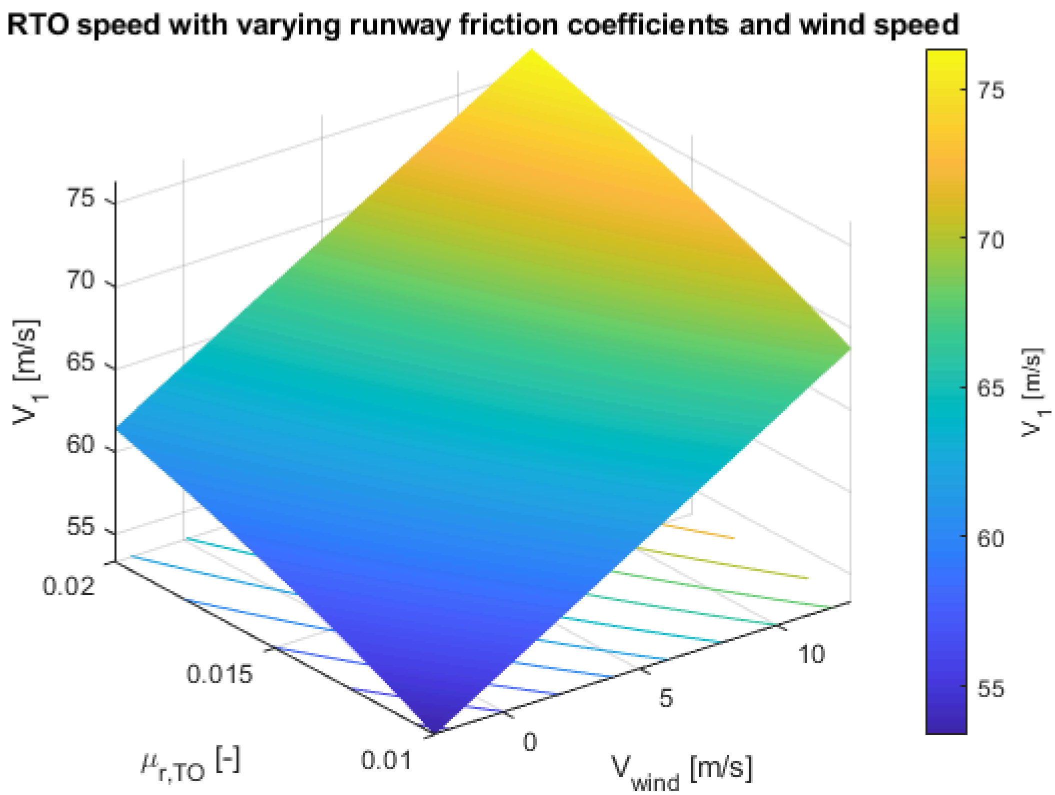

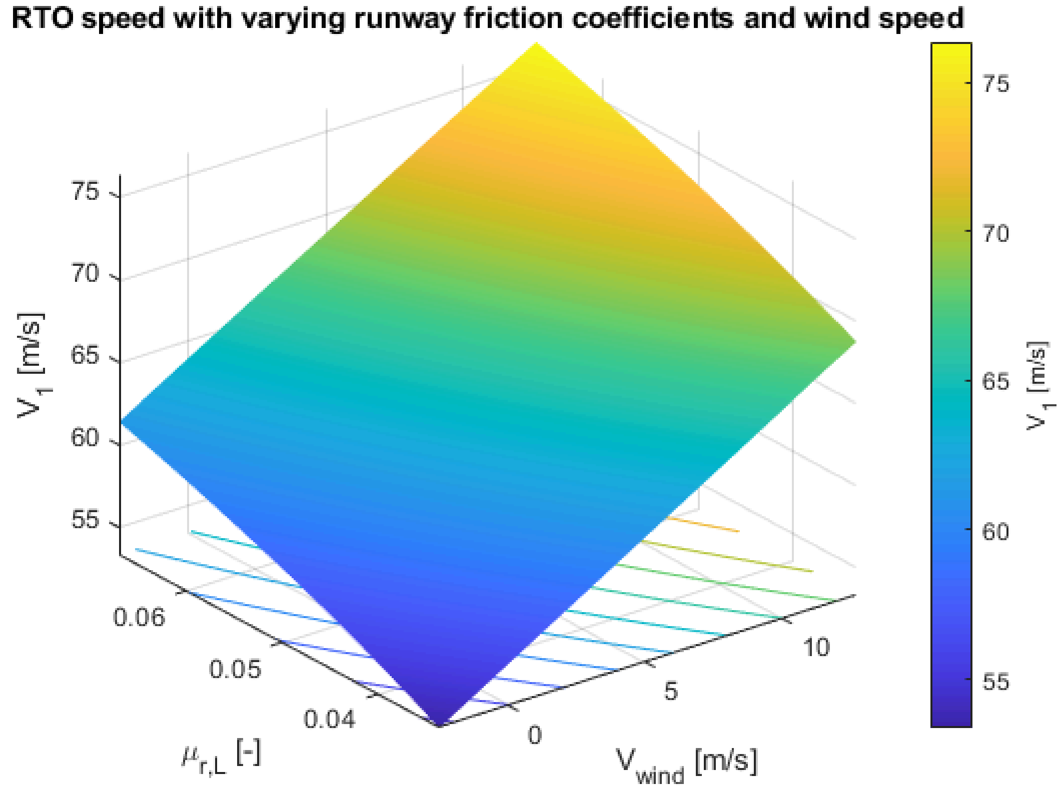
RTO speed with varying runway friction coefficients and wind speed
V1 [m/s]
75
70
65
60
55
0.06
0.05
0.04
μr,L [-]
0
5
10
Vwind [m/s]
75
70
65
60
55
V1 [m/s]

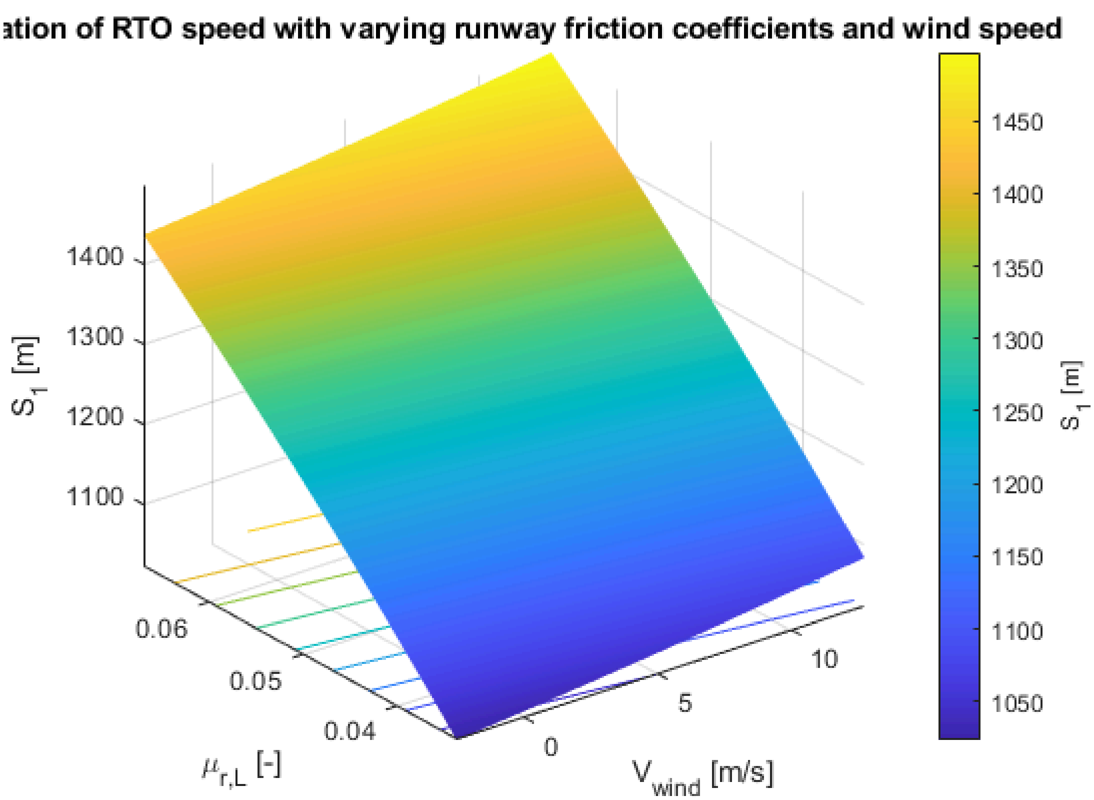
ation of RTO speed with varying runway friction coefficients and wind speed
S1 [m]
1400
1300
1200
1100
0.06
0.05
0.04
μr,L [-]
0
5
10
Vwind [m/s]
1450
1400
1350
1300
1250
1200
1150
1100
1050
S1 [m]

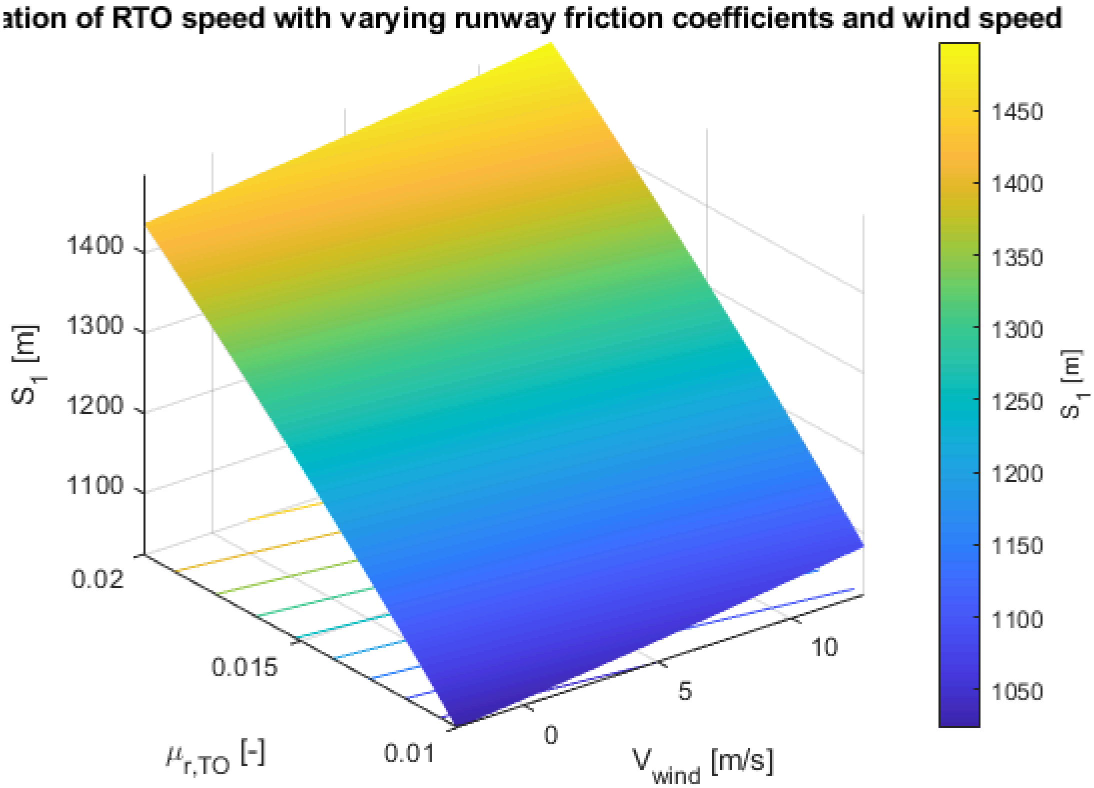
ation of RTO speed with varying runway friction coefficients and wind speed
S1 [m]
1400
1300
1200
1100
0.02
0.015
0.01
μr,TO [-]
0
5
10
Vwind [m/s]
1450
1400
1350
1300
1250
1200
1150
1100
1050

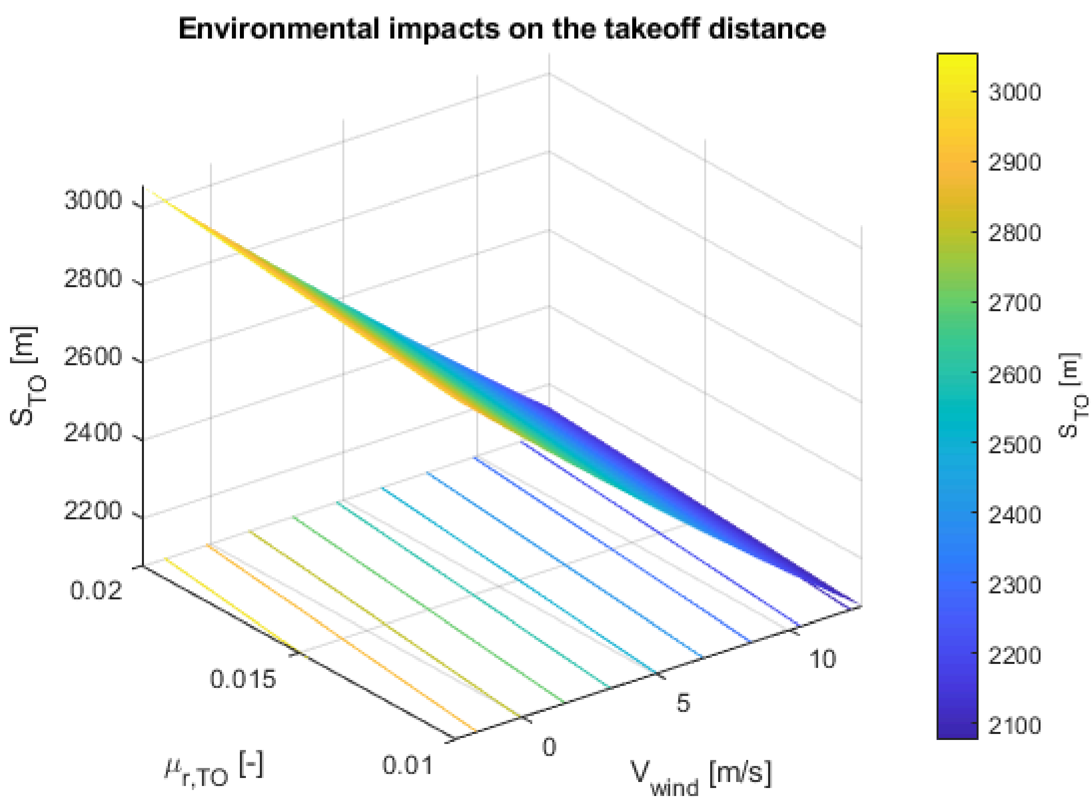
Environmental impacts on the takeoff distance
STO [m]
3000
2800
2600
2400
2200
0.02
0.015
0.01
μr,TO [-]
0
5
10
Vwind [m/s]
3000
2900
2800
2700
2600
2500
2400
2300
2200
2100

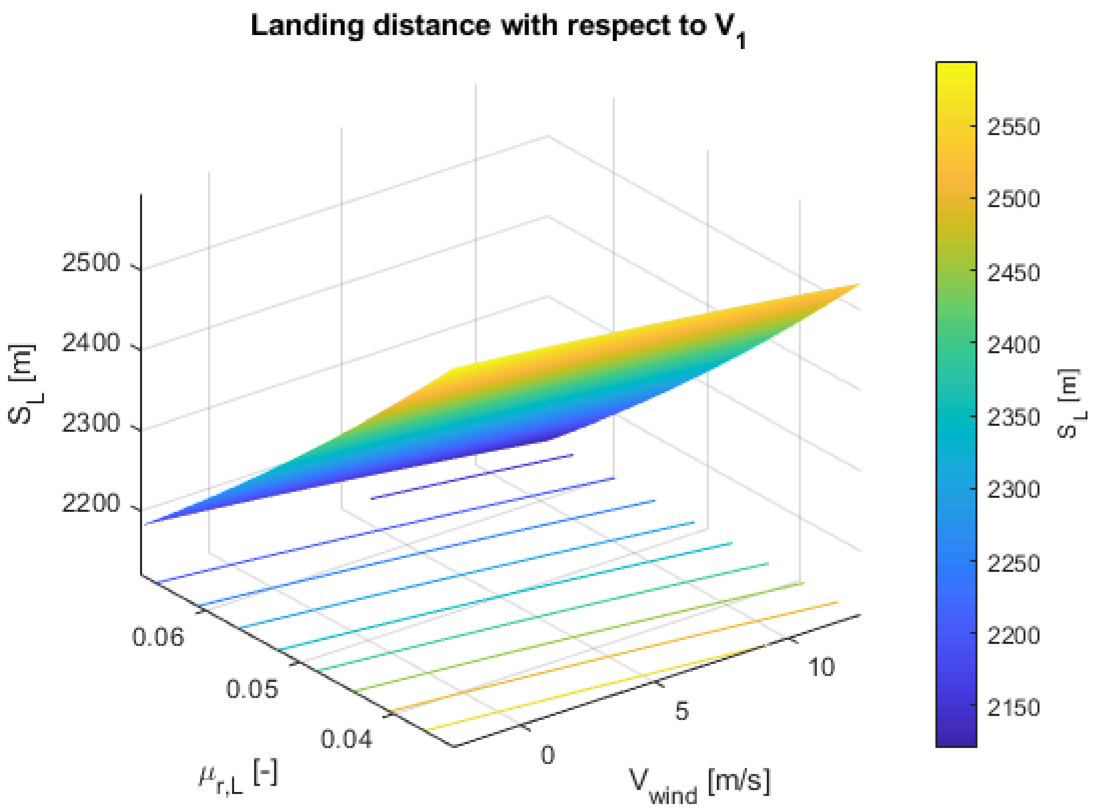
Landing distance with respect to V_1
S_L [m]
2500
2400
2300
2200
0.06
0.05
0.04
$\mu_{r,L}$ [-]
0
5
10
V_{wind} [m/s]
2550
2500
2450
2400
2350
2300
2250
2200
2150

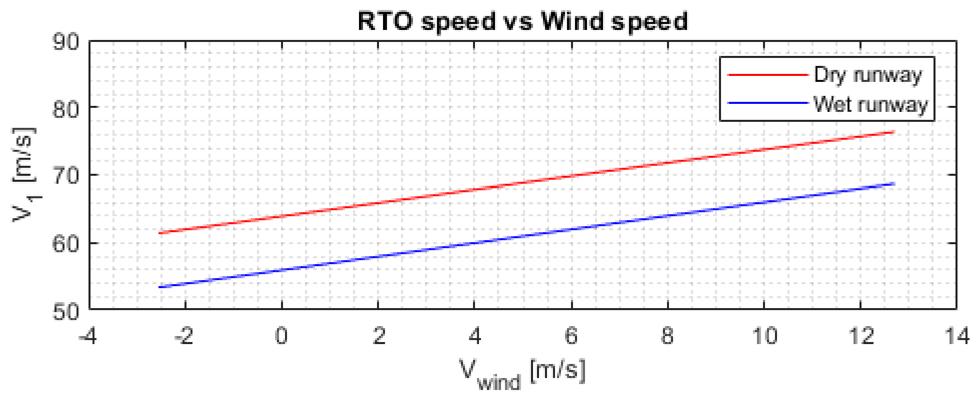
RTO speed vs Wind speed
Dry runway
Wet runway
V_1 [m/s]
V_{wind} [m/s]

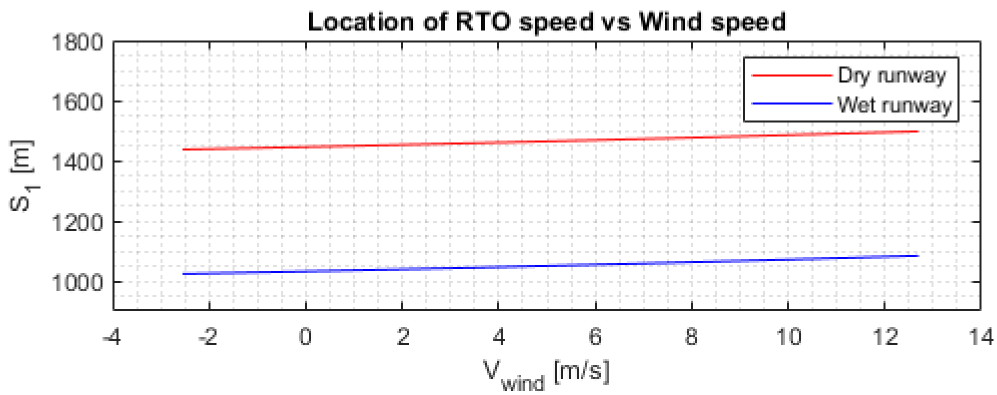
Location of RTO speed vs Wind speed
Dry runway
Wet runway
S_1 [m]
V_{wind} [m/s]

Published with MATLAB® R2022b

Appendix C:
Sample 2022 KSFO METAR Data

station	valid	tmpf	dwpf	relh	drct	sknt	p01i	alti	mslp	vsby	gust	skyc1	skyc2	skyc3	skyc4	skyl1	skyl2	skyl3	skyl4	wxcodes	ice_accreti	ice_accreti	ice_accreti	peak_wind	peak_wind	peak_wind	feel	metar
SFO	1/1/2022 0:56	51.1	41	68.23	300	14	0	29.91	1012.8	10	M	SCT	M	M	M	2000	M	M	M	M	M	M	M	M	M	M	51.1	KSFO 0100
SFO	1/1/2022 1:56	50	39.9	68.1	300	10	0	29.92	1013.3	10	M	FEW	M	M	M	1900	M	M	M	M	M	M	M	M	M	M	50	KSFO 0101
SFO	1/1/2022 2:56	48.9	39.9	70.95	290	10	0	29.95	1014	10	M	CLR	M	M	M	M	M	M	M	M	M	M	M	M	M	M	44.16	KSFO 0102
SFO	1/1/2022 3:56	48.9	41	74.05	310	10	0	29.96	1014.6	10	M	FEW	M	M	M	3000	M	M	M	M	M	M	M	M	M	M	44.16	KSFO 0103
SFO	1/1/2022 4:56	48	41	76.58	330	5	0	29.99	1015.5	10	M	CLR	M	M	M	M	M	M	M	M	M	M	M	M	M	M	45.4	KSFO 0104
SFO	1/1/2022 5:56	46.9	37.9	70.73	310	5	0	30.02	1016.4	10	M	CLR	M	M	M	M	M	M	M	M	M	M	M	M	M	M	44.09	KSFO 0105
SFO	1/1/2022 6:56	48	36	62.97	M	5	0	30.04	1017.3	10	M	CLR	M	M	M	M	M	M	M	M	M	M	M	M	M	M	45.4	KSFO 0106
SFO	1/1/2022 7:56	46	37	70.64	300	6	0	30.06	1017.8	10	M	CLR	M	M	M	M	M	M	M	M	M	M	M	M	M	M	42.39	KSFO 0107
SFO	1/1/2022 8:56	43	37.9	82.04	220	4	0	30.07	1018.3	10	M	CLR	M	M	M	M	M	M	M	M	M	M	M	M	M	M	40.27	KSFO 0108
SFO	1/1/2022 9:56	42.1	37	81.98	0	0	0	30.08	1018.6	10	M	CLR	M	M	M	M	M	M	M	M	M	M	M	M	M	M	42.1	KSFO 0109
SFO	1/1/2022 10:56	41	36	82.22	190	3	0	30.09	1019	10	M	CLR	M	M	M	M	M	M	M	M	M	M	M	M	M	M	38.98	KSFO 0110
SFO	1/1/2022 11:56	43	37	79.19	M	5	0	30.09	1019	10	M	CLR	M	M	M	M	M	M	M	M	M	M	M	M	M	M	39.46	KSFO 0111
SFO	1/1/2022 12:56	46	39	76.4	360	9	0	30.11	1019.6	10	M	FEW	M	M	M	20000	M	M	M	M	M	M	M	M	M	M	40.92	KSFO 0112
SFO	1/1/2022 13:56	41	36	82.22	0	0	0	30.15	1020.8	10	M	FEW	M	M	M	20000	M	M	M	M	M	M	M	M	M	M	41	KSFO 0113
SFO	1/1/2022 14:56	41	35.1	79.34	0	0	0	30.17	1021.6	10	M	SCT	M	M	M	20000	M	M	M	M	M	M	M	M	M	M	41	KSFO 0114
SFO	1/1/2022 15:56	39	35.1	85.76	220	3	0	30.2	1022.5	10	M	SCT	M	M	M	20000	M	M	M	M	M	M	M	M	M	M	36.69	KSFO 0115
SFO	1/1/2022 16:56	44.1	37.9	78.66	200	4	0	30.21	1023	10	M	SCT	M	M	M	20000	M	M	M	M	M	M	M	M	M	M	41.55	KSFO 0116
SFO	1/1/2022 17:56	48	36	62.97	0	0	0	30.24	1024	10	M	FEW	M	M	M	20000	M	M	M	M	M	M	M	M	M	M	48	KSFO 0117
SFO	1/1/2022 18:56	48.9	35.1	58.75	110	7	0	30.24	1024	10	M	FEW	M	M	M	20000	M	M	M	M	M	M	M	M	M	M	45.38	KSFO 0118
SFO	1/1/2022 19:56	48.9	28.9	45.75	110	4	0	30.23	1023.5	10	M	FEW	M	M	M	20000	M	M	M	M	M	M	M	M	M	M	47.16	KSFO 0119
SFO	1/1/2022 20:56	50	30.9	47.64	70	3	0	30.19	1022.3	10	M	SCT	M	M	M	20000	M	M	M	M	M	M	M	M	M	M	50	KSFO 0120
SFO	1/1/2022 21:56	51.1	32	47.81	0	0	0	30.19	1022.3	10	M	SCT	M	M	M	20000	M	M	M	M	M	M	M	M	M	M	51.1	KSFO 0121
SFO	1/1/2022 22:56	52	33.1	48.34	30	3	0	30.2	1022.6	10	M	SCT	M	M	M	20000	M	M	M	M	M	M	M	M	M	M	52	KSFO 0122
SFO	1/1/2022 23:56	51.1	36	56.1	50	5	0	30.2	1022.6	10	M	SCT	M	M	M	20000	M	M	M	M	M	M	M	M	M	M	51.1	KSFO 0123
SFO	1/2/2022 0:56	50	37	60.79	40	5	0	30.21	1023	10	M	SCT	M	M	M	20000	M	M	M	M	M	M	M	M	M	M	50	KSFO 0200
SFO	1/2/2022 1:56	48.9	37.9	65.62	50	4	0	30.22	1023.2	10	M	FEW	M	M	M	20000	M	M	M	M	M	M	M	M	M	M	47.16	KSFO 0201
SFO	1/2/2022 2:56	46.9	36	65.63	210	3	0	30.23	1023.7	10	M	CLR	M	M	M	M	M	M	M	M	M	M	M	M	M	M	45.72	KSFO 0202
SFO	1/2/2022 3:56	44.1	35.1	70.43	0	0	0	30.25	1024.3	10	M	CLR	M	M	M	M	M	M	M	M	M	M	M	M	M	M	44.1	KSFO 0203
SFO	1/2/2022 4:56	43	34	70.3	270	3	0	30.27	1025	10	M	CLR	M	M	M	M	M	M	M	M	M	M	M	M	M	M	41.26	KSFO 0204
SFO	1/2/2022 5:56	43	34	70.3	0	0	0	30.28	1025.3	10	M	CLR	M	M	M	M	M	M	M	M	M	M	M	M	M	M	43	KSFO 0205
SFO	1/2/2022 6:56	41	33.1	73.25	0	0	0	30.28	1025.5	10	M	CLR	M	M	M	M	M	M	M	M	M	M	M	M	M	M	41	KSFO 0206
SFO	1/2/2022 7:56	41	34	75.94	0	0	0	30.29	1025.5	10	M	CLR	M	M	M	M	M	M	M	M	M	M	M	M	M	M	41	KSFO 0207
SFO	1/2/2022 8:56	39	34	82.08	200	3	0	30.28	1025.3	10	M	CLR	M	M	M	M	M	M	M	M	M	M	M	M	M	M	36.69	KSFO 0208
SFO	1/2/2022 9:56	37.9	33.1	82.66	0	0	0	30.29	1025.5	10	M	CLR	M	M	M	M	M	M	M	M	M	M	M	M	M	M	37.9	KSFO 0209
SFO	1/2/2022 10:56	37	32	81.93	220	4	0	30.29	1025.6	10	M	CLR	M	M	M	M	M	M	M	M	M	M	M	M	M	M	33.26	KSFO 0210
SFO	1/2/2022 11:56	37	32	81.93	0	0	0	30.28	1025.3	10	M	CLR	M	M	M	M	M	M	M	M	M	M	M	M	M	M	37	KSFO 0211
SFO	1/2/2022 12:56	36	30.9	81.53	230	3	0	30.27	1024.9	10	M	CLR	M	M	M	M	M	M	M	M	M	M	M	M	M	M	33.26	KSFO 0212
SFO	1/2/2022 13:56	36	32	85.23	220	3	0	30.29	1025.5	10	M	CLR	M	M	M	M	M	M	M	M	M	M	M	M	M	M	33.26	KSFO 0213
SFO	1/2/2022 14:56	37	33.1	85.64	210	3	0	30.29	1025.7	10	M	FEW	M	M	M	20000	M	M	M	M	M	M	M	M	M	M	34.4	KSFO 0214
SFO	1/2/2022 15:56	37.9	34	85.69	210	3	0	30.3	1026.1	10	M	FEW	M	M	M	20000	M	M	M	M	M	M	M	M	M	M	35.43	KSFO 0215
SFO	1/2/2022 16:56	42.1	34	72.78	170	3	0	30.32	1026.5	10	M	FEW	M	M	M	20000	M	M	M	M	M	M	M	M	M	M	40.23	KSFO 0216
SFO	1/2/2022 17:56	45	33.1	62.83	90	3	0	30.33	1026.9	10	M	FEW	M	M	M	20000	M	M	M	M	M	M	M	M	M	M	43.55	KSFO 0217
SFO	1/2/2022 18:56	46	35.1	65.52	100	3	0	30.3	1026	10	M	FEW	FEW	M	M	3600	20000	M	M	M	M	M	M	M	M	M	44.69	KSFO 0218
SFO	1/2/2022 19:56	46.9	35.1	63.33	70	4	0	30.27	1024.9	10	M	FEW	FEW	M	M	3800	20000	M	M	M	M	M	M	M	M	M	44.82	KSFO 0219
SFO	1/2/2022 20:56	48	35.1	60.76	60	3	0	30.24	1024	10	M	SCT	SCT	M	M	3500	20000	M	M	M	M	M	M	M	M	M	46.98	KSFO 0220
SFO	1/2/2022 21:56	50	35.1	56.39	20	4	0	30.23	1023.5	10	M	FEW	SCT	SCT	M	2900	3600	20000	M	M	M	M	M	M	M	M	50	KSFO 0221
SFO	1/2/2022 22:56	52	37.9	58.48	10	4	0	30.22	1023.2	10	M	FEW	SCT	SCT	M	2700	5000	20000	M	M	M	M	M	M	M	M	52	KSFO 0222
SFO	1/2/2022 23:56	51.1	42.1	71.19	360	5	0	30.22	1023.2	10	M	FEW	BKN	BKN	M	2700	4300	20000	M	M	M	M	M	M	M	M	51.1	KSFO 0223
SFO	1/3/2022 0:56	51.1	44.1	76.86	20	4	0	30.21	1022.9	10	M	FEW	SCT	BKN	BKN	1700	2700	4000	20000	M	M	M	M	M	M	M	51.1	KSFO 0300
SFO	1/3/2022 1:56	52	45	76.94	180	6	0	30.19	1022.2	10	M	FEW	BKN	M	M	1500	4100	M	M	M	M	M	M	M	M	M	52	KSFO 0301
SFO	1/3/2022 2:56	50	43	76.76	130	4	0	30.19	1022.4	10	M	FEW	BKN	M	M	1300	4000	M	M	M	M	M	M	M	M	M	50	KSFO 0302
SFO	1/3/2022 3:56	51.1	45	79.54	200	8	0	30.19	1022.4	10	M	FEW	SCT	M	M	2300	3500	M	M	M	M	M	M	M	M	M	51.1	KSFO 0303
SFO	1/3/2022 4:56	51.1	45	79.54	170	6	0	30.2	1022.5	10	M	FEW	BKN	BKN	M	1300	3300	4000	M	M	M	M	M	M	M	M	51.1	KSFO 0304
SFO	1/3/2022 5:56	52	46	79.92	170	5	0	30.2	1022.7	10	M	FEW	BKN	BKN	M	1500	2800	3700	M	M	M	M	M	M	M	M	52	KSFO 0305
SFO	1/3/2022 6:15	52	46	79.92	0	0	0	30.21	M	10	M	SCT	OVC	M	M	2800	3900	M	M	M	M	M	M	M	M	M	52	KSFO 0306
SFO	1/3/2022 6:43	51.1	44.1	76.86	280	4	0	30.22	M	10	M	BKN	OVC	M	M	2800	3800	M	M	M	M	M	M	M	M	M	51.1	KSFO 0306
SFO	1/3/2022 6:56	51.1	45	79.54	240	5	0	30.22	1023.3	10	M	SCT	OVC	M	M	2300	3000	M	M	M	M	M	M	M	M	M	51.1	KSFO 0306
SFO	1/3/2022 7:18	52	44.1	74.35	230	6	0	30.23	M	10	M	FEW	BKN	OVC	M	2100	2900	3700	M	M	M	M	M	M	M	M	52	KSFO 0307
SFO	1/3/2022 7:56	51.1	44.1	76.86	220	4	0	30.22	1023.4	10	M	FEW	BKN	OVC	M	2100	2600	4000	M	M	M	M	M	M	M	M	51.1	KSFO 0307
SFO	1/3/2022 8:50	50	42.8	76.18	170	6	0	30.21	M	10	M	SCT	OVC	M	M	2700	3900	M	M	M	M	M	M	M	M	M	50	KSFO 0308
SFO	1/3/2022 8:56	50	43	76.76	180	7	0	30.21	1022.9	10	M	SCT	OVC	M	M	2700	3900	M	M	M	M	M	M	M	M	M	50	KSFO 0308
SFO	1/3/2022 9:56	48	42.1	79.91	170	4	0	30.21	1023	10	M	SCT	M	M	M	3900	M	M	M	M	M	M	M	M	M	M	46.1	KSFO 0309
SFO	1/3/2022 10:56	46.9	42.1	83.28	150	5	0	30.21	1023	10	M	FEW	SCT	M	M	2800	3700	M	M	M	M	M	M	M	M	M	44.09	KSFO 0310
SFO	1/3/2022 11:14	48.2	42.8	81.47	160	4	0	30.21	M	10	M	BKN	M	M	M	2900	M	M	M	M	M	M	M	M	M	M	46.34	KSFO 0311
SFO	1/3/2022 11:56	48.9	43	79.98	150	7	0	30.19	1022.4	10	M	BKN	M	M	M	2900	M	M	M	M	M	M	M	M	M	M	45.38	KSFO 0311
SFO	1/3/2022 12:56	50	43	76.76	130	5	0	30.19	1022.2	10	M	BKN	M	M	M	2900	M	M	M	M	M	M	M	M	M	M	50	KSFO 0312
SFO	1/3/2022 13:47	50	43	76.76	150	9	0	30.18	M	10	M	SCT	OVC	M	M	2900	4300	M	M	M	M	M	M	M	M	M	50	KSFO 0313
SFO	1/3/2022 13:56	50	43	76.76	170	11	0	30.18	1022	10	M	SCT	OVC	M	M	2900	4300	M	M	M	M	M	M	M	M	M	50	KSFO 0313
SFO	1/3/2022 14:56	48.9	43	79.98	150	7	0	30.19	1022.2	10	M	BKN	OVC	M	M	2600	3800	M	M	M	M	M	M	M	M	M	45.38	KSFO 0314
SFO	1/3/2022 15:56	48.9	43	79.98	110	8	0	30.18	1021.9	10	M	SCT	BKN	BKN	M	2200	3700	20000	M	M	M	M	M	M	M	M	44.93	KSFO 0315
SFO	1/3/2022 16:56	48.9	44.1	83.42	110	7	0	30.21	1023	10	M	BKN	BKN	BKN	M	2300	4000	6000	M	M	M	M	M	M	M	M	45.38	KSFO 0316
SFO	1/3/2022 17:56	52	44.1	74.35	160	11	0	30.22	1023.3	10	M	BKN	BKN	BKN	M	2300	4000	6000	M	M	M	M	M	M	M	M	52	KSFO 0317
SFO	1/3/2022 18:56	53.1	45	73.89	170	13	0	30.21	1022.9	10	M	SCT	BKN	M	M	2000	6500	M	M	M	M	M	M	M	M	M	53.1	KSFO 0318
SFO	1/3/2022 19:56	55	46	71.6	160	8	0	30.2	1022.4	10	M	FEW	BKN	BKN	M	800	2000	5500	M	M	M	M	M	M	M	M	55	KSFO 0319
SFO	1/3/2022 20:56	55	46	71.6	200	20	0	30.18	1021.9	10	28	FEW	SCT	OVC	M	800	2500	7000	M	M	M	M	M	28	200	########	55	KSFO 0320
SFO	1/3/2022 21:56	55	46.9	74.08	190	17	0	30.17	1021.7	10	25	FEW	BKN	OVC	M	800	6000	7500	M	M	M	M	M	M	M	M	55	KSFO 0321

SFO	1/3/2022 22:56	53.1	48.9	85.59	180	15	0	30.16	1021.4	8	25	FEW	BKN	OVC	M	900	4700	6500	M	M	M	M	M	M	M	M	53.1	KSFO 0322
SFO	1/3/2022 23:56	54	50	86.29	180	15	T	30.17	1021.5	8	M	FEW	BKN	OVC	M	900	4700	6500	M	#NAME?	M	M	M	M	M	M	54	KSFO 0323
SFO	1/4/2022 0:56	53.1	50	89.18	170	13	T	30.17	1021.7	7	22	FEW	BKN	OVC	M	900	4900	7000	M	#NAME?	M	M	M	M	M	M	53.1	KSFO 0400
SFO	1/4/2022 1:56	53.1	51.1	92.89	160	10	0.02	30.18	1021.8	4	M	FEW	BKN	OVC	M	900	2300	3200	M	#NAME?	M	M	M	M	M	M	53.1	KSFO 0401
SFO	1/4/2022 2:56	52	51.1	96.73	150	10	0.04	30.19	1022.3	4	M	FEW	BKN	OVC	M	800	2000	2900	M	#NAME?	M	M	M	M	M	M	52	KSFO 0402
SFO	1/4/2022 3:56	53.1	52	96.03	190	8	0.04	30.21	1023	4	M	FEW	BKN	OVC	M	800	2500	3500	M	#NAME?	M	M	M	M	M	M	53.1	KSFO 0403
SFO	1/4/2022 4:56	54	52	92.92	170	4	0.04	30.22	1023.4	5	M	FEW	OVC	M	M	800	2400	M	M	#NAME?	M	M	M	M	M	M	54	KSFO 0404
SFO	1/4/2022 5:56	54	52	92.92	170	6	0.02	30.24	1024.1	8	M	FEW	BKN	OVC	M	800	2800	3800	M	#NAME?	M	M	M	M	M	M	54	KSFO 0405
SFO	1/4/2022 6:05	54	52	92.92	160	6	0.01	30.24	M	2.5	M	FEW	BKN	OVC	M	600	2800	3700	M	#NAME?	M	M	M	M	M	M	54	KSFO 0406
SFO	1/4/2022 6:18	54	52	92.92	160	6	0.02	30.24	M	4	M	FEW	BKN	OVC	M	600	2800	3700	M	#NAME?	M	M	M	M	M	M	54	KSFO 0406
SFO	1/4/2022 6:26	54	52	92.92	160	4	0.02	30.24	M	2.5	M	FEW	BKN	OVC	M	600	2600	3100	M	#NAME?	M	M	M	M	M	M	54	KSFO 0406
SFO	1/4/2022 6:56	54	53.1	96.76	170	4	0.05	30.24	1024	2.5	M	FEW	BKN	OVC	M	600	2500	3000	M	#NAME?	M	M	M	M	M	M	54	KSFO 0406
SFO	1/4/2022 7:36	54	52	92.92	250	4	0.03	30.25	M	1.75	M	FEW	BKN	OVC	M	600	2500	3000	M	#NAME?	M	M	M	M	M	M	54	KSFO 0407
SFO	1/4/2022 7:50	55.4	53.6	93.65	250	6	0	30.25	M	2.5	M	FEW	BKN	OVC	M	600	2400	2900	M	#NAME?	M	M	M	M	M	M	55.4	KSFO 0407
SFO	1/4/2022 7:56	55	53.1	93.29	250	10	0.06	30.25	1024.3	2.5	M	FEW	BKN	OVC	M	600	2400	2900	M	#NAME?	M	M	M	M	M	M	55	KSFO 0407
SFO	1/4/2022 8:29	55	53.1	93.29	270	4	0.02	30.25	M	6	M	FEW	OVC	M	M	600	1800	M	M	BR	M	M	M	M	M	M	55	KSFO 0408
SFO	1/4/2022 8:40	52	51.1	96.73	80	10	0.02	30.25	M	2	M	FEW	OVC	M	M	600	1500	M	M	#NAME?	M	M	M	M	M	M	52	KSFO 0408
SFO	1/4/2022 8:50	51.8	50	93.55	90	7	0.03	30.25	M	3	M	FEW	BKN	OVC	M	600	1400	2500	M	#NAME?	M	M	M	M	M	M	51.8	KSFO 0408
SFO	1/4/2022 8:56	51.1	50	96	90	8	0.03	30.25	1024.5	3	M	FEW	BKN	OVC	M	600	1400	2500	M	BR	M	M	M	M	M	M	51.1	KSFO 0408
SFO	1/4/2022 9:14	52	50	92.86	100	5	0.01	30.26	M	4	M	FEW	SCT	OVC	M	600	1300	2000	M	#NAME?	M	M	M	M	M	M	52	KSFO 0409
SFO	1/4/2022 9:27	52	50	92.86	120	5	0.01	30.26	M	5	M	SCT	BKN	OVC	M	600	1300	2600	M	BR	M	M	M	M	M	M	52	KSFO 0409
SFO	1/4/2022 9:49	52	50	92.86	120	5	0.01	30.26	M	4	M	FEW	SCT	OVC	M	600	1800	3400	M	BR	M	M	M	M	M	M	52	KSFO 0409
SFO	1/4/2022 9:56	52	50	92.86	130	5	0.01	30.26	1024.7	7	M	FEW	SCT	OVC	M	600	1800	3400	M	M	M	M	M	M	M	M	52	KSFO 0409
SFO	1/4/2022 10:12	52	50	92.86	150	3	0	30.27	M	10	M	FEW	BKN	OVC	M	600	2400	3300	M	M	M	M	M	M	M	M	52	KSFO 0410
SFO	1/4/2022 10:56	52	51.1	96.73	140	5	0.01	30.26	1024.8	4	M	FEW	BKN	OVC	M	600	1700	2400	M	BR	M	M	M	M	M	M	52	KSFO 0410
SFO	1/4/2022 11:49	52	51.1	96.73	140	6	0.01	30.26	M	5	M	FEW	BKN	OVC	M	600	3100	4800	M	#NAME?	M	M	M	M	M	M	52	KSFO 0411
SFO	1/4/2022 11:56	51.1	50	96	130	4	0.01	30.26	1024.5	7	M	FEW	BKN	OVC	M	600	3100	4800	M	M	M	M	M	M	M	M	51.1	KSFO 0411
SFO	1/4/2022 12:04	51.1	51.1	100	140	3	0	30.26	M	6	M	FEW	BKN	OVC	M	600	2700	3200	M	BR	M	M	M	M	M	M	51.1	KSFO 0412
SFO	1/4/2022 12:56	52	51.1	96.73	160	3	0	30.27	1024.8	5	M	FEW	BKN	OVC	M	600	2100	3200	M	BR	M	M	M	M	M	M	52	KSFO 0412
SFO	1/4/2022 13:11	52	51.1	96.73	170	4	0	30.27	M	6	M	FEW	BKN	OVC	M	600	1200	2500	M	BR	M	M	M	M	M	M	52	KSFO 0413
SFO	1/4/2022 13:56	53.1	51.1	92.89	110	3	0	30.28	1025.2	8	M	FEW	OVC	M	M	600	1000	M	M	M	M	M	M	M	M	M	53.1	KSFO 0413
SFO	1/4/2022 14:05	52	50	92.86	110	5	0	30.28	M	8	M	BKN	OVC	M	M	600	1100	M	M	M	M	M	M	M	M	M	52	KSFO 0414
SFO	1/4/2022 14:56	53.1	51.1	92.89	60	3	0.04	30.3	1025.9	5	M	OVC	M	M	M	500	M	M	M	#NAME?	M	M	M	M	M	M	53.1	KSFO 0414
SFO	1/4/2022 14:58	52	51.1	96.73	70	3	0.01	30.3	M	1.75	M	BKN	OVC	M	M	500	900	M	M	#NAME?	M	M	M	M	M	M	52	KSFO 0414
SFO	1/4/2022 15:29	52	51.1	96.73	60	3	0.02	30.3	M	3	M	OVC	M	M	M	500	M	M	M	BR	M	M	M	M	M	M	52	KSFO 0415
SFO	1/4/2022 15:56	51.1	51.1	100	100	4	0.02	30.31	1026.3	8	M	SCT	OVC	M	M	500	1300	M	M	M	M	M	M	M	M	M	51.1	KSFO 0415
SFO	1/4/2022 16:05	51.1	50	96	80	4	0	30.31	M	8	M	BKN	OVC	M	M	600	1300	M	M	M	M	M	M	M	M	M	51.1	KSFO 0416
SFO	1/4/2022 16:56	52	51.1	96.73	0	0	0	30.33	1027	3	M	BKN	OVC	M	M	500	1300	M	M	BR	M	M	M	M	M	M	52	KSFO 0416
SFO	1/4/2022 17:45	52	50	92.86	70	4	0	30.34	M	9	M	FEW	SCT	OVC	M	900	2000	2600	M	M	M	M	M	M	M	M	52	KSFO 0417
SFO	1/4/2022 17:56	52	51.1	96.73	80	3	0	30.35	1027.6	9	M	FEW	SCT	OVC	M	900	2000	2600	M	M	M	M	M	M	M	M	52	KSFO 0417
SFO	1/4/2022 18:41	52	51.1	96.73	120	3	0.02	30.35	M	1	M	FEW	OVC	M	M	500	1400	M	M	#NAME?	M	M	M	M	M	M	52	KSFO 0418
SFO	1/4/2022 18:56	53.1	52	96.03	0	0	0.03	30.34	1027.4	1	M	FEW	OVC	M	M	500	1400	M	M	BR	M	M	M	M	M	M	53.1	KSFO 0418
SFO	1/4/2022 18:58	53.1	52	96.03	0	0	0	30.34	M	3	M	FEW	BKN	OVC	M	1300	2100	2800	M	BR	M	M	M	M	M	M	53.1	KSFO 0418
SFO	1/4/2022 19:56	53.1	52	96.03	110	5	0	30.31	1026.3	9	M	SCT	BKN	OVC	M	1100	1700	11000	M	M	M	M	M	M	M	M	53.1	KSFO 0419
SFO	1/4/2022 20:22	53.1	52	96.03	90	4	0	30.31	M	9	M	FEW	BKN	OVC	M	1100	1400	2200	M	M	M	M	M	M	M	M	53.1	KSFO 0420
SFO	1/4/2022 20:56	53.1	51.1	92.89	90	4	0	30.3	1025.9	9	M	OVC	M	M	M	1800	M	M	M	M	M	M	M	M	M	M	53.1	KSFO 0420
SFO	1/4/2022 21:56	54	52	92.92	0	0	0	30.3	1025.9	9	M	BKN	BKN	OVC	M	1700	2400	3400	M	M	M	M	M	M	M	M	54	KSFO 0421
SFO	1/4/2022 22:34	55.9	53.1	90.29	0	0	0	30.29	M	10	M	FEW	BKN	BKN	M	1700	3100	10000	M	M	M	M	M	M	M	M	55.9	KSFO 0422
SFO	1/4/2022 22:56	54	51.1	89.88	0	0	0	30.29	1025.8	10	M	FEW	SCT	BKN	M	1700	3000	10000	M	M	M	M	M	M	M	M	54	KSFO 0422
SFO	1/4/2022 23:56	57.9	53.1	84	280	5	0	30.29	1025.7	10	M	FEW	SCT	BKN	M	1000	11000	20000	M	M	M	M	M	M	M	M	57.9	KSFO 0423
SFO	1/5/2022 0:56	55	51.1	86.66	300	7	0	30.3	1025.8	10	M	FEW	SCT	BKN	M	1000	1800	20000	M	M	M	M	M	M	M	M	55	KSFO 0500
SFO	1/5/2022 1:56	54	50	86.29	330	6	0	30.31	1026.4	10	M	FEW	BKN	M	M	800	20000	M	M	M	M	M	M	M	M	M	54	KSFO 0501
SFO	1/5/2022 2:56	54	51.1	89.88	270	5	0	30.31	1026.5	10	M	FEW	SCT	BKN	M	800	1200	20000	M	M	M	M	M	M	M	M	54	KSFO 0502
SFO	1/5/2022 3:08	54	51.1	89.88	M	5	0	30.31	M	10	M	FEW	SCT	BKN	M	800	1000	1400	M	M	M	M	M	M	M	M	54	KSFO 0503
SFO	1/5/2022 3:56	54	51.1	89.88	300	5	0	30.32	1026.7	10	M	FEW	SCT	BKN	M	800	1000	1200	M	M	M	M	M	M	M	M	54	KSFO 0503
SFO	1/5/2022 4:56	53.1	50	89.18	300	7	0	30.33	1027.1	10	M	SCT	BKN	M	M	800	2400	M	M	M	M	M	M	M	M	M	53.1	KSFO 0504
SFO	1/5/2022 5:46	53.1	50	89.18	230	7	0	30.33	M	10	M	FEW	SCT	BKN	M	800	1000	9000	M	M	M	M	M	M	M	M	53.1	KSFO 0505
SFO	1/5/2022 5:56	53.1	50	89.18	260	9	0	30.34	1027.3	10	M	FEW	SCT	BKN	M	800	1100	9000	M	M	M	M	M	M	M	M	53.1	KSFO 0505
SFO	1/5/2022 5:59	54	50	86.29	270	9	0	30.34	M	10	M	FEW	BKN	BKN	M	600	1200	8500	M	M	M	M	M	M	M	M	54	KSFO 0505
SFO	1/5/2022 6:56	53.1	48.9	85.59	210	4	0	30.34	1027.5	10	M	FEW	BKN	M	M	600	1500	M	M	M	M	M	M	M	M	M	53.1	KSFO 0506
SFO	1/5/2022 7:34	53.1	50	89.18	0	0	0	30.34	M	10	M	FEW	BKN	M	M	600	1400	M	M	M	M	M	M	M	M	M	53.1	KSFO 0507
SFO	1/5/2022 7:56	54	48.9	82.82	290	4	0	30.34	1027.3	10	M	FEW	BKN	M	M	600	1300	M	M	M	M	M	M	M	M	M	54	KSFO 0507
SFO	1/5/2022 8:56	53.1	50	89.18	0	0	0	30.33	1027.1	10	M	FEW	BKN	M	M	600	1200	M	M	M	M	M	M	M	M	M	53.1	KSFO 0508
SFO	1/5/2022 9:56	52	50	92.86	180	3	0	30.33	1026.9	10	M	FEW	BKN	M	M	600	1000	M	M	M	M	M	M	M	M	M	52	KSFO 0509
SFO	1/5/2022 10:56	52	50	92.86	160	3	0	30.32	1026.8	10	M	FEW	BKN	M	M	600	1100	M	M	M	M	M	M	M	M	M	52	KSFO 0510
SFO	1/5/2022 11:56	52	50	92.86	160	3	0	30.32	1026.5	10	M	FEW	BKN	M	M	400	1300	M	M	M	M	M	M	M	M	M	52	KSFO 0511
SFO	1/5/2022 12:56	53.1	50	89.18	0	0	0	30.31	1026.4	10	M	FEW	BKN	M	M	400	1200	M	M	M	M	M	M	M	M	M	53.1	KSFO 0512
SFO	1/5/2022 13:56	52	50	92.86	0	0	0	30.31	1026.5	10	M	FEW	BKN	M	M	400	1100	M	M	M	M	M	M	M	M	M	52	KSFO 0513
SFO	1/5/2022 14:56	52	51.1	96.73	10	3	0	30.31	1026.4	10	M	BKN	M	M	M	1000	M	M	M	M	M	M	M	M	M	M	52	KSFO 0514
SFO	1/5/2022 15:56	52	50	92.86	120	5	0	30.32	1026.5	9	M	BKN	OVC	M	M	900	1700	M	M	M	M	M	M	M	M	M	52	KSFO 0515
SFO	1/5/2022 16:56	53.1	50	89.18	160	3	0	30.32	1026.7	9	M	BKN	OVC	M	M	900	1400	M	M	M	M	M	M	M	M	M	53.1	KSFO 0516
SFO	1/5/2022 17:56	53.1	48.9	85.59	110	6	0	30.33	1027.1	9	M	OVC	M	M	M	1000	M	M	M	M	M	M	M	M	M	M	53.1	KSFO 0517
SFO	1/5/2022 18:56	53.1	50	89.18	80	6	0	30.32	1026.6	9	M	OVC	M	M	M	1000	M	M	M	M	M	M	M	M	M	M	53.1	KSFO 0518
SFO	1/5/2022 19:56	54	50	86.29	60	3	0	30.3	1025.9	9	M	OVC	M	M	M	1000	M	M	M	M	M	M	M	M	M	M	54	KSFO 0519
SFO	1/5/2022 20:56	54	51.1	89.88	70	3	0	30.25	1024.3	9	M	FEW	OVC	M	M	800	1100	M	M	M	M	M	M	M	M	M	54	KSFO 0520
SFO	1/5/2022 21:56	55	51.1	86.66	40	6	0	30.23	1023.7	9	M	FEW	BKN	M	M	900	1200	M	M	M	M	M	M	M	M	M	55	KSFO 0521
SFO	1/5/2022 22:07	55	52	89.59	40	6	0	30.23	M	10	M	FEW	SCT	BKN	M	900	1200	20000	M	M	M	M	M	M	M	M	55	KSFO 0522

SFO	1/5/2022 22:56	55.9	52	86.71	360	7	0	30.23	1023.5	10	M	FEW	BKN	BKN	M	500	1300	20000	M	M	M	M	M	M	M	M	55.9	KSFO 0522
SFO	1/5/2022 23:56	57	53.1	86.77	310	7	0	30.22	1023.2	10	M	FEW	BKN	BKN	M	400	1000	20000	M	M	M	M	M	M	M	M	57	KSFO 0523
SFO	1/6/2022 0:56	55.9	52	86.71	300	4	0	30.21	1022.9	10	M	FEW	SCT	BKN	M	400	800	20000	M	M	M	M	M	M	M	M	55.9	KSFO 0600
SFO	1/6/2022 1:17	55.9	52	86.71	290	5	0	30.21	M	10	M	FEW	SCT	BKN	BKN	400	900	1700	20000	M	M	M	M	M	M	M	55.9	KSFO 0601
SFO	1/6/2022 1:56	55	52	89.59	300	3	0	30.2	1022.8	10	M	FEW	BKN	OVC	M	300	1400	1700	M	M	M	M	M	M	M	M	55	KSFO 0601
SFO	1/6/2022 2:56	55.9	53.1	90.29	0	0	0	30.21	1022.8	10	M	FEW	OVC	M	M	400	1200	M	M	M	M	M	M	M	M	M	55.9	KSFO 0602
SFO	1/6/2022 3:56	57	53.1	86.77	0	0	0	30.2	1022.6	10	M	FEW	OVC	M	M	400	1500	M	M	M	M	M	M	M	M	M	57	KSFO 0603
SFO	1/6/2022 4:56	57	53.1	86.77	0	0	0	30.2	1022.6	10	M	FEW	OVC	M	M	400	1500	M	M	M	M	M	M	M	M	M	57	KSFO 0604
SFO	1/6/2022 5:56	55.9	52	86.71	350	4	0	30.19	1022.4	10	M	FEW	OVC	M	M	400	1300	M	M	M	M	M	M	M	M	M	55.9	KSFO 0605
SFO	1/6/2022 6:56	54	52	92.92	20	3	0	30.18	1022	10	M	FEW	OVC	M	M	400	1200	M	M	M	M	M	M	M	M	M	54	KSFO 0606
SFO	1/6/2022 7:56	54	52	92.92	340	5	0	30.18	1022.1	10	M	FEW	BKN	OVC	M	500	800	1000	M	M	M	M	M	M	M	M	54	KSFO 0607
SFO	1/6/2022 8:56	54	51.1	89.88	40	7	0	30.17	1021.6	10	M	FEW	BKN	OVC	M	500	800	1000	M	M	M	M	M	M	M	M	54	KSFO 0608
SFO	1/6/2022 9:56	54	52	92.92	360	3	0	30.17	1021.5	10	M	FEW	BKN	OVC	M	400	600	800	M	M	M	M	M	M	M	M	54	KSFO 0609
SFO	1/6/2022 10:56	54	52	92.92	30	5	0	30.16	1021.3	10	M	FEW	BKN	OVC	M	400	600	800	M	M	M	M	M	M	M	M	54	KSFO 0610
SFO	1/6/2022 11:56	54	52	92.92	0	0	0	30.15	1020.8	10	M	FEW	BKN	OVC	M	400	600	800	M	M	M	M	M	M	M	M	54	KSFO 0611
SFO	1/6/2022 12:56	54	52	92.92	0	0	0	30.13	1020.3	10	M	FEW	BKN	OVC	M	400	600	800	M	M	M	M	M	M	M	M	54	KSFO 0612
SFO	1/6/2022 13:56	53.1	51.1	92.89	360	4	0	30.13	1020.3	10	M	FEW	BKN	OVC	M	500	800	1000	M	M	M	M	M	M	M	M	53.1	KSFO 0613
SFO	1/6/2022 14:56	53.1	51.1	92.89	0	0	0	30.13	1020.2	4	M	OVC	M	M	M	600	M	M	M	BR	M	M	M	M	M	M	53.1	KSFO 0614
SFO	1/6/2022 15:56	53.1	52	96.03	0	0	0	30.12	1020	4	M	OVC	M	M	M	500	M	M	M	BR	M	M	M	M	M	M	53.1	KSFO 0615
SFO	1/6/2022 16:56	53.1	51.1	92.89	80	3	0	30.11	1019.7	4	M	OVC	M	M	M	500	M	M	M	BR	M	M	M	M	M	M	53.1	KSFO 0616
SFO	1/6/2022 17:56	53.1	51.1	92.89	50	3	0	30.12	1019.9	4	M	OVC	M	M	M	600	M	M	M	BR	M	M	M	M	M	M	53.1	KSFO 0617
SFO	1/6/2022 18:56	53.1	51.1	92.89	20	4	0	30.12	1019.9	4	M	OVC	M	M	M	600	M	M	M	BR	M	M	M	M	M	M	53.1	KSFO 0618
SFO	1/6/2022 19:56	54	51.1	89.88	20	6	0	30.09	1018.8	4	M	OVC	M	M	M	700	M	M	M	BR	M	M	M	M	M	M	54	KSFO 0619
SFO	1/6/2022 20:56	54	51.1	89.88	360	4	0	30.05	1017.7	4	M	OVC	M	M	M	600	M	M	M	BR	M	M	M	M	M	M	54	KSFO 0620
SFO	1/6/2022 21:56	54	51.1	89.88	20	4	0	30.02	1016.6	4	M	OVC	M	M	M	500	M	M	M	BR	M	M	M	M	M	M	54	KSFO 0621
SFO	1/6/2022 22:56	53.1	51.1	92.89	40	4	0	30	1015.9	3	M	OVC	M	M	M	500	M	M	M	BR	M	M	M	M	M	M	53.1	KSFO 0622
SFO	1/6/2022 23:56	53.1	51.1	92.89	0	0	0	30	1015.9	4	M	OVC	M	M	M	500	M	M	M	BR	M	M	M	M	M	M	53.1	KSFO 0623
SFO	1/7/2022 0:56	53.1	51.1	92.89	0	0	0	29.99	1015.5	5	M	OVC	M	M	M	500	M	M	M	BR	M	M	M	M	M	M	53.1	KSFO 0700
SFO	1/7/2022 1:56	53.1	50	89.18	30	5	0	29.99	1015.4	7	M	OVC	M	M	M	600	M	M	M	M	M	M	M	M	M	M	53.1	KSFO 0701
SFO	1/7/2022 2:56	53.1	50	89.18	50	4	0	29.98	1015.2	8	M	SCT	OVC	M	M	400	700	M	M	M	M	M	M	M	M	M	53.1	KSFO 0702
SFO	1/7/2022 3:56	53.1	50	89.18	180	3	0	29.99	1015.3	6	M	SCT	BKN	OVC	M	400	700	1300	M	BR	M	M	M	M	M	M	53.1	KSFO 0703
SFO	1/7/2022 4:21	53.1	50	89.18	0	0	0	29.99	M	6	M	FEW	SCT	OVC	M	400	700	1100	M	BR	M	M	M	M	M	M	53.1	KSFO 0704
SFO	1/7/2022 4:37	53.1	50	89.18	280	3	0	29.99	M	5	M	FEW	BKN	OVC	M	400	800	1100	M	BR	M	M	M	M	M	M	53.1	KSFO 0704
SFO	1/7/2022 4:56	52	51.1	96.73	0	0	0	29.99	1015.4	4	M	FEW	BKN	OVC	M	300	600	2400	M	BR	M	M	M	M	M	M	52	KSFO 0704
SFO	1/7/2022 5:56	53.1	50	89.18	290	6	0	30	1015.7	7	M	FEW	BKN	OVC	M	300	800	2100	M	M	M	M	M	M	M	M	53.1	KSFO 0705
SFO	1/7/2022 6:56	53.1	50	89.18	0	0	0	29.98	1015	9	M	FEW	BKN	BKN	M	300	900	1600	M	M	M	M	M	M	M	M	53.1	KSFO 0706
SFO	1/7/2022 7:56	53.1	50	89.18	210	3	0	29.97	1014.9	10	M	FEW	BKN	OVC	M	300	1000	1700	M	M	M	M	M	M	M	M	53.1	KSFO 0707
SFO	1/7/2022 8:56	52	50	92.86	220	3	T	29.97	1014.7	8	M	FEW	BKN	OVC	M	400	800	1500	M	#NAME?	M	M	M	M	M	M	52	KSFO 0708
SFO	1/7/2022 9:28	52	50	92.86	0	0	T	29.96	M	8	M	FEW	BKN	OVC	M	400	1100	3900	M	M	M	M	M	M	M	M	52	KSFO 0709
SFO	1/7/2022 9:56	52	50	92.86	180	3	T	29.97	1014.7	6	M	FEW	BKN	OVC	M	800	1700	2300	M	BR	M	M	M	M	M	M	52	KSFO 0709
SFO	1/7/2022 10:37	50	48.9	95.98	140	4	0	29.96	M	10	M	FEW	BKN	M	M	800	3300	M	M	M	M	M	M	M	M	M	50	KSFO 0710
SFO	1/7/2022 10:56	51.1	50	96	150	3	0	29.96	1014.6	10	M	FEW	SCT	SCT	M	800	3400	20000	M	M	M	M	M	M	M	M	51.1	KSFO 0710
SFO	1/7/2022 11:56	51.1	50	96	0	0	0	29.97	1014.8	10	M	FEW	BKN	M	M	400	4000	M	M	M	M	M	M	M	M	M	51.1	KSFO 0711
SFO	1/7/2022 12:56	50	48	92.8	150	5	0	29.95	1014.2	10	M	FEW	SCT	SCT	M	900	6000	20000	M	M	M	M	M	M	M	M	50	KSFO 0712
SFO	1/7/2022 13:56	50	48	92.8	170	5	0	29.96	1014.4	10	M	FEW	BKN	BKN	M	1400	4000	6000	M	M	M	M	M	M	M	M	50	KSFO 0713
SFO	1/7/2022 14:56	51.1	48	89.09	140	5	0	29.96	1014.4	10	M	FEW	SCT	OVC	M	1400	3500	5000	M	M	M	M	M	M	M	M	51.1	KSFO 0714
SFO	1/7/2022 15:56	53.1	45	73.89	150	5	0	29.95	1014.2	10	M	FEW	SCT	OVC	M	1400	3500	5000	M	M	M	M	M	M	M	M	53.1	KSFO 0715
SFO	1/7/2022 16:56	53.1	46.9	79.4	160	12	0	29.95	1014.2	10	M	OVC	M	M	M	2700	M	M	M	M	M	M	M	M	M	M	53.1	KSFO 0716
SFO	1/7/2022 17:56	53.1	48	82.76	150	9	T	29.98	1015.1	6	M	FEW	FEW	OVC	M	1500	2500	3000	M	HZ	M	M	M	M	M	M	53.1	KSFO 0717
SFO	1/7/2022 18:56	54	48.9	82.82	160	11	0	29.97	1014.9	9	M	BKN	OVC	M	M	2900	3600	M	M	M	M	M	M	M	M	M	54	KSFO 0718
SFO	1/7/2022 19:56	55.9	50	80.52	180	8	0	29.95	1014.3	10	M	SCT	OVC	M	M	2900	3800	M	M	M	M	M	M	M	M	M	55.9	KSFO 0719
SFO	1/7/2022 20:56	55.9	50	80.52	220	11	0	29.95	1014	10	M	FEW	SCT	BKN	M	2800	3500	18000	M	M	M	M	M	M	M	M	55.9	KSFO 0720
SFO	1/7/2022 21:56	55.9	50	80.52	230	11	0	29.94	1013.8	10	M	SCT	BKN	M	M	2800	18000	M	M	M	M	M	M	M	M	M	55.9	KSFO 0721
SFO	1/7/2022 22:56	55.9	50	80.52	280	14	0	29.94	1013.8	10	M	FEW	BKN	OVC	M	1000	1800	2800	M	M	M	M	M	M	M	M	55.9	KSFO 0722
SFO	1/7/2022 23:56	55.9	48	74.72	300	12	0	29.96	1014.4	10	M	BKN	BKN	M	M	1600	18000	M	M	M	M	M	M	M	M	M	55.9	KSFO 0723
SFO	1/8/2022 0:11	55.9	48	74.72	280	11	0	29.96	M	10	M	SCT	BKN	M	M	1700	18000	M	M	M	M	M	M	M	M	M	55.9	KSFO 0800
SFO	1/8/2022 0:56	54	48	80.07	290	10	0	29.97	1015	10	M	FEW	SCT	BKN	M	900	1600	18000	M	M	M	M	M	M	M	M	54	KSFO 0800
SFO	1/8/2022 1:15	54	48	80.07	300	9	0	29.97	M	10	M	FEW	BKN	BKN	M	900	1600	18000	M	M	M	M	M	M	M	M	54	KSFO 0801
SFO	1/8/2022 1:27	53.1	46.9	79.4	280	9	0	29.97	M	10	M	FEW	SCT	M	M	900	1600	M	M	M	M	M	M	M	M	M	53.1	KSFO 0801
SFO	1/8/2022 1:56	53.1	48	82.76	260	9	0	29.98	1015	10	M	FEW	SCT	M	M	900	1600	M	M	M	M	M	M	M	M	M	53.1	KSFO 0801
SFO	1/8/2022 2:32	53.1	48	82.76	290	8	0	29.98	M	10	M	FEW	BKN	M	M	900	1400	M	M	M	M	M	M	M	M	M	53.1	KSFO 0802
SFO	1/8/2022 2:56	52	48	86.17	290	9	0	29.98	1015.3	10	M	FEW	SCT	M	M	900	1400	M	M	M	M	M	M	M	M	M	52	KSFO 0802
SFO	1/8/2022 3:56	52	48	86.17	280	8	0	30	1015.7	10	M	FEW	FEW	M	M	700	1400	M	M	M	M	M	M	M	M	M	52	KSFO 0803
SFO	1/8/2022 4:34	52	48	86.17	280	9	0	30.01	M	10	M	FEW	BKN	M	M	700	1100	M	M	M	M	M	M	M	M	M	52	KSFO 0804
SFO	1/8/2022 4:56	52	46.9	82.68	290	12	0	30.01	1016.2	10	M	FEW	BKN	M	M	600	1100	M	M	M	M	M	M	M	M	M	52	KSFO 0804
SFO	1/8/2022 5:56	51.1	46.9	85.48	280	14	0	30.03	1016.8	10	M	FEW	BKN	M	M	400	1000	M	M	M	M	M	M	M	M	M	51.1	KSFO 0805
SFO	1/8/2022 6:56	51.1	46.9	85.48	300	10	0	30.03	1016.8	10	M	FEW	BKN	M	M	400	1000	M	M	M	M	M	M	M	M	M	51.1	KSFO 0806
SFO	1/8/2022 7:17	51.1	46.9	85.48	300	5	0	30.02	M	10	M	FEW	SCT	M	M	400	1000	M	M	M	M	M	M	M	M	M	51.1	KSFO 0807
SFO	1/8/2022 7:56	50	46	86.06	310	3	0	30.02	1016.6	10	M	FEW	SCT	M	M	400	1000	M	M	M	M	M	M	M	M	M	50	KSFO 0807
SFO	1/8/2022 8:24	51.8	46.4	81.74	320	4	0	30.04	M	10	M	FEW	BKN	M	M	400	1100	M	M	M	M	M	M	M	M	M	51.8	KSFO 0808
SFO	1/8/2022 8:56	51.1	46.9	85.48	300	3	0	30.05	1017.4	10	M	FEW	BKN	M	M	400	1100	M	M	M	M	M	M	M	M	M	51.1	KSFO 0808
SFO	1/8/2022 9:56	50	46	86.06	270	3	0	30.06	1017.8	10	M	FEW	BKN	M	M	600	1100	M	M	M	M	M	M	M	M	M	50	KSFO 0809
SFO	1/8/2022 10:16	50	46	86.06	0	0	0	30.06	M	10	M	FEW	BKN	M	M	600	900	M	M	M	M	M	M	M	M	M	50	KSFO 0810
SFO	1/8/2022 10:50	48.2	44.6	87.28	280	4	0	30.07	M	10	M	FEW	SCT	M	M	300	700	M	M	M	M	M	M	M	M	M	46.34	KSFO 0810
SFO	1/8/2022 10:56	46.9	45	93.06	280	4	0	30.07	1018.3	10	M	FEW	FEW	M	M	300	700	M	M	M	M	M	M	M	M	M	44.82	KSFO 0810
SFO	1/8/2022 11:56	46.9	44.1	89.92	280	6	0	30.08	1018.7	10	M	FEW	FEW	M	M	400	1200	M	M	M	M	M	M	M	M	M	43.48	KSFO 0811
SFO	1/8/2022 12:34	46.4	44.6	93.4	300	4	0	30.1	M	10	M	FEW	BKN	M	M	400	1800	M	M	M	M	M	M	M	M	M	44.24	KSFO 0812

Appendix D:
Sample 2022 KDEN METAR Data

station	valid	tmpf	dwpf	relh	drct	sknt	p01i	alti	mslp	vsby	gust	skyc1	skyc2	skyc3	skyc4	skyl1	skyl2	skyl3	skyl4	wxcodes	ice_accreti	ice_accreti	ice_accreti	peak_wind	peak_wind	peak_wind_time	feel	metar	snowdepth
DEN	6/11/2022 22:53	99	35.1	10.87	320	5	0	29.88	1001.7	10	15	SCT	SCT	BKN	M	11000	16000	22000	M	M	M	M	M	M	M	M	93.48	KDEN 1122	M
DEN	7/9/2022 21:53	99	32	9.6	30	8	0	30.23	1013.9	10	M	SCT	SCT	M	M	13000	22000	M	M	M	M	M	M	M	M	M	93.03	KDEN 0921	M
DEN	7/10/2022 21:53	99	35.1	10.87	320	14	0	30.13	1010.2	10	20	FEW	BKN	BKN	M	11000	15000	22000	M	M	M	M	M	M	M	M	93.48	KDEN 1021	M
DEN	7/18/2022 18:53	99	39.9	13.13	M	3	0	30.08	1008.4	10	M	FEW	FEW	SCT	M	9000	12000	22000	M	M	M	M	M	M	M	M	94.35	KDEN 1818	M
DEN	8/5/2022 20:53	99	43	14.8	0	0	0	30.01	1005.8	10	M	SCT	SCT	BKN	M	11000	15000	22000	M	M	M	M	M	M	M	M	94.72	KDEN 0520	M
DEN	6/11/2022 21:34	98.1	33.1	10.32	330	7	0	29.9	M	10	15	FEW	FEW	M	M	11000	22000	M	M	M	M	M	M	M	M	M	92.42	KDEN 1121	M
DEN	6/11/2022 21:53	98.1	33.1	10.32	290	11	0	29.9	1002.4	10	17	SCT	SCT	M	M	11000	22000	M	M	M	M	M	M	M	M	M	92.42	KDEN 1121	M
DEN	6/13/2022 22:53	98.1	19	5.75	200	14	0	29.56	990.5	10	24	FEW	M	M	M	12000	M	M	M	M	M	M	M	27	180	6/13/2022 22:43	91.05	KDEN 1322	M
DEN	7/9/2022 19:53	98.1	30.9	9.44	360	11	0	30.27	1014.9	10	15	FEW	FEW	M	M	11000	22000	M	M	M	M	M	M	M	M	M	92.13	KDEN 0919	M
DEN	7/9/2022 20:53	98.1	33.1	10.32	80	3	0	30.25	1014.2	10	M	SCT	SCT	M	M	13000	22000	M	M	M	M	M	M	M	M	M	92.42	KDEN 0920	M
DEN	7/9/2022 23:53	98.1	32	9.87	M	M	0	30.21	1013	10	M	SCT	BKN	BKN	M	12000	16000	22000	M	M	M	M	M	M	M	M	92.27	KDEN 0923	M
DEN	7/10/2022 17:53	98.1	32	9.87	30	5	0	30.21	1012.7	10	M	FEW	BKN	BKN	M	11000	15000	22000	M	M	M	M	M	M	M	M	92.27	KDEN 1017	M
DEN	7/10/2022 18:53	98.1	35.1	11.17	70	6	0	30.19	1011.6	10	M	FEW	BKN	BKN	M	11000	15000	22000	M	M	M	M	M	M	M	M	92.73	KDEN 1018	M
DEN	7/10/2022 20:53	98.1	34	10.7	60	3	0	30.15	1010.2	10	M	SCT	BKN	BKN	M	11000	15000	22000	M	M	M	M	M	M	M	M	92.55	KDEN 1020	M
DEN	7/10/2022 22:05	98.1	35.1	11.17	350	14	0	30.13	M	10	19	FEW	BKN	BKN	M	11000	15000	22000	M	M	M	M	M	M	M	M	92.73	KDEN 1022	M
DEN	7/14/2022 20:53	98.1	39.9	13.5	260	5	0	30.17	1011.3	10	M	FEW	SCT	SCT	M	10000	12000	22000	M	M	M	M	M	M	M	M	93.51	KDEN 1420	M
DEN	8/1/2022 21:53	98.1	37.9	12.48	30	10	0	30.09	1009	10	15	FEW	SCT	BKN	M	12000	17000	22000	M	M	M	M	M	M	M	M	93.22	KDEN 0121	M
DEN	8/5/2022 19:53	98.1	43	15.21	20	7	0	30.02	1006.3	10	M	SCT	SCT	SCT	M	10000	15000	22000	M	M	M	M	M	M	M	M	93.85	KDEN 0519	M
DEN	9/7/2022 20:53	98.1	30	9.1	0	0	0	30.23	1013.9	10	M	FEW	FEW	M	M	10000	14000	M	M	M	M	M	M	M	M	M	92.02	KDEN 0720	M
DEN	9/8/2022 18:53	98.1	28	8.39	320	8	0	29.97	1004.4	10	M	FEW	SCT	SCT	M	10000	15000	22000	M	M	M	M	M	M	M	M	91.79	KDEN 0818	M
DEN	6/11/2022 20:53	97	34	11.06	M	M	0	29.92	1003	10	M	FEW	FEW	M	M	12000	22000	M	M	M	M	M	M	M	M	M	91.64	KDEN 1120	M
DEN	6/11/2022 20:57	97	34	11.06	160	7	0	29.91	M	10	14	FEW	FEW	M	M	11000	22000	M	M	M	M	M	M	M	M	M	91.64	KDEN 1120	M
DEN	6/13/2022 20:53	97	25	7.66	190	8	0	29.61	992.3	10	14	FEW	M	M	M	14000	M	M	M	M	M	M	M	M	M	M	90.58	KDEN 1320	M
DEN	6/13/2022 21:53	97	21.9	6.73	170	8	0	29.59	991.5	10	22	FEW	M	M	M	14000	M	M	M	M	M	M	M	26	220	6/13/2022 21:40	90.33	KDEN 1321	M
DEN	6/13/2022 23:53	97	18	5.7	230	17	0	29.54	990	10	27	FEW	M	M	M	12000	M	M	M	M	M	M	M	29	200	6/13/2022 23:22	90.07	KDEN 1323	M
DEN	6/17/2022 19:53	97	37	12.46	130	19	0	30.01	1006.5	10	28	FEW	SCT	M	M	10000	22000	M	M	M	M	M	M	32	150	6/17/2022 18:57	92.13	KDEN 1719	M
DEN	6/17/2022 20:53	97	33.1	10.67	140	16	0	29.99	1006	10	28	FEW	SCT	M	M	10000	22000	M	M	M	M	M	M	31	160	6/17/2022 20:12	91.5	KDEN 1720	M
DEN	6/17/2022 21:53	97	32	10.21	140	23	0	29.96	1004.9	10	29	FEW	SCT	SCT	M	10000	14000	22000	M	M	M	M	M	32	150	6/17/2022 21:17	91.35	KDEN 1721	M
DEN	6/17/2022 22:53	97	32	10.21	170	20	0	29.96	1004.9	10	28	FEW	SCT	SCT	M	10000	14000	22000	M	M	M	M	M	32	150	6/17/2022 22:19	91.35	KDEN 1722	M
DEN	7/9/2022 17:53	97	39	13.48	M	3	0	30.31	1016.1	10	M	FEW	SCT	M	M	11000	22000	M	M	M	M	M	M	M	M	M	92.4	KDEN 0917	M
DEN	7/9/2022 22:53	97	30.9	9.76	0	0	0	30.22	1013.8	10	M	SCT	SCT	M	M	12000	22000	M	M	M	M	M	M	M	M	M	91.21	KDEN 0922	M
DEN	7/9/2022 23:55	97	32	10.21	40	10	0	30.21	M	10	M	SCT	BKN	BKN	M	12000	16000	22000	M	M	M	M	M	M	M	M	91.35	KDEN 0923	M
DEN	7/10/2022 19:53	97	32	10.21	50	6	0	30.16	1010.9	10	M	FEW	BKN	BKN	M	11000	15000	22000	M	M	M	M	M	M	M	M	91.35	KDEN 1019	M
DEN	7/13/2022 20:53	97	33.1	10.67	90	5	0	30.12	1010.3	10	M	SCT	SCT	SCT	M	9000	14000	22000	M	M	M	M	M	M	M	M	91.5	KDEN 1320	M
DEN	7/18/2022 19:53	97	39.9	13.96	0	0	0	30.07	1007.6	10	M	FEW	SCT	BKN	M	10000	14000	18000	M	M	M	M	M	M	M	M	92.48	KDEN 1819	M
DEN	7/19/2022 20:53	97	43	15.73	M	6	0	30.07	1007.7	10	M	SCT	BKN	BKN	M	11000	15000	22000	M	VCTS	M	M	M	M	M	M	92.79	KDEN 1920	M
DEN	7/19/2022 20:56	97	43	15.73	M	3	0	30.07	M	10	M	FEW	BKN	BKN	M	11000	15000	22000	M	M	M	M	M	M	M	M	92.79	KDEN 1920	M
DEN	7/21/2022 20:53	97	34	11.06	310	7	0	30.09	1009.1	10	M	SCT	SCT	BKN	M	9000	12000	22000	M	M	M	M	M	M	M	M	91.64	KDEN 2120	M
DEN	7/22/2022 20:53	97	34	11.06	M	4	0	30.07	1008.1	10	M	FEW	SCT	SCT	M	9000	12000	22000	M	M	M	M	M	M	M	M	91.64	KDEN 2220	M
DEN	8/4/2022 22:53	97	39	13.48	M	3	0	30.07	1008.2	10	M	FEW	FEW	SCT	M	9000	13000	22000	M	M	M	M	M	M	M	M	92.4	KDEN 0422	M
DEN	8/5/2022 18:53	97	46	17.64	10	6	0	30.05	1007.1	10	M	FEW	FEW	SCT	M	10000	15000	22000	M	M	M	M	M	M	M	M	93.19	KDEN 0518	M
DEN	9/5/2022 22:53	97	37	12.46	M	4	0	30.09	1008.9	10	M	FEW	FEW	M	M	11000	15000	M	M	M	M	M	M	M	M	M	92.13	KDEN 0522	M
DEN	9/6/2022 23:53	97	32	10.21	0	0	0	30.22	1013.4	10	M	FEW	FEW	M	M	11000	22000	M	M	M	M	M	M	M	M	M	91.35	KDEN 0623	M
DEN	9/7/2022 19:53	97	32	10.21	340	3	0	30.26	1014.9	10	M	FEW	FEW	M	M	9000	13000	M	M	M	M	M	M	M	M	M	91.35	KDEN 0719	M
DEN	9/7/2022 21:53	97	30.9	9.76	210	5	0	30.2	1012.9	10	M	FEW	FEW	M	M	10000	14000	M	M	M	M	M	M	M	M	M	91.21	KDEN 0721	M
DEN	9/8/2022 20:53	97	28	8.67	280	5	0	29.91	1002.6	10	M	FEW	SCT	SCT	M	10000	15000	22000	M	M	M	M	M	M	M	M	90.87	KDEN 0820	M
DEN	6/13/2022 20:20	96.1	25	7.88	200	9	0	29.63	M	10	16	FEW	M	M	M	14000	M	M	M	M	M	M	M	M	M	M	89.84	KDEN 1320	M
DEN	7/9/2022 18:53	96.1	32	10.49	60	7	0	30.28	1015.6	10	18	FEW	SCT	M	M	11000	22000	M	M	M	M	M	M	M	M	M	90.61	KDEN 0918	M
DEN	7/10/2022 16:53	96.1	36	12.31	310	6	0	30.22	1013.1	10	16	FEW	BKN	BKN	M	11000	15000	22000	M	M	M	M	M	M	M	M	91.21	KDEN 1016	M
DEN	7/13/2022 18:53	96.1	36	12.31	20	11	0	30.16	1011.7	10	18	FEW	SCT	SCT	M	9000	14000	22000	M	M	M	M	M	M	M	M	91.21	KDEN 1318	M
DEN	7/13/2022 19:53	96.1	34	11.37	M	4	0	30.14	1011	10	15	FEW	SCT	SCT	M	9000	14000	22000	M	M	M	M	M	M	M	M	90.89	KDEN 1319	M
DEN	7/13/2022 21:53	96.1	35.1	11.88	220	5	0	30.11	1010	10	16	SCT	BKN	BKN	M	11000	14000	22000	M	M	M	M	M	M	M	M	91.07	KDEN 1321	M
DEN	7/13/2022 22:29	96.1	35.1	11.88	10	9	0	30.11	M	10	M	SCT	BKN	BKN	M	11000	14000	22000	M	M	M	M	M	M	M	M	91.07	KDEN 1322	M
DEN	7/14/2022 21:36	96.1	41	14.97	0	0	0	30.17	M	10	M	SCT	BKN	BKN	M	12000	16000	22000	M	M	M	M	M	M	M	M	91.73	KDEN 1421	M
DEN	7/15/2022 20:53	96.1	46	18.13	110	6	0	30.18	1012.1	10	M	FEW	SCT	BKN	M	10000	15000	22000	M	M	M	M	M	M	M	M	92.3	KDEN 1520	M
DEN	7/18/2022 17:53	96.1	42.1	15.62	210	6	0	30.11	1009	10	M	FEW	FEW	SCT	M	11000	15000	22000	M	M	M	M	M	M	M	M	91.83	KDEN 1817	M
DEN	7/18/2022 20:10	96.1	39	13.85	190	4	0	30.07	M	10	M	SCT	BKN	BKN	M	10000	16000	22000	M	VCTS	M	M	M	M	M	M	91.57	KDEN 1820	M
DEN	7/19/2022 19:53	96.1	41	14.97	180	5	0	30.08	1008.1	10	M	FEW	SCT	BKN	M	10000	15000	22000	M	M	M	M	M	M	M	M	91.73	KDEN 1919	M
DEN	7/21/2022 19:53	96.1	28.9	9.25	10	11	0	30.11	1009.5	10	M	SCT	SCT	M	M	9000	12000	M	M	M	M	M	M	M	M	M	90.23	KDEN 2119	M
DEN	7/22/2022 19:53	96.1	35.1	11.88	20	9	0	30.1	1008.8	10	M	FEW	FEW	SCT	M	9000	12000	22000	M	M	M	M	M	M	M	M	91.07	KDEN 2219	M
DEN	7/23/2022 17:53	96.1	39	13.85	60	9	0	30.06	1007.4	10	M	FEW	FEW	BKN	M	10000	15000	22000	M	M	M	M	M	M	M	M	91.57	KDEN 2317	M
DEN	7/23/2022 18:40	96.1	39	13.85	360	16	0	30.06	M	10	24	FEW	FEW	BKN	M	10000	15000	22000	M	M	M	M	M	M	M	M	91.57	KDEN 2318	M
DEN	8/1/2022 20:53	96.1	35.1	11.88	30	6	0	30.11	1009.6	10	M	FEW	SCT	SCT	M	10000	17000	22000	M	M	M	M	M	M	M	M	91.07	KDEN 0120	M
DEN	8/4/2022 20:53	96.1	39	13.85	170	9	0	30.1	1009.2	10	14	SCT	SCT	SCT	M	9000	13000	22000	M	M	M	M	M	M	M	M	91.57	KDEN 0420	M
DEN	8/4/2022 23:53	96.1	39	13.85	M	4	0	30.05	1007.8	10	M	FEW	SCT	SCT	M	9000	13000	22000	M	M	M	M	M	M	M	M	91.57	KDEN 0423	M
DEN	8/11/2022 19:53	96.1	43	16.17	360	4	0	30.2	1012.8	10	M	FEW	FEW	M	M	9000	22000	M	M	M	M	M	M	M	M	M	91.93	KDEN 1119	M
DEN	8/11/2022 20:53	96.1	41	14.97	300	3	0	30.18	1012.1	10	M	FEW	FEW	M	M	10000	20000	M	M	M	M	M	M	M	M	M	91.73	KDEN 1120	M
DEN	9/5/2022 21:53	96.1	36	12.31	330	7	0	30.09	1009.1	10	M	FEW	FEW	M	M	11000	15000	M	M	M	M	M	M	M	M	M	91.21	KDEN 0521	M
DEN	9/6/2022 20:53	96.1	34	11.37	M	3	0	30.22	1013.3	10	M	FEW	FEW	M	M	14000	22000	M	M	M	M	M	M	M	M	M	90.89	KDEN 0620	M
DEN	9/6/2022 21:53	96.1	30	9.68	90	4	0	30.21	1013.1	10	M	FEW	FEW	M	M	14000	22000	M	M	M	M	M	M	M	M	M	90.35	KDEN 0621	M
DEN	9/6/2022 22:53	96.1	30.9	10.04	130	4	0	30.22	1013.5	10	M	FEW	FEW	M	M	14000	22000	M	M	M	M	M	M	M	M	M	90.46	KDEN 0622	M
DEN	9/7/2022 22:53	96.1	30.9	10.04	170	13	0	30.19	1012.8	10	24	FEW	SCT	M	M	10000	15000	M	M	M	M	M	M	M	M	M	90.46	KDEN 0722	M
DEN	9/8/2022 17:53	96.1	28.9	9.25	M	6	0	30.01	1005.8	10	M	FEW	FEW	M	M	11000	15000	M	M	M	M	M	M	M	M	M	90.23	KDEN 0817	M
DEN	9/8/2022 19:53	96.1	27	8.56	330	6	0	29.95	1003.8	10	M	FEW	SCT	SCT	M	10000	15000	22000	M	M	M	M	M	M	M	M	90.03	KDEN 0819	M
DEN	9/8/2022 21:53	96.1	28	8.92	40	9	0	29.89	1002	10	M	FEW	BKN	BKN	M	10000	15000	20000	M	M	M	M	M	M	M	M	90.13	KDEN 0821	M
DEN	6/11/2022 18:53	95	37	13.25	280	7	0	29.97	1004.5	10	M	FEW	FEW	M	M	11000	22000	M	M	M	M	M	M	M	M	M	90.44	KDEN 1118	M
DEN	6/11/2022 19:53	95	35.1	12.29	0	0	0	29.94	1003.6	10	M	FEW	FEW	M	M	11000	22000	M	M	M	M	M	M	M	M	M	90.17	KDEN 1119	M
DEN	6/11/2022 23:53	95	33.1	11.34	300	8	0	29.87	1001.7	10	17	SCT	SCT	BKN	M	11000	16000	22000	M	M	M	M	M	M	M	M	89.86	KDEN 1123	M
DEN	6/13/2022 19:53	95	25	8.15	M	M	0	29.65	993.7	9	M	FEW	M	M	M	14000	M	M	M	M	M	M	M	M	M	M	88.93	KDEN 1319	M
DEN	6/17/2022 18:53	95	39	14.33	130	18	0	30.05	1007.7	10	28	FEW	SCT	M	M	10000	22000	M	M	M	M	M	M	31	130	6/17/2022 18:05	90.55	KDEN 1718	M
DEN	7/4/2022 21:53	95	39	14.33	50	10	0	30.01	1006.4	10	15	SCT	BKN	BKN	M	10000	15000	22000	M	M	M	M	M	M	M	M	90.55	KDEN 0421	M
DEN	7/10/2022 22:53	95	36	12.73	340	13	0	30.13	1010.2	10	M	FEW	BKN	BKN	M	11000	15000	22000	M	M	M	M	M	M	M	M	90.32	KDEN 1022	M
DEN	7/13/2022 22:53	95	35.1	12.29	10	4	0	30.1	1010.3	10	M	FEW	BKN	BKN	M	11000	13000	22000	M	M	M	M	M	M	M	M	90.17	KDEN 1322	M
DEN	7/14/2022 18:53	95	41	15.49	M	3	0	30.2	1012.7	10	M	FEW	SCT	SCT	M	9000	12000	22000	M	M	M	M	M	M	M	M	90.7	KDEN 1418	M
DEN	7/14/2022 19:53	95	41	15.49	M	3	0	30.19	1012.2	10	M	FEW	SCT	SCT	M	10000	12000	22000	M	M	M	M	M	M	M	M	90.7	KDEN 1419	M
DEN	7/14/2022 21:53	95	39.9	14.84	250	6	0	30.16	1011.5	10	M	BKN	BKN	BKN	M	12000	16000	22000	M	M	M	M	M	M	M	M	90.61	KDEN 1421	M

DEN	7/14/2022 22:41	95	39.9	14.84	M	5	0	30.16	M	10	M	SCT	BKN	BKN	M	12000	16000	22000	M	VCTS	M	M	M	M	M	M	90.61	KDEN 1422	M
DEN	7/17/2022 19:53	95	42.1	16.16	M	5	0	30.18	1012.2	10	M	SCT	SCT	M	M	10000	22000	M	M	M	M	M	M	M	M	M	90.79	KDEN 1719	M
DEN	7/17/2022 21:53	95	42.1	16.16	M	M	0	30.15	1011.2	10	M	FEW	SCT	M	M	11000	25000	M	M	M	M	M	M	M	M	M	90.79	KDEN 1721	M
DEN	7/17/2022 21:57	95	42.1	16.16	150	5	0	30.14	M	10	15	FEW	SCT	M	M	11000	25000	M	M	M	M	M	M	M	M	M	90.79	KDEN 1721	M
DEN	7/17/2022 22:53	95	43	16.73	140	8	0	30.14	1011	10	20	FEW	SCT	M	M	11000	25000	M	M	M	M	M	M	M	M	M	90.88	KDEN 1722	M
DEN	7/18/2022 22:53	95	41	15.49	160	7	0	30.05	1007.2	10	M	BKN	BKN	BKN	M	12000	16000	22000	M	M	M	M	M	M	M	M	90.7	KDEN 1822	M
DEN	7/19/2022 17:53	95	41	15.49	30	7	0	30.11	1009.1	10	M	FEW	SCT	SCT	M	10000	14000	22000	M	M	M	M	M	M	M	M	90.7	KDEN 1917	M
DEN	7/19/2022 18:53	95	41	15.49	M	5	0	30.1	1008.7	10	M	FEW	SCT	SCT	M	10000	14000	22000	M	M	M	M	M	M	M	M	90.7	KDEN 1918	M
DEN	7/19/2022 20:42	95	43	16.73	350	7	0	30.07	M	10	M	SCT	BKN	BKN	M	11000	15000	22000	M	VCTS	M	M	M	M	M	M	90.88	KDEN 1920	M
DEN	7/20/2022 20:53	95	43	16.73	30	10	0	30.13	1010.4	10	M	FEW	SCT	SCT	M	10000	14000	17000	M	M	M	M	M	M	M	M	90.88	KDEN 2020	M
DEN	7/21/2022 23:53	95	35.1	12.29	360	13	0	30.06	1008.5	10	M	FEW	SCT	BKN	M	10000	15000	22000	M	M	M	M	M	M	M	M	90.17	KDEN 2123	M
DEN	7/22/2022 21:53	95	35.1	12.29	M	M	0	30.06	1007.6	10	M	FEW	SCT	BKN	M	9000	12000	22000	M	M	M	M	M	M	M	M	90.17	KDEN 2221	M
DEN	7/22/2022 21:59	95	35.1	12.29	180	6	0	30.06	M	10	M	FEW	SCT	BKN	M	9000	12000	22000	M	M	M	M	M	M	M	M	90.17	KDEN 2221	M
DEN	7/22/2022 22:53	95	35.1	12.29	220	7	0	30.05	1007.8	10	15	FEW	SCT	BKN	M	9000	15000	20000	M	M	M	M	M	M	M	M	90.17	KDEN 2222	M
DEN	7/23/2022 16:53	95	39.9	14.84	360	6	0	30.05	1007.2	10	M	FEW	FEW	BKN	M	10000	15000	22000	M	M	M	M	M	M	M	M	90.61	KDEN 2316	M
DEN	7/23/2022 19:53	95	41	15.49	20	14	0	30.06	1007.8	10	27	FEW	SCT	BKN	BKN	7000	10000	15000	22000	M	M	M	M	36	10	7/23/2022 18:58	90.7	KDEN 2319	M
DEN	8/1/2022 18:53	95	43	16.73	40	7	0	30.15	1011.5	10	17	FEW	FEW	SCT	M	9000	14000	22000	M	M	M	M	M	M	M	M	90.88	KDEN 0118	M
DEN	8/1/2022 22:53	95	34	11.76	340	4	0	30.08	1009.1	10	M	FEW	BKN	BKN	M	10000	13000	18000	M	M	M	M	M	M	M	M	90	KDEN 0122	M
DEN	8/4/2022 21:53	95	39.9	14.84	M	3	0	30.08	1009	10	M	FEW	FEW	SCT	M	9000	13000	22000	M	M	M	M	M	M	M	M	90.61	KDEN 0421	M
DEN	8/5/2022 0:53	95	39	14.33	120	9	0	30.04	1007.7	10	M	FEW	SCT	BKN	M	9000	13000	22000	M	M	M	M	M	M	M	M	90.55	KDEN 0500	M
DEN	8/5/2022 17:53	95	50	21.79	M	5	0	30.06	1007.7	10	M	FEW	FEW	SCT	M	10000	15000	22000	M	M	M	M	M	M	M	M	91.89	KDEN 0517	M
DEN	8/9/2022 22:53	95	37.9	13.73	M	M	0	30.19	1012.7	10	M	SCT	M	M	M	11000	M	M	M	M	M	M	M	M	M	M	90.48	KDEN 0922	M
DEN	8/9/2022 22:56	95	37.9	13.73	90	6	0	30.19	M	10	M	SCT	M	M	M	11000	M	M	M	M	M	M	M	M	M	M	90.48	KDEN 0922	M
DEN	9/5/2022 20:53	95	35.1	12.29	350	3	0	30.1	1009.6	10	M	FEW	M	M	M	11000	M	M	M	M	M	M	M	M	M	M	90.17	KDEN 0520	M
DEN	9/5/2022 23:53	95	36	12.73	0	0	0	30.09	1009	10	M	FEW	FEW	FEW	M	11000	15000	22000	M	M	M	M	M	M	M	M	90.32	KDEN 0523	M
DEN	9/6/2022 19:53	95	35.1	12.29	0	0	0	30.24	1013.8	10	M	FEW	M	M	M	14000	M	M	M	M	M	M	M	M	M	M	90.17	KDEN 0619	M
DEN	6/14/2022 0:53	93.9	25	8.43	280	6	0	29.54	989.8	10	M	FEW	M	M	M	12000	M	M	M	M	M	M	M	26	220	6/14/2022 0:02	88.1	KDEN 1400	M
DEN	6/16/2022 21:53	93.9	44.1	18.05	80	9	0	30.1	1010.8	10	20	FEW	M	M	M	10000	M	M	M	M	M	M	M	M	M	M	89.95	KDEN 1621	M
DEN	6/28/2022 20:53	93.9	26.1	8.82	290	8	0	30.21	1014.2	10	M	SCT	SCT	SCT	M	10000	14000	22000	M	M	M	M	M	M	M	M	88.2	KDEN 2820	M
DEN	7/10/2022 0:53	93.9	39.9	15.35	120	12	0	30.21	1013	10	16	FEW	BKN	BKN	M	12000	15000	22000	M	M	M	M	M	M	M	M	89.6	KDEN 1000	M
DEN	7/10/2022 1:08	93.9	45	18.68	140	12	0	30.21	M	10	M	FEW	BKN	BKN	M	12000	15000	22000	M	M	M	M	M	M	M	M	90.05	KDEN 1001	M
DEN	7/12/2022 21:53	93.9	43	17.31	160	13	0	30.1	1010.4	10	22	SCT	SCT	BKN	M	10000	14000	22000	M	M	M	M	M	M	M	M	89.84	KDEN 1221	M
DEN	7/13/2022 17:53	93.9	42.1	16.72	20	9	0	30.17	1012.1	10	15	FEW	SCT	SCT	M	9000	15000	22000	M	M	M	M	M	M	M	M	89.76	KDEN 1317	M
DEN	7/14/2022 22:53	93.9	41	16.02	210	13	0	30.17	1011.6	10	18	SCT	BKN	BKN	M	12000	16000	22000	M	M	M	M	M	M	M	M	89.68	KDEN 1422	M
DEN	7/15/2022 19:53	93.9	46	19.4	M	M	0	30.2	1013	10	M	CLR	M	M	M	M	M	M	M	M	M	M	M	M	M	M	90.17	KDEN 1519	M
DEN	7/15/2022 20:20	93.9	46.9	20.07	110	6	0	30.2	M	10	M	FEW	SCT	BKN	M	10000	15000	22000	M	M	M	M	M	M	M	M	90.29	KDEN 1520	M
DEN	7/17/2022 18:53	93.9	42.1	16.72	80	5	0	30.2	1012.8	10	M	SCT	SCT	M	M	10000	22000	M	M	M	M	M	M	M	M	M	89.76	KDEN 1718	M
DEN	7/17/2022 20:53	93.9	41	16.02	M	5	0	30.16	1011.8	10	M	SCT	SCT	M	M	11000	22000	M	M	M	M	M	M	M	M	M	89.68	KDEN 1720	M
DEN	7/17/2022 23:53	93.9	45	18.68	140	14	0	30.13	1010.7	10	M	FEW	FEW	M	M	11000	25000	M	M	M	M	M	M	M	M	M	90.05	KDEN 1723	M
DEN	7/18/2022 21:53	93.9	43	17.31	130	11	0	30.05	1007.2	10	19	SCT	BKN	BKN	M	9000	14000	20000	M	M	M	M	M	M	M	M	89.84	KDEN 1821	M
DEN	7/18/2022 23:53	93.9	43	17.31	240	9	0	30.04	1007.4	10	M	BKN	BKN	BKN	M	12000	16000	22000	M	M	M	M	M	M	M	M	89.84	KDEN 1823	M
DEN	7/19/2022 21:39	93.9	45	18.68	160	17	0	30.07	M	10	M	BKN	BKN	BKN	M	11000	15000	22000	M	M	M	M	M	M	M	M	90.05	KDEN 1921	M
DEN	7/20/2022 20:15	93.9	44.1	18.05	310	7	0	30.15	M	10	M	FEW	SCT	BKN	M	10000	14000	17000	M	M	M	M	M	M	M	M	89.95	KDEN 2020	M
DEN	7/21/2022 22:53	93.9	36	13.17	340	17	0	30.08	1009.2	10	27	FEW	SCT	BKN	M	10000	14000	22000	M	M	M	M	M	27	360	7/21/2022 22:48	89.4	KDEN 2122	M
DEN	7/22/2022 18:53	93.9	39.9	15.35	40	9	0	30.12	1009.5	10	M	FEW	FEW	SCT	M	9000	12000	22000	M	M	M	M	M	M	M	M	89.6	KDEN 2218	M
DEN	7/31/2022 21:02	93.9	44.1	18.05	360	11	0	30.19	M	10	19	SCT	BKN	BKN	M	10000	15000	22000	M	M	M	M	M	M	M	M	89.95	KDEN 3121	M
DEN	8/2/2022 19:53	93.9	43	17.31	290	9	0	30.02	1006.5	10	16	SCT	SCT	BKN	M	10000	14000	22000	M	M	M	M	M	M	M	M	89.84	KDEN 0219	M
DEN	8/4/2022 19:53	93.9	39	14.82	150	4	0	30.12	1010.1	10	M	FEW	SCT	M	M	9000	22000	M	M	M	M	M	M	M	M	M	89.54	KDEN 0419	M
DEN	8/9/2022 21:53	93.9	39	14.82	50	13	0	30.19	1013.3	10	16	SCT	SCT	M	M	11000	15000	M	M	M	M	M	M	M	M	M	89.54	KDEN 0921	M
DEN	8/10/2022 21:53	93.9	39.9	15.35	70	5	0	30.27	1015.3	10	M	SCT	M	M	M	10000	M	M	M	M	M	M	M	M	M	M	89.6	KDEN 1021	M
DEN	8/11/2022 21:53	93.9	44.1	18.05	M	3	0	30.15	1011.4	10	M	FEW	SCT	M	M	10000	20000	M	M	M	M	M	M	M	M	M	89.95	KDEN 1121	M
DEN	8/12/2022 21:53	93.9	46	19.4	M	3	0	30.18	1012.2	10	M	FEW	SCT	M	M	11000	22000	M	M	M	M	M	M	M	M	M	90.17	KDEN 1221	M
DEN	8/12/2022 22:53	93.9	42.1	16.72	M	3	0	30.16	1011.5	10	M	SCT	SCT	M	M	11000	22000	M	M	M	M	M	M	M	M	M	89.76	KDEN 1222	M
DEN	8/13/2022 22:53	93.9	42.1	16.72	30	6	0	30.13	1010.9	10	M	FEW	FEW	FEW	M	10000	16000	22000	M	M	M	M	M	M	M	M	89.76	KDEN 1322	M
DEN	8/14/2022 20:53	93.9	46.9	20.07	M	6	0	30.1	1009.5	10	17	FEW	SCT	SCT	M	9000	14000	22000	M	M	M	M	M	M	M	M	90.29	KDEN 1420	M
DEN	8/14/2022 21:00	93.9	46.9	20.07	20	6	0	30.1	M	10	M	FEW	SCT	SCT	M	9000	14000	22000	M	M	M	M	M	M	M	M	90.29	KDEN 1421	M
DEN	9/2/2022 20:53	93.9	36	13.17	50	8	0	30.17	1011.9	10	16	FEW	FEW	M	M	13000	22000	M	M	M	M	M	M	M	M	M	89.4	KDEN 0220	M
DEN	9/2/2022 22:53	93.9	35.1	12.71	20	11	0	30.17	1012.1	10	16	FEW	FEW	SCT	M	9000	13000	22000	M	M	M	M	M	M	M	M	89.29	KDEN 0222	M
DEN	9/4/2022 22:53	93.9	33.1	11.74	100	5	0	30.11	1010.4	10	M	FEW	M	M	M	10000	M	M	M	M	M	M	M	M	M	M	89	KDEN 0422	M
DEN	9/6/2022 18:53	93.9	33.1	11.74	0	0	0	30.25	1014.3	10	M	FEW	M	M	M	13000	M	M	M	M	M	M	M	M	M	M	89	KDEN 0618	M
DEN	9/7/2022 18:53	93.9	35.1	12.71	240	5	0	30.28	1016	10	M	FEW	FEW	M	M	9000	13000	M	M	M	M	M	M	M	M	M	89.29	KDEN 0718	M
DEN	6/11/2022 17:53	93	39.9	15.79	180	6	0	29.99	1005.3	10	M	FEW	FEW	M	M	11000	22000	M	M	M	M	M	M	M	M	M	88.78	KDEN 1117	M
DEN	6/13/2022 18:53	93	26.1	9.07	0	0	0	29.67	994.6	8	M	FEW	M	M	M	14000	M	M	M	M	M	M	M	M	M	M	87.52	KDEN 1318	M
DEN	6/28/2022 22:53	93	26.1	9.07	40	10	0	30.18	1013.1	10	14	SCT	BKN	BKN	M	11000	15000	22000	M	M	M	M	M	M	M	M	87.52	KDEN 2822	M
DEN	6/28/2022 23:53	93	26.1	9.07	350	5	0	30.17	1012.6	10	M	FEW	BKN	BKN	M	11000	15000	22000	M	M	M	M	M	M	M	M	87.52	KDEN 2823	M
DEN	6/29/2022 17:53	93	35.1	13.07	240	8	0	30.16	1011.5	10	M	SCT	SCT	BKN	M	10000	15000	22000	M	M	M	M	M	M	M	M	88.56	KDEN 2917	M
DEN	7/3/2022 20:06	93	44.1	18.56	350	9	0	29.98	M	10	15	SCT	SCT	BKN	M	9000	13000	22000	M	M	M	M	M	M	M	M	89.11	KDEN 0320	M
DEN	7/4/2022 19:53	93	39.9	15.79	30	9	0	30.04	1007.3	10	M	SCT	SCT	BKN	M	10000	15000	20000	M	M	M	M	M	M	M	M	88.78	KDEN 0419	M
DEN	7/4/2022 20:53	93	37.9	14.6	M	3	0	30.03	1006.9	10	M	BKN	BKN	BKN	M	10000	15000	20000	M	M	M	M	M	M	M	M	88.67	KDEN 0420	M
DEN	7/4/2022 22:53	93	37	14.09	70	8	0	30	1006.5	10	M	SCT	BKN	BKN	M	11000	16000	22000	M	M	M	M	M	M	M	M	88.63	KDEN 0422	M
DEN	7/4/2022 23:53	93	37	14.09	50	6	0	30	1006.2	10	M	SCT	BKN	BKN	M	10000	16000	22000	M	M	M	M	M	M	M	M	88.63	KDEN 0423	M
DEN	7/5/2022 18:53	93	41	16.48	300	7	0	30.03	1007.4	10	M	FEW	SCT	BKN	M	9000	13000	22000	M	M	M	M	M	M	M	M	88.85	KDEN 0518	M
DEN	7/5/2022 19:53	93	42.1	17.19	70	9	0	30.02	M	10	M	FEW	SCT	BKN	BKN	8000	11000	15000	22000	M	M	M	M	M	M	M	88.93	KDEN 0519	M
DEN	7/8/2022 21:53	93	46.9	20.64	100	10	0	30.23	1015	10	21	SCT	SCT	SCT	M	9500	12000	20000	M	M	M	M	M	M	M	M	89.43	KDEN 0821	M
DEN	7/8/2022 22:53	93	45	19.21	110	11	0	30.23	1014.8	10	19	SCT	BKN	BKN	M	10000	13000	20000	M	M	M	M	M	M	M	M	89.2	KDEN 0822	M
DEN	7/10/2022 1:30	93	46.9	20.64	130	9	0	30.2	M	10	M	FEW	BKN	BKN	M	12000	15000	22000	M	VCTS	M	M	M	M	M	M	89.43	KDEN 1001	M
DEN	7/12/2022 19:53	93	42.1	17.19	90	8	0	30.14	1011.8	10	15	FEW	FEW	SCT	M	10000	14000	20000	M	M	M	M	M	M	M	M	88.93	KDEN 1219	M
DEN	7/12/2022 20:53	93	36	13.55	40	6	0	30.13	1011.2	10	M	SCT	SCT	SCT	M	10000	14000	22000	M	M	M	M	M	M	M	M	88.59	KDEN 1220	M
DEN	7/13/2022 23:53	93	34	12.51	0	0	0	30.12	1010.9	10	M	BKN	BKN	M	M	13000	22000	M	M	M	M	M	M	M	M	M	88.42	KDEN 1323	M
DEN	7/16/2022 19:53	93	51.1	24.15	10	15	0	30.17	1012	10	26	SCT	BKN	BKN	M	8000	12000	22000	M	M	M	M	M	26	10	7/16/2022 19:50	90.11	KDEN 1619	M
DEN	7/18/2022 0:53	93	46.9	20.64	150	16	0	30.12	1010.6	10	22	FEW	FEW	M	M	11000	25000	M	M	M	M	M	M	M	M	M	89.43	KDEN 1800	M
DEN	7/19/2022 0:01	93	44.1	18.56	240	14	0	30.04	M	10	19	BKN	BKN	BKN	M	12000	16000	22000	M	VCTS	M	M	M	M	M	M	89.11	KDEN 1900	M
DEN	7/19/2022 16:53	93	44.1	18.56	M	6	0	30.11	1009.3	10	M	FEW	FEW	SCT	M	10000	14000	22000	M	M	M	M	M	M	M	M	89.11	KDEN 1916	M
DEN	7/19/2022 21:53	93	44.1	18.56	160	12	0	30.06	1007.9	10	M	SCT	BKN	BKN	M	11000	15000	22000	M	M	M	M	M	M	M	M	89.11	KDEN 1921	M
DEN	7/20/2022 21:53	93	43	17.8	30	11	0	30.13	1010.6	10	M	SCT	BKN	BKN	M	10000	14000	18000	M	M	M	M	M	M	M	M	89	KDEN 2021	M
DEN	7/21/2022 17:53	93	34	12.51	290	7	0	30.15	1011.4	10	M	FEW	FEW	M	M	9000	12000	M	M	M	M	M	M	M	M	M	88.42	KDEN 2117	M
DEN	7/21/2022 18:53	93	28.9	10.18	M	5	0	30.12	1010.3	10	M	SCT	SCT	M	M	9000	12000	M	M	M	M	M	M	M	M	M	87.79	KDEN 2118	M

DEN	7/21/2022 21:29	93	34	12.51	330	15	0	30.09	M	10	25	SCT	BKN	BKN	M	9000	14000	22000	M	M	M	M	M		30	320	7/21/2022 21:18	88.42	KDEN 2121M
DEN	7/21/2022 21:53	93	34	12.51	330	13	0	30.09	1009.6	10	24	SCT	BKN	BKN	M	9000	14000	22000	M	M	M	M	M		31	340	7/21/2022 21:34	88.42	KDEN 2121M
DEN	7/22/2022 23:53	93	41	16.48	210	13	0	30.05	1007.7	10	23	FEW	BKN	BKN	M	10000	15000	20000	M	M	M	M	M	M	M	M		88.85	KDEN 2223M
DEN	7/23/2022 18:53	93	42.1	17.19	10	24	0	30.06	1007.8	10	37	SCT	BKN	BKN	M	10000	14000	22000	M	M	M	M	M		37	20	7/23/2022 18:47	88.93	KDEN 2318M
DEN	8/1/2022 19:53	93	37.9	14.6	M	3	0	30.13	1011.2	10	M	FEW	SCT	BKN	M	10000	18000	22000	M	M	M	M	M	M	M	M		88.67	KDEN 0119M
DEN	8/2/2022 20:09	93	43	17.8	100	5	0	30.02	M	10	M	SCT	SCT	BKN	M	10000	14000	22000	M	M	M	M	M	M	M	M		89	KDEN 0220M
DEN	8/2/2022 20:53	93	43	17.8	10	11	0	30.01	1006.1	10	17	SCT	BKN	BKN	M	10000	14000	22000	M	M	M	M	M	M	M	M		89	KDEN 0220M
DEN	8/2/2022 21:53	93	43	17.8	20	5	0	29.99	1005.3	10	M	FEW	BKN	BKN	M	10000	13000	22000	M	M	M	M	M	M	M	M		89	KDEN 0221M
DEN	8/9/2022 20:53	93	42.1	17.19	M	4	0	30.21	1013.7	10	16	SCT	SCT	M	M	11000	15000	M	M	M	M	M	M	M	M	M		88.93	KDEN 0920M
DEN	8/9/2022 20:59	93	41	16.48	80	9	0	30.21	M	10	M	SCT	SCT	M	M	11000	15000	M	M	M	M	M	M	M	M	M		88.85	KDEN 0920M
DEN	8/10/2022 20:07	93	41	16.48	130	9	0	30.3	M	10	M	FEW	M	M	M	9000	M	M	M	M	M	M	M	M	M	M		88.85	KDEN 1020M
DEN	8/10/2022 20:53	93	39.9	15.79	130	9	0	30.28	1015.8	10	M	SCT	M	M	M	10000	M	M	M	M	M	M	M	M	M	M		88.78	KDEN 1020M
DEN	8/10/2022 22:53	93	39.9	15.79	70	7	0	30.25	1015.2	10	M	FEW	M	M	M	11000	M	M	M	M	M	M	M	M	M	M		88.78	KDEN 1022M
DEN	8/10/2022 23:53	93	44.1	18.56	140	14	0	30.24	1014.6	10	20	FEW	M	M	M	11000	M	M	M	M	M	M	M	M	M	M		89.11	KDEN 1023M
DEN	8/11/2022 22:53	93	45	19.21	130	12	0	30.14	1011	10	22	SCT	BKN	M	M	11000	20000	M	M	M	M	M	M	M	M	M		89.2	KDEN 1122M
DEN	8/12/2022 20:53	93	46.9	20.64	340	7	0	30.2	1012.9	10	M	SCT	SCT	M	M	11000	22000	M	M	M	M	M	M	M	M	M		89.43	KDEN 1220M
DEN	8/12/2022 23:53	93	44.1	18.56	M	4	0	30.14	1010.9	10	15	SCT	SCT	M	M	11000	20000	M	M	M	M	M	M	M	M	M		89.11	KDEN 1223M
DEN	8/13/2022 20:53	93	46	19.95	130	10	0	30.17	1012.1	10	M	FEW	FEW	FEW	M	10000	16000	22000	M	M	M	M	M	M	M	M		89.31	KDEN 1320M
DEN	8/13/2022 23:53	93	43	17.8	90	11	0	30.12	1010.7	10	M	FEW	SCT	SCT	M	10000	16000	22000	M	M	M	M	M	M	M	M		89	KDEN 1323M
DEN	9/4/2022 20:53	93	33.1	12.07	40	7	0	30.14	1011.3	10	M	FEW	M	M	M	10000	M	M	M	M	M	M	M	M	M	M		88.29	KDEN 0420M
DEN	9/4/2022 21:53	93	32	11.55	60	9	0	30.12	1010.9	10	15	FEW	M	M	M	9000	M	M	M	M	M	M	M	M	M	M		88.15	KDEN 0421M
DEN	9/4/2022 23:53	93	34	12.51	0	0	0	30.1	1010.2	10	M	FEW	M	M	M	10000	M	M	M	M	M	M	M	M	M	M		88.42	KDEN 0423M
DEN	9/6/2022 17:53	93	35.1	13.07	20	4	0	30.27	1014.8	10	M	FEW	M	M	M	13000	M	M	M	M	M	M	M	M	M	M		88.56	KDEN 0617M
DEN	9/7/2022 23:53	93	30	10.65	160	16	0	30.18	1012.7	10	M	FEW	M	M	M	15000	M	M	M	M	M	M	M	M	M	M		87.91	KDEN 0723M
DEN	6/12/2022 18:53	91.9	43	18.42	M	M	0	29.86	1001.1	10	M	SCT	SCT	BKN	M	11000	15000	22000	M	M	M	M	M	M	M	M		87.99	KDEN 1218M
DEN	6/12/2022 18:58	91.9	44.1	19.21	60	5	0	29.86	M	10	M	SCT	SCT	BKN	M	11000	15000	22000	M	M	M	M	M	M	M	M		88.09	KDEN 1218M
DEN	6/16/2022 20:53	91.9	37	14.58	100	8	0	30.13	1011.6	10	M	FEW	M	M	M	10000	M	M	M	M	M	M	M	M	M	M		87.65	KDEN 1620M
DEN	6/16/2022 22:53	91.9	46	20.65	110	15	0	30.08	1010.7	10	27	SCT	M	M	M	10000	M	M	M	M	M	M	M		27	80	6/16/2022 22:46	88.28	KDEN 1622M
DEN	6/16/2022 23:53	91.9	44.1	19.21	100	16	0	30.06	1009.5	10	23	SCT	SCT	M	M	11000	13000	M	M	M	M	M	M	M	M	M		88.09	KDEN 1623M
DEN	6/23/2022 22:53	91.9	26.1	9.39	40	5	0	29.98	1006.3	10	M	FEW	SCT	SCT	M	10000	15000	22000	M	M	M	M	M	M	M	M		86.69	KDEN 2322M
DEN	6/29/2022 18:53	91.9	30.9	11.43	M	3	0	30.15	1011.2	10	M	SCT	SCT	BKN	M	11000	15000	22000	M	M	M	M	M	M	M	M		87.17	KDEN 2918M
DEN	7/3/2022 20:53	91.9	42.1	17.79	310	5	0	29.97	1005.6	10	M	SCT	BKN	BKN	M	9000	13000	20000	M	M	M	M	M	M	M	M		87.92	KDEN 0320M
DEN	7/3/2022 21:53	91.9	41	17.05	320	4	0	29.97	1005.2	10	M	FEW	BKN	BKN	M	9000	15000	20000	M	M	M	M	M	M	M	M		87.85	KDEN 0321M
DEN	7/5/2022 0:27	91.9	41	17.05	320	15	0	30	M	10	22	SCT	BKN	BKN	M	10000	16000	22000	M	M	M	M	M	M	M	M		87.85	KDEN 0500M
DEN	7/5/2022 0:53	91.9	39	15.77	340	13	0	30	1006.2	10	M	SCT	BKN	BKN	M	11000	16000	22000	M	M	M	M	M	M	M	M		87.74	KDEN 0500M
DEN	7/8/2022 20:53	91.9	39.9	16.34	M	M	0	30.23	1015.2	10	M	SCT	SCT	SCT	M	9000	12000	20000	M	M	M	M	M	M	M	M		87.78	KDEN 0820M
DEN	7/8/2022 20:57	91.9	37.9	15.11	120	5	0	30.23	M	10	M	SCT	SCT	SCT	M	9000	12000	20000	M	M	M	M	M	M	M	M		87.69	KDEN 0820M
DEN	7/9/2022 16:53	91.9	44.1	19.21	M	3	0	30.31	1016.6	10	M	FEW	SCT	M	M	10000	22000	M	M	M	M	M	M	M	M	M		88.09	KDEN 0916M
DEN	7/15/2022 21:53	91.9	48	22.26	120	3	0	30.17	1012	10	M	SCT	BKN	BKN	M	10000	15000	22000	M	M	M	M	M	M	M	M		88.53	KDEN 1521M
DEN	7/17/2022 17:53	91.9	50	23.99	40	8	0	30.21	1013.2	10	M	FEW	FEW	M	M	10000	22000	M	M	M	M	M	M	M	M	M		88.84	KDEN 1717M
DEN	7/18/2022 16:53	91.9	44.1	19.21	290	4	0	30.12	1009.5	10	M	FEW	FEW	SCT	M	11000	15000	22000	M	M	M	M	M	M	M	M		88.09	KDEN 1816M
DEN	7/19/2022 22:09	91.9	45	19.88	180	8	0	30.07	M	10	M	SCT	BKN	BKN	M	10000	15000	22000	M	VCTS	M	M	M	M	M	M		88.17	KDEN 1922M
DEN	7/20/2022 18:53	91.9	46.9	21.36	20	4	0	30.17	1011.8	10	M	FEW	SCT	SCT	M	9000	15000	22000	M	M	M	M	M	M	M	M		88.39	KDEN 2018M
DEN	7/20/2022 22:53	91.9	43	18.42	50	8	0	30.13	1010.9	10	M	FEW	SCT	BKN	M	6000	8500	14000	M	M	M	M	M	M	M	M		87.99	KDEN 2022M
DEN	7/23/2022 20:53	91.9	39.9	16.34	60	10	0	30.06	1008.2	10	20	SCT	SCT	BKN	BKN	8000	11000	15000	22000	M	M	M	M		27	10	7/23/2022 20:02	87.78	KDEN 2320M
DEN	7/27/2022 22:53	91.9	48.9	23.03	40	11	0	30.08	1009.6	10	M	FEW	BKN	BKN	M	10000	14000	22000	M	M	M	M	M	M	M	M		88.66	KDEN 2722M
DEN	8/1/2022 17:53	91.9	44.1	19.21	M	4	0	30.17	1012.3	10	M	FEW	FEW	SCT	M	9000	14000	22000	M	M	M	M	M	M	M	M		88.09	KDEN 0117M
DEN	8/2/2022 17:53	91.9	45	19.88	100	7	0	30.06	1007.6	10	M	FEW	FEW	SCT	M	10000	14000	22000	M	M	M	M	M	M	M	M		88.17	KDEN 0217M
DEN	8/2/2022 22:53	91.9	45	19.88	320	14	0	30	1005.8	10	M	SCT	BKN	BKN	M	11000	14000	22000	M	M	M	M	M		28	330	8/2/2022 22:08	88.17	KDEN 0222M
DEN	8/4/2022 18:53	91.9	44.1	19.21	0	0	0	30.13	1010.7	10	M	FEW	SCT	M	M	9000	22000	M	M	M	M	M	M	M	M	M		88.09	KDEN 0418M
DEN	8/5/2022 16:53	91.9	51.1	24.99	20	4	0	30.08	1008.2	10	M	FEW	FEW	SCT	M	10000	15000	22000	M	M	M	M	M	M	M	M		89.04	KDEN 0516M
DEN	8/9/2022 18:53	91.9	51.1	24.99	80	11	0	30.23	1014.1	10	M	FEW	FEW	SCT	M	10000	12000	15000	M	M	M	M	M	M	M	M		89.04	KDEN 0918M
DEN	8/9/2022 23:53	91.9	43	18.42	110	10	0	30.18	1012.9	10	18	SCT	SCT	M	M	11000	15000	M	M	M	M	M	M	M	M	M		87.99	KDEN 0923M
DEN	8/10/2022 18:53	91.9	42.1	17.79	90	13	0	30.32	1016.9	10	20	FEW	M	M	M	9000	M	M	M	M	M	M	M	M	M	M		87.92	KDEN 1018M
DEN	8/10/2022 19:53	91.9	42.1	17.79	170	9	0	30.3	1016.5	10	16	FEW	M	M	M	9000	M	M	M	M	M	M	M	M	M	M		87.92	KDEN 1019M
DEN	8/11/2022 23:53	91.9	43	18.42	150	14	0	30.13	1011	10	M	SCT	BKN	M	M	11000	20000	M	M	M	M	M	M	M	M	M		87.99	KDEN 1123M
DEN	8/13/2022 0:53	91.9	42.1	17.79	60	7	0	30.14	1011	10	M	FEW	SCT	M	M	11000	20000	M	M	M	M	M	M	M	M	M		87.92	KDEN 1300M
DEN	8/13/2022 21:53	91.9	45	19.88	M	5	0	30.14	1011.5	10	19	FEW	FEW	FEW	M	10000	16000	22000	M	M	M	M	M	M	M	M		88.17	KDEN 1321M
DEN	8/13/2022 21:55	91.9	45	19.88	60	7	0	30.14	M	10	M	FEW	FEW	FEW	M	10000	16000	22000	M	M	M	M	M	M	M	M		88.17	KDEN 1321M
DEN	8/30/2022 22:53	91.9	43	18.42	40	11	0	30.23	1014.7	10	M	FEW	FEW	M	M	10000	13000	M	M	M	M	M	M	M	M	M		87.99	KDEN 3022M
DEN	8/31/2022 21:53	91.9	34	12.95	30	11	0	30.19	1012.5	10	M	SCT	BKN	BKN	M	10000	16000	22000	M	M	M	M	M	M	M	M		87.56	KDEN 3121M
DEN	9/1/2022 19:53	91.9	33.1	12.49	M	3	0	30.11	1010.1	10	M	FEW	SCT	SCT	M	10000	15000	22000	M	M	M	M	M	M	M	M		87.44	KDEN 0119M
DEN	9/1/2022 20:53	91.9	33.1	12.49	40	4	0	30.09	1009.5	10	M	FEW	SCT	SCT	M	10000	15000	22000	M	M	M	M	M	M	M	M		87.44	KDEN 0120M
DEN	9/2/2022 19:53	91.9	37	14.58	360	11	0	30.18	1012.2	10	M	FEW	FEW	M	M	13000	22000	M	M	M	M	M	M	M	M	M		87.65	KDEN 0219M
DEN	9/2/2022 21:53	91.9	36	14.02	M	6	0	30.17	1012	10	M	FEW	FEW	SCT	M	9000	13000	22000	M	M	M	M	M	M	M	M		87.62	KDEN 0221M
DEN	9/2/2022 23:53	91.9	36	14.02	40	12	0	30.17	1012.3	10	18	FEW	SCT	SCT	M	10000	13000	22000	M	M	M	M	M	M	M	M		87.62	KDEN 0223M
DEN	9/4/2022 19:53	91.9	35.1	13.53	50	7	0	30.17	1012.4	10	M	FEW	M	M	M	10000	M	M	M	M	M	M	M	M	M	M		87.6	KDEN 0419M
DEN	9/5/2022 19:53	91.9	37	14.58	280	4	0	30.12	1010.2	10	M	FEW	M	M	M	11000	M	M	M	M	M	M	M	M	M	M		87.65	KDEN 0519M
DEN	9/20/2022 20:53	91.9	24.1	8.64	M	5	0	30.07	1009.2	10	M	FEW	SCT	SCT	M	10000	14000	20000	M	M	M	M	M	M	M	M		86.53	KDEN 2020M
DEN	6/11/2022 16:53	91	39.9	16.8	180	4	0	30	1006.1	10	M	FEW	FEW	M	M	11000	22000	M	M	M	M	M	M	M	M	M		86.98	KDEN 1116M
DEN	6/12/2022 0:53	91	36	14.42	180	3	0	29.88	1001.9	10	M	SCT	BKN	BKN	M	11000	15000	22000	M	M	M	M	M	M	M	M		86.83	KDEN 1200M
DEN	6/12/2022 1:53	91	34	13.32	30	7	0	29.88	1001.7	10	M	SCT	BKN	BKN	M	10000	15000	22000	M	M	M	M	M	M	M	M		86.79	KDEN 1201M
DEN	6/12/2022 21:53	91	46	21.24	40	16	0	29.81	1000	10	M	SCT	BKN	BKN	M	11000	15000	20000	M	M	M	M	M	M	M	M		87.45	KDEN 1221M
DEN	6/13/2022 17:53	91	24.1	8.89	M	3	0	29.7	995.4	7	M	FEW	M	M	M	14000	M	M	M	M	M	M	M	M	M	M		85.86	KDEN 1317M
DEN	6/17/2022 17:53	91	46.9	21.97	140	16	0	30.09	1009	10	23	FEW	SCT	M	M	11000	22000	M	M	M	M	M	M	M	M	M		87.55	KDEN 1717M
DEN	6/17/2022 23:53	91	39	16.23	300	13	0	29.97	1006.1	10	M	SCT	SCT	SCT	M	11000	14000	22000	M	M	M	M	M		31	160	6/17/2022 22:54	86.94	KDEN 1723M
DEN	6/23/2022 19:53	91	25	9.23	140	7	0	30.03	1007.5	10	M	FEW	SCT	BKN	M	9000	15000	22000	M	M	M	M	M	M	M	M		85.93	KDEN 2319M
DEN	6/23/2022 20:53	91	24.1	8.89	110	5	0	30	1007.2	10	M	FEW	SCT	BKN	M	10000	15000	22000	M	M	M	M	M	M	M	M		85.86	KDEN 2320M
DEN	6/23/2022 21:53	91	24.1	8.89	M	M	0	29.99	1006.7	10	M	FEW	SCT	SCT	M	10000	15000	22000	M	M	M	M	M	M	M	M		85.86	KDEN 2321M
DEN	6/23/2022 21:55	91	24.1	8.89	40	7	0	29.99	M	10	M	FEW	SCT	SCT	M	10000	15000	22000	M	M	M	M	M	M	M	M		85.86	KDEN 2321M
DEN	6/24/2022 19:55	91	35.1	13.91	30	5	0	29.99	M	10	M	SCT	SCT	SCT	M	10000	14000	22000	M	M	M	M	M	M	M	M		86.81	KDEN 2419M
DEN	6/28/2022 18:53	91	28.9	10.84	130	7	0	30.25	1015.5	10	M	FEW	FEW	M	M	10000	14000	M	M	M	M	M	M	M	M	M		86.27	KDEN 2818M
DEN	6/28/2022 19:53	91	27	10.02	360	8	0	30.23	1015	10	M	SCT	SCT	M	M	10000	14000	M	M	M	M	M	M	M	M	M		86.1	KDEN 2819M
DEN	6/28/2022 21:53	91	24.1	8.89	310	7	0	30.2	1014.4	10	M	SCT	SCT	SCT	M	10000	14000	22000	M	M	M	M	M	M	M	M		85.86	KDEN 2821M
DEN	6/29/2022 22:53	91	37.9	15.54	300	8	0	30.11	1010.3	10	M	FEW	BKN	BKN	M	11000	14000	22000	M	M	M	M	M		29	310	6/29/2022 22:01	86.9	KDEN 2922M
DEN	7/3/2022 19:53	91	43	18.94	M	3	0	29.98	1006	10	16	SCT	SCT	BKN	M	9000	13000	22000	M	M	M	M	M	M	M	M		87.18	KDEN 0319M
DEN	7/4/2022 18:53	91	42.1	18.3	350	7	0	30.05	1007.9	10	16	SCT	SCT	M	M	10000	22000	M	M	M	M	M	M	M	M	M		87.11	KDEN 0418M

Appendix E:
Sample 2022 SEQM METAR Data

station	valid	tmpf	tmpc	alti	dwpf	relh	drct	sknt	p01i	mslp	vsby	gust	skyc1	skyc2	skyc3	skyc4	skyl1	skyl2	skyl3	skyl4	wxcodes	ice_accreti	ice_accreti	ice_accreti	peak_wind	peak_wind	peak_wind	feel	metar	snowdepth
SEQM	5/1/2022 6:00	M	#VALUE!	30.27	M	M	130	2	0	M	M	M	M	M	M	M	M	M	M	M	M	M	M	M	M	M	M	M	SEQM 010	M
SEQM	5/7/2022 21:40	M	#VALUE!	M	M	M	40	7	0	M	M	M	FEW	BKN	BKN	M	3000	3300	30000	M	#NAME?	M	M	M	M	M	M	M	SEQM 072	M
SEQM	7/6/2022 17:00	M	#VALUE!	M	M	M	310	3	0	M	6.21	M	BKN	SCT	M	M	3000	8000	M	M	M	M	M	M	M	M	M	M	SEQM 061	M
SEQM	11/19/2022 18:00	80.6	27	30.15	46.4	30.07	M	3	0	M	6.21	M	SCT	M	M	M	3000	M	M	M	M	M	M	M	M	M	M	79.56	SEQM 191	M
SEQM	9/8/2022 19:00	80.6	27	30.18	28.4	14.81	80	11	0	M	6.21	M	FEW	SCT	M	M	4000	30000	M	M	M	M	M	M	M	M	M	78.72	SEQM 081	M
SEQM	5/3/2022 19:00	80.6	27	30.21	44.6	28.08	240	5	0	M	6.21	M	SCT	M	M	M	4000	M	M	M	M	M	M	M	M	M	M	79.42	SEQM 031	M
SEQM	7/19/2022 20:00	78.8	26	30.15	39.2	24.19	270	12	0	M	6.21	M	FEW	M	M	M	3000	M	M	M	M	M	M	M	M	M	M	78.8	SEQM 192	M
SEQM	8/23/2022 19:00	78.8	26	30.15	30.2	16.9	340	13	0	M	6.21	M	FEW	SCT	M	M	3000	30000	M	M	M	M	M	M	M	M	M	78.8	SEQM 231	M
SEQM	9/9/2022 19:00	78.8	26	30.18	37.4	22.54	60	9	0	M	6.21	M	M	M	M	M	M	M	M	M	M	M	M	M	M	M	M	78.8	SEQM 091	M
SEQM	12/22/2022 18:00	78.8	26	30.18	39.2	24.19	360	4	0	M	6.21	M	FEW	SCT	M	M	4000	30000	M	M	M	M	M	M	M	M	M	78.8	SEQM 221	M
SEQM	9/9/2022 18:00	78.8	26	30.21	37.4	22.54	40	10	0	M	6.21	M	SCT	SCT	M	M	5000	30000	M	M	M	M	M	M	M	M	M	78.8	SEQM 091	M
SEQM	9/13/2022 18:00	78.8	26	30.21	35.6	21	350	12	0	M	6.21	M	FEW	SCT	M	M	4000	30000	M	M	M	M	M	M	M	M	M	78.8	SEQM 131	M
SEQM	9/15/2022 18:00	78.8	26	30.21	44.6	31.62	300	9	0	M	6.21	M	BKN	M	M	M	4000	M	M	M	M	M	M	M	M	M	M	77	COR SEQM	M
SEQM	9/23/2022 19:00	78.8	26	30.21	37.4	22.54	M	4	0	M	6.21	M	FEW	M	M	M	4000	M	M	M	M	M	M	M	M	M	M	78.8	SEQM 231	M
SEQM	5/7/2022 19:00	78.8	26	30.24	50	36.51	360	11	0	M	6.21	M	BKN	M	M	M	3300	M	M	M	VCSH	M	M	M	M	M	M	78.8	SEQM 071	M
SEQM	5/7/2022 18:00	78.8	26	30.27	44.6	29.79	190	4	0	M	6.21	M	BKN	M	M	M	3300	M	M	M	M	M	M	M	M	M	M	78.8	SEQM 071	M
SEQM	1/21/2022 20:00	77	25	30.15	41	27.53	90	7	0	M	6.21	M	FEW	SCT	BKN	M	3000	3300	7000	M	M	M	M	M	M	M	M	77	SEQM 212	M
SEQM	4/30/2022 19:00	77	25	30.15	48.2	36.22	60	10	0	M	6.21	M	BKN	M	M	M	4000	M	M	M	M	M	M	M	M	M	M	77	SEQM 301	M
SEQM	7/19/2022 20:15	77	25	30.15	41	27.53	340	15	0	M	6.21	M	FEW	M	M	M	3000	M	M	M	M	M	M	M	M	M	M	77	SEQM 192	M
SEQM	7/19/2022 20:38	77	25	30.15	42.8	29.51	320	12	0	M	6.21	M	FEW	M	M	M	3000	M	M	M	M	M	M	M	M	M	M	77	SEQM 192	M
SEQM	8/18/2022 19:00	77	25	30.15	46.4	33.85	360	15	0	M	6.21	M	SCT	M	M	M	3000	M	M	M	M	M	M	M	M	M	M	77	SEQM 181	M
SEQM	8/19/2022 20:00	77	25	30.15	39.2	25.67	330	6	0	M	6.21	M	SCT	BKN	M	M	4000	30000	M	M	M	M	M	M	M	M	M	77	SEQM 192	M
SEQM	9/2/2022 19:00	77	25	30.15	41	27.53	360	7	0	M	6.21	M	BKN	M	M	M	4000	M	M	M	M	M	M	M	M	M	M	77	SEQM 021	M
SEQM	9/13/2022 19:00	77	25	30.15	46.4	33.85	350	19	0	M	6.21	M	SCT	BKN	M	M	4000	30000	M	M	M	M	M	M	M	M	M	77	SEQM 131	M
SEQM	11/1/2022 19:00	77	25	30.15	50	38.74	340	14	0	M	6.21	M	SCT	M	M	M	4000	M	M	M	M	M	M	M	M	M	M	77	SEQM 011	M
SEQM	11/30/2022 18:00	77	25	30.15	39.2	25.67	340	14	0	M	6.21	M	SCT	M	M	M	3000	M	M	M	M	M	M	M	M	M	M	77	SEQM 301	M
SEQM	12/23/2022 19:00	77	25	30.15	46.4	33.85	360	13	0	M	6.21	M	SCT	M	M	M	3000	M	M	M	M	M	M	M	M	M	M	77	SEQM 231	M
SEQM	1/19/2022 19:00	77	25	30.18	44.6	31.62	50	11	0	M	6.21	M	SCT	SCT	M	M	4000	30000	M	M	M	M	M	M	M	M	M	77	SEQM 191	M
SEQM	5/8/2022 20:00	77	25	30.18	46.4	33.85	20	5	0	M	6.21	M	SCT	SCT	M	M	3300	10000	M	M	M	M	M	M	M	M	M	77	SEQM 082	M
SEQM	7/19/2022 19:00	77	25	30.18	41	27.53	270	11	0	M	6.21	M	FEW	M	M	M	3600	M	M	M	M	M	M	M	M	M	M	77	SEQM 191	M
SEQM	7/30/2022 20:00	77	25	30.18	41	27.53	270	4	0	M	6.21	M	FEW	BKN	M	M	4000	10000	M	M	M	M	M	M	M	M	M	77	SEQM 302	M
SEQM	8/17/2022 20:00	77	25	30.18	42.8	29.51	350	12	0	M	6.21	M	SCT	M	M	M	4000	M	M	M	M	M	M	M	M	M	M	77	SEQM 172	M
SEQM	8/18/2022 18:00	77	25	30.18	41	27.53	350	13	0	M	6.21	M	SCT	M	M	M	3000	M	M	M	M	M	M	M	M	M	M	77	SEQM 181	M
SEQM	8/23/2022 18:00	77	25	30.18	26.6	15.48	360	11	0	M	6.21	M	FEW	SCT	M	M	3000	30000	M	M	M	M	M	M	M	M	M	77	SEQM 231	M
SEQM	9/13/2022 18:31	77	25	30.18	44.6	31.62	350	18	0	M	6.21	M	FEW	SCT	M	M	4000	30000	M	M	M	M	M	M	M	M	M	77	SEQM 131	M
SEQM	9/23/2022 19:18	77	25	30.18	42.8	29.51	350	16	0	M	6.21	M	FEW	M	M	M	4000	M	M	M	M	M	M	M	M	M	M	77	SEQM 231	M
SEQM	9/25/2022 18:00	77	25	30.18	42.8	29.51	350	7	0	M	6.21	M	BKN	M	M	M	3300	M	M	M	M	M	M	M	M	M	M	77	SEQM 251	M
SEQM	10/1/2022 20:00	77	25	30.18	39.2	25.67	160	12	0	M	6.21	M	FEW	SCT	M	M	3000	3300	M	M	M	M	M	M	M	M	M	77	SEQM 012	M
SEQM	10/10/2022 20:00	77	25	30.18	39.2	25.67	90	9	0	M	6.21	M	FEW	M	M	M	4000	M	M	M	M	M	M	M	M	M	M	77	SEQM 102	M
SEQM	11/1/2022 18:00	77	25	30.18	42.8	29.51	350	9	0	M	6.21	M	FEW	BKN	M	M	3300	4000	M	M	M	M	M	M	M	M	M	77	SEQM 011	M
SEQM	11/18/2022 18:00	77	25	30.18	44.6	31.62	250	5	0	M	6.21	M	FEW	SCT	M	M	2300	3000	M	M	VCSH	M	M	M	M	M	M	77	SEQM 181	M
SEQM	12/23/2022 18:00	77	25	30.18	46.4	33.85	20	8	0	M	6.21	M	SCT	M	M	M	3000	M	M	M	M	M	M	M	M	M	M	77	SEQM 231	M
SEQM	1/19/2022 18:00	77	25	30.21	44.6	31.62	60	10	0	M	6.21	M	SCT	SCT	M	M	4000	30000	M	M	M	M	M	M	M	M	M	77	SEQM 191	M
SEQM	5/2/2022 18:00	77	25	30.21	42.8	29.51	M	2	0	M	6.21	M	SCT	M	M	M	3600	M	M	M	M	M	M	M	M	M	M	77	SEQM 021	M
SEQM	5/7/2022 20:00	77	25	30.21	48.2	36.22	340	12	0	M	6.21	M	BKN	M	M	M	4000	M	M	M	VCSH	M	M	M	M	M	M	77	SEQM 072	M
SEQM	7/29/2022 18:00	77	25	30.21	44.6	31.62	280	6	0	M	6.21	M	FEW	M	M	M	3000	M	M	M	M	M	M	M	M	M	M	77	SEQM 291	M
SEQM	7/31/2022 18:00	77	25	30.21	46.4	33.85	320	8	0	M	6.21	M	FEW	M	M	M	4000	M	M	M	M	M	M	M	M	M	M	77	SEQM 311	M
SEQM	8/17/2022 19:00	77	25	30.21	41	27.53	350	11	0	M	6.21	M	BKN	M	M	M	4000	M	M	M	M	M	M	M	M	M	M	77	SEQM 171	M
SEQM	9/1/2022 18:00	77	25	30.21	41	27.53	360	10	0	M	6.21	M	BKN	M	M	M	4000	M	M	M	M	M	M	M	M	M	M	77	SEQM 011	M
SEQM	9/8/2022 18:00	77	25	30.21	39.2	25.67	350	12	0	M	6.21	M	SCT	M	M	M	4000	M	M	M	M	M	M	M	M	M	M	77	SEQM 081	M
SEQM	9/12/2022 19:00	77	25	30.21	46.4	33.85	350	19	0	M	6.21	M	SCT	M	M	M	3300	M	M	M	M	M	M	M	M	M	M	77	SEQM 121	M
SEQM	9/18/2022 18:00	77	25	30.21	41	27.53	10	13	0	M	6.21	M	SCT	BKN	M	M	4000	30000	M	M	M	M	M	M	M	M	M	77	SEQM 181	M
SEQM	10/1/2022 19:00	77	25	30.21	39.2	25.67	150	10	0	M	6.21	M	FEW	SCT	M	M	3000	3300	M	M	M	M	M	M	M	M	M	77	SEQM 011	M
SEQM	10/10/2022 19:00	77	25	30.21	39.2	25.67	60	9	0	M	6.21	M	SCT	M	M	M	4000	M	M	M	M	M	M	M	M	M	M	77	SEQM 101	M
SEQM	5/3/2022 18:00	77	25	30.24	44.6	31.62	240	4	0	M	6.21	M	SCT	M	M	M	4000	M	M	M	M	M	M	M	M	M	M	77	SEQM 031	M
SEQM	5/8/2022 19:00	77	25	30.24	48.2	36.22	200	7	0	M	6.21	M	SCT	SCT	M	M	3300	10000	M	M	M	M	M	M	M	M	M	77	SEQM 081	M
SEQM	9/8/2022 17:00	77	25	30.24	35.6	22.28	M	4	0	M	6.21	M	SCT	M	M	M	4000	M	M	M	M	M	M	M	M	M	M	77	SEQM 081	M
SEQM	9/9/2022 17:00	77	25	30.24	35.6	22.28	240	8	0	M	6.21	M	SCT	SCT	M	M	4000	30000	M	M	M	M	M	M	M	M	M	77	SEQM 091	M
SEQM	9/10/2022 19:00	77	25	30.24	41	27.53	160	12	0	M	6.21	25	SCT	M	M	M	4000	M	M	M	M	M	M	M	M	M	M	77	SEQM 101	M
SEQM	9/12/2022 18:00	77	25	30.24	39.2	25.67	320	10	0	M	6.21	M	SCT	M	M	M	3300	M	M	M	M	M	M	M	M	M	M	77	SEQM 121	M
SEQM	9/15/2022 17:00	77	25	30.24	42.8	29.51	M	4	0	M	6.21	M	SCT	M	M	M	3000	M	M	M	M	M	M	M	M	M	M	77	SEQM 151	M
SEQM	9/23/2022 18:00	77	25	30.24	37.4	23.93	M	6	0	M	6.21	M	SCT	SCT	M	M	4000	30000	M	M	M	M	M	M	M	M	M	77	SEQM 231	M
SEQM	10/2/2022 18:00	77	25	30.24	37.4	23.93	210	11	0	M	6.21	M	FEW	SCT	BKN	M	4000	10000	30000	M	M	M	M	M	M	M	M	77	SEQM 021	M
SEQM	10/3/2022 18:00	77	25	30.24	39.2	25.67	70	3	0	M	6.21	M	FEW	SCT	M	M	4000	8000	M	M	M	M	M	M	M	M	M	77	SEQM 031	M
SEQM	10/12/2022 17:00	77	25	30.24	41	27.53	330	7	0	M	6.21	M	FEW	SCT	M	M	4000	30000	M	M	M	M	M	M	M	M	M	77	SEQM 121	M
SEQM	11/7/2022 18:00	77	25	30.24	39.2	25.67	330	11	0	M	6.21	M	SCT	M	M	M	3000	M	M	M	M	M	M	M	M	M	M	77	SEQM 071	M
SEQM	5/2/2022 17:00	77	25	30.27	44.6	31.62	M	3	0	M	6.21	M	SCT	M	M	M	4000	M	M	M	M	M	M	M	M	M	M	77	SEQM 021	M
SEQM	5/3/2022 17:00	77	25	30.27	44.6	31.62	210	4	0	M	6.21	M	FEW	M	M	M	4000	M	M	M	M	M	M	M	M	M	M	77	SEQM 031	M
SEQM	8/14/2022 18:00	77	25	30.27	41	27.53	290	6	0	M	6.21	M	SCT	SCT	M	M	4000	10000	M	M	M	M	M	M	M	M	M	77	SEQM 141	M
SEQM	8/24/2022 18:00	77	25	30.27	35.6	22.28	280	8	0	M	6.21	M	SCT	M	M	M	4000	M	M	M	M	M	M	M	M	M	M	77	SEQM 241	M
SEQM	10/2/2022 17:00	77	25	30.27	39.2	25.67	200	5	0	M	6.21	M	FEW	SCT	BKN	M	4000	10000	30000	M	M	M	M	M	M	M	M	77	SEQM 021	M
SEQM	11/7/2022 17:00	77	25	30.27	37.4	23.93	M	4	0	M	6.21	M	SCT	M	M	M	3000	M	M	M	M	M	M	M	M	M	M	77	SEQM 071	M
SEQM	8/12/2022 18:00	77	25	30.3	35.6	22.28	310	9	0	M	6.21	M	SCT	M	M	M	3600	M	M	M	M	M	M	M	M	M	M	77	SEQM 121	M
SEQM	11/30/2022 20:00	75.2	24	30.09	44.6	33.57	360	17	0	M	6.21	M	FEW	SCT	M	M	2600	3000	M	M	M	M	M	M	M	M	M	75.2	SEQM 302	M
SEQM	9/15/2022 20:00	75.2	24	30.12	48.2	38.46	340	20	0	M	6.21	M	SCT	SCT	M	M	4000	30000	M	M	M	M	M	M	M	M	M	75.2	SEQM 152	M
SEQM	11/19/2022 19:00	75.2	24	30.12	53.6	46.98	360	14	0	M	6.21	M	FEW	SCT	M	M	2600	3000	M	M	M	M	M	M	M	M	M	75.2	SEQM 191	M
SEQM	12/22/2022 20:00	75.2	24	30.12	46.4	35.94	350	16	0	M	6.21	M	FEW	SCT	M	M	4000	10000	M	M	M	M	M	M	M	M	M	75.2	SEQM 222	M
SEQM	1/19/2022 20:00	75.2	24	30.15	42.8	31.34	60	11	0	M	6.21	M	SCT	BKN	M	M	3600	30000	M	M	M	M	M	M	M	M	M	75.2	SEQM 192	M
SEQM	1/20/2022 20:00	75.2	24	30.15	41	29.23	150	11	0	M	6.21	M	BKN	BKN	M	M	3000	10000	M	M	M	M	M	M	M	M	M	75.2	SEQM 202	M
SEQM	1/24/2022 18:00	75.2	24	30.15	53.6	46.98	350	16	0	M	6.21	M	FEW	M	M	M	3000	M	M	M	M	M	M	M	M	M	M	75.2	SEQM 241	M
SEQM	5/3/2022 20:00	75.2	24	30.15	48.2	38.46	350	15	0	M	6.21	M	SCT	M	M	M	4000	M	M	M	M	M	M	M	M	M	M	75.2	SEQM 032	M
SEQM	7/19/2022 21:00	75.2	24	30.15	48.2	38.46	350	13	0	M	6.21	M	FEW	M	M	M	3000	M	M	M	M	M	M	M	M	M	M	75.2	SEQM 192	M
SEQM	7/29/2022 20:00	75.2	24	30.15	42.8	31.34	M	4	0	M	6.21	M	FEW	SCT	M	M	2600	3000	M	M	VCSH	M	M	M	M	M	M	75.2	SEQM 292	M
SEQM	7/29/2022 21:00	75.2	24	30.15	50	41.14	340	11	0	M	6.21	M	FEW	SCT	M	M	2600	3000	M	M	M	M	M	M	M	M	M	75.2	SEQM 292	M
SEQM	7/30/2022 21:00	75.2	24	30.15	50	41.14	360	13	0	M	6.21	M	FEW	SCT	M	M	4000	10000	M	M	M	M	M	M	M	M	M	75.2	SEQM 302	M
SEQM	8/7/2022 20:00	75.2	24	30.15	39.2	27.26	100	11	0	M	6.21	M	SCT	M	M	M	3000	M	M	M	M	M	M	M	M	M	M	75.2	SEQM 072	M

SEQM	8/8/2022 20:00	75.2	24	30.15	37.4	25.4	110	12	0	M	6.21	23	SCT	M	M	M	3000	M	M	M	M	M	M	M	M	M	M	75.2	SEQM 0820	M
SEQM	8/23/2022 20:00	75.2	24	30.15	32	20.49	60	9	0	M	6.21	M	FEW	M	M	M	3000	M	M	M	M	M	M	M	M	M	M	75.2	COR SEQM	M
SEQM	9/8/2022 20:00	75.2	24	30.15	44.6	33.57	10	12	0	M	6.21	M	FEW	BKN	M	M	4000	30000	M	M	M	M	M	M	M	M	M	75.2	SEQM 0820	M
SEQM	9/9/2022 20:00	75.2	24	30.15	37.4	25.4	70	7	0	M	6.21	M	FEW	BKN	M	M	4000	30000	M	M	M	M	M	M	M	M	M	75.2	SEQM 0920	M
SEQM	9/26/2022 20:00	75.2	24	30.15	37.4	25.4	100	7	0	M	6.21	M	SCT	SCT	M	M	3000	30000	M	M	M	M	M	M	M	M	M	75.2	SEQM 2620	M
SEQM	10/7/2022 19:00	75.2	24	30.15	48.2	38.46	350	16	0	M	6.21	M	SCT	SCT	M	M	2300	30000	M	M	M	M	M	M	M	M	M	75.2	SEQM 0719	M
SEQM	10/10/2022 21:00	75.2	24	30.15	41	29.23	110	10	0	M	6.21	M	FEW	SCT	M	M	3300	30000	M	M	M	M	M	M	M	M	M	75.2	SEQM 1021	M
SEQM	10/14/2022 19:00	75.2	24	30.15	44.6	33.57	40	9	0	M	6.21	M	FEW	SCT	M	M	3000	3300	M	M	VCSH	M	M	M	M	M	M	75.2	SEQM 1419	M
SEQM	10/30/2022 19:00	75.2	24	30.15	41	29.23	360	13	0	M	6.21	M	FEW	M	M	M	3300	M	M	M	M	M	M	M	M	M	M	75.2	SEQM 3019	M
SEQM	10/31/2022 19:00	75.2	24	30.15	48.2	38.46	340	15	0	M	6.21	M	SCT	M	M	M	3000	M	M	M	M	M	M	M	M	M	M	75.2	SEQM 3119	M
SEQM	11/14/2022 19:00	75.2	24	30.15	48.2	38.46	340	19	0	M	6.21	M	FEW	SCT	M	M	2600	3000	M	M	VCSH	M	M	M	M	M	M	75.2	COR SEQM	M
SEQM	12/12/2022 18:27	75.2	24	30.15	48.2	38.46	350	22	0	M	6.21	M	SCT	BKN	M	M	4000	30000	M	M	M	M	M	M	M	M	M	75.2	SEQM 1218	M
SEQM	12/21/2022 19:00	75.2	24	30.15	46.4	35.94	350	14	0	M	6.21	M	SCT	M	M	M	3300	M	M	M	M	M	M	M	M	M	M	75.2	SEQM 2119	M
SEQM	12/22/2022 19:00	75.2	24	30.15	41	29.23	350	12	0	M	6.21	M	FEW	BKN	M	M	4000	8000	M	M	M	M	M	M	M	M	M	75.2	SEQM 2219	M
SEQM	1/18/2022 18:00	75.2	24	30.18	44.6	33.57	350	11	0	M	6.21	M	SCT	BKN	M	M	4000	30000	M	M	M	M	M	M	M	M	M	75.2	SEQM 1818	M
SEQM	1/23/2022 18:00	75.2	24	30.18	48.2	38.46	330	12	0	M	6.21	M	SCT	M	M	M	4000	M	M	M	M	M	M	M	M	M	M	75.2	SEQM 2318	M
SEQM	5/2/2022 19:00	75.2	24	30.18	48.2	38.46	350	12	0	M	6.21	M	BKN	M	M	M	3600	M	M	M	M	M	M	M	M	M	M	75.2	SEQM 0219	M
SEQM	5/8/2022 21:00	75.2	24	30.18	53.6	46.98	360	12	0	M	6.21	M	FEW	SCT	M	M	3000	3300	M	M	VCSH	M	M	M	M	M	M	75.2	SEQM 0821	M
SEQM	7/7/2022 19:00	75.2	24	30.18	39.2	27.26	250	5	0	M	6.21	M	FEW	BKN	M	M	3000	7000	M	M	M	M	M	M	M	M	M	75.2	SEQM 0719	M
SEQM	7/29/2022 19:00	75.2	24	30.18	42.8	31.34	330	11	0	M	6.21	M	SCT	M	M	M	3000	M	M	M	M	M	M	M	M	M	M	75.2	SEQM 2919	M
SEQM	8/7/2022 19:00	75.2	24	30.18	37.4	25.4	90	11	0	M	6.21	22	SCT	M	M	M	3000	M	M	M	M	M	M	M	M	M	M	75.2	SEQM 0719	M
SEQM	8/8/2022 19:00	75.2	24	30.18	39.2	27.26	110	12	0	M	6.21	23	SCT	M	M	M	3000	M	M	M	M	M	M	M	M	M	M	75.2	SEQM 0819	M
SEQM	8/16/2022 20:00	75.2	24	30.18	44.6	33.57	340	13	0	M	6.21	M	FEW	SCT	M	M	3000	3300	M	M	VCSH	M	M	M	M	M	M	75.2	SEQM 1620	M
SEQM	9/15/2022 19:00	75.2	24	30.18	48.2	38.46	350	17	0	M	6.21	M	BKN	M	M	M	4000	M	M	M	M	M	M	M	M	M	M	75.2	SEQM 1519	M
SEQM	9/18/2022 19:00	75.2	24	30.18	46.4	35.94	350	18	0	M	6.21	M	SCT	SCT	M	M	4000	30000	M	M	M	M	M	M	M	M	M	75.2	SEQM 1819	M
SEQM	9/26/2022 19:00	75.2	24	30.18	37.4	25.4	M	4	0	M	6.21	M	SCT	SCT	M	M	3000	30000	M	M	M	M	M	M	M	M	M	75.2	SEQM 2619	M
SEQM	9/27/2022 20:00	75.2	24	30.18	33.8	22.02	190	4	0	M	6.21	M	SCT	M	M	M	4000	M	M	M	M	M	M	M	M	M	M	75.2	SEQM 2720	M
SEQM	10/2/2022 20:00	75.2	24	30.18	39.2	27.26	210	10	0	M	6.21	M	SCT	BKN	M	M	4000	30000	M	M	M	M	M	M	M	M	M	75.2	SEQM 0220	M
SEQM	10/2/2022 21:00	75.2	24	30.18	41	29.23	50	8	0	M	6.21	M	FEW	BKN	M	M	4000	30000	M	M	M	M	M	M	M	M	M	75.2	SEQM 0221	M
SEQM	10/30/2022 18:00	75.2	24	30.18	42.8	31.34	M	6	0	M	6.21	M	FEW	M	M	M	3000	M	M	M	M	M	M	M	M	M	M	75.2	SEQM 3018	M
SEQM	10/31/2022 18:00	75.2	24	30.18	42.8	31.34	320	12	0	M	6.21	M	SCT	M	M	M	3000	M	M	M	M	M	M	M	M	M	M	75.2	SEQM 3118	M
SEQM	11/11/2022 19:00	75.2	24	30.18	46.4	35.94	360	12	0	M	6.21	M	SCT	M	M	M	3000	M	M	M	VCSH	M	M	M	M	M	M	75.2	SEQM 1119	M
SEQM	11/13/2022 18:00	75.2	24	30.18	44.6	33.57	340	12	0	M	6.21	M	SCT	M	M	M	3000	M	M	M	M	M	M	M	M	M	M	75.2	SEQM 1318	M
SEQM	11/14/2022 18:00	75.2	24	30.18	44.6	33.57	340	8	0	M	6.21	M	SCT	M	M	M	3000	M	M	M	M	M	M	M	M	M	M	75.2	SEQM 1418	M
SEQM	11/15/2022 19:00	75.2	24	30.18	48.2	38.46	360	10	0	M	6.21	M	SCT	M	M	M	3000	M	M	M	M	M	M	M	M	M	M	75.2	SEQM 1519	M
SEQM	12/12/2022 18:00	75.2	24	30.18	41	29.23	10	9	0	M	6.21	M	SCT	BKN	M	M	4000	30000	M	M	M	M	M	M	M	M	M	75.2	SEQM 1218	M
SEQM	12/20/2022 19:00	75.2	24	30.18	44.6	33.57	350	12	0	M	6.21	M	SCT	BKN	M	M	4000	30000	M	M	M	M	M	M	M	M	M	75.2	SEQM 2019	M
SEQM	1/23/2022 17:00	75.2	24	30.21	44.6	33.57	280	4	0	M	6.21	M	FEW	M	M	M	4000	M	M	M	M	M	M	M	M	M	M	75.2	SEQM 2317	M
SEQM	2/3/2022 18:00	75.2	24	30.21	44.6	33.57	330	9	0	M	6.21	M	FEW	BKN	M	M	2600	30000	M	M	M	M	M	M	M	M	M	75.2	SEQM 0318	M
SEQM	4/3/2022 18:00	75.2	24	30.21	50	41.14	350	9	0	M	6.21	M	SCT	M	M	M	4000	M	M	M	M	M	M	M	M	M	M	75.2	SEQM 0318	M
SEQM	4/30/2022 16:34	75.2	24	30.21	48.2	38.46	M	2	0	M	6.21	M	SCT	SCT	M	M	4000	30000	M	M	M	M	M	M	M	M	M	75.2	SEQM 3016	M
SEQM	5/1/2022 18:00	75.2	24	30.21	48.2	38.46	360	5	0	M	6.21	M	BKN	M	M	M	4000	M	M	M	M	M	M	M	M	M	M	75.2	SEQM 0118	M
SEQM	7/3/2022 20:00	75.2	24	30.21	48.2	38.46	340	5	0	M	6.21	M	FEW	SCT	M	M	2600	3000	M	M	VCSH	M	M	M	M	M	M	75.2	SEQM 0320	M
SEQM	7/19/2022 18:00	75.2	24	30.21	39.2	27.26	130	7	0	M	6.21	M	FEW	M	M	M	3600	M	M	M	M	M	M	M	M	M	M	75.2	SEQM 1918	M
SEQM	7/30/2022 19:00	75.2	24	30.21	41	29.23	310	7	0	M	6.21	M	FEW	SCT	M	M	4000	10000	M	M	M	M	M	M	M	M	M	75.2	SEQM 3019	M
SEQM	8/7/2022 18:00	75.2	24	30.21	41	29.23	90	9	0	M	6.21	M	BKN	M	M	M	3000	M	M	M	M	M	M	M	M	M	M	75.2	SEQM 0718	M
SEQM	8/18/2022 17:00	75.2	24	30.21	39.2	27.26	330	6	0	M	6.21	M	FEW	M	M	M	2600	M	M	M	M	M	M	M	M	M	M	75.2	SEQM 1817	M
SEQM	8/27/2022 19:00	75.2	24	30.21	35.6	23.66	90	10	0	M	6.21	M	BKN	M	M	M	4000	M	M	M	M	M	M	M	M	M	M	75.2	SEQM 2719	M
SEQM	8/30/2022 19:00	75.2	24	30.21	41	29.23	150	16	0	M	6.21	26	SCT	M	M	M	4000	M	M	M	VCSH	M	M	M	M	M	M	75.2	SEQM 3019	M
SEQM	9/2/2022 18:00	75.2	24	30.21	39.2	27.26	260	7	0	M	6.21	M	BKN	M	M	M	4000	M	M	M	M	M	M	M	M	M	M	75.2	SEQM 0218	M
SEQM	9/4/2022 18:00	75.2	24	30.21	39.2	27.26	230	12	0	M	6.21	M	SCT	SCT	BKN	M	4000	8000	30000	M	M	M	M	M	M	M	M	75.2	SEQM 0418	M
SEQM	9/9/2022 17:37	75.2	24	30.21	35.6	23.66	360	14	0	M	6.21	M	SCT	SCT	M	M	5000	30000	M	M	M	M	M	M	M	M	M	75.2	SEQM 0917	M
SEQM	9/10/2022 20:00	75.2	24	30.21	41	29.23	120	8	0	M	6.21	M	SCT	SCT	M	M	4000	10000	M	M	M	M	M	M	M	M	M	75.2	SEQM 1020	M
SEQM	9/14/2022 18:00	75.2	24	30.21	42.8	31.34	30	8	0	M	6.21	M	FEW	SCT	M	M	4000	8000	M	M	M	M	M	M	M	M	M	75.2	SEQM 1418	M
SEQM	9/22/2022 18:00	75.2	24	30.21	41	29.23	320	10	0	M	6.21	M	SCT	M	M	M	4000	M	M	M	M	M	M	M	M	M	M	75.2	SEQM 2218	M
SEQM	9/25/2022 17:00	75.2	24	30.21	42.8	31.34	M	4	0	M	6.21	M	FEW	M	M	M	3000	M	M	M	M	M	M	M	M	M	M	75.2	SEQM 2517	M
SEQM	9/27/2022 19:00	75.2	24	30.21	35.6	23.66	100	11	0	M	6.21	M	SCT	M	M	M	4000	M	M	M	M	M	M	M	M	M	M	75.2	SEQM 2719	M
SEQM	9/29/2022 18:00	75.2	24	30.21	44.6	33.57	20	9	0	M	6.21	M	SCT	SCT	M	M	3300	10000	M	M	M	M	M	M	M	M	M	75.2	SEQM 2918	M
SEQM	10/2/2022 19:00	75.2	24	30.21	37.4	25.4	150	10	0	M	6.21	M	SCT	SCT	BKN	M	4000	10000	30000	M	M	M	M	M	M	M	M	75.2	SEQM 0219	M
SEQM	10/3/2022 19:00	75.2	24	30.21	39.2	27.26	70	12	0	M	6.21	M	FEW	BKN	M	M	4000	8000	M	M	M	M	M	M	M	M	M	75.2	SEQM 0319	M
SEQM	10/5/2022 18:00	75.2	24	30.21	44.6	33.57	340	8	0	M	6.21	M	FEW	SCT	M	M	3000	3300	M	M	M	M	M	M	M	M	M	75.2	SEQM 0518	M
SEQM	10/27/2022 18:00	75.2	24	30.21	50	41.14	330	11	0	M	6.21	M	SCT	M	M	M	3000	M	M	M	VCSH	M	M	M	M	M	M	75.2	SEQM 2718	M
SEQM	11/7/2022 19:00	75.2	24	30.21	44.6	33.57	350	14	0	M	6.21	M	SCT	M	M	M	3600	M	M	M	M	M	M	M	M	M	M	75.2	SEQM 0719	M
SEQM	11/11/2022 18:00	75.2	24	30.21	44.6	33.57	20	9	0	M	6.21	M	SCT	M	M	M	3000	M	M	M	M	M	M	M	M	M	M	75.2	SEQM 1118	M
SEQM	11/18/2022 17:00	75.2	24	30.21	46.4	35.94	M	5	0	M	6.21	M	SCT	SCT	M	M	3000	30000	M	M	M	M	M	M	M	M	M	75.2	SEQM 1817	M
SEQM	11/19/2022 17:00	75.2	24	30.21	44.6	33.57	M	4	0	M	6.21	M	FEW	M	M	M	3000	M	M	M	M	M	M	M	M	M	M	75.2	SEQM 1917	M
SEQM	11/25/2022 18:00	75.2	24	30.21	44.6	33.57	M	4	0	M	6.21	M	SCT	SCT	M	M	3300	10000	M	M	M	M	M	M	M	M	M	75.2	SEQM 2518	M
SEQM	12/12/2022 17:00	75.2	24	30.21	44.6	33.57	M	4	0	M	6.21	M	FEW	BKN	M	M	3300	30000	M	M	M	M	M	M	M	M	M	75.2	SEQM 1217	M
SEQM	12/19/2022 18:00	75.2	24	30.21	46.4	35.94	350	12	0	M	6.21	M	FEW	M	M	M	3600	M	M	M	M	M	M	M	M	M	M	75.2	SEQM 1918	M
SEQM	12/20/2022 18:00	75.2	24	30.21	44.6	33.57	M	6	0	M	6.21	M	SCT	BKN	M	M	4000	30000	M	M	M	M	M	M	M	M	M	75.2	SEQM 2018	M
SEQM	12/21/2022 18:00	75.2	24	30.21	44.6	33.57	360	10	0	M	6.21	M	SCT	M	M	M	3300	M	M	M	M	M	M	M	M	M	M	75.2	SEQM 2118	M
SEQM	12/22/2022 17:00	75.2	24	30.21	39.2	27.26	310	7	0	M	6.21	M	FEW	SCT	M	M	4000	30000	M	M	M	M	M	M	M	M	M	75.2	SEQM 2217	M
SEQM	12/29/2022 19:00	75.2	24	30.21	44.6	33.57	10	11	0	M	6.21	M	SCT	M	M	M	3300	M	M	M	M	M	M	M	M	M	M	75.2	SEQM 2919	M
SEQM	1/3/2022 18:00	75.2	24	30.24	42.8	31.34	360	8	0	M	6.21	M	FEW	SCT	M	M	3000	30000	M	M	M	M	M	M	M	M	M	75.2	SEQM 0318	M
SEQM	1/21/2022 17:00	75.2	24	30.24	44.6	33.57	290	6	0	M	6.21	M	BKN	BKN	M	M	4000	10000	M	M	M	M	M	M	M	M	M	75.2	SEQM 2117	M
SEQM	6/5/2022 17:00	75.2	24	30.24	50	41.14	M	3	0	M	6.21	M	FEW	FEW	SCT	M	2600	3000	30000	M	M	M	M	M	M	M	M	75.2	SEQM 0517	M
SEQM	7/2/2022 17:00	75.2	24	30.24	44.6	33.57	30	7	0	M	6.21	M	SCT	SCT	M	M	4000	10000	M	M	M	M	M	M	M	M	M	75.2	SEQM 0217	M
SEQM	7/19/2022 17:00	75.2	24	30.24	39.2	27.26	180	14	0	M	6.21	M	FEW	M	M	M	3600	M	M	M	M	M	M	M	M	M	M	75.2	SEQM 1917	M
SEQM	8/12/2022 21:00	75.2	24	30.24	33.8	22.02	360	13	0	M	6.21	M	FEW	M	M	M	3600	M	M	M	M	M	M	M	M	M	M	75.2	SEQM 1221	M
SEQM	8/17/2022 18:00	75.2	24	30.24	39.2	27.26	300	4	0	M	6.21	M	BKN	M	M	M	4000	M	M	M	M	M	M	M	M	M	M	75.2	SEQM 1718	M
SEQM	8/24/2022 19:00	75.2	24	30.24	37.4	25.4	110	16	0	M	6.21	M	SCT	M	M	M	4000	M	M	M	M	M	M	M	M	M	M	75.2	SEQM 2419	M
SEQM	8/24/2022 20:00	75.2	24	30.24	37.4	25.4	110	15	0	M	6.21	M	SCT	M	M	M	4000	M	M	M	M	M	M	M	M	M	M	75.2	SEQM 2420	M
SEQM	8/27/2022 18:00	75.2	24	30.24	37.4	25.4	320	6	0	M	6.21	M	BKN	M	M	M	4000	M	M	M	M	M	M	M	M	M	M	75.2	SEQM 2718	M
SEQM	9/2/2022 17:00	75.2	24	30.24	41	29.23	M	5	0	M	6.21	M	BKN	M	M	M	4000	M	M	M	M	M	M	M	M	M	M	75.2	SEQM 0217	M
SEQM	9/13/2022 17:00	75.2	24	30.24	35.6	23.66	10	9	0	M	6.21	M	FEW	SCT	M	M	4000	30000	M	M	M	M	M	M	M	M	M	75.2	SEQM 1317	M
SEQM	9/18/2022 17:00	75.2	24	30.24	39.2	27.26	M	5	0	M	6.21	M	FEW	BKN	M	M	4000	30000	M	M	M	M	M	M	M	M	M	75.2	SEQM 1817	M
SEQM	9/26/2022 17:00	75.2	24	30.24	41	29.23	M	3	0	M	6.21	M	SCT	SCT	M	M	3000	30000	M	M	M	M	M	M	M	M	M	75.2	SEQM 2617	M

SEQM	9/27/2022 18:00	75.2	24	30.24	33.8	22.02	100	6	0	M	6.21	M	SCT	M	M	M	4000	M	M	M	M	M	M	M	M	M	M	75.2	SEQM 271	M
SEQM	10/1/2022 17:00	75.2	24	30.24	42.8	31.34	180	12	0	M	6.21	M	SCT	SCT	M	M	3300	30000	M	M	M	M	M	M	M	M	M	75.2	SEQM 011	M
SEQM	10/1/2022 18:00	75.2	24	30.24	41	29.23	140	13	0	M	6.21	M	SCT	SCT	M	M	3300	10000	M	M	M	M	M	M	M	M	M	75.2	SEQM 011	M
SEQM	10/10/2022 18:00	75.2	24	30.24	37.4	25.4	60	8	0	M	6.21	M	SCT	M	M	M	4000	M	M	M	M	M	M	M	M	M	M	75.2	SEQM 101	M
SEQM	10/11/2022 19:00	75.2	24	30.24	41	29.23	240	11	0	M	6.21	M	BKN	SCT	M	M	3300	10000	M	M	M	M	M	M	M	M	M	75.2	SEQM 111	M
SEQM	10/16/2022 17:00	75.2	24	30.24	46.4	35.94	300	5	0	M	6.21	M	SCT	SCT	M	M	3000	30000	M	M	M	M	M	M	M	M	M	75.2	SEQM 161	M
SEQM	11/1/2022 17:00	75.2	24	30.24	42.8	31.34	M	4	0	M	6.21	M	SCT	BKN	M	M	4000	8000	M	M	M	M	M	M	M	M	M	75.2	SEQM 011	M
SEQM	12/29/2022 18:00	75.2	24	30.24	42.8	31.34	350	10	0	M	6.21	M	SCT	M	M	M	3300	M	M	M	M	M	M	M	M	M	M	75.2	SEQM 291	M
SEQM	5/8/2022 18:00	75.2	24	30.27	50	41.14	210	4	0	M	6.21	M	SCT	BKN	M	M	3300	10000	M	M	M	M	M	M	M	M	M	75.2	SEQM 081	M
SEQM	7/12/2022 17:00	75.2	24	30.27	42.8	31.34	M	3	0	M	6.21	M	SCT	M	M	M	4000	M	M	M	M	M	M	M	M	M	M	75.2	SEQM 121	M
SEQM	7/28/2022 18:00	75.2	24	30.27	42.8	33.29	360	5	0	M	6.21	M	BKN	M	M	M	3000	M	M	M	M	M	M	M	M	M	M	73.4	COR SEQM	M
SEQM	8/12/2022 19:00	75.2	24	30.27	33.8	22.02	70	5	0	M	6.21	17	SCT	M	M	M	3600	M	M	M	M	M	M	M	M	M	M	75.2	SEQM 121	M
SEQM	8/12/2022 20:00	75.2	24	30.27	33.8	22.02	100	9	0	M	6.21	M	FEW	SCT	M	M	3600	30000	M	M	M	M	M	M	M	M	M	75.2	SEQM 122	M
SEQM	8/27/2022 17:00	75.2	24	30.27	37.4	25.4	210	8	0	M	6.21	M	SCT	M	M	M	4000	M	M	M	M	M	M	M	M	M	M	75.2	SEQM 271	M
SEQM	9/8/2022 16:00	75.2	24	30.27	39.2	27.26	290	6	0	M	6.21	M	FEW	M	M	M	4000	M	M	M	M	M	M	M	M	M	M	75.2	SEQM 081	M
SEQM	9/10/2022 18:00	75.2	24	30.27	41	29.23	160	12	0	M	6.21	22	BKN	SCT	M	M	4000	30000	M	M	M	M	M	M	M	M	M	75.2	SEQM 101	M
SEQM	9/11/2022 19:00	75.2	24	30.27	39.2	27.26	180	7	0	M	6.21	M	BKN	M	M	M	4000	M	M	M	M	M	M	M	M	M	M	75.2	SEQM 111	M
SEQM	9/15/2022 16:00	75.2	24	30.27	44.6	33.57	280	6	0	M	6.21	M	FEW	M	M	M	3000	M	M	M	M	M	M	M	M	M	M	75.2	SEQM 151	M
SEQM	9/23/2022 17:00	75.2	24	30.27	37.4	25.4	M	5	0	M	6.21	M	SCT	SCT	M	M	4000	30000	M	M	M	M	M	M	M	M	M	75.2	SEQM 231	M
SEQM	9/27/2022 17:00	75.2	24	30.27	33.8	22.02	340	8	0	M	6.21	M	FEW	M	M	M	4000	M	M	M	M	M	M	M	M	M	M	75.2	SEQM 271	M
SEQM	10/3/2022 17:00	75.2	24	30.27	39.2	27.26	M	3	0	M	6.21	M	SCT	M	M	M	4000	M	M	M	M	M	M	M	M	M	M	75.2	SEQM 031	M
SEQM	8/13/2022 18:00	75.2	24	30.3	28.4	17.7	350	10	0	M	6.21	M	FEW	M	M	M	3000	M	M	M	M	M	M	M	M	M	M	75.2	SEQM 131	M
SEQM	8/17/2022 17:00	75.2	24	30.3	39.2	27.26	M	3	0	M	6.21	M	FEW	M	M	M	4000	M	M	M	M	M	M	M	M	M	M	75.2	SEQM 171	M
SEQM	8/25/2022 18:00	75.2	24	30.3	39.2	27.26	80	9	0	M	6.21	M	BKN	M	M	M	4000	M	M	M	M	M	M	M	M	M	M	75.2	SEQM 251	M
SEQM	9/10/2022 17:00	75.2	24	30.3	41	29.23	160	14	0	M	6.21	M	SCT	M	M	M	3300	M	M	M	M	M	M	M	M	M	M	75.2	SEQM 101	M
SEQM	10/2/2022 16:00	75.2	24	30.3	37.4	25.4	360	7	0	M	6.21	M	FEW	SCT	BKN	M	4000	10000	30000	M	M	M	M	M	M	M	M	75.2	SEQM 021	M
SEQM	10/3/2022 16:00	75.2	24	30.3	41	29.23	300	5	0	M	6.21	M	SCT	M	M	M	4000	M	M	M	M	M	M	M	M	M	M	75.2	SEQM 031	M
SEQM	10/4/2022 16:00	75.2	24	30.3	42.8	31.34	330	8	0	M	6.21	M	SCT	BKN	M	M	3300	30000	M	M	M	M	M	M	M	M	M	75.2	SEQM 041	M
SEQM	11/2/2022 17:00	75.2	24	30.3	44.6	33.57	220	4	0	M	6.21	M	SCT	BKN	M	M	4000	8000	M	M	M	M	M	M	M	M	M	75.2	SEQM 021	M
SEQM	5/7/2022 17:00	75.2	24	30.33	50	41.14	290	3	0	M	6.21	M	BKN	M	M	M	3300	M	M	M	M	M	M	M	M	M	M	75.2	SEQM 071	M
SEQM	1/23/2022 20:00	73.4	23	30.12	55.4	53.29	10	15	0	M	6.21	M	SCT	M	M	M	4000	M	M	M	M	M	M	M	M	M	M	73.4	SEQM 232	M
SEQM	2/2/2022 20:00	73.4	23	30.12	53.6	49.9	350	17	0	M	6.21	M	FEW	SCT	M	M	3000	30000	M	M	M	M	M	M	M	M	M	73.4	SEQM 022	M
SEQM	10/30/2022 20:00	73.4	23	30.12	46.4	38.18	340	18	0	M	6.21	M	FEW	M	M	M	3300	M	M	M	M	M	M	M	M	M	M	73.4	SEQM 302	M
SEQM	11/1/2022 20:00	73.4	23	30.12	51.8	46.71	340	18	0	M	6.21	M	SCT	M	M	M	4000	M	M	M	M	M	M	M	M	M	M	73.4	SEQM 012	M
SEQM	11/30/2022 19:00	73.4	23	30.12	35.6	25.13	350	12	0	M	6.21	M	SCT	M	M	M	3000	M	M	M	M	M	M	M	M	M	M	73.4	SEQM 301	M
SEQM	1/19/2022 21:00	73.4	23	30.15	42.8	33.29	50	9	0	M	6.21	M	SCT	SCT	M	M	3600	30000	M	M	M	M	M	M	M	M	M	73.4	SEQM 192	M
SEQM	1/20/2022 21:00	73.4	23	30.15	41	31.05	180	15	0	M	6.21	M	SCT	SCT	M	M	3000	10000	M	M	M	M	M	M	M	M	M	73.4	SEQM 202	M
SEQM	1/23/2022 19:00	73.4	23	30.15	51.8	46.71	350	19	0	M	6.21	M	SCT	M	M	M	4000	M	M	M	M	M	M	M	M	M	M	73.4	SEQM 231	M
SEQM	2/2/2022 19:00	73.4	23	30.15	48.2	40.85	350	13	0	M	6.21	M	SCT	SCT	M	M	4000	30000	M	M	M	M	M	M	M	M	M	73.4	SEQM 021	M
SEQM	4/30/2022 21:00	73.4	23	30.15	46.4	38.18	330	9	0	M	6.21	M	SCT	M	M	M	4000	M	M	M	M	M	M	M	M	M	M	73.4	SEQM 302	M
SEQM	5/2/2022 21:00	73.4	23	30.15	53.6	49.9	340	13	0	M	6.21	M	SCT	M	M	M	3300	M	M	M	M	M	M	M	M	M	M	73.4	SEQM 022	M
SEQM	5/3/2022 21:00	73.4	23	30.15	55.4	53.29	350	16	0	M	6.21	M	SCT	M	M	M	3300	M	M	M	M	M	M	M	M	M	M	73.4	SEQM 032	M
SEQM	8/7/2022 21:00	73.4	23	30.15	39.2	28.96	100	10	0	M	6.21	M	SCT	M	M	M	3000	M	M	M	M	M	M	M	M	M	M	73.4	SEQM 072	M
SEQM	8/18/2022 20:00	73.4	23	30.15	51.8	46.71	360	16	0	M	6.21	M	SCT	M	M	M	3000	M	M	M	M	M	M	M	M	M	M	73.4	SEQM 182	M
SEQM	8/23/2022 21:00	73.4	23	30.15	41	31.05	340	18	0	M	6.21	M	SCT	M	M	M	3000	M	M	M	M	M	M	M	M	M	M	73.4	SEQM 232	M
SEQM	9/3/2022 21:00	73.4	23	30.15	42.8	33.29	190	10	0	M	6.21	M	BKN	SCT	M	M	3000	30000	M	M	M	M	M	M	M	M	M	73.4	COR SEQM	M
SEQM	9/9/2022 21:00	73.4	23	30.15	48.2	40.85	340	15	0	M	6.21	M	FEW	BKN	M	M	4000	30000	M	M	M	M	M	M	M	M	M	73.4	SEQM 092	M
SEQM	9/13/2022 20:00	73.4	23	30.15	50	43.69	350	20	0	M	6.21	M	FEW	BKN	M	M	4000	30000	M	M	M	M	M	M	M	M	M	73.4	SEQM 132	M
SEQM	9/13/2022 20:10	73.4	23	30.15	51.8	46.71	360	18	0	M	6.21	28	FEW	BKN	M	M	4000	30000	M	M	M	M	M	M	M	M	M	73.4	SEQM 132	M
SEQM	9/23/2022 20:00	73.4	23	30.15	50	43.69	350	18	0	M	6.21	M	FEW	M	M	M	4000	M	M	M	M	M	M	M	M	M	M	73.4	SEQM 232	M
SEQM	9/27/2022 21:00	73.4	23	30.15	44.6	35.66	340	16	0	M	6.21	M	SCT	M	M	M	4000	M	M	M	M	M	M	M	M	M	M	73.4	SEQM 272	M
SEQM	10/5/2022 19:00	73.4	23	30.15	51.8	46.71	350	19	0	M	6.21	M	FEW	SCT	BKN	M	3000	3300	30000	M	M	M	M	M	M	M	M	73.4	SEQM 051	M
SEQM	10/14/2022 19:03	73.4	23	30.15	46.4	38.18	50	7	0	M	6.21	M	FEW	SCT	M	M	3000	3300	M	M	TS VCSH	M	M	M	M	M	M	73.4	SEQM 141	M
SEQM	11/20/2022 18:00	73.4	23	30.15	44.6	35.66	340	7	0	M	6.21	M	SCT	SCT	M	M	3000	30000	M	M	M	M	M	M	M	M	M	73.4	SEQM 201	M
SEQM	11/24/2022 19:00	73.4	23	30.15	48.2	40.85	350	16	0	M	6.21	M	SCT	M	M	M	3000	M	M	M	M	M	M	M	M	M	M	73.4	SEQM 241	M
SEQM	11/25/2022 19:00	73.4	23	30.15	48.2	40.85	340	13	0	M	6.21	M	FEW	SCT	M	M	3000	3300	M	M	M	M	M	M	M	M	M	73.4	SEQM 251	M
SEQM	12/1/2022 19:00	73.4	23	30.15	46.4	38.18	350	13	0	M	6.21	M	SCT	M	M	M	3300	M	M	M	M	M	M	M	M	M	M	73.4	SEQM 011	M
SEQM	12/5/2022 18:00	73.4	23	30.15	41	31.05	340	11	0	M	6.21	M	SCT	M	M	M	4000	M	M	M	M	M	M	M	M	M	M	73.4	SEQM 051	M
SEQM	12/6/2022 18:00	73.4	23	30.15	44.6	35.66	340	9	0	M	6.21	M	FEW	M	M	M	4000	M	M	M	M	M	M	M	M	M	M	73.4	SEQM 061	M
SEQM	12/10/2022 19:00	73.4	23	30.15	42.8	33.29	M	7	0	M	6.21	M	SCT	SCT	M	M	3000	30000	M	M	M	M	M	M	M	M	M	73.4	SEQM 101	M
SEQM	12/12/2022 19:00	73.4	23	30.15	51.8	46.71	350	21	0	M	6.21	M	SCT	BKN	M	M	4000	30000	M	M	M	M	M	M	M	M	M	73.4	SEQM 121	M
SEQM	12/19/2022 19:00	73.4	23	30.15	50	43.69	360	17	0	M	6.21	M	SCT	M	M	M	3600	M	M	M	M	M	M	M	M	M	M	73.4	SEQM 191	M
SEQM	12/24/2022 19:00	73.4	23	30.15	50	43.69	350	17	0	M	6.21	27	FEW	M	M	M	3000	M	M	M	M	M	M	M	M	M	M	73.4	SEQM 241	M
SEQM	12/29/2022 20:00	73.4	23	30.15	48.2	40.85	350	16	0	M	6.21	M	SCT	SCT	M	M	3300	10000	M	M	M	M	M	M	M	M	M	73.4	SEQM 292	M
SEQM	1/16/2022 20:00	73.4	23	30.18	44.6	35.66	350	10	0	M	6.21	M	SCT	BKN	M	M	4000	10000	M	M	M	M	M	M	M	M	M	73.4	SEQM 162	M
SEQM	1/20/2022 18:00	73.4	23	30.18	44.6	35.66	320	4	0	M	6.21	M	BKN	BKN	M	M	3000	4000	M	M	M	M	M	M	M	M	M	73.4	SEQM 201	M
SEQM	1/22/2022 19:00	73.4	23	30.18	53.6	49.9	350	16	0	M	6.21	M	BKN	SCT	M	M	3000	10000	M	M	M	M	M	M	M	M	M	73.4	SEQM 221	M
SEQM	1/24/2022 17:00	73.4	23	30.18	48.2	40.85	360	8	0	M	6.21	M	FEW	M	M	M	3000	M	M	M	M	M	M	M	M	M	M	73.4	SEQM 241	M
SEQM	2/2/2022 18:00	73.4	23	30.18	50	43.69	350	9	0	M	6.21	M	FEW	SCT	M	M	4000	30000	M	M	M	M	M	M	M	M	M	73.4	SEQM 021	M
SEQM	2/17/2022 19:00	73.4	23	30.18	53.6	49.9	350	17	0	M	6.21	M	FEW	SCT	BKN	M	3000	3300	30000	M	M	M	M	M	M	M	M	73.4	SEQM 171	M
SEQM	4/2/2022 21:00	73.4	23	30.18	46.4	38.18	320	9	0	M	6.21	M	SCT	SCT	M	M	3000	30000	M	M	M	M	M	M	M	M	M	73.4	SEQM 022	M
SEQM	4/3/2022 19:00	73.4	23	30.18	53.6	49.9	350	17	0	M	6.21	M	SCT	M	M	M	4000	M	M	M	M	M	M	M	M	M	M	73.4	SEQM 031	M
SEQM	4/6/2022 19:00	73.4	23	30.18	50	43.69	270	4	0	M	6.21	M	BKN	SCT	M	M	3300	8000	M	M	M	M	M	M	M	M	M	73.4	SEQM 061	M
SEQM	4/14/2022 19:00	73.4	23	30.18	42.8	33.29	140	5	0	M	6.21	M	SCT	SCT	M	M	3300	10000	M	M	M	M	M	M	M	M	M	73.4	SEQM 141	M
SEQM	4/15/2022 19:00	73.4	23	30.18	50	43.69	10	8	0	M	6.21	M	SCT	SCT	M	M	3300	10000	M	M	M	M	M	M	M	M	M	73.4	SEQM 151	M
SEQM	4/30/2022 18:00	73.4	23	30.18	48.2	40.85	M	5	0	M	6.21	M	BKN	M	M	M	4000	M	M	M	M	M	M	M	M	M	M	73.4	SEQM 301	M
SEQM	5/1/2022 19:00	73.4	23	30.18	51.8	46.71	10	12	0	M	6.21	M	SCT	SCT	M	M	4000	8000	M	M	M	M	M	M	M	M	M	73.4	SEQM 011	M
SEQM	5/24/2022 19:00	73.4	23	30.18	48.2	40.85	350	10	0	M	6.21	M	SCT	SCT	M	M	3000	30000	M	M	M	M	M	M	M	M	M	73.4	SEQM 241	M
SEQM	5/29/2022 19:00	73.4	23	30.18	41	31.05	300	6	0	M	6.21	M	SCT	M	M	M	4000	M	M	M	M	M	M	M	M	M	M	73.4	SEQM 291	M
SEQM	6/21/2022 20:00	73.4	23	30.18	51.8	46.71	330	12	0	M	6.21	M	SCT	BKN	M	M	3300	8000	M	M	M	M	M	M	M	M	M	73.4	SEQM 212	M
SEQM	7/1/2022 19:00	73.4	23	30.18	44.6	35.66	360	5	0	M	6.21	M	BKN	M	M	M	3000	M	M	M	M	M	M	M	M	M	M	73.4	SEQM 011	M
SEQM	7/7/2022 20:00	73.4	23	30.18	39.2	28.96	120	6	0	M	6.21	M	SCT	M	M	M	3000	M	M	M	M	M	M	M	M	M	M	73.4	SEQM 072	M
SEQM	7/7/2022 21:00	73.4	23	30.18	39.2	28.96	100	8	0	M	6.21	20	FEW	SCT	M	M	3000	8000	M	M	M	M	M	M	M	M	M	73.4	SEQM 072	M
SEQM	7/31/2022 19:00	73.4	23	30.18	51.8	46.71	350	21	0	M	6.21	M	SCT	M	M	M	4000	M	M	M	M	M	M	M	M	M	M	73.4	SEQM 311	M
SEQM	8/8/2022 18:39	73.4	23	30.18	39.2	28.96	90	12	0	M	6.21	M	SCT	M	M	M	3000	M	M	M	M	M	M	M	M	M	M	73.4	SEQM 081	M
SEQM	8/19/2022 19:00	73.4	23	30.18	39.2	28.96	40	8	0	M	6.21	M	SCT	SCT	M	M	4000	30000	M	M	M	M	M	M	M	M	M	73.4	SEQM 191	M
SEQM	8/22/2022 21:00	73.4	23	30.18	33.8	23.39	120	6	0	M	6.21	M	FEW	SCT	M	M	4000	30000	M	M	M	M	M	M	M	M	M	73.4	SEQM 222	M

Appendix F:
METAR Data Analysis

RejectedTakeoffSpeed_METAR

June 29, 2023

[1]:
```python
# Import libraries
import numpy as np
import pandas as pd
import datetime as dt
import matplotlib.pyplot as plot
import glob
```

[2]:
```python
# Grab the METAR csv files for each facility:
files = glob.glob('c:/Users/pilot/OneDrive/Desktop/San Jose State University/
 ↪Masters_Project/Rejected_Takeoff_Speed/Data/*.csv')

# Create an empty list to store METAR Dataframes:
frame = []
for file in files:
    frame.append(pd.read_csv(file))

# Concatenate Dataframes into a single Dataframe:
df = pd.concat(frame)
```

[3]:
```python
# Get METAR data from the concatenated database - select airport/station here:
# stations: SFO, DEN,SEQM
df = df.loc[df["station"] == "SFO"]
```

[4]:
```python
# Rename columns for readability:
df = df[["station","valid","tmpf","drct","sknt","alti","gust"]]
df.rename(columns={'station':'Airport','valid':'Datetime_UTC','tmpf':
 ↪'Temp_F','drct':'Wind_direction','sknt':
                   'Avg_wind_speed','alti':'Altimeter','gust':
 ↪'Gust_Conditions','metar':'METAR'}, inplace = True)

# Create a dictionary to convert specific columns to float type:
convert_dict = {'Temp_F': float, 'Wind_direction': float, 'Avg_wind_speed':␣
 ↪float}

# Since "M"s exist throughout the dataframe, replace with 'nan' to avoid errors:
df = df.replace('M',np.nan,regex=True)
df = df.astype(convert_dict)
```

[5]:
```
# Convert the date in the .csv file to datetime format:
df["Datetime_UTC"] = pd.to_datetime(df.Datetime_UTC)
df["Date_UTC"] = df["Datetime_UTC"].dt.strftime('%m/%d/%Y')

# Reposition Date_UTC, adjacent to Datetime_UTC:
df = df[["Airport","Datetime_UTC","Date_UTC","Temp_F","Wind_direction",
        "Avg_wind_speed",'Altimeter',"Gust_Conditions"]]
```

[6]:
```
# Obtain the average wind speed conditions, grouped by Date:
Wind_conditions = df.groupby(['Date_UTC']).mean().
 ↪sort_values('Avg_wind_speed',ascending = False)
Wind_conditions
```

[6]:

Date_UTC	Temp_F	Wind_direction	Avg_wind_speed	Altimeter
04/11/2022	52.675862	277.241379	22.206897	29.938621
04/26/2022	56.088000	283.600000	20.760000	30.030800
05/08/2022	54.711111	289.629630	20.259259	30.021481
05/19/2022	61.529167	288.333333	19.833333	29.985417
05/16/2022	57.582143	274.642857	19.571429	30.058929
…	…	…	…	…
01/11/2022	51.064000	47.600000	1.840000	30.374000
11/21/2022	52.433333	70.000000	1.833333	30.198333
01/28/2022	53.237500	82.083333	1.791667	30.267083
02/13/2022	59.470833	67.083333	1.750000	30.186667
01/27/2022	51.476000	64.400000	1.600000	30.192000

[364 rows x 4 columns]

[7]:
```
# Obtain the average altimeter and temperature readings, used for density␣
 ↪calculations:
Alti = df.groupby(['Date_UTC']).mean().
 ↪sort_values(['Altimeter',"Temp_F"],ascending = True)
Alti
```

[7]:

Date_UTC	Temp_F	Wind_direction	Avg_wind_speed	Altimeter
09/09/2022	67.245833	305.833333	11.916667	29.592083
09/18/2022	64.276923	174.400000	11.769231	29.660769
11/08/2022	50.922581	173.870968	10.290323	29.669355
03/28/2022	56.644444	166.800000	9.153846	29.700741
12/11/2022	50.641379	237.586207	11.517241	29.718276
…	…	…	…	…
12/24/2022	50.966667	78.750000	2.500000	30.344583
02/04/2022	51.041667	140.416667	3.833333	30.348333
01/11/2022	51.064000	47.600000	1.840000	30.374000
02/27/2022	54.150000	108.750000	3.708333	30.377917

```
01/10/2022  52.025000      107.083333        2.916667  30.383750

[364 rows x 4 columns]
```

[8]:
```python
# Create pivot table for the average wind speed and wind direction:
Wind_conditions_pivot = Wind_conditions.
 ↪pivot_table(index='Date_UTC',columns=None,values=['Avg_wind_speed',
 ↪           'Wind_direction'])
Wind_conditions_pivot
```

[8]:
```
            Avg_wind_speed  Wind_direction
Date_UTC
01/01/2022        4.791667      168.181818
01/02/2022        2.625000      114.166667
01/03/2022        7.700000      162.666667
01/04/2022        4.604167      122.291667
01/05/2022        4.551724      165.000000
…                      …             …
12/26/2022        5.357143       82.857143
12/27/2022       13.034483      182.068966
12/28/2022        5.750000      180.434783
12/29/2022        4.117647      102.058824
12/30/2022       11.227273      176.818182

[364 rows x 2 columns]
```

[9]:
```python
# Create pivot table for altimeter readings:
Alti_pivot = Alti.
 ↪pivot_table(index='Date_UTC',columns=None,values=['Altimeter','Temp_F'])
Alti_pivot
```

[9]:
```
            Altimeter     Temp_F
Date_UTC
01/01/2022  30.104583  46.583333
01/02/2022  30.268750  43.200000
01/03/2022  30.198667  51.016667
01/04/2022  30.271458  52.906250
01/05/2022  30.306552  53.548276
…                 …          …
12/26/2022  30.157500  50.825000
12/27/2022  29.904138  56.982759
12/28/2022  29.971250  51.237500
12/29/2022  29.904118  50.482353
12/30/2022  29.939091  57.631818

[364 rows x 2 columns]
```

[10]:
```
# Export pivot tables to Excel for plot/chart generation:
#Wind_conditions_pivot.to_excel('Plot.xlsx')
#Alti_pivot.to_excel('Plot.xlsx')
```

Appendix G: Crosswind Analysis

```
clc
close all
clear

% James D. Gonzalez III
% Dr. Lombaerts

%%%%%%%%%%%%%%%%%%%%%%%%%%%%%%%%%%%%%%%%%%%%%%%%%%%%%%%%%%%%%%%%%%%%%%%%%%%%%%%%%%%%%%%%%%%%%%%%%%%%%%%%%%%%%%%%%%%%%%%%%%%%%%%%%%%%%%%%%%%%%%%%%%%%%%%%%%%%%%%%%%%%%%%%%%%%
%%%%%%%%%%%%%%%%%%%%%%%%%%%%%%%%%%%%%%%%%%%%%%%%%%%%%%%%%%%%%%%%%%%%%%%%%%%%%%%%%%%%%%%%%%%%%%%%%%%%%%%%%%%%%%%%%%%%%%%%%%%%%%%%%%%%%%%%%%%%%%%%%%%%%%%%%%%%%%%%%%%%%%%%%%%%
% Step 1: Identify and define aircraft and airfield parameters:

% KSFO Airport Information:
l_28R = 3618;                                       % Length of the runway 29R
 at KSFO [m]
rho_0 = 1.225;                                      % Density of air at sea-
level conditions [kg/m^3].
%%%%%%%%%%%%%%%%%%%%%%%%%%%%%%%%%%%%%%%%%%%%%%%%%%%%%%%%%%%%%%%%%%%%%%%%%%%%%%%%%%%%%%%%%%%%%%%
% Runway surface conditions
l_28R_MagHeading = 284;                             % Magnetic heading of RWY
 28R at KSFO [deg]
mu_roll_dry_TO = 0.02;                              % Rolling coefficient for
 a dry, paved runway [-]
%%%%%%%%%%%%%%%%%%%%%%%%%%%%%%%%%%%%%%%%%%%%%%%%%%%%%%%%%%%%%%%%%%%%%%%%%%%%%%%%%%%%%%%%%%%%%%%
% Wind conditions obtained from METAR observation:
V_wind_avg = 35;                                    % Average wind speed,
 obtained from METAR observation [kts]
%V_wind_avg = 0.001;                                % Uncomment to implement
 zero wind condition [kts]
V_wind_avg = V_wind_avg*0.51444;                    % Average wind speed [m/s]
V_wind_dir = 312;                                   % Wind direction, obtained
 from METAR observation [deg]
V_wind_dir_angle = V_wind_dir-l_28R_MagHeading;     % Wind direction with
 respect to the aircraft body [deg]
%%%%%%%%%%%%%%%%%%%%%%%%%%%%%%%%%%%%%%%%%%%%%%%%%%%%%%%%%%%%%%%%%%%%%%%%%%%%%%%%%%%%%%%%%%%%%%%
% Nose and Main gear parameters:
W_b_x = 28.605;                                     % Distance from main wheel
 to nose wheel (center-to-center) [m]
W_b_y = 12.456;                                     % Distance from left main
 wheel to right main wheel (center-to-center) [m]
W_b_z = 5.5;                                        % Vertical distance from
 wheels to C.G., approximated from maintenance document [m]
```

```
r1 = 28.61;                                     % Horizontal distance from
 C.G. to center of nose wheel [m]
r4 = 1.0;                                       % Horizontal distance from
 C.G. to center of main wheels [m]
r_y_eng_inboard = 14.8;                         % Lateral distance between
 C.G. and center of inboard engines [m]
r_y_eng_outboard = 25.7;                        % Lateral distance between
 C.G. and center of outboard engines [m]
%%%%%%%%%%%%%%%%%%%%%%%%%%%%%%%%%%%%%%%%%%%%%%%%%%%%%%%%%%%%%%%%%%%%%%%%%%%%%%
%%%%%%%%%%%%%%%%%%%%%%%%%%%%%%%%%%%%%%%%%%%%%%%%%%%%%%%%%%%%%%%%%%%%%%%%%%%%%%%
%%%%%
% Aerodynamic parameters:
S = 845;                                        % Total wing surface area
 [m^2]
b = 79.75;                                      % Wingspan [m]
T_eng_1 = 0.704*348e3;                          % Maximum thrust generated
 by engine #1 [N]
T_eng_2 = 0.704*348e3;                          % Maximum thrust generated
 by engine #2 [N]
T_eng_3 = 0.704*348e3;                          % Maximum thrust generated
 by engine #3 [N]
T_eng_4 = 0.704*348e3;                          % Maximum thrust generated
 by engine #4 [N]
T_max = T_eng_1+T_eng_2+T_eng_3+T_eng_4;        % Total thrust generated
 by engines [N]
T_rev = T_max*.15;                              % Maximum reverse thrust
 (i.e. 15% of maximum thrust) [N]
r_y_eng_in = 14.8;                              % Horizontal distance
 between C.G. and inboard engines (#2 and #3) [m]
r_y_eng_out = 25.7;                             % Horizontal distance
 between C.G. and outboard engines (#1 and #4) [m]
z1 = 1.25;                                      % Vertical distance
 between C.G. and center of #1 and #4 engines (estimation)
z2 = 2.25;                                       % Vertical distance
 between C.G. and center of #2 and #3 engines
I_zz = 13.53103E7;                              % Mass moment of inertia
 about the z-axis (I_zz = 0.037*M_MTOW*b^2) [kg m^2)
del_r_max = 26;                                 % Max. rudder deflection
 angle [deg]
del_nw_max = 10;                                % Max. nose wheel
 deflection angle [deg]
C_l_beta = -0.221;                              % Non-dimensional measure
 of the change in roll rate due to a change in sideslip angle [1/rad]
C_l_delr = 0.007;                               % Non-dimensional measure
 of the change in roll rate due to a change in rudder deflection angle [1/rad]
C_l_r = 0.101;                                  % Non-dimensional measure
 of the change in roll rate due to a change in yaw rate [1/rad]
C_Y_beta = -0.96;                               % Non-dimensional measure
 of the change in side force due to a change in sideslip angle [1/rad]
C_Y_delr = 0.175;                               % Non-dimensional measure
 of the change in side force due to a change in rudder deflection angle [1/
rad]
C_n_beta = 0.150;                               % Non-dimensional measure
 of the change in yaw moment due to a change in sideslip angle [1/rad]
```

```
C_n_delr = -0.109;                                     % Non-dimensional measure
 of the change in yaw moment due to a change in rudder deflection angle [1/
rad]
C_n_r = -0.30;                                         % Non-dimensional measure
 of the change in yaw moment due to a change in yaw rate [1/rad]
C_L = 0.75;                                            % Lift coefficient [-]
C_D = 0.013;                                           % Drag coefficient [-]
%%%%%%%%%%%%%%%%%%%%%%%%%%%%%%%%%%%%%%%%%%%%%%%%%%%%%%%%%%%%%%%%%%%%%%%%%%%%%
%%%%%%%%%%%%%%%%%%%%%%%%%%%%%%%%%%%%%%%%%%%%%%%%%%%%%%%%%%%%%%%%%%%%%%%%%%%%%%
%%%%%
% Simulation parameters and Conversion factors:
epsilon_precision = 1E-9;                              % Safeguard for
 singularities [-]
rad2deg=180/pi;                                        % Convert radians to
 degrees [deg]
deg2rad = pi/180;                                      % Convert degrees to
 radians [1/deg]
dt = 0.001;                                              % Timestep [s]
%%%%%%%%%%%%%%%%%%%%%%%%%%%%%%%%%%%%%%%%%%%%%%%%%%%%%%%%%%%%%%%%%%%%%%%%%%%%%
%%%%%%%%%%%%%%%%%%%%%%%%%%%%%%%%%%%%%%%%%%%%%%%%%%%%%%%%%%%%%%%%%%%%%%%%%%%%%%
%%%%%
% Aircraft Mass and Weight specifications:
g_0 = 9.80665;                                         % Acceleration due to
 gravity at sea-level [m/s^2]
M_MTOW = 575000;                                       % Maximum takeoff mass
 [kg]
W_MTOW = M_MTOW*g_0;                                   % Maximum takeoff weight
 (MTOW) [N]
%%%%%%%%%%%%%%%%%%%%%%%%%%%%%%%%%%%%%%%%%%%%%%%%%%%%%%%%%%%%%%%%%%%%%%%%%%%%%
%%%%%%%%%%%%%%%%%%%%%%%%%%%%%%%%%%%%%%%%%%%%%%%%%%%%%%%%%%%%%%%%%%%%%%%%%%%%%%
%%%%%
%%%%%%%%%%%%%%%%%%%%%%%%%%%%%%%%%%%%%%%%%%%%%%%%%%%%%%%%%%%%%%%%%%%%%%%%%%%%%
%%%%%%%%%%%%%%%%%%%%%%%%%%%%%%%%%%%%%%%%%%%%%%%%%%%%%%%%%%%%%%%%%%%%%%%%%%%%%%
%%%%%
% Step 2: Apply EOMs and initial conditions:

% First, initialize the parameters for the takeoff roll:
i = 1;
  % First index, parameters evaluated at x = 0 m [-]

% Initial position and longitudinal/lateral speed:
s_x_TO(i) = 0;
  % Initial position of aircraft on runway (x-dir) [m]
s_y_TO(i) = 0;
  % Initial position of aircraft on runway (y-dir) [m]
u(i) = 0;
  % Forward velocity with respect to the body frame [m/s]
v(i) = 0;
  % Lateral velocity with respect to the body frame [m/s]
beta_g(i) = atan(v(i)/max([u(i) epsilon_precision]));
  % Tire sideslip angle [rad]
V_g(i)  = sqrt(u(i)^2+v(i)^2);
  % Inertial velocity relative to the ground [m/s]
```

```
r(i) = 0;
  % Initial yaw rate [rad/s]
r_psi(i) = 0;
  % Initial heading with respect to the body frame and RWY centerline [rad]
kappa(i) = r_psi(i) + beta_g(i);
  % Track angle relative to the ground [rad]
V_g_x(i) = V_g(i)*cos(kappa(i));
  % Ground speed component in the inertial frame (x-dir) [m/s]
V_g_y(i) = V_g(i)*sin(kappa(i));
  % Ground speed component in the inertial frame (y-dir) [m/s]
V_wind_x(i) = V_wind_avg*cos(V_wind_dir_angle*pi/180 - r_psi(i));
  % Horizontal wind component (i.e., headwind) [m/s]
V_wind_y(i) = V_wind_avg*sin(V_wind_dir_angle*pi/180 - r_psi(i));
  % Orthogonal wind component with respect to RWY (i.e., crosswind) [m/s]
beta(i) = atan((v(i)+V_wind_y(i))/max([(u(i)+V_wind_x(i))
 epsilon_precision])); % Aerodynamic sideslip angle [rad]

% Initialize gear sideslip and nose wheel deflection angle:
beta_g_mw_left(i) = atan((v(i)-(r(i)*r4))/max([(u(i)+(r(i)*(W_b_y/2)))
 epsilon_precision]));    % Left main wheel sideslip angle [rad]
beta_g_mw_right(i) = atan((v(i)-(r(i)*r4))/max([(u(i)-(r(i)*(W_b_y/2)))
 epsilon_precision]));   % Right main wheel sideslip angle [rad]
del_nw(i) = 0;
                  % Nose wheel deflection angle [rad]
beta_g_nw(i) = del_nw(i) + atan((v(i)+r(i)*r1)/max([u(i) epsilon_precision]));
                  % Nose wheel sideslip angle [rad]
del_r(i) = 0;
                  % Rudder deflection angle [rad]

% Initialize the aerodynamic forces:
V_air(i) = sqrt((V_g_x(i)+V_wind_x(i))^2+(V_g_y(i)+V_wind_y(i))^2);
                  % Airspeed magnitude [m/s]
q(i) = 0.5*rho_0*V_air(i)^2;
                  % Dynamic pressure [N/m^2]
V_air_lift(i) = sqrt((V_g_x(i)+V_wind_x(i))^2);
                  % Airspeed magnitude for lift calculations [m/s]
q_lift(i) = 0.5*rho_0*V_air_lift(i)^2;
                  % Dynamic pressure for lift calculations [N/m^2]
F_x_aero(i) = T_max - q(i)*S*C_D;
                   % Aerodynamic force along \hat{b_x} direciton in body frame
 [N]
F_y_aero(i) = q(i)*S*(C_Y_beta*beta(i) + C_Y_delr*del_r(i));
                   % Aerodynamic force along \hat{b_y} direciton in body frame
 [N]
F_z_aero(i) = W_MTOW - q_lift(i)*S*C_L;
                   % Aerodynamic force along \hat{b_z} direciton in body frame
 [N]

% Initialize the aerodynamic moments:
M_x_aero(i) = q(i)*S*b*(C_l_beta*beta(i) + C_l_delr*del_r(i) + C_l_r*(r(i)*b)/
(2*V_air(i)));    % Aerodynamic moment about the roll axis [N m]
M_y_aero(i) = z1*(T_eng_1 + T_eng_4) + z2*(T_eng_2 + T_eng_3);
                  % Aerodynamic moment about the pitch axis [N m]
```

```
M_z_aero(i) = q(i)*S*b*(C_n_beta*beta(i)+C_n_delr*del_r(i)+C_n_r*((r(i)*b)/
(2*V_air(i))))...    % Aerodynamic moment about the yaw axis [N m]
    + (T_eng_1 - T_eng_4)*T_eng_4*r_y_eng_outboard + (T_eng_2 -
 T_eng_3)*r_y_eng_inboard;

% Initialize the lateral runway friction coefficients for the nose wheel and
 both main gears:
mu_s_nw(i) =
 abs(0.39*exp(-0.015*sqrt(V_g(i)))*atan(0.33*beta_g_nw(i)*rad2deg));
      % Lateral runway friction coeff. nose wheel [-]
mu_s_mw_left(i) =
 abs(0.39*exp(-0.015*sqrt(V_g(i)))*atan(0.33*beta_g_mw_left(i)*rad2deg));
  % Lateral runway friction coeff. left main wheel [-]
mu_s_mw_right(i) =
 abs(0.39*exp(-0.015*sqrt(V_g(i)))*atan(0.33*beta_g_mw_right(i)*rad2deg));
  % Lateral runway friction coeff. right main wheel [-]

% Implement correction factors for the lateral runway friction coefficients:
mu_s_nw_corr(i) = mu_s_nw(i)*cos(beta_g_nw(i)) +
 mu_roll_dry_TO*sin(beta_g_nw(i));
mu_s_mw_left_corr(i) = mu_s_mw_left(i)*cos(beta_g_mw_left(i)) +
 mu_roll_dry_TO*sin(beta_g_mw_left(i));
mu_s_mw_right_corr(i) = mu_s_mw_right(i)*cos(beta_g_mw_right(i)) +
 mu_roll_dry_TO*sin(beta_g_mw_right(i));

% Setup the gear submodel A and B matrices for calculating all three normal
 forces:
B = [M_x_aero(i);
     M_y_aero(i);
     F_z_aero(i)];

A = [(-W_b_z*mu_s_nw_corr(i)*(sign(beta_g_nw(i)))) (-
W_b_z*mu_s_mw_left_corr(i)*(sign(beta_g_mw_left(i))) - 0.5*W_b_y)...
    (-W_b_z*mu_s_mw_right_corr(i)*(sign(beta_g_mw_right(i))) + 0.5*W_b_y);
    (-W_b_z*mu_roll_dry_TO - r1) (-W_b_z*mu_roll_dry_TO+r4) (-
W_b_z*mu_roll_dry_TO+r4);
    1 1 1];

% Initialize all three normal forces:
X = A\(-1*B);
F_z_nw(i) = X(1,:);                                                    %
 Normal force on the nose wheel [N]
F_z_mw_left(i) = X(2,:);                                               %
 Normal force on the left main wheel [N]
F_z_mw_right(i) = X(3,:);                                              %
 Normal force on the right main wheel [N]

% Setup dummy variables to validate calculations related to the gear submodel:
normal_force_total(i) = F_z_nw(i)+F_z_mw_left(i)+F_z_mw_right(i);
test(i) = normal_force_total(i) + F_z_aero(i);

% Initialize the forces acting on the gear:
F_x_gear(i) = F_z_nw(i)*mu_roll_dry_TO + F_z_mw_left(i)*mu_roll_dry_TO +
 F_z_mw_right(i)*mu_roll_dry_TO;
```

```
F_y_gear(i) = F_z_nw(i)*mu_s_nw_corr(i)*(sign(beta_g_nw(i))) +
 F_z_mw_left(i)*mu_s_mw_left_corr(i)*sign(beta_g_mw_left(i))...
    + F_z_mw_right(i)*mu_s_mw_right_corr(i)*sign(beta_g_mw_right(i));

% Initialize the moments acting on the gear:
M_x_gear(i) = -W_b_z*(F_z_nw(i)*mu_s_nw_corr(i)*sign(beta_g_nw(i)) +...
                                              % Gear moment about roll axis [N
 m]
    F_z_mw_left(i)*mu_s_mw_left_corr(i)*sign(beta_g_mw_left(i))...
    + F_z_mw_right(i)*mu_s_mw_right_corr(i)*sign(beta_g_mw_right(i)));

M_y_gear(i) = -W_b_z*(F_z_nw(i)*mu_roll_dry_TO + F_z_mw_left(i)*mu_roll_dry_TO
 + F_z_mw_right(i)*mu_roll_dry_TO);           % Gear moment about pitch axis
 [N m]
M_z_gear(i) = -(F_z_mw_left(i)*mu_s_mw_left_corr(i)*sign(beta_g_mw_left(i))...
    + F_z_mw_right(i)*mu_s_mw_right_corr(i)*sign(beta_g_mw_right(i)))*r4 +
 F_z_nw(i)*mu_s_nw_corr(i)*sign(beta_g_nw(i))...  % Gear moment about yaw axis
 [N m]
    *r1 + F_z_mw_left(i)*mu_roll_dry_TO*(W_b_y/2) -
 F_z_mw_right(i)*mu_roll_dry_TO*(W_b_y/2);

% Initialize the longitudinal, lateral, and rotational accelection:
u_dot(i) = (F_x_aero(i) + F_x_gear(i))/M_MTOW + r(i)*v(i);  % Acceleration
 along \hat{b_x} direciton in body frame [N]
v_dot(i) = (F_y_aero(i) + F_y_gear(i))/M_MTOW - r(i)*u(i);  % Acceleration
 along \hat{b_y} direciton in body frame [N]
r_dot(i) = (M_z_aero(i) + M_z_gear(i))/I_zz;                % Acceleration
 along \hat{b_z} direciton in body frame [N]

% Initialize time variable:
time(i) = 0;                                        % Initialize the total
 time to zero [s]

%%%%%%%%%%%%%%%%%%%%%%%%%%%%%%%%%%%%%%%%%%%%%%%%%%%%%%%%%%%%%%%%%%%%%%%%%%%%%%%%%
%%%%%%%%%%%%%%%%%%%%%%%%%%%%%%%%%%%%%%%%%%%%%%%%%%%%%%%%%%%%%%%%%%%%%%%%%%%%%%%%%%
%%%%%
%%%%%%%%%%%%%%%%%%%%%%%%%%%%%%%%%%%%%%%%%%%%%%%%%%%%%%%%%%%%%%%%%%%%%%%%%%%%%%%%%
%%%%%%%%%%%%%%%%%%%%%%%%%%%%%%%%%%%%%%%%%%%%%%%%%%%%%%%%%%%%%%%%%%%%%%%%%%%%%%%%%%
%%%%%
% Step 2: Apply EOMs for the takeoff procedure:
 while s_x_TO < l_28R
    i = i+1;                          % Advance to the next timestep

    % Apply an explicit Euler method and approximate velocities in the
 \hat{b_x},\hat{b_y}, and \hat{b_z} directions:
    u(i) = u(i-1) + dt*u_dot(i-1);      % Forward velocity with respect to the
 body frame [m/s]
    v(i) = v(i-1) + dt*v_dot(i-1);      % Lateral velocity with respect to the
 body frame [m/s]
    r(i) = r(i-1) + dt*r_dot(i-1);      % yaw rate [rad/s]

    % Apply an explicit Euler method and approximate distances/heading in the
 \hat{b_x},\hat{b_y}, and \hat{b_z} directions:
```

```
    s_x_TO(i) = s_x_TO(i-1) + dt*u(i);  % Position of aircraft on runway (x-
dir) [m]
    s_y_TO(i) = s_y_TO(i-1) + dt*v(i);  % Position of aircraft on runway (y-
dir) [m]
    r_psi(i) = r_psi(i-1) + dt*r(i);    % Heading angle [rad]

    % Calculate new sideslip angles and velocity magnitudes:
    beta_g(i) = atan(v(i)/max([u(i) epsilon_precision]));
      % Tire sideslip angle [rad]
    V_g(i)  = sqrt(u(i)^2+v(i)^2);
      % Inertial velocity relative to the ground [m/s]
    kappa(i) = r_psi(i) + beta_g(i);
      % Track angle relative to the ground [rad]
    V_g_x(i) = V_g(i)*cos(kappa(i));
      % Ground speed component in the inertial frame (x-dir) [m/s]
    V_g_y(i) = V_g(i)*sin(kappa(i));
      % Ground speed component in the inertial frame (y-dir) [m/s]
    V_wind_x(i) = V_wind_avg*cos(V_wind_dir_angle*pi/180 - r_psi(i));
      % Horizontal wind component (i.e., headwind) [m/s]
    V_wind_y(i) = V_wind_avg*sin(V_wind_dir_angle*pi/180 - r_psi(i));
      % Orthogonal wind component with respect to RWY (i.e., crosswind) [m/s]
    beta(i) = atan((v(i)+V_wind_y(i))/max([(u(i)+V_wind_x(i))
 epsilon_precision])); % Aerodynamic sideslip angle [rad]

    % Gear sideslip and nose wheel deflection angle:
    beta_g_mw_left(i) = atan((v(i)-(r(i)*r4))/max([(u(i)+(r(i)*(W_b_y/2)))
 epsilon_precision]));
    beta_g_mw_right(i) = atan((v(i)-(r(i)*r4))/max([(u(i)-(r(i)*(W_b_y/2)))
 epsilon_precision]));
    K_nw = -0.01/0.95;
    del_nw(i) = K_nw*s_y_TO(i); % Feedback loop; choose k-value (tuning)
    beta_g_nw(i) = del_nw(i) + atan((v(i)+(r(i)*r1))/max([u(i)
 epsilon_precision]));
    del_r(i) = del_nw(i)*(del_r_max/del_nw_max);%0;
      % Rudder deflection angle [rad]

    % Aerodynamic forces:
    V_air(i) = sqrt((V_g_x(i)+V_wind_x(i))^2+(V_g_y(i)+V_wind_y(i))^2);
    q(i) = 0.5*rho_0*V_air(i)^2;
    V_air_lift(i) = sqrt((V_g_x(i)+V_wind_x(i))^2);
    q_lift(i) = 0.5*rho_0*V_air_lift(i)^2;
    F_x_aero(i) = T_max - q(i)*S*C_D;
    F_y_aero(i) = q(i)*S*(C_Y_beta*beta(i) + C_Y_delr*del_r(i));
    F_z_aero(i) = W_MTOW - q_lift(i)*S*C_L;

    % Aerodynamic Moments:
    M_x_aero(i) = q(i)*S*b*(C_l_beta*beta(i) + C_l_delr*del_r(i) +
 C_l_r*(r(i)*b)/(2*V_air(i)));
    M_y_aero(i) = z1*(T_eng_1 + T_eng_4) + z2*(T_eng_2 + T_eng_3);
    M_z_aero(i) =
 q(i)*S*b*(C_n_beta*beta(i)+C_n_delr*del_r(i)+C_n_r*((r(i)*b)/
(2*V_air(i))))...
        + (T_eng_1 - T_eng_4)*T_eng_4*r_y_eng_outboard + (T_eng_2 -
 T_eng_3)*r_y_eng_inboard;
```

```
    % Calculate lateral runway friction coefficients for the nose wheel and
 both main gears:
    mu_s_nw(i) =
 abs(0.39*exp(-0.015*sqrt(V_g(i)))*atan(0.33*beta_g_nw(i)*rad2deg));
    mu_s_mw_left(i) =
 abs(0.39*exp(-0.015*sqrt(V_g(i)))*atan(0.33*beta_g_mw_left(i)*rad2deg));
    mu_s_mw_right(i) =
 abs(0.39*exp(-0.015*sqrt(V_g(i)))*atan(0.33*beta_g_mw_right(i)*rad2deg));

    % Implement correction factors for the lateral runway friction
 coefficients:
    mu_s_nw_corr(i) = mu_s_nw(i)*cos(beta_g_nw(i)) +
 mu_roll_dry_TO*sin(beta_g_nw(i));
    mu_s_mw_left_corr(i) = mu_s_mw_left(i)*cos(beta_g_mw_left(i)) +
 mu_roll_dry_TO*sin(beta_g_mw_left(i));
    mu_s_mw_right_corr(i) = mu_s_mw_right(i)*cos(beta_g_mw_right(i)) +
 mu_roll_dry_TO*sin(beta_g_mw_right(i));

    % Setup the gear submodel A and B matrices for calculating all three
 normal forces:
    B = [M_x_aero(i);
         M_y_aero(i);
         F_z_aero(i)];

    A = [(-W_b_z*mu_s_nw_corr(i)*(sign(beta_g_nw(i)))) (-
W_b_z*mu_s_mw_left_corr(i)*(sign(beta_g_mw_left(i))) - 0.5*W_b_y)...
        (-W_b_z*mu_s_mw_right_corr(i)*(sign(beta_g_mw_right(i))) + 0.5*W_b_y);
        (-W_b_z*mu_roll_dry_TO - r1) (-W_b_z*mu_roll_dry_TO+r4) (-
W_b_z*mu_roll_dry_TO+r4);
        1 1 1];

    % Calculate three normal forces:
    X = A\(-1*B);
    F_z_nw(i) = X(1,:);
    F_z_mw_left(i) = X(2,:);
    F_z_mw_right(i) = X(3,:);

    % Dummy calculations to validate gear submodel:
    normal_force_total(i) = F_z_nw(i)+F_z_mw_left(i)+F_z_mw_right(i);
    test(i) = normal_force_total(i) + F_z_aero(i);

    % Initialize the forces acting on the gear:
    F_x_gear(i) = F_z_nw(i)*mu_roll_dry_TO + F_z_mw_left(i)*mu_roll_dry_TO +
 F_z_mw_right(i)*mu_roll_dry_TO;
    F_y_gear(i) = F_z_nw(i)*mu_s_nw_corr(i)*(sign(beta_g_nw(i))) +
 F_z_mw_left(i)*mu_s_mw_left_corr(i)*sign(beta_g_mw_left(i))...
        + F_z_mw_right(i)*mu_s_mw_right_corr(i)*sign(beta_g_mw_right(i));

    % Initialize the moments acting on the gear:
    M_x_gear(i) = -W_b_z*(F_z_nw(i)*mu_s_nw_corr(i)*sign(beta_g_nw(i)) +...
        F_z_mw_left(i)*mu_s_mw_left_corr(i)*sign(beta_g_mw_left(i))...
        + F_z_mw_right(i)*mu_s_mw_right_corr(i)*sign(beta_g_mw_right(i)));
```

```
    M_y_gear(i) = -W_b_z*(F_z_nw(i)*mu_roll_dry_TO +
 F_z_mw_left(i)*mu_roll_dry_TO + F_z_mw_right(i)*mu_roll_dry_TO);
    M_z_gear(i) = -
(F_z_mw_left(i)*mu_s_mw_left_corr(i)*sign(beta_g_mw_left(i))...
        + F_z_mw_right(i)*mu_s_mw_right_corr(i)*sign(beta_g_mw_right(i)))*r4 +
 F_z_nw(i)*mu_s_nw_corr(i)*sign(beta_g_nw(i))...
        *r1 + F_z_mw_left(i)*mu_roll_dry_TO*(W_b_y/2) -
 F_z_mw_right(i)*mu_roll_dry_TO*(W_b_y/2);

    % Dynamic submodel:
    u_dot(i) = (F_x_aero(i) + F_x_gear(i))/M_MTOW + r(i)*v(i);
    v_dot(i) = (F_y_aero(i) + F_y_gear(i))/M_MTOW - r(i)*u(i);
    r_dot(i) = (M_z_aero(i) + M_z_gear(i))/I_zz;

    % Time array:
    time(i) = time(i-1) + dt;
 end

%%%%%%%%%%%%%%%%%%%%%%%%%%%%%%%%%%%%%%%%%%%%%%%%%%%%%%%%%%%%%%%%%%%%%%%%%%%%%%
%%%%%%%%%%%%%%%%%%%%%%%%%%%%%%%%%%%%%%%%%%%%%%%%%%%%%%%%%%%%%%%%%%%%%%%%%%%%%%%
%%%%%
%%%%%%%%%%%%%%%%%%%%%%%%%%%%%%%%%%%%%%%%%%%%%%%%%%%%%%%%%%%%%%%%%%%%%%%%%%%%%%
%%%%%%%%%%%%%%%%%%%%%%%%%%%%%%%%%%%%%%%%%%%%%%%%%%%%%%%%%%%%%%%%%%%%%%%%%%%%%%%
%%%%%
% Step 3: Plot the results:
figure(1)
subplot(2,1,1)
plot(s_x_TO(1,:),u(1,:))
ylabel('u [m/s]')
xlabel('s_x_{TO} [m]')
title('Inertial Velocity in x-direction [m/s]')
grid on

subplot(2,1,2)
plot(-1*flip(s_y_TO(1,:)),v(1,:))
ylabel('v [m/s]')
xlabel('s_y_{TO} [m]')
title('Inertial Velocity in y-direction [m/s]')
grid on

figure(2)
subplot(2,1,1)
plot(s_x_TO(1,:),u(1,:))
ylabel('u [m/s]')
xlabel('s_x_{TO} [m]')
title('Inertial Velocity in x-direction [m/s]')
grid on

subplot(2,1,2)
plot(s_x_TO(1,:),v(1,:))
ylabel('v [m/s]')
xlabel('s_x_{TO} [m]')
title('Inertial Velocity in y-direction [m/s]')
grid on
```

```
figure(3)
plot(s_x_TO(1,:),s_y_TO(1,:))
set(gca, 'YDir','reverse')
ylabel('s_y_{TO} [m]')
xlabel('s_x_{TO} [m]')
title('ground track of takeoff roll [m]')
axis equal

figure(4)
plot(s_x_TO(1,:),r_psi(1,:)*rad2deg)
ylabel('psi [deg]')
xlabel('s_x_{TO} [m]')
title('aircraft heading during takeoff roll [deg]')
grid on

% zeros_plot = zeros(size(s_x_TO));
% figure(5)
% axes1 = axes('Parent', figure(5));
% hold(axes1,'on');
% rectangle('Parent',axes1,'Position',[0 -60.96/2 3000 60.96],'FaceColor',[0 0
 1 0.5]); % Plots the rectangle
% hold on
% trajectory3(s_x_TO,s_y_TO,zeros_plot,zeros_plot,zeros_plot,r_psi
+pi/2,0.01,50,'A380',[0 90])
% set(gca, 'YDir','reverse')
% grid on
% %axis equal
% axis manual
% %ylim([-500 500])
% %xlim([0 s_x_TO(end)])
% ylabel('Runway Width [m]')
% xlabel('Runway Length [m]')

figure(6)
subplot(2,1,1)
plot(s_x_TO(1,:),del_nw(1,:)*rad2deg)
ylabel('\delta_{nw} [deg]')
xlabel('s_x_{TO} [m]')
grid on

subplot(2,1,2)
plot(s_x_TO(1,:),del_r(1,:)*rad2deg)
ylabel('\delta_{r} [deg]')
xlabel('s_x_{TO} [m]')
grid on


figure(7)
plot(V_air, F_z_nw)
hold on
plot(V_air, F_z_mw_left)
plot(V_air,F_z_mw_right)
ylabel('Normal Forces [N]')
```

```
xlabel('V_{air} [m/s]')
legend('Nose wheel','Left Main Wheel','Right Main Wheel')
title('aircraft heading during takeoff roll [deg]')
grid on

figure(8)
plot(s_x_TO, test)
ylim([-1,1])
ylabel('F_{z} - F_{aero} [N]')
xlabel('s_x_TO [m]')
title('Normal forces and Aerodynamic Force in z-direction Check')
grid on

figure(9)
subplot(1,2,1)
plot(time, V_g/0.51444)
xlim([0 30])
ylabel('V_g [knots]')
xlabel('Time (s)')
grid on
title('V_g vs. time')

subplot(1,2,2)
plot(time,r_psi*rad2deg)
hold on
plot(time,beta*rad2deg)
plot(time,del_r*rad2deg)
xlim([0 30])
ylabel('Degrees')
xlabel('Time (s)')
legend('hdg','\beta','\delta_r')
title('Figure 10b in Paper')
grid on
```

Appendix H:
Gear Submodel Derivation

Gear submodel Derivation:

$$\begin{Bmatrix} 0 \\ 0 \\ 0 \end{Bmatrix} = \begin{bmatrix} M_{x,aero} + M_{x,gear} \\ M_{y,aero} + M_{y,gear} \\ \underbrace{Mg - \bar{q}_{Lift} S C_L}_{F_{z,aero}\ (\text{Eqn. } 6)} \end{bmatrix} + \begin{bmatrix} 0 & -\frac{1}{2} W_{b_y} & +\frac{1}{2} W_{b_y} \\ -|r_1| & r_4 & r_4 \\ 1 & 1 & 1 \end{bmatrix} \begin{Bmatrix} F_{z,nw} \\ F_{z,mw,left} \\ F_{z,mw,right} \end{Bmatrix}$$

$$0 = M_{x,aero} + M_{x,gear} + 0\,F_{z,nw} - \frac{1}{2} W_{b_y} F_{z,mw,left} + \frac{1}{2} W_{b_y} F_{z,mw,right} \quad (1^*)$$

* signs for W_{b_y} makes sense to me. $\underline{F_{z,mw,right}} \downarrow$ wants to cause a positive rolling motion, where the right wing would move down & the left wing move up. $F_{z,mw,left} \downarrow$ wants to cause a negative rolling motion, or left wing down & right wing up.

$$M_{x,aero} = \bar{q} S b \left(C_{l_\beta} \beta + C_{l_{\delta_r}} \delta_r + C_{l_r} \frac{r b}{2V} \right) + T_{left}\, r_{y,eng} - T_{left}\, r_{y,eng} \quad (\text{Eqn } 7)$$

$$M_{x,gear} = -W_{b_z} \left(F_{y,mw,left} + F_{y,mw,right} + F_{y,nw} \right) \quad (\text{Eqn } 13)$$

$$F_{y,gear} = F_{z,nw} \mu_{s,nw} \operatorname{sign}(\beta_{g,nw}) + F_{z,mw,left} \mu_{s,mw,left} \operatorname{sign}(\beta_{g,mw,left})$$
$$+ F_{z,mw,right} \mu_{s,mw,right} \operatorname{sign}(\beta_{g,mw,right}) = F_{y,nw} + F_{y,mw,left} + F_{y,mw,right} \quad (\text{Eqn } 12)$$

where $\mu_s = 0.39 \exp(-0.015\sqrt{V_g}) \tan^{-1}(0.33\beta_g)$ (Eqn 14)

↳ β_g in deg. here; checked by plotting

∴ (Eqn 13 becomes)

$$M_{x,gear} = -W_{b_z} \Big[\left(F_{z,mw,left} \mu_{s,mw,left} \operatorname{sign}(\beta_{g,mw,left})\right) + \left(F_{z,mw,right} \mu_{s,mw,right} \operatorname{sign}(\beta_{g,mw,right})\right)$$
$$+ \left(F_{z,nw} \mu_{s,nw} \operatorname{sign}(\beta_{g,nw})\right) \Big] \quad (12^*)$$

Sub. Eqn 2^* into Eq 1^* to get:

$$0 = M_{x,aero} - W_{b_z} F_{z,mw,left} \mu_{s,mw,left} \operatorname{Sign}(\beta_{g,mw,left}) - W_{b_z} F_{z,mw,right} \mu_{s,mw,right} \operatorname{Sign}(\beta_{g,mw,right})$$
$$- W_{b_z} F_{z,nw} \mu_{s,nw} \operatorname{Sign}(\beta_{g,nw}) - \frac{1}{2} W_{b_y} F_{z,mw,left} + \frac{1}{2} W_{b_y} F_{z,mw,right}$$

$$0 = M_{x,aero} - W_{b_z} \mu_{s,nw} \operatorname{Sign}(\beta_{g,nw}) F_{z,nw} + \left[-W_{b_z} \mu_{s,mw,left} \operatorname{Sign}(\beta_{g,mw,left}) - \frac{1}{2} W_{b_y} \right] F_{z,mw,left}$$
$$+ \left[-W_{b_z} \mu_{s,mw,right} \operatorname{sign}(\beta_{g,mw,right}) + \frac{1}{2} W_{b_y} \right] F_{z,mw,right} \quad (4^*)$$

$$0 = M_{y,aero} + \underbrace{M_{y,gear}} - r_1 F_{z,nw} + r_4 F_{z,mw,left} + r_4 F_{z,mw,right} \quad (5^*)$$

$$M_{y,gear} = -W_{bz}\left(F_{x,nw} + F_{x,mw,left} + F_{x,mw,right}\right) \quad (\text{Eqn. } 14)$$

$$F_{x,gear} = \underbrace{F_{z,nw}\mu_{roll}}_{F_{x,nw}} + \underbrace{F_{z,mw,left}\mu_{roll}}_{F_{x,mw,left}} + \underbrace{F_{z,mw,right}\mu_{roll}}_{F_{x,mw,right}} \quad (\text{Eqn } 11)$$

where $\mu_{roll} = 0.015$

$$\therefore M_{y,gear} = -W_{bz}\left[F_{z,nw}\mu_{roll} + F_{z,mw,left}\mu_{roll} + F_{z,mw,right}\mu_{roll}\right] \quad (6^*)$$

<u>Sub Eqn 6* into Eqn 5*</u>

$$0 = M_{y,aero} - W_{bz}F_{z,nw}\mu_{roll} - W_{bz}F_{z,mw,left}\mu_{roll} - W_{bz}F_{z,mw,right}\mu_{roll} - r_1 F_{z,nw} + r_4 F_{z,mw,left} + r_4 F_{z,mw,right}$$

$$0 = M_{y,aero} + \left[-W_{bz}\mu_{roll} - r_1\right]F_{z,nw} + \left[-W_{bz}\mu_{roll} + r_4\right]F_{z,mw,left} + \left[-W_{bz}\mu_{roll} + r_4\right]F_{z,mw,right} \quad (7^*)$$

$\therefore$ Given Eqn 4^* & Eqn 7^*

$$\underbrace{\begin{Bmatrix} 0 \\ 0 \\ 0 \end{Bmatrix} = \begin{Bmatrix} M_{x,aero} \\ M_{y,aero} \\ F_{z,aero} \end{Bmatrix}}_{B_{3\times1}} + \underbrace{\begin{bmatrix} -W_{bz}\mu_{s,nw}\,\text{sign}(\beta_{g,nw}) & \left(-W_{bz}\mu_{s,mw,left}\,\text{sign}(\beta_{g,mw,left}) - \tfrac{1}{2}W_{by}\right) & \left(-W_{bz}\mu_{s,mw,right}\,\text{sign}(\beta_{g,mw,right}) + \tfrac{1}{2}W_{by}\right) \\ \left(-W_{bz}\mu_{roll} - r_1\right) & \left(-W_{bz}\mu_{roll} + r_4\right) & \left(-W_{bz}\mu_{roll} + r_4\right) \\ 1 & 1 & 1 \end{bmatrix}}_{A_{3\times3}} \underbrace{\begin{Bmatrix} F_{z,nw} \\ F_{z,mw,left} \\ F_{z,mw,right} \end{Bmatrix}}_{X_{3\times1}}$$

$$\begin{Bmatrix} -M_{x,aero} \\ -M_{y,aero} \\ -F_{z,aero} \end{Bmatrix} = [A] \begin{Bmatrix} F_{z,nw} \\ F_{z,mw,left} \\ F_{z,mw,right} \end{Bmatrix} \Rightarrow \begin{Bmatrix} F_{z,nw} \\ F_{z,mw,left} \\ F_{z,mw,right} \end{Bmatrix} = [A]^{-1}_{3\times3} \begin{Bmatrix} -M_{x,aero} \\ -M_{y,aero} \\ -F_{z,aero} \end{Bmatrix}$$